Spin network Entanglement and Bulk-Boundary Map in Loop Quantum Gravity

Qian Chen

Numéro National de Thèse : 2022ENSL0035

THÈSE
en vue de l'obtention du grade de Docteur, délivré par
l'ECOLE NORMALE SUPERIEURE DE LYON

École Doctorale N° 52
Physique et Astrophysique de Lyon (PHAST)

Discipline :Physique

Soutenue publiquement le 17/11/2022, par :
Qian CHEN

Spin Network Entanglement and Bulk-Boundary Map in Loop Quantum Gravity

Intrication quantique des réseaux de spin et états de frontière en Gravité Quantique à Boucles

---

Devant le jury composé de :

DITTRICH, Bianca	Professeure	Perimeter Institute	Rapporteur
MA, Yongge	Professeur	Beijing Normal University	Rapporteur
SPEZIALE, Simone	Directeur de Recherche	Université Aix-Marseille	Examinateur
ORITI, Daniele	Professeur	Arnold Sommerfeld Center	Examinateur
LIVINE, Etera	Directeur de Recherche	ENS de Lyon	Directeur de thèse

Acknowledgement

There are many individuals who have helped me get here. First and foremost, I would like to express my sincere gratitude to my thesis supervisor Etera Livine for welcoming me, teaching me and helping me navigate the world of mathematics and physics, encouraging and supporting me, and also criticizing me, to let me become better. It has been a real pleasure working with him. Trying to keep up with his very quick mind and immense knowledge is of challenge, but I really learn much from that, and I will always be grateful to him for his patience, motivation and enthusiasm.

I am also grateful to all the members of my committee. To Bianca Dittrich and Yongge Ma, who took the time to be my examiners and read my manuscript. To Daniele Oriti and Simone Speziale for being part of my jury.

At ENS de Lyon, I am indebted to my colleagues, friends. To Marc Geiller and Francesco Sartini for sharing their enthusiasm and experience in quantum gravity. To Laurent Chevillard, Thierry Dauxois, Andrei Fedorenko, Jean-Christophe Geminard, Jean-Michel Maillet, Laurence Mauduit, Marc Magro, Alain Pumir, Erika Sattler, for their kindness and care. To my office mates, Jan, Salvish, Joonas, Qiaoyin, Corentin, for the funny and easy days we spent together. Especially thanks to Christophe Goeller, who sacrificed his own time to answer me a ridiculous amount of questions. I can not thank him enough for his great patience with me.

To the colleagues and teachers around the world, Carlo Rovelli, Cong Zhang, Kristina Giesel, Hongguang Liu, Muxin Han, Mehdi Assanioussi, Iñaki Garay, Jerzy Lewandowski, Alejandro Perez and all adorable group members in CPT, Marseille (including Simone, of course), I am so lucky to meet you and learn much from you. I am really appreciated to your generosity and the knowledges, ideas, insights shared from you.

To my friends, Haoran, Yunlong, Qingyi, Haixiu, Bin, Qiyun, Shijia, Jingru, Jun, Jie, Tingting(s), Lulu, Junqing, Changjiang, Shuaipeng, Bingyu, Jiandi, Yisheng, Yicheng, Zhe, Yidi & Xuening, Wei & Tian, Sicheng & Yaqi, very happy to have your accompany, and thanks for your toleration with me. I especially must thank to my dearest friends, Shangqiang Ning, Xiangjing Liu, Ning Guo, Weizhen Jia, for sharing your delight with me, in other journeys of mathematics and physics, as well as your selfless support and assistance.

Last but not least, my deepest gratitude to my family: my parents, aunt and cousin, who have been a constant source of support and love, and always help me when needed. As a final note, I have to thank Edelgard, who know why.

Finally, I would like to acknowledge the financial support I have received from the CSC and ENS de Lyon in the form of a generous scholarship.

Résumé de la Thèse (English version below)

Cette thèse explore la question de la gravitation quantique, qui vise l'unification de la théorie de la relativité générale et de la théorie quantique des champs et étudie les conséquences phénoménologiques d'une telle théorie physique nouvelle. Récemment, les efforts sur cette ligne de recherche se sont concentrés sur l'idée d'holographie gravitationnelle et sur l'interface entre géométrie et information quantique. Dans ce contexte, la présente thèse est consacrée à l'implémentation et l'analyse de ces problématiques à la théorie de la gravitation quantique à boucles (loop quantum gravity). L'objectif est double, il s'agit de: (1) formuler une description quasi-locale de la gravitation quantique à boucle explicitant avec la relation entre états de géométries 4D et états de frontière 3D ; (2) formuler la géométrie quantique à l'échelle de Planck en termes d'information quantique et de flux quantique.

Ainsi, nous étudions les réseaux de spin ouverts (open spin networks), qui définissent les états quantiques de géométrie de variété 4D avec frontière. Nous les formulons comme des fonctions d'onde envoyant les géométries d'espace-temps 4D sur les états quantiques de bord. La question de l'holographie gravitationnelle est alors de comprendre à quel point il est possible de reconstruire la géométrie 4D à partir d'un état quantique de bord. En termes d'information quantique, il s'agit de la purification de l'état mixte de la frontière en un état pur de de la géométrie de l'intérieur. Nous prouvons un théorème de reconstruction universelle: pour un état de frontière quelconque, il est toujours possible de reconstruire un état pur de géométrie 4D sans profondeur. Cela constitue le point de départ de l'étude de l'holographie de la gravitation quantique à boucles. Poussant l'étude de l'intrication quantique multipartite dans les réseaux de spin, en particulier son comportement sous l'action de l'opérateur d'holonomie, nous prouvons l'invariance de l'intrication quantique sous coarse-graining de l'état quantique.

Summary of the Thesis

General relativity is the most widely accepted gravitational theory to date which describes cosmological scale in terms of differential geometry of spacetime, and quantum theory is the most accurate physical theory which describes microscopic scale in terms of non-commutative algebra. While the two fundamental physical theories have not been put into one picture. Loop quantum gravity is a tentative theory of quantum gravity that inherits the essences from the two theories. One of the crucial properties of loop quantum gravity is diffeomorphism invariance, which, however, leads to the absence of locality in the theory. Inspired by the insights of holography and relational perspective, the issue involved to locality could be resolved by the prescriptions of quasi-locality and emergent geometry. Following the two insights, it is conceivable that the diffeomorphism invariant operators are entirely described by a theory living on boundary, and the quantum geometry could be reconstructed/emerged from entanglement and correlation. This thesis is dedicated to the relevant explorations: (1) to formulate a quasi-local description for loop quantum gravity with bulk-to-boundary relation; (2) to formulate quantum geometry in terms of the notions of quantum information theory. We wish these formulations shed light on the holography and renormalization flow in loop quantum gravity.

We study open spin networks, which are embedded in manifolds with non-empty boundaries, from the viewpoint of bulk-boundary maps. Based on it, we formulate quasi-local descriptions of loop quantum gravity. We investigate the coarse-graining procedure via tracing over bulk degrees of freedom, which encodes all that we can know about the quantum state of geometry from probing the boundary. We prove a boundary-to-bulk universal reconstruction procedure, to be understood as a purification of the mixed boundary state into a pure bulk state. We then move to define multipartite entanglement in spin networks and show the computation of entanglement excitation from holonomy operator, which also allows us to glimpse bulk curvature from entanglement. Moreover, by investigating another coarse-graining procedure - via gauge-fixing, which does not trace over any bulk degrees of freedom, we show a new interesting connection between bulk geometry and boundary observables via the dynamics of entanglement. Finally, we define the spin network entanglement between spin sub-networks, which correspond to spatial sub-regions. We then generalize the coarse-graining approach and prove that the entanglement between spin sub-networks is preserved under the coarse-graining (via gauge-fixing), which exhibits a holographic perspective for the topic of entanglement.

Contents

Acknowledgements iii
Summary of the Thesis v

Introduction **1**

I Quantum Gravity and Quantum Information in a nutshell **9**

1 General Relativity **11**
1.1 Lagrangian formalism of General Relativity 12
1.1.1 The action of general relativity 12
1.1.2 General covariance and tetrad formalism 14
1.2 ADM Formulation 16
1.2.1 Geometrodynamics 16
1.2.2 Diffeomorphism invariance in Lagrangian and Hamiltonian formalism 20
1.3 Ashtekar-Barbero Formulation 22

2 Loop Quantum Gravity **26**
2.1 Holonomy-Flux Algebra 27
2.1.1 Holonomies 27
2.1.2 Fluxes 28
2.2 The Kinematical Hilbert Space: Cylindrical Functions 29
2.3 Operators on Kinematical Hilbert Space 32
2.3.1 Holonomy Operators 32
2.3.2 Flux Operators 33
2.4 Gauge-Invariant Hilbert Space: Spin Networks 34
2.5 Diffeomorphism Constraint: Abstract Spin Networks 38
2.6 The Hamiltonian Constraint 42

3 Quantum Information Theory **47**

3.1 Quantum Entanglement 48
3.1.1 Bipartite Entanglement and Purification 49
3.1.2 Multipartite Entanglement 50
3.1.3 Entanglement Measures 51
3.2 Mathematical Formalism of Quantum Operations 53
3.2.1 Classical Operations: Stochastic Process 54
3.2.2 Quantum Operations: Choi-Kraus Theorem and Kraus Operators 54
3.2.3 Examples of Quantum Operations 58

4 Two-body Entanglement in Newtonian Gravity 62
4.1 Quantum theory of Newtonian gravity 62
4.1.1 Two-body states 62
4.1.2 Solutions of bound states and SO(4) symmetry 64
4.2 Two-body entanglement in non-relativistic theory 67
4.2.1 Reduced state for two-body state 67
4.2.2 Correlation functions of two-body operators 70
4.2.3 Expectations of relative momentum and relative distance for Newtonian gravity 72
4.3 Two-body entanglement entropy 73
4.3.1 Two-body momentum entropy 73
4.3.2 Momentum entropy for Newtonian gravity bound states 74
4.3.3 An observation about entanglement reconstruction for interaction and geometry 76

II Entanglement and Bulk-Boundary Map in Quantum Gravity 80

5 Bulk-Boundary Maps 82
5.1 Spin Networks as Bulk-Boundary Maps 83
5.1.1 Corners 83
5.1.2 Boundary States and Maps 84
5.1.3 Spin Network Maps as Quantum Circuits 87
5.2 Coarse-graining via Gauge-fixing 89
5.2.1 Coarse-grained States 89
5.2.2 Bulk Probability 91
5.3 The closure defect basis 93
5.4 Boundary Hilbert Space and Dual Boundary Hilbert Space 94
5.4.1 Scalar Products of Dual Boundary Hilbert Space 94
5.4.2 Unitary transformations underlying dual boundary Hilbert spaces 96

6 Boundary Density Matrices and Reconstructed Bulk States 101
6.1 Boundary Density Matrices: Coarse-Graining via Tracing-Bulk 102
6.1.1 Bulk state to boundary density matrix 104
6.1.2 SU(2)-invariance of the boundary density matrix 104
6.2 Universal bulk reconstruction from the boundary density matrix 106

6.3 Probing the first layer of the bulk: bouquets of boundary edges 107
6.4 Examples: Boundary Density Matrix for Candy Graphs 111
6.4.1 The four-qubit candy graph 111
6.4.2 The six-qubit candy graph 113

7 Intertwiner Entanglement Excitation 119
7.1 Loop holonomy operator on spin networks 120
7.2 Multipartite entanglement and geometric measure of entanglement 126
7.2.1 Separable and entangled spin network states 127
7.2.2 The leading order evolution of geometric entanglement 132
7.2.3 Entanglement excitation and closure defect distribution 135
7.3 Example: Bipartite entanglement on candy graph 138
7.3.1 Entanglement entropy excitation on candy graph with truncated dynamics 138
7.3.2 Geometric entanglement and holonomy operator dispersion 141
7.3.3 Geometric interpretation of the entanglement in the semi-classical regime . 143
7.4 Example: Tripartite entanglement on triangle graph 149
7.4.1 Tripartite entanglement 152

8 Spin Network Entanglement: Coarse-graining 160
8.1 Entanglement between spin sub-networks 161
8.1.1 Reduced density matrices on spin network 161
8.1.2 Spin network entanglement and cluster intertwiner entanglement 164
8.2 Coarse-graining: holonomy operators 167
8.2.1 The transformation between holonomy operators based on finer and coarser graph 167
8.3 Examples 170
8.3.1 Triangle graph 170
8.3.2 Square graph 173
8.3.3 Path-dependency on simplest two-loop graph 175

Conclusion 180

A Examples of entanglement evolution 185
A.1 Time-dependent Bell state 185
A.2 Black hole evaporation toy model 185

B Proof of Proposition 5.2 187

C Proof of Result 8.3 189

Bibliography 192

Introduction

Modern physics develops on two cornerstones: general relativity describes the world of cosmological scale, and quantum physics describes the world of microscopic scale. However, they have not been formulated coherently: each theory underlies assumptions contradicting the other. General relativity is formulated with differential geometry, describing space-time by metric deterministically. In turn, quantum physics is formalized with non-commutative algebra, admitting discrete quanta and predicting measurements probabilistically. The quantum theory of gravity is supposed to offer a coherent picture merging and reconciling the two theories.

Why quantum theory of gravity is necessary

A natural question is whether a quantum theory of gravity is necessary or not for us to describe and understand the universe. General relativity is the best classical description for gravity so far. It has been verified by experiments to date, from its early success in the anomalous precession of Mercury, and in the deflection of starlight, to the recent direct detection of gravitational waves. Though, there is still mathematical risk in general relativity since it admits the existence of singularity that would spoil the smoothness of the space-time manifold and causes problematic divergence.

On the other hand, quantum field theory is going on the road to unifying four known fundamental interactions. After a series of triumphs in using quantum field theory [1], the standard model was established, which unifies the electromagnetic, weak, and strong interactions. It was then appealing to apply the same logic to general relativity and gravity and to see if the problem of singularity could be cured. But a long-standing obstacle is that general relativity in four dimensions is *non-renormalizable* in quantum field theory. Namely, applying perturbative quantum field theory to general relativity causes an infinite number of undetermined coupling constants. Non-renormalizability also occurs in other effective theories, e.g., Fermi interaction. Thus perturbative quantum field theory implies that general relativity is just an effective field theory of gravity.

A tentative path to study quantum phenomena in a gravitational field is to apply quantum field theory to curved space-time. This semi-classical description treats matter fields as quantum and the gravitational field as classical. These semi-classical approaches indeed proposed falsifiable phenomena, at least in principle, e.g., black hole entropy and Hawking radiation. Nevertheless, they are not the end of the story. Some paradoxes still need to be clarified and resolved, e.g., information paradox. Moreover, the semi-

classical approaches lead to infinitely degenerate vacua, immensely bringing mathematical difficulties to the theory.

Without a quantum theory of gravity, it is risky to incorporate the pictures of quantum mechanics and gravity. For instance, suppose a massive particle in a spatial superposition. What about the gravitational field it generates, i.e., should the gravitational field itself be considered as in quantum superposition (c.f. [2, 3, 4] and recent literature [5])? Then, should space-time itself be considered as being quantum superposition? If so, how do we figure out the quantum measurements that take place in space-time? Which phenomena may emerge if the quantum jump is allowed, say, quantum jump amongst particle's energy level? Furthermore, many concepts that have been accepted for a long time should be revised. For instance, the locality should be considered cautiously, as Bronstein argued: if we do not disregard general relativity, quantum theory does prevent the measurability of the field in an arbitrarily small region (c.f. [6]).

The theories built on semi-classical frameworks are unsatisfactory. In order to reconcile the problematic issues, it is necessary to have a genuine quantum theory of gravity. This theory is supposed: (i) cure the problematic issues in both general relativity and quantum field theory and (ii) resolve the problems arising from semi-classical approaches. Moreover, as a rigorous mathematical theory, quantum gravity should also tell us: (iii) which observables are relevant to the physical context and how quantum theory is related to measurements.

The approaches to quantum gravity

A quantum theory of gravity means the unification of general relativity and quantum field theory, following the working philosophy of theoretical physics prevalent in the 20th century. To embark on the road of unification is crucial to argue which principles should be deemed fundamental and which should be relaxed.

The most important lesson that general relativity taught us is that space-time geometry should be considered a dynamic object—space-time equals matter fields as in Einstein equation $G_{\mu\nu} = \frac{\kappa}{2} T_{\mu\nu}$. In general relativity, the gravitational interaction is encoded in space-time geometry as the manifestation of the curvature of space-time.

According to quantum field theory and the philosophy of unification, the next step is to quantize gravitational interaction as a dynamical object. However, this is extremely difficult, as one may think. The perturbative techniques are set up with a specific fixed background, e.g., Minkowski space-time, whereas the gravitational field is the dynamical object to be quantized. Thus any quantum fluctuation or quantum perturbation would nevertheless affect the background space-time and even the quantization, which comes with technical and philosophical difficulties. Another obstacle is the non-renormalizability of general relativity, as already mentioned, which entails to infinite number of to-be-determined coupling constants from perturbative techniques, which implies that general relativity should be an effective field theory of gravity.

The exploration of a quantum theory of gravity is a big challenge to modern physics, especially in the lack of experiments. Beyond semi-classical approaches, progress con-

tinues, and many approaches to quantum gravity have been developed in recent decades. Roughly, these approaches to quantum gravity diverge in two directions: one views general relativity as a low energy limit of a more fundamental theory, whereas one takes general relativity seriously. Two significant representatives of the two directions are string theory and loop quantum gravity (c.f. [7, 8] for more on the different approaches).

For string theory, it is not only a theory of gravity but an attempt to incorporate four fundamental interactions, following the idea of unification for physics. String theory views general relativity as a low energy limit of a more fundamental theory [9, 10, 11]. Its basic idea is to describe fundamental particles not as point-like objects but as one-dimensional strings in spatial dimensions or two-dimensional worldsheets in space-time. In string theory, the properties of a fundamental particle, such as mass, and charge, are determined by the vibrational state of the string, and one of which vibrational states of a string gives rise to the graviton, carrying the gravitational interaction. In this way, string theory quantizes gravitational field through quantizing graviton à la particle physics.

Apart from canonical quantization, loop quantum gravity also admits a covariant non-perturbative quantization, i.e., spin foam formalism [12, 13, 14, 15, 16, 17], introduced as an alternative method to implement the dynamics in loop quantum gravity. In spin foam, we define the quantum theory based on a discretized and regularized path integral for quantum gravity. To go beyond the formal definition of the path integral, we consider a cellular-decomposition to discretize the manifold and write the path integral as a state sum-model over the building blocks of the cellular-decomposition. These building blocks are fundamentally interpreted as the building blocks of space-time arising from the intrinsic discrete nature at the Planck scale. The resulting spin foam models, constructed from (extended) topological quantum field theories (TQFTs) with defects, define transition amplitudes for histories of spin networks. Though closely related, the spin foam formalism and the canonical loop quantum gravity are considered to be independent approaches.

Apart from canonical quantization, loop quantum gravity also admits a covariant non-perturbative quantization, i.e. spin foam formalism [18, 19, 20, 21, 22, 23, 24, 25, 6, 26, 27], introduced as an alternative method to implement the dynamics in loop quantum gravity. In spin foam, we define the quantum theory based on a discretized and regularized path integral for quantum gravity. To go beyond the formal definition of the path integral, we consider a cellular-decomposition to discretize the manifold and write the path integral as a state sum-model over the building blocks of the cellular-decomposition. These building blocks are fundamentally interpreted as the building blocks of space-time arising from the intrinsic discrete nature at the Planck scale. The resulting spin foam models, constructed from (extended) topological quantum field theories (TQFTs) with defects, define transition amplitudes for histories of spin networks. Though closely related, the spin foam formalism, and the canonical loop quantum gravity are considered to be independent approaches.

The spin foam formalism then evolves in a third quantization, where so-called "group field theories" define non-perturbative sums over random spin network histories in a similar way that matrix model partition functions define sums over random 2d discrete surfaces [28, 29, 30, 31, 32, 33]. The quantum theory sets up in a path integral formulation where the fields and the interaction terms carry a combinatorial and non-local character,

distinguishing it from the standard local quantum field theories. It is a general formalism that could be related to several approaches to quantum gravity, including loop quantum gravity and causal dynamical triangulations. It can play an important role in proposing new ways to formulate and investigate those theories [34].

The challenges from background independence

The significant successes of loop quantum gravity are the rigorous mathematical definition of the Hilbert space of quantum geometry, representing the physical states of the theory, and the definition of geometrical observables, such as area and volume operators. This approach predicts the intrinsic discreteness of geometry at the Planck scale. In this sense, the smooth geometry in general relativity will be replaced by the picture portraying discreteness and fuzziness, and the discrete structure of geometry will prevent space-time from collapsing below the Planck scale. Hence the singularity problem is cured.

Moreover, background independence has been taken seriously in loop quantum gravity, which is believed to be inherited from the very insight of Einstein: a physical theory should be established without referring to any artificial settings. This is the essential aspect of general relativity and implies the symmetry of the theory. Especially in general relativity, the diffeomorphism invariance is the manifestation of background independence.

Whereas background independence also brings new challenges that would change the long-standing notions rooted in minds. The diffeomorphism invariance is the symmetry of loop quantum gravity inherited from general relativity. Any diffeomorphic-equivalent state should be gauge-equivalent from the perspective of quantum theory, which raises new questions about background independence: how do we localize subsystems in the gravitational system?

In some sense, this challenge resembles the development of special relativity. As Einstein had done, he promoted the constancy of the speed of light and symmetry between inertial reference frames to be the fundamental principles (or axioms). Then based on that, he deliberated the relational notions, in theory, especially the simultaneity for measuring time and length, and finally reconciled electrodynamics and mechanics.

In exploring quantum gravity, the locality issue compels us to pay attention to relational notions. According to the relational perspective, any formulation concerning an individual dynamical object does not make sense. A formulation only makes sense when it involves the *relation* between dynamical objects. General relativity is formulated in this sense, thus in accord with background independence: space-time is a genuine dynamical object interacting with matter fields instead of a background anymore. There is no place for preferred background. Any physics should be talked about regarding certain relations.

The relational perspective, complementary to the requirement of background independence, bred a profound interpretation for the foundation of quantum theory, which is referred to as the relational interpretation of quantum mechanics delineated in [35, 36]. In the relational interpretation, the fundamental questions regarding quantum states, measurements, and observer-observed distinction should be addressed following the spirit of relationalism. In contrast, in non-relativistic quantum mechanics, it is necessary to put an artificial setting for physical interpretation, namely, an observer-observed distinc-

tion, where the observer-side (measurement apparatus) is assumed to be entirely classical, and observed-side (quantum object) is assumed to be quantum mechanical. Note that semi-classical approaches follow the artificial setting that assumes gravitational field to be classical. From the relational perspective, the observer-observed distinction is discarded, and gravitational field is also supposed to be quantum mechanical. That is to say, the relational perspective is innately compatible with the idea that gravitational field should be quantized. Moreover, the relational perspective prescribes the locality by prohibiting the absolute locality. Instead, we can only talk about locality in the sense of relations, meaning that the physical description ineluctably admits non-local observables.

So far, we have seen why the fundamental degrees of freedom can be innately non-local in the picture of quantum geometry and why relational perspective is necessary for the requirement of background independence. It is then interested to apply the relation perspective to the loop quantum gravity proposal to figure out how the classical picture of our daily lives emanates from quantum geometry and how localization emerges from superposition and probabilistic features of quantum theory. In the following, we would like to mention some open and relevant topics in the loop quantum gravity:

- *Quantum information prespective.* Loop quantum gravity is formulated as a diffeomorphism invariant theory in which we do not have a background space-time where to locate things. This raises a series of questions related to the locality in loop quantum gravity: How do we define reference frames? How does the notion of locality enter the theory?

  Since any physical quantities should emerge from the relations, it is natural to conceive the possibility that these relations get reflected in correlations. In quantum theory, some correlations cannot be interpreted classically, which is the notion of entanglement. Suppose we are given a composite system and want to study the relations between subsystems. Quantum theory requires us to consider the relations encoded by entanglement and quantum correlations. Thus, in the case of quantum gravity, the space-time and geometric notions are to be reconstructed from the notions of quantum information theory. Furthermore, in most interesting physical cases, the information is carried by the boundaries between subsystems [37], giving interesting relation that entanglement entropy satisfies area law.

- *Macroscopic and semi-classical regime.* At the Planck scale, the picture provided by loop quantum gravity is visualized as full of discreteness and fuzziness in the sense that quantum states are superposed within discrete spectra. How do we tame them to have a smooth and familiar picture for the macroscopic scale? In addition, does the smooth picture match the classical theory of general relativity?

  The main road toward the classical description is through coarse-graining procedures on the discrete quantum states [38, 39, 40, 41, 42, 43, 44], which are designed to reduce the number of tremendously many degrees of freedom within quantum superpositions and fluctuations for the sake of recovering macroscopic description. What is the connection between the various coarse-graining procedures? Furthermore, the evolutional and dynamic behavior under coarse-graining can be seen as renormalization flows. How do we properly define renormalization flows in quantum

gravity? The research will undeniably provide a deeper understanding of quantum gravity's dynamics.

- *Holography.* At the dynamical level, inspired by the black hole entropy formula, the gravitational degrees of freedom in a d-dimensional bounded region can be encoded on its $d-1$-dimensional boundary. This conjecture is usually referred to holographic principle. In some recent developments, boundaries play an important role in the works on classical edge modes (also referred to as 'local holography') for general relativity in its first-order formulation in terms of connection-vierbein variables [45, 46, 47, 48, 49], which are conserved charges of gravitational system. It is fascinating to construct loop quantum gravity's dynamics under the guidance of the holographic principle. What is the connection between boundary dynamics and bulk dynamics? Can we get the entropic area law in the context of loop quantum gravity? Furthermore, can holographic principle be emerged/derived from the semi-classical regime of loop quantum gravity?

Furthermore, the quantum information perspective and bulk-to-boundary relation advocate the idea that space-time is emergent [50]. Emergence is an essential idea in modern physics born from effective field theories, renormalization groups, and condensed matter physics. It also applies to other sciences involved in complex behavior, such as system science and even biology. Putting the spirit of "more is different" into practice [51], the idea of emergence states that phenomena that are unforeseen from the point of view of microscopic physics (e.g., phase transition and formation of crystal lattice), appear at macroscopic scales from the complex collective behavior of the fundamental degrees of freedom. That is, the connectivity and relation between the objects in a complex system constitute the diverse and fascinating macroscopic world! In the context of quantum gravity, the geometric information can be emerged from quantum information. The quantum-to-classical transition can be understood from the perspective of decoherence: the observer-observed distinction emerges on a physical boundary such that the coherence between the measuring apparatus and the observed quantum object is destroyed due to the randomness over the information from both sides.

This thesis is motivated by the above insights. We follow relational and holographic perspectives, focusing on entanglement and bulk-to-boundary relations. The goals are to formalize loop quantum gravity in a quasi-local framework, understand diffeomorphism invariant operators in this quasi-local framework, and reconstruct quantum geometry in terms of the notions of quantum information. We wish the exploration shed light on the further research involved in dynamics and eventually reveal the holography and renormalization flow in loop quantum gravity.

Outline of the thesis

This thesis is organized into eight chapters divided into two parts.

The first part comprises the background materials presenting the core concepts for the project in the second part. In the first part of the thesis, Chapter 1, we quickly review the framework of general relativity and present in more detail the Hamiltonian formulations,

the ADM formalism, and Ashtekar-Barbero formalism, where the later is the foundation of loop quantization. Particular attention is given to the diffeomorphism invariance, which is relevant to background independence. We discuss the subtlety between diffeomorphism invariances in the Lagrangian formulation and Hamiltonian formulation. The following Chapter 2 focuses on the canonical loop quantum gravity. It aims to give the basics of its construction as a canonical quantization of a suitable formulation of general relativity and then review its kinematical states called spin network states which are the building block of the quantum description of space. Then we will discuss how the diffeomorphism invariance is represented in canonical loop quantum gravity. We end this chapter with a brief introduction to the Hamiltonian constraint operator, which is still an open issue in this theory. The Chapter 3 is a narrow review of quantum information theory. It aims at giving the background materials for the rest of the thesis, focusing on two topics, entanglement and quantum operation formalism (Kraus representation). The two topics can be related closely through the purification concept. Finally, the first part ends with Chapter 4. It is a work on the study of non-relativistic quantum theory for Newtonian gravity, where the bipartite entanglement between two particles interacted with the Newtonian gravitational force studied. This chapter aims to provide a closer look at gravitational entanglement where the dynamics are well-established and investigate the idea of entanglement-geometry reconstruction.

The second part of the thesis is dedicated to the bulk-boundary map and the relevant quantum information perspective in loop quantum gravity, aiming at the goals of quasi-local formulation for loop quantum gravity and understanding quantum geometry from quantum information theory. In Chapter 5, based on [52], we consider the cases of spin networks with non-empty boundaries. We then introduce spin network state as a map from bulk holonomies to boundary Hilbert space. Namely, we construct the bulk-boundary à la spin foam or extended topological field theory with bulk holonomies as defects. The chapter starts with defining boundary Hilbert space and regarding functional represented by spin networks, then we introduce the coarse-graining procedure via gauge-fixing. It ends with defining dual boundary Hilbert space equipped with the scalar product of spin network Hilbert space. The following Chapter 6 explores the induced boundary density matrix via tracing the degrees of freedom of bulk holonomies. The approach actually defines another coarse-graining procedure where the information is conveyed to the recoupling of boundary spins. We prove that any induced boundary density matrix must be a SU(2)-invariant state with integer recoupled spin (closed defect), and conversely any SU(2)-invariant state with integer recoupled spin can be reconstructed (purified) from bulk with a single loop and single vertex. The chapter ends with proposing that boundary dynamics could be represented by SU(2)-invariant quantum operations (Kraus operators). Chapter 7, based on [53], explores the intertwiner entanglement excitation by loop holonomy operator and proposes a multipartite entanglement measure for loop quantum gravity. i.e., the *geometric measure of entanglement*. The chapter starts with the implementation of the loop holonomy operator on spin network states. We then explore the notion of multipartite entanglement and define the notion of geometric measure of entanglement for spin networks. The main result of this chapter is the computation of the growth of entanglement due to the action of the holonomy on a spin network basis state. In particular, the 2nd-order derivative to the geometric measure of entanglement

with respect to time can be computed from the dispersion of the loop holonomy operator. Moreover, we show that the computation can be expressed in terms of closure defect. The following Chapter 8 generalizes the intertwiner entanglement and defines the spin network entanglement between subgraphs. It is based on [54] and explores the spin network entanglement under coarse-graining (via gauge-fixing). We prove that the spin network entanglement is preserved under the coarse-graining method. Then we study the actions of loop holonomy operator under the coarse-graining procedure, giving the transformation rule between the implementations of holonomy operator on a fined graph and its corresponding coarse-grained graph, which leads to the statement that the evolution of spin network entanglement is still preserved under the coarse-graining method.

Part I

Quantum Gravity and Quantum Information in a nutshell

Chapter 1

General Relativity

General relativity is a beautiful theory describing gravitation in the language of differential geometry in terms of metric on a manifold. Despite its early successful interpretation of the anomalous precession of the perihelion of Mercury, and the prediction of deflection of starlight by the Sun during the solar eclipse, general relativity also suggested the existence of black holes and the expansion of the universe. A few years ago, the direct detection of gravitational waves, a crucial prediction of general relativity, was observed by LIGO. This opened a new door to the era of gravitational-wave astronomical observations. Even though there are still predictions of general relativity awaiting experimental verification, it has been widely thought of as the most successful theory of gravitation to date.

Indeed, general relativity unravels the profound connection between space, time, geometry, and matter. Especially general relativity is a representative example of the theories that can be constructed by considering diffeomorphism invariance.

Section 1.1 of this chapter quickly introduces general relativity in Lagrangian for- malism. In this section, we emphasize the importance of boundary terms in the Lagrangian formalism of general relativity. We also look at the difference between first-order formalism and second-order formalism. In fact, there are much more content and literatures on boundary terms and first/second-order formalisms, but we could only mention a small piece of them. Following this brief introduction to general relativity, we will then focus on a brief discussion on general covariance, which historically inspired general relativity. Then we introduce the Hamiltonian formalism of general relativity. We first look at the ADM formulation in Section 1.2, the prototype toward canonical quantization. Then we discuss the diffeomorphism, which may be considered the most important lesson that general relativity teaches us. In there, the diffeomorphism invariances in Lagrangian and Hamiltonian formalism are reviewed. We will also mention the 'problem of time' in Hamiltonian formalism and see how it can be resolved from the perspective of relationalism. Finally, we turn to the Ashtekar-Barbero formulation in Section 1.3, which is the first step toward canonical loop quantum gravity.

1.1 Lagrangian formalism of General Relativity

1.1.1 The action of general relativity

Historically, Einstein established his general relativity by seeking a proper way to integrate space-time geometry and matter with the help of constructing conservative law [55]. His attempt eventually achieved the celebrated field equation

$$\mathcal{R}_{\mu\nu} - \frac{1}{2}g_{\mu\nu}\mathcal{R} + \Lambda g_{\mu\nu} = \frac{\kappa}{2}T_{\mu\nu}\,, \tag{1.1.1}$$

where $\kappa = 16\pi G$ with gravitational constant in unit $c = 1$, and Λ the cosmological constant introduced by Einstein, initially to avoid the solution of expansion of the universe. The left-hand side of the field equation is all about the geometry of space-time, the space-time metric $g_{\mu\nu}$, and the associative Ricci curvature $\mathcal{R}_\mu$, while the right-hand side is about matter fields, encoded in energy-momentum tensor $T_{\mu\nu}$. The conservative law is realized in a very geometric manner,

$$\nabla^\nu\left(\mathcal{R}_{\mu\nu} - \frac{1}{2}g_{\mu\nu}\mathcal{R} + \Lambda g_{\mu\nu}\right) = \frac{\kappa}{2}\nabla^\nu T_{\mu\nu} = 0\,, \tag{1.1.2}$$

where ∇ is the covariant derivative compatible with metric $g_{\mu\nu}$. Einstein's equation elegantly links the space-time geometry to matter fields. As Wheeler said, matter tells space how to curve, and curved space tells matter how to move. Even in vacuum cases, i.e., the solutions for the cases of $T_{\mu\nu} = 0$ that energy-momentum tensor vanishes everywhere, e.g., Schwarzschild metric, Kerr metric, Reissner-Nordström metric, are nontrivial, which unravel fascinating pictures about our universe, e.g. black holes, horizons, etc.

The most important and rigorous way to derive the equation would be to start with the action principle. Historically, Einstein and Hilbert sought a gravitational action that does not rely on one's choice of coordinates. Thus the Lagrangian is purely a geometric quantity. Almost at the same time, they proposed the so-called Einstein-Hilbert action in the absence of a boundary, from which the field equation can be derived. Moreover, it admits straightforward generalization to D-dimensional ($D \geq 2$) manifold $\mathcal{M}$, i.e.,

$$S_{\text{EH}} = \frac{1}{\kappa}\int_{\mathcal{M}} \mathrm{d}^D x\,\sqrt{g}(\mathcal{R} - 2\Lambda)\,, \tag{1.1.3}$$

where $g = \det(g_{\mu\nu})$ the determinant of metric $g_{\mu\nu}$, and $\mathcal{R}$ the scalar curvature of the manifold. So far it is quite good, as a manifestation of genuine aesthetics.

While going further, in the cases of the manifold with a non-empty boundary, it is well-known that some terms must be added to the action for the action principle to be still well-defined [55]. For instance, in metric formalism (also called *second-order formulation*), the $\delta S_{\text{EH}}[g]$ gives the derivative of variational metric, say $\nabla\delta g_{\mu\nu}$, on boundary $\partial\mathcal{M}$. Thus, the variational condition on the boundary, i.e., $\delta g_{\mu\nu}|_{\partial\mathcal{M}} = 0$, would be not enough.

Basically, there are two resolutions: One prescription is to consider the connection formalism (also called *first-order formulation*), e.g., Palatini action (c.f. [55]) that takes

the metric $g_{\mu\nu}$ and connection $\omega^{\rho}_{\mu\nu}$ as independent variables. In the first-order formulation, the variation gives $\delta\omega^{\rho}_{\mu\nu}$ on boundary $\partial\mathcal{M}$, which is going to be fixed by imposing boundary condition $\delta\omega^{\rho}_{\mu\nu}|_{\partial\mathcal{M}} = 0$. The Einstein equation is recovered from varying the action without boundary term if no matter field is considered.

Another strategy is to consider adding boundary terms to the action. To remedy these boundary terms produced by variation, the well-known Gibbons-Hawking-York (GHY) term is added into the action [56, 57]

$$S_{\mathrm{GHY}} = \frac{2}{\kappa}\int_{\partial\mathcal{M}} \mathrm{d}^{D-1}x\,\sqrt{h}K\,, \tag{1.1.4}$$

where K is the extrinsic curvature, and h is the induced boundary metric on $\partial\mathcal{M}$. The covariant derivative term $\nabla\delta g_{\mu\nu}$ from varying Einstein-Hilbert action S_{EH} is then balanced by the variation from the boundary term, i.e., δS_{GHY}.

For general relativity without coupling matter field, the first-order formulation and the second-order formulation are equivalent, whereas gravity coupled to matter fields are not entirely equivalent. In particular, metric variables are insufficient for coupling Fermionic matter and spinor fields. Instead, we must introduce a tetrad field that allows us to couple these matter fields to the gravitational field. It is very likely to encounter the situation when one attempts to extend metric formalism to tetrad formalism. There are many possibilities for the extension, such as the Holst term, Euler class, Pontryagin class, and Nieh-Yan class [58, 59, 60, 61]. Following these considerations, some issues are involved, such as torsion and parity violation [60].

Note that the request of coupling Fermionic matter does not mean the strategy of adding boundary terms worse than first-order formalism. It is likely to construct a more sophisticated action containing the equations of motion of general relativity while the boundary condition $\delta\omega^{\rho}_{\mu\nu}|_{\partial\mathcal{M}} = 0$ is not enough. Moreover, a subtler situation occurs in the cases of space-time with non-smooth boundaries. For instance, one has to foliate space-time to derive a Hamiltonian formalism. In order to apply generalized Gauss's law to translating bulk integration to boundary integration, the corner term

$$S_{\mathrm{Hayward}} = \frac{2}{\kappa}\int_{\mathcal{S}} \mathrm{d}^{D-2}\sigma\sqrt{\gamma}(\theta - \pi) \tag{1.1.5}$$

is required to eliminate the discontinuity of derivatives [62, 63, 64], where $\mathcal{S}$ is the corner (the wedge between two surfaces, e.g., between time-like boundary and space-like boundary), θ the angle between two surfaces, and γ_{ij} the induced metric on $\mathcal{S}$. It turns out that boundary terms (1.1.4) and (1.1.5) contribute to the gravitational quasi-local energy [65, 66, 67, 68]. Indeed, boundary terms are crucial in the formalism of general relativity, and it is remarkable to note the role of boundaries. Whereas at this moment, we will not look into them too much.

Although it is far from to claim that general relativity has interpreted anything about gravity since one may envision the possibility that future experiments compel classical corrections when matter fields are taken into account, it is indeed withstood all the experimental tests to date. A tremendous amount of work has been done on this subject.

Beyond the research of an extension of general relativity at a classical level and the knowledge of quasi-local symmetry group, what we are still missing today is a coherent description of what we call quantum gravity, i.e. a consistent description of the law of gravity at the quantum level (if it exists).

1.1.2 General covariance and tetrad formalism

The prototype of the *general covariance* originates from the *equivalence principle* inspired by Einstein's ideal experiment that imagines someone in a falling elevator where he/she will not feel gravity in a sufficiently small region. This is the key insight guiding Einstein to go from special relativity to general relativity. It tells us that, locally, gravitation and inertia are equivalent. From this principle, Einstein deduces that gravitation is better understood not as a force but rather through the geometry of space and time.

It is possible to argue that one can distinguish acceleration or gravity if a more extensive region is accessible. For instance, he/she could measure the tidal force between the head and feet. However, this is not the case discussed here since we have accented the indistinguishability under the adverb "locally".

What we mostly care about is the freedom to choose inertial reference frames or non-inertial reference frames, or indistinguishability between gravitational force and fictitious force. Locally, one can take $\{\xi^I\}$ as the coordinates associated to Lorentz metric η_{IJ} such that the space-time distance is given in the manner of Minkowski $\mathrm{d}s^2 = \eta_{IJ}\mathrm{d}\eta^I\mathrm{d}\eta^J$. On the other side, the event can be described from other coordinates, say $\{x^\mu\}$. Since the space-time distance between events should be preserved, one has

$$\eta_{IJ}\mathrm{d}\xi^I\mathrm{d}\xi^J = g_{\mu\nu}\mathrm{d}x^\mu\mathrm{d}x^\nu\,, \tag{1.1.6}$$

from which the local reference frame fields can be defined, say

$$e^I_\mu(x) = \frac{\partial\xi^I}{\partial x^\mu}\,. \tag{1.1.7}$$

Admitting all possibilities to define the local reference frame field amounts to admitting a local Lorentz transformation Λ, i.e.,

$$\widetilde{e}^I_\mu(x) = \Lambda^I{}_J(x)e^J_\mu(x)\,. \tag{1.1.8}$$

The introduce of local reference frames beautifully captures Einstein's intuition that gravitation can be transformed away locally and space-time looks like Minkowski space. At every point x there exist four space-time vector fields e^μ_I which provide an orthonormal frame in which the metric reduces to η_{IJ}. As an added benefit, the local reduction to Minkowski space-time allows us to define fermions using standard techniques. However, there is more to this formalism. In fact, the Minkowski indices do more than just distinguish between the four vector fields e^μ_I. space-time would be thought as being equipped with two distinct vectorial structures (i.e., being a vector bundle [69]) — the tangent bundle on one hand side (associated to greek indices μ) and a collection of Minkowski spaces (associated to latin indices I) attached to every space-time point x on the other

hand side. Such a terminology is often encountered in particle physics where internal spaces are used as representation spaces for gauge groups.

So the metric is reformulated by solder form with local Lorentz metric η and the local reference frame field (also called co-tetrad),

$$g_{\mu\nu}(x) = \eta_{IJ} e^I_\mu(x) e^J_\nu(x)\,. \tag{1.1.9}$$

Note that we don't need to write x as an argument for η_{IJ} since η_{IJ} is universal to the manifold to be considered. The metric $g_{\mu\nu}$ defined so is clearly $\mathrm{SO}(3,1)$ invariant, because of $\Lambda^I{}_K(x)\eta_{IJ}\Lambda^J{}_L(x) = \eta_{KL}$ at every x. The definition does not demand the co-tetrad field invertible. The tetrad field is well-defined if e^I_μ does,

$$e^\mu_I = \frac{1}{3!}\frac{1}{e}\varepsilon^{\mu\nu\rho\lambda}\,\varepsilon_{IJKL}\,e^J_\nu\,e^K_\rho\,e^L_\lambda\,, \tag{1.1.10}$$

where $e = \frac{1}{4!}\varepsilon^{\mu\nu\rho\lambda}\,\varepsilon_{IJKL}\,e^I_\mu\,e^J_\nu\,e^K_\rho\,e^L_\lambda$ is the determinant of the co-tetrad e^I_μ. It is easy to check that they are commutatively inverse,

$$e^I_\mu\,e^\nu_I = \delta^\nu_\mu\,, \qquad \text{and} \qquad e^\mu_I\,e^J_\mu = \delta^J_I\,. \tag{1.1.11}$$

Given that besides general covariance we also have an internal gauge symmetry, and there are two distinct vectorial spaces associated to the manifold $\mathcal{M}$. We can still employ the usual covariant derivative ∇_μ in terms of the Levi-Civita connection $\Gamma^\rho_{\mu\nu}$ for space-time tensor fields associated to greek indices, and introduce a connection 1-form $\omega_\mu{}^I{}_J$ for gauge symmetry associated to latin indices. Therefore, we can then define the covariant derivative for both space-time tensor and internal tensor field, e.g.,

$$\mathcal{D}_\mu v^I_\nu(x) := \partial_\mu v^I_\nu(x) + \omega_\mu{}^I{}_J(x) v^J_\nu(x) - \Gamma^\rho_{\mu\nu}(x) v^I_\rho(x)\,. \tag{1.1.12}$$

We can consider an internal Lorentz rotation $\widetilde{v}^I = \Lambda^I{}_J(x) v^J$. Based on that we require $\widetilde{\mathcal{D}}_\mu \widetilde{v}^I = \Lambda^I{}_J \mathcal{D}_\mu v^J$, which implies the transformation rule associated to the connection 1-form $\omega_\mu{}^I{}_J$,

$$\widetilde{\omega}_\mu{}^I{}_J = (\Lambda^{-1})^I{}_K \omega_\mu{}^K{}_L \Lambda^L{}_J + (\Lambda^{-1})^I{}_K \partial_\mu \Lambda^K{}_J\,. \tag{1.1.13}$$

As to be seen, this is how connection should be transformed under local transformation. In addition, $\mathcal{D}_\mu$ will annihilate the Lorentz metric, i.e. $\mathcal{D}_\mu \eta_{IJ} = 0$, implying the antisymmetry of the connection 1-form, i.e., $\omega^{IJ}_\mu = -\omega^{JI}_\mu$, where we have used η^{IJ} to raise (or one could lower by η_{IJ}) the internal indices. Therefore, ω^{IJ}_μ is a $\mathfrak{so}(3,1)$-valued field.

Moreover, we can define the torsion 1-form and curvature 2-form associated to the connection 1-form ω as follow,

$$T^I = \mathrm{d}e^I + \omega^I{}_J \wedge e^J\,, \tag{1.1.14}$$

$$F^I{}_J = \mathrm{d}\omega^I{}_J + \omega^I{}_K \wedge \omega^K{}_J\,. \tag{1.1.15}$$

One can then formulate the Einstein-Hilbert action in terms of connection 1-form and tetrad field, which entails the tetradic Palatini action

$$S_P[e,\omega] = \int_{\mathcal{M}} \epsilon_{IJKL} e^I \wedge e^J \wedge F^{KL}[\omega]\,, \tag{1.1.16}$$

where $F^{KL}[\omega]$ is the curvature 2-form associated to the connection 1-form ω. In the case of vacuum, variation gives two equations of motion: one is almost to be the Einstein equation, another is an equation telling the connection torsion-free. The two equations are combined into Einstein equation. Moreover, this action is viewed as a constrained BF theory. By adding Holst term [70], i.e. Holst-Palatini action, it can be furthermore promoted as the starting point of spin-foam model [23, 24, 25, 6].

We have seen the importance of connection 1-form and tetrad field in the framework of general relativity, putting general relativity in a $\mathrm{SO}(3,1)$ or $\mathrm{SL}(2,\mathbb{C})$ gauge theory. While it is still hard to implement the quantization. One of reasons is that both $\mathrm{SO}(3,1)$ and $\mathrm{SL}(2,\mathbb{C})$ are non-compact groups. A way out is to seek a canonical theory to implement canonical quantization program in which the gauge group is compact. That will be Ashtekar-Barbero formulation on which loop quantum gravity is based. Before going into it, we first look at the first Hamiltonian formulation of general relativity in the history, which was very successful in developing new methods in order to investigate classical solutions, even though it has failed to be quantized towards a quantum theory of gravity.

1.2 ADM Formulation

1.2.1 Geometrodynamics

The Hamiltonian formulation of general relativity in terms of ADM (abbreviation for Arnowitt, Deser, Misner) variables is constrained system with induced spatial metric $q_{ab},\ a,b=1,2,3$ as configuration variables and its conjugate π_{ab} as momentum variables. The idea is to recover the picture of space evolving in time. The formulation starts with assuming that space-time manifold $\mathcal{M}$ is globally hyperbolic and diffeomorphic to $\Sigma\times\mathbb{R}$. We then consider a foliation of space-time by a family of space-like three dimensional hypersurface Σ_t parameterized by a scalar field t called coordinate time, i.e., $\Sigma_t=\left\{p\in\mathcal{M}\middle|t(p)=t\right\}$. A coordinates system $\left\{x^1,x^2,x^3,t\right\}$ is naturally adapted to the foliation where $x^a,\ a=1,2,3$ coordinate spatial splice Σ_t. Then the space-time metric $g_{\mu\nu}$ will be decomposed into induced metric associated to the spatial slice and extrinsic data related to the embedding and evolution. Essentially, one will have $g_{\mu\nu}=q_{\mu\nu}-n_\mu n_\nu$.

We illustrate the decomposition in Fig, 1.1 and explain how it is acquired: on each hypersurface Σ_t the coordinate t is a constant thus defining normal co-vector with gradient $\nabla_\mu t$ vertical to the tangent space $T\Sigma_t$, i.e. $v^\mu\nabla_\mu t=0,\ \forall\, v^\mu\in T_p\Sigma_t$ at each $p\in\Sigma_t$. On the other hand, at $p\in\mathcal{M}$ tangent vector $t^\mu\equiv\left(\frac{\partial}{\partial t}\right)^\mu$ of t-coordinate line is defined rather arbitrarily provided that $t^\mu\nabla_\mu=1$. In fact, the vector t^μ can be understood as a tangent vector of world line of observer at that point. It can be decomposed along four directions: three components are projected onto $T^*\Sigma_t$ (for defining shift vector later) and another component is projected onto the normal co-vector of Σ_t. Now we define the lapse function N as the proportional factor $n_\mu=-N\nabla_\mu t$ where n_μ is the unit co-vector with respect to Σ_t. Hence one has $t^\mu=N^\mu+Nn^\mu$ where $N^\mu\in T\Sigma$ is the shift vector and N lapse function.

A remark is pointed here: since the local observers are too arbitrary to be set, the shift vector N^μ and lapse function N inherit the arbitrariness from t^μ, presenting the spatial diffeomorphism and freedom of re-parameterization with respect to t.

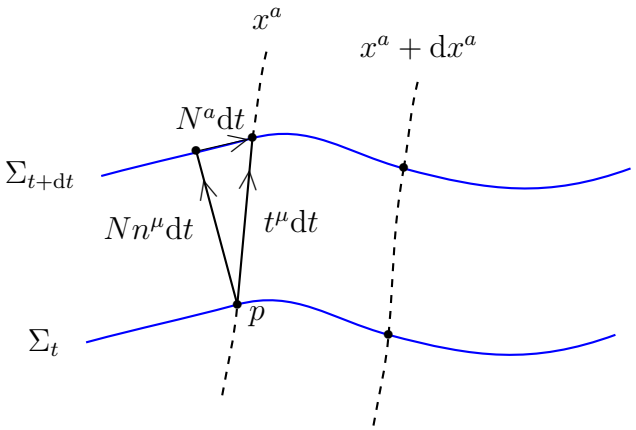

Figure 1.1: The illustration of the decomposition for lapse function N and shift vector N^a.

After the preparation, the space-time metric $g_{\mu\nu}$ is decomposed into the

$$g_{\mu\nu} = \begin{pmatrix} -N^2 + N_c N^c & N_b \\ N_a & q_{ab} \end{pmatrix} , \tag{1.2.1}$$

where $N_a = q_{ab}N^b = g_{ab}N^b$ are component of co-vector. Conversely, one can verify the inverse metric written as

$$g^{\mu\nu} = \begin{pmatrix} -\frac{1}{N^2} & \frac{N^b}{N^2} \\ \frac{N^a}{N^2} & q^{ab} - \frac{N^a N^b}{N^2} \end{pmatrix} . \tag{1.2.2}$$

The 4d configuration $g_{\mu\nu}$, is now converted to 3d configuration (q_{ab}, N^a, N). The Einstein-Hilbert action is rewritten in terms of 3d configuration (q_{ab}, N^a, N) as follow [71, 72]:

$$S[q_{ab}, N^a, N] = \frac{1}{\kappa}\int \mathrm{d}t \int_{\Sigma_t} \mathrm{d}^3x\, N\sqrt{q}\left(R + K_{ab}K^{ab} - K^2\right) + \frac{2}{\kappa}\int_{S_t} \mathrm{d}^2x\, N\sqrt{\sigma}k\,. \tag{1.2.3}$$

Here R is the scalar curvature of the spatial metric q_{ab}, $K^{ab} = q^\mu_a q^\nu_b \nabla_\mu n_\nu$ the extrinsic curvature of spatial slice Σ_t and $K = q_{ab}K^{ab}$, and q the determinant of 3d metric q_{ab}. The second term term of the action correspond to the $3+1$ decomposition of the boundary term with S_t the boundary of spatial slice Σ_t where σ_{ij} is the induced metric on S_t, and k^{ij} the extrinsic curvature of S_t embedding in Σ_t.

It turns out that boundary terms give the energy associated to the gravitational system [65, 66]. As seen immediately, bulk's contribution are constraints thus contributing nothing to the energy, while boundary terms contributes genuinely to energy. This explains the so-called 'quasi-local' energy: the energy is defined on boundary and seems

to be defined by boundary! In addition, the quasi-local energy depends on the choice of boundary conditions [68].

The generalized velocity of the theory is defined via Lie derivative with respect to vector field t^μ

$$\mathcal{L}_t q_{ab} = 2NK_{ab} + \mathcal{L}_{\vec{N}} q_{ab}\,, \tag{1.2.4}$$

while there is no respect velocity $\dot{N}^a$ or $\dot{N}$ meaning their respect conjugate momentum π_{Na} and π_N constrained at zero. The conjugate momentum variables are then defined via Legendre transform,

$$\pi^{ab} = \frac{1}{\kappa}\sqrt{q}(K^{ab} - q^{ab}K)\,, \qquad C_a = \pi_{Na}\,, \qquad C = \pi_N\,, \tag{1.2.5}$$

where the last two terms are primary constraints in Dirac's program [73, 74].

The velocity $\mathcal{L}_t q_{ab}$ is then solved in terms of q_{ab}, π^{ab} and N^a, N, defining the canonical form of action (without boundary terms)

$$S[q_{ab}, \pi^{ab}, N^a, N] = \int \mathrm{d}t \int_{\Sigma_t} \mathrm{d}^3x \, \left(\pi^{ab}\dot{q}_{ab} + \pi_{Na}\dot{N}^a + \pi\dot{N} - (\lambda C + \lambda^a C_a + N^a H_a + NH)\right)\,, \tag{1.2.6}$$

where H_a and H are secondly constraints in Dirac's program

$$H_a = -2q_{ac}D_b\pi^{bc}\,, \tag{1.2.7}$$

$$H = \frac{\kappa}{\sqrt{q}}\left(q_{ac}q_{bd} - \frac{1}{2}q_{ab}q_{cd}\right)\pi^{ab}\pi^{cd} - \frac{1}{\kappa}\sqrt{q}\,R\,, \tag{1.2.8}$$

called diffeomorphism constraint and Hamiltonian constraint, respectively.

These constraints are functions on hypersurface Σ_t thus are actually an infinite collection of constraints. In order to remove the distributional δ in Poisson algebra, we consider smeared field with respect to phase space test function field ϕ in the following manner:

$$\phi(f) = \int_{\Sigma_t} \mathrm{d}^3\,\phi(x)f(x) \tag{1.2.9}$$

where f is a test function with suitable boundary condition. We group up all constraints into a total bulk Hamiltonian (since no boundary term) in canonical action (1.2.6)

$$\mathbf{H} := \int_{\Sigma_t} \mathrm{d}^3x \, (\lambda C + \lambda^a C_a + N^a H_a + NH) = C(\lambda) + \vec{C}(\vec{\lambda}) + \vec{H}(\vec{N}) + H(N)\,. \tag{1.2.10}$$

Here we adopt vector sign to label $\vec{C}$ and $\vec{H}$ since their test fields carry a vector indices. In particular, the diffeomorphism constraint H_a is also referred to as vectorial constraint in some literatures, and Hamiltonian constraint H as scalar constraint.

The kinematical phase space is parametrized by the variables (q_{ab}, π^{cd}) equipped with the Poisson bracket structure

$$\left\{q_{ab}(x)\,, \pi^{cd}(y)\right\} = \kappa\delta^c_{(a}\delta^d_{b)}\delta^{(3)}(x, y)\,. \tag{1.2.11}$$

The total Hamiltonian determines the dynamics and evolution of the theory. The evolutions of primary constraints are given by

$$\left\{C(\lambda)\,,\mathbf{H}\right\}=H(\lambda)\,,\qquad\text{and}\qquad\left\{\vec{C}(\vec{\lambda})\,,\mathbf{H}\right\}=\vec{H}(\vec{\lambda})\tag{1.2.12}$$

respectively, concluding $H=0$ and $H_a=0$ on constraint surface. This is why $H=0$ and $H_a=0$ are referred to as secondly constraints: they are the consistent conditions to ensure that primary conditions are never out of constraint surface along the evolution.

Beside $\pi_{Na}=0$ and $\pi=0$ in phase space, the physical configurations (also called on-shell configurations) of the theory must extra satisfy diffeomorphism constraint $H_a=0$ and Hamiltonian constraint $H=0$. As mentioned, the gravitational energy vanishes if boundary items are not considered.

The secondly constraint are also required to be consistent in that sense, so we look at the Poisson algebra between diffeomorphism constraint and Hamiltonian constraint. Given test vector field V^a and test function field f, the smeared constraints form a closed Poisson algebra on the constraint surface,

$$\left\{\vec{H}(\vec{V})\,,\vec{H}(\vec{V}')\right\}=\kappa\vec{H}(\mathcal{L}_{\vec{V}}\vec{V}')\,,\tag{1.2.13}$$

$$\left\{\vec{H}(\vec{V})\,,H(f)\right\}=\kappa H(\mathcal{L}_{\vec{V}}f)\,,\tag{1.2.14}$$

$$\left\{H(f)\,,H(f')\right\}=\kappa\vec{H}(\vec{Y}_{[f,f',q]})\,,\tag{1.2.15}$$

where $\vec{Y}^a_{[f,f',q]}=q^{ab}(f\partial_b f'-f'\partial_b f)$ is the vector field in the third bracket. Poisson brackets above verify the consistency of the constrained system. The closed Poisson algebra is also called *hypersurface deformation algebra*, which is preserved under the motions generated by the constraints.

In the terminology of Dirac [73], all constraints in ADM formulation are of first class. A first class constrained system defines a degenerate symplectic form (understood as reducible phase space). Using exponential mapping, we can define a final transformation with respect to a phase space function X in the following way [14]: for any phase space function f,

$$\exp\left(\{X\,,\cdot\}\right)\triangleright f:=\sum_{n=0}^{\infty}\frac{1}{n!}\{X\,,f\}_{(n)}\tag{1.2.16}$$

where $\{X\,,\cdot\}_{(n)}$ stands for the iteration $\{X\,,f\}_{(0)}:=f\,,\{X\,,f\}_{(1)}:=\{X\,,f\}\,,\{X\,,f\}_{(2)}:=\left\{X\,,\{X\,,f\}\right\}$ and so on. On one hand, the constraints C and C_a generate the variations on lapse function and shift vector, respectively, complying with the setting of the theory. In the case of Hamiltonian general relativity, every constraint generates a transformation which maps to a state into a physically equivalent one. On the other hand, the constraints H and H_a generate the spatial diffeomorphism and time diffeomorphism,

$$\left\{q_{ab}\,,\vec{H}(\vec{V})\right\}=\mathcal{L}_V q_{ab}\,,\qquad\left\{\pi^{ab}\,,\vec{H}(\vec{V})\right\}=\mathcal{L}_V\pi^{ab}\,,\tag{1.2.17}$$

$$\left\{q_{ab}\,,H(f)\right\}=\mathcal{L}_{fn}q_{ab}\,,\qquad\left\{\pi^{ab}\,,H(f)\right\}=\mathcal{L}_{fn}\pi^{ab}+\frac{1}{2}q^{ab}fH-2f\sqrt{q}q^{a[c}q^{b]d}\mathcal{R}_{cd}\,.\tag{1.2.18}$$

Note that here the $\mathcal{R}_{\mu\nu}$ is the 4d Ricci curvature tensor. That is, only on the constraint surface and only when the vacuum Einstein equation $\mathcal{R}_{\mu\nu} = 0$ hold, the Hamiltonian flow of π^{ab} with respect to $H(f)$ can be interpreted as the action of a diffeomorphism in the direction fn^μ perpendicular to 3d hypersurface Σ_t.

While it turns out that the canonical quantization program cannot be completed in a rigorous and fully background independent way due to various technical difficulties [14]. The tentative quantization based on ADM formulation would start with elementary variables 3d metric q_{ab} and momentum π^{ab} from which elementary operators are promoted. Then the Hilbert space would be the space of wave functions of form $\Psi[q_{ab}]$ in which the precise definition for the scalar product is lack. In addition, one would write down the quantum constraints in terms of elementary operators. In particular, the quantum Hamiltonian constraint derived from ADM formulation, which is referred to as Wheeler-DeWitt equation, is not a polynomial functions of the variables (q_{ab}, π^{ab}), which in quantum theory become operator-valued distributions, thus non-polynomial expressions of these are hopelessly divergent.

A new Hamiltonian formulation, based on connection and triad variables, was introduced by Ashtekar [75], which finally allowed to elegantly perform major steps in canonical quantization program, opening the door to loop quantum gravity. We will introduce the Ashtekar-Barbero formulation in later section. Before doing it, we would like to discuss a subtlety about diffeomorphism invariance.

1.2.2 Diffeomorphism invariance in Lagrangian and Hamiltonian formalism

Diffeomorphism invariance actually admits many probable gravitational actions. Amongst them, general relativity is very special, according to the so-called Lovelock's theorem [76], which tells us that it is the only possible three or four-dimensional local theory depending on a metric up to second order derivatives. The number of admissible theories becomes enormous if we relax at least one constraint, see [77, 78, 79] for some reviews on the subject. In particular, in more than four dimensions, General relativity provides only a part of the full admissible action for gravity.

In metric formalism, in absence of matter, the only restriction on the action principle is general covariance and any gauge invariant functional of the metric $g_{\mu\nu}$ can be used to construct an action. The most general action for a covariant theory of gravity in terms of metric variables is formally given by

$$S[g_{\mu\nu}] = \int_{\mathcal{M}} \mathrm{d}^4x \sqrt{-g} \left(\mathcal{R} - 2\Lambda + \sum_{n=2}^{\infty} \alpha_n \mathcal{R}^n + \beta_1 \mathcal{R}_{\mu\nu\rho\sigma}\mathcal{R}^{\mu\nu\rho\sigma} + \cdots \right) , \qquad (1.2.19)$$

where the α_n's and β_i's stand for infinitely many coupling constants that need to be determined through experiments and observations. The metric general relativity is the simplest case with $\alpha_n = \beta_i = 0$ and acceptable for all tests so far, but it is also true that higher order curvature terms could make an appearance in future observations. But such a generalization of general relativity is not the subject of this thesis, and we restrict

ourselves to the usual Einstein formulation of gravity. What we are most interested is the diffeomorphism invariance revealed in the theory.

We briefly review the definition of diffeomorphism which has two equivalent versions: active diffeomorphism and passive diffeomorphism [55]. The active diffeomorphism is defined by moving points around, namely, $\varphi : \mathcal{M} \to \mathcal{N}$ sending $x \in \mathcal{M}$ to $\varphi(x) \in \mathcal{N}$, as well as the push forward φ_* and pull back φ^* for tensor field associated to the diffeomorphic manifolds $\mathcal{M}$ and $\mathcal{N}$. As for passive diffeomorphism, it is defined via coordinates transformation, namely, let $\{x^\mu\}$ and $\{y^\nu\}$ be any coordinates on $\mathcal{M}$ and $\mathcal{N}$ respectively, then diffeomorphism maps the coordinate chart at $p \in \mathcal{M}$ to the counterpart at $\varphi(p) \in \mathcal{N}$ but does not move the point p. The two manners look differently, but in fact they are equivalent. We specially concern the cases that $\varphi : \mathcal{M} \to \mathcal{M}$. In particular, φ is said to be a symmetry transformation for the tensor field T if $\varphi^* T = T$.

We collect all diffeomorphism $\varphi : \mathcal{M} \to \mathcal{M}$ to define the set $\mathrm{Diff}(\mathcal{M})$. Note that the form of action (1.2.19) satisfies $\varphi^* S[g_{\mu\nu}] = S[\varphi^* g_{\mu\nu}]$. Then diffeomorphism $\mathrm{Diff}(\mathcal{M})$ implies a statement as follows: an equation is said to be invariant under some set of transformation if, when written explicitly, for instance in terms of $g_{\mu\nu}$, it keeps the same functional form. This is an invariant property no matter whether the field equations hold or not. Such an invariance can be used to generate new solutions: Given a solution g of field equation $E(g) = 0$ and a diffeomorphism φ, then $g' = \varphi_* g$ is again a solution of $E(g) = 0$, provided the initial conditions are preserved.

As mentioned earlier, the derivation from action principle embarked on seeking quantity independent on the choice of coordinates. This independence is also referred to as diffeomorphism $\mathrm{Diff}(\mathcal{M})$. A gravitational action is invariant under $\mathrm{Diff}(\mathcal{M})$ provided that is invariant under the change of coordinates, also referred to as passive diffeomorphisms. The passive diffeomorphism is equivalent to active diffeomorphism that moves points in $\mathcal{M}$ around. In one word, $\mathrm{Diff}(\mathcal{M})$ is the case whether the equations of motion hold or not. While it is too early to state that any formulation of general relativity is necessary to be invariant under $\mathrm{Diff}(\mathcal{M})$. In fact, as seen in the Hamiltonian formalism, the diffeomorphism is realized a different way, which requires the equations of motion hold. This kind of diffeomorphism is referred to as $\mathrm{BK}(\mathcal{M})$, the Bergmann-Komar group [14]. The distinction is that $\mathrm{Diff}(\mathcal{M})$ is a kind of kinematical symmetry of any diffeomorphism-invariant action, while $\mathrm{BK}(\mathcal{M})$ is a kind of dynamical symmetry generated by constraints in Hamiltonian formalism. They are unnecessary to be same *in prior*.

Though the very elegance, diffeomorphism comes with some technical and philosophical difficulties to quantization. In contrast to quantum field theory as a local theory. The observables of general relativity are necessarily diffeomorphism invariant, implying that they are non-local and hence not well described by quantum field theory.

Another issue is about the evolution of a gravitational system. Quantum field theory tells us that the evolution is given by the Hamiltonian of the system. Whereas in the Hamiltonian formalism of general relativity (in more general, any covariant theory [80]), the Hamiltonian for a quantum theory of gravity is identically zero on-shell. The issue is usually referred to as 'problem of time'. In loop quantum gravity, the relationalism provides an answer for it [81, 82, 14]. That is, the notion of time should be represented à la dynamical relation, i.e. time is nothing but the relation between the movement of a

clock pointer and the movement of an object. We can not discuss time without referring dynamical relation. Similarly, the issue of spatial diffeomorphism can be answered in this way, namely, the locality is actually defined by the relation between two objects. Again, we can not talk about locality without referring relation.

The next section returns to the main thread and introduces Ashtekar-Barbero formulation, the Hamiltonian formalism in terms of connection-triad instead of metric and extrinsic curvature.

1.3 Ashtekar-Barbero Formulation

The Hamiltonian formulation of general relativity in terms of Ashtekar-Barbero variables can be understood as an extension of the ADM phase space along with a change of coordinates on this extended phase space through a canonical transformation [75, 83, 84]. The construction can be carried out by starting with solder form of 3d metric q_{ab},

$$q_{ab} = \delta_{ij} e^i_a e^j_b \,, \tag{1.3.1}$$

where $e^i_a,\ i = 1, 2, 3$ are co-triad field with $\mathfrak{so}(3)$-valued. It is free to say co-triad field e^i_a a $\mathfrak{su}(2)$-valued field, since $\mathfrak{so}(3) \cong \mathfrak{su}(2)$. The co-triad field admits inverse, the triad field e^a_i defined by

$$e^a_i = \frac{1}{2e}\epsilon_{ijk}\epsilon^{abc} e^j_b e^k_c \,, \qquad \text{where} \quad e = \det(e^i_a) = \frac{1}{3!}\epsilon_{ijk}\epsilon^{abc} e^i_a e^j_b e^k_c \,, \tag{1.3.2}$$

provided that e^i_a is invertible. It is easy to see $e = \sqrt{q}$ from the solder form.

The next is to define the extrinsic curvature 1-form $K^i_a = K_{ab} e^b_i$. The symmetric K_{ab} introduces a constraint on K^i_a,

$$K^i_{[a} e^i_{b]} = 0 \,. \tag{1.3.3}$$

But K^i_a does not transform as a connection under the action of SO(3) generated by the constraint. To obtain a connection variable thus get close to gauge theory, the spin connection Γ^i_a is introduced,

$$\Gamma^i_a = -\frac{1}{2}\epsilon^i{}_{jk} e^b_k (\partial_a e^j_b - \Gamma^c_{ab} e^j_c) \,, \qquad \text{with} \quad D_a v^i = \partial_a v^i + \epsilon^i{}_{jk}\Gamma^j_a v^k \,, \tag{1.3.4}$$

where the right-hand side defines the action on Lie algebra indices with respect to covariant derivative D associated to spin connection Γ^i_a. Moreover, the covariant derivative D is compatible with co-triad field e^i_a in the sense of combining spatial covariant derivative associated to 3d Levi-Civita connection, i.e., $D_a e^i_b = \partial_a e^i_b + \epsilon^i{}_{jk}\Gamma^j_a e^k_b - \Gamma^c_{ab} e^i_c = 0$.

Then the Ashtekar-Barbero connection is introduced

$$A^i_a := \beta K^i_a + \Gamma^i_a \,, \tag{1.3.5}$$

where β is a real number called Barbero-Immirzi parameter [84, 85, 86]. The conjugate part (A, E) is equipped kinematical phase space with Poisson structure:

$$\left\{ A^i_a(x) \,, E^b_j(y) \right\} = \frac{\kappa\beta}{2}\delta^b_a \delta^i_j \delta(x, y) \,. \tag{1.3.6}$$

Note that the connection A_a^i is not a space-time connection. It is an elaborate combination of extrinsic and intrinsic connection, depending explicitly on both the embedding of the spatial hypersurface into space-time, and the intrinsic geometry of Σ_t [87].

Similar to spin connection Γ_a^i, the Ashtekar-Barbero connection introduces a new covariant derivative $\mathcal{D}$,

$$\mathcal{D}_a v^i = \partial_a v^i + \epsilon^i{}_{jk} A_a^j v^k \,, \tag{1.3.7}$$

and rewrite the constraint (1.3.3) as

$$G_i = \frac{2}{\kappa\beta} \mathcal{D}_a E_i^a \,. \tag{1.3.8}$$

Ashtekar-Barbero connection defines a connection curvature,

$$F_a^i = \partial_a A_b^i - \partial_b A_a^i + \epsilon^i{}_{jk} A_a^j A_b^k \,. \tag{1.3.9}$$

Grouping these ingredients up, it eventually leads to the following reformulation of canonical general relativity,

$$S[A, E, N^a, N] = \frac{1}{\kappa\beta} \int \mathrm{d}t \int_{\Sigma_t} \mathrm{d}^3x \, \left(2E_i^a \dot{A}_a^i - N^a H_a - NH - \Lambda^i G_i \right) \,, \tag{1.3.10}$$

$$G_i = \mathcal{D}_a E_i^a = \partial_a E_i^a + \epsilon_{ijk} A_a^j E_k^a \,, \tag{1.3.11}$$

$$H_a = \frac{2}{\kappa\beta} F_{ab}^i E_i^a \,, \tag{1.3.12}$$

$$H = \frac{1}{\kappa} \frac{E_i^a E_j^b}{\sqrt{\det E}} \left(\epsilon^{ij}{}_k F_{ab}^k - (1+\beta^2)(K_a^i K_b^j - K_a^j K_b^i) \right) \,. \tag{1.3.13}$$

In this new formulation, the Gauss constraints G_i (1.3.11) are new due to the introduce of three extra internal degrees of freedom. The smearing function

$$G(\Lambda) = \int_{\Sigma_t} \mathrm{d}^3x \, \Lambda^i G_i \tag{1.3.14}$$

generates SU(2) gauge transformation

$$\left\{ A_a^i \,, G(\Lambda) \right\} = -\mathcal{D}_a \Lambda^i \,, \qquad \left\{ E_i^a \,, G(\Lambda) \right\} = \epsilon_{ij}{}^k \Lambda^j E_k^a \,. \tag{1.3.15}$$

The expressions are understood as an infinitesimal version of the gauge transformation in the sense of

$$A_a \longrightarrow g A_a g^{-1} + g \partial_a g^{-1} \,, \qquad E \longrightarrow g E g^{-1} \tag{1.3.16}$$

where $A = A_a^i \tau_i$ and $E = E_i^a \tau_i$ with $\mathfrak{su}(2)$ basis τ_i. The diffeomorphism constraints (with slight modification) and Hamiltonian constraint are smeared

$$\vec{H}(\vec{N}) = \int_{\Sigma_t} \mathrm{d}^3x \, N^a \left(H_a - A_a^i G_i \right) \,, \tag{1.3.17}$$

$$H(N) = \int_{\Sigma_t} \mathrm{d}^3x \, NH \,. \tag{1.3.18}$$

These smeared $G, \vec{H}, H$ form a closed constraint algebra as follow:

$$\{G(\Lambda), G(\mu)\} = G([\Lambda, \mu]), \tag{1.3.19}$$

$$\left\{\vec{H}(\vec{N}), G(\Lambda)\right\} = G(\mathcal{L}_N \Lambda), \tag{1.3.20}$$

$$\left\{\vec{H}(\vec{M}), \vec{H}(\vec{N})\right\} = \vec{H}(\mathcal{L}_M \vec{N}), \tag{1.3.21}$$

$$\left\{\vec{H}(\vec{M}), H(N)\right\} = H(\mathcal{L}_M N), \tag{1.3.22}$$

$$\{G(\Lambda), H(N)\} = 0, \tag{1.3.23}$$

$$\{H(M), H(N)\} = \vec{H}(\vec{Y}_{[M,N,E]}) + G(W_{[M,N,A,E]}). \tag{1.3.24}$$

Here we have adopted shorthand $[\Lambda, \mu] = \epsilon^i{}_{jk}\Lambda^j\mu^k$ of $\mathfrak{su}(2)$ Lie algebra commutator, and

$$\vec{Y}^a_{[M,N,E]} = \beta^2 \frac{E^a_i E^{bi}}{\det E}(M\partial_a N - N\partial_a M) \tag{1.3.25}$$

similar in Eq.(1.2.15), and a complicated function $W^i_{M,N}$ whose explicit expression can be found in [12]. Again, the constraint algebra in Ashtekar-Barbero formulation is of first class in Dirac's terminology.

At the end of the day, we have seen that the Ashtekar-Barbero formulation is defined in terms of connection-triad variables, which resembles to the formulation of Yang-Mills gauge field. Although they are different, Yang-Mills gauge field was the motivation of the Ashtekar-Barbero formulation in some historical sense. Nevertheless, the formulation allows us to construct quantum theory in favour of non-perturbative approaches, as done in lattice gauge theories. This is what we will see in the next chapter.

Chapter 2

Loop Quantum Gravity

The canonical loop quantum gravity follows the general framework for the quantization of constrained systems which was first formulated by Dirac [73, 74]. The first step of the program is to define a kinematical Hilbert space on which the Poisson brackets between the elementary classical variables are represented by the commutation relations between the corresponding elementary operators. In the case of loop quantum gravity, the elementary classical variables are chosen as Ashtekar-Barbero connection field A and triad field E. The following step of the program is to represent the constraint algebra as the constraint operators in the Hilbert space. Based on the step, one will look for the sector of the kinematical Hilbert space, which is annihilated by all of the constraint operators, i.e., constructing the physical Hilbert space of the theory. Once the physical Hilbert space has been constructed, the physical content of the theory will be encoded in the set of physical observables, which are represented by Dirac operators commuting with all constraint operators. Meanwhile, the transition amplitudes between the physical states are defined by the scalar product of the physical Hilbert space.

This chapter is meant to provide a review as complete as possible for the canonical loop quantum gravity. Section 2.1 follows the step of Ashtekar-Barbero formulation in the last chapter, defining the so-called holonomy-flux algebra, which represents the connection-triad variables to implement Dirac canonical quantization. Section 2.2 embarks on establishing the kinematical Hilbert space based on the holonomy-flux algebra, introducing cylindrical functions and kinematical scalar product. This section ends with the harmonic analysis of SU(2) function. In there, the Peter-Weyl theorem is stated, and the orthonormal basis with respect to the space of cylindrical functions is given. Section 2.3 introduces the operators on kinematical Hilbert space, i.e., holonomy operator and flux operator, as well as their actions on cylindrical functions. Particular attention is given to the non-commutativity of the commutator between two flux operators because this non-commutativity has something to do with the local holography developed in recent literatures. Section 2.4 is dedicated to solving Gauss constraints. In there, we will show the relation between Gauss constraints and gauge invariance and finally define the spin network states. We also define intertwining maps in a style of representation theory. Section 2.5 aims to introduce the solutions to diffeomorphism constraints. Note that the solutions are picked in the dual space instead of the kinematical Hilbert space. Based on

the solutions, we introduce the concept of abstract spin networks, moving to the framework of algebraic quantum gravity (AQG). The chapter ends with Section 2.6. Its aim is to give a basic introduction to the construction of Hamiltonian. In fact, the Hamiltonian operator and the corresponding dynamics are topics that still need exploration and to be understood. We refer the interested reader to the reference therein.

2.1 Holonomy-Flux Algebra

The first step from classical to quantum theory is to choose an appropriate set of elementary variables on the classical phase space. In order to fulfill the requirement of background independence, we are not allowed to use any background metric in defining elementary variables. Moreover, the distributional (singular) nature of the Poisson bracket (which is to be promoted into a commutator in the quantum theory) between the field variables entails considering a specific set of smeared variables, which must still satisfy the requirement to separate the points of (A, E) on the phase space. Further desirable properties of the chosen variables would be simple behavior under gauge transformations and spatial diffeomorphisms.

Although the raw Ashtekar-Barbero variables (A_a^i, E_j^b) do not provide a suitable starting point for quantization, their smearing geometric objects — holonomies of connection along curves (1d) and fluxes of the triad over surfaces (2d), do. These smeared variables generate a Lie algebra known as the holonomy-flux algebra [88, 89, 90, 91]. Moreover, holonomies are variables analogous to Wilson lines well-known in the context of lattice gauge theories, so some insights from the two fields could be potentially connected.

Therefore, loop quantum gravity is based on choosing these holonomies and fluxes as the elementary classical variables. This choice turns out to fulfill all the requirements outlined above.

2.1.1 Holonomies

We start by defining holonomies through parallel transport. Let $A_a^{ij}(x)$ be a smooth connection field, and $\gamma(t)$ an analytic curve with parameter t supported on manifold Σ. The holonomy operator $U_\gamma^{ij}(t_0\,, t_1)$ is defined by the solution of parallel transport equation with initial condition $U_\gamma^{ij}(t_0\,, t_0) = \delta^{ij}$, i.e.,

$$\frac{\mathrm{d}}{\mathrm{d}t}\, U_\gamma^{ij}(t_0\,, t_1) = -\dot{\gamma}^a\, A_a^{ik} U_\gamma^{kj}(t_0\,, t_1)\,, \tag{2.1.1}$$

where $\dot{\gamma}^a$ is the tangent vector along the curve $\gamma(t)$.

The definition by Eq.(2.1.1) leads to the crucial transformation rule for holonomy under local gauge transformation: consider local gauge transformation $A_a \longrightarrow gA_ag^{-1} + g\partial_a g^{-1}$ at every point in Σ, then the holonomy solved from Eq.(2.1.1) has to be transformed as

$$U_\gamma(t_0\,, t_1) \longrightarrow g(t_1) U_\gamma(t_0\,, t_1) g^{-1}(t_0)\,. \tag{2.1.2}$$

To prove it, we denote $\widetilde{U}_\gamma(t_0, t_1)$ the holonomy, solution of Eq.(2.1.1), transformed by the local gauge transformation such that the equation becomes

$$\frac{\mathrm{d}}{\mathrm{d}t}\widetilde{U}_\gamma(t) = -\dot{\gamma}^a g A_a g^{-1}\widetilde{U}_\gamma(t) - g\frac{\mathrm{d}g^{-1}}{\mathrm{d}t}\widetilde{U}_\gamma(t)\,. \tag{2.1.3}$$

We then act g^{-1} from left and notice the transformed equation is again an equation of parallel transport with respect to $g^{-1}\widetilde{U}_\gamma$ but with different initial condition $[g^{-1}\widetilde{U}_\gamma](t_0) = g^{-1}(t_0)$ due to $\widetilde{U}_\gamma(t_0) = \mathbb{I}$ the requirement of parallel transport. To remedy the initial condition, we act $g(t_0)$ from right, i.e.,

$$\frac{\mathrm{d}[g^{-1}\widetilde{U}_\gamma](t)}{\mathrm{d}t}g(t_0) = -\dot{\gamma}^a A_a[g^{-1}\widetilde{U}_\gamma(t)]g(t_0)\,. \tag{2.1.4}$$

Note that $g^{-1}(t_0)$ is a constant SU(2)-transformation with respect to t, the holonomy to be solved is $\widetilde{U}'_\gamma(t) = g^{-1}(t)\widetilde{U}_\gamma(t)g(t_0)$ with initial condition $\widetilde{U}'_\gamma(t_0) = \mathbb{I}$, i.e. $\frac{\mathrm{d}\widetilde{U}'(t)}{\mathrm{d}t} = -\dot{\gamma}^\mu A_\mu \widetilde{U}'_\gamma(t)$, which shares same solution as $U_\gamma(t)$ associated to connection field A_a, thus $\widetilde{U}'_\gamma(t) = U_\gamma(t)$. Finally, we arrive the wanted $\widetilde{U}_\gamma(t) = g(t)U_\gamma(t)g^{-1}(t_0)$.

Following the same logic, a diffeomorphism φ changes the Eq.(2.1.1) by replacing $A(x)$ with pull back $\varphi^* A(x)$, which are related by $(\varphi^* A)_a(\gamma(t)) = A_a(\varphi\circ\gamma(t))$. Thus the change is just to solve the parallel transport along curve $\varphi\circ\gamma$, meaning

$$U_\gamma(\varphi^* A) = U_{\varphi(\gamma)}(A)\,. \tag{2.1.5}$$

Therefore, the transform rules meet the 'desirable properties' mentioned at the beginning of this section, namely, holonomies behavior simply under gauge transformations and spatial diffeomorphisms: (1) One only need to look at the gauge transformation at endpoints, instead of concerning the gauge transformation within curves. (2) One only need to move the curves to fulfill diffeomorphisms.

We therefore see that the holonomy and the flux have simple and natural transformation properties under gauge transformations and diffeomorphisms.

2.1.2 Fluxes

The conjugate variable to the holonomy is given by the flux of the densitized triad E^a_i smeared on 2d surface. It is a nature geometric object since E^a is dual to 2-form field in 3d space, which eventually entails the non-commutativity of fluxes in quantum theory, as seen later. Let (σ^1, σ^2) be the coordinates on the surface S, then the flux is defined by smearing

$$E_i(S) = \int_S \epsilon_{abc}E^c_i = \int_S \mathrm{d}^2\sigma\, E^a_i n_a\,. \tag{2.1.6}$$

Moreover, we make $\mathfrak{su}(2)$-valued function f_i to define $f = f^i\tau_i$ then consider the following smearing flux variable:

$$E_f(S) = \int_S \mathrm{d}^2\sigma\, f^i E^a_i n_a\,. \tag{2.1.7}$$

Since $g\partial_a g^{-1}$ term is absent in the infinitesimal gauge transformation for triad field E^a_i induced by Eq.(1.3.15), smearing flux admits a simple rule for gauge transformation: $\tau_i \longrightarrow g\tau_i g^{-1}$ amounts to transform $f^i \longrightarrow g^{-1}f^i g$, thus

$$E_f(S) \longrightarrow E_{g^{-1}fg}(S)\,. \tag{2.1.8}$$

As for diffeomorphisms, the situation is similar: one moves the 2d surface by diffeomorphism φ,

$$(\varphi^* E)_f(S) = E_{f\circ\varphi^{-1}}(\varphi(S))\,. \tag{2.1.9}$$

It concludes that holonomy-flux algebra admits natural transformation properties under gauge transformations and spatial diffeomorphisms. In next section, we will construct the quantum theory based on holonomy-flux algebra.

2.2 The Kinematical Hilbert Space: Cylindrical Functions

The kinematical Hilbert space of loop quantum gravity is defined in terms of so-called cylindrical functions of a (generalized, distributional) connection A [12, 13, 14] which have to be square integrable with respect to a suitable gauge invariant and diffeomorphism invariant measure $\mathrm{d}\mu_{AL}[A]$. The difficulty at this stage comes from the fully dynamical feature of the metric. We do not have a background metric at disposal to define the integration measure. We need to define a measure on the space of connections without relying on any fixed background metric. The key to do this relies on the notion of cylindrical functions.

Suppose Γ is a graph consisting of N oriented edges (paths) $e_1\,,\cdots e_E$ embedded in the spatial manifold Σ. Then a cylindrical function is a functional of the form

$$\Psi_\Gamma[A] = \psi(g_{e_1}[A]\,,\cdots g_{e_E}[A])\,, \tag{2.2.1}$$

where ψ is any (complex-valued) function on $\mathrm{SU}(2)^E$, and E stands for the number of edges on the graph Γ. The function $\Psi_\Gamma[A]$ is called cylindrical with respect to the graph Γ. The set of all functions cylindrical with respect to Γ is denoted by Cyl_Γ.

It turns out that a natural quantity associated with a connection consists is the holonomy along edge. The holonomy is a functional of the connection that provides a rule for the parallel transport of SU(2) spinors along the edge e. Since the holonomy of the connection along a path $e(\epsilon)$ of infinitesimal parameter length ϵ is given by

$$g_{e(\epsilon)}[A] = 1 - \epsilon\dot{e}^a A^i_a \tau_i + O(\epsilon^2)\,, \tag{2.2.2}$$

we can think of it as a functional of the edge e and it is clear that it captures the information about the field A^i_a. More important, it has a very simple behavior under gauge transformations generated by Gauss constraint G_i,

$$G \triangleright g_e = h_{t(e)}\, g_e\, h^{-1}_{s(e)}\,, \tag{2.2.3}$$

are respectively the source and the target points of the edge e. The transformation is very meaningful, because it means the gauge transformation to be accumulated to the endpoints of e, so one only needs to look at the gauge transformation local at $s(e)$ and $t(e)$, i.e. $h_{s(e)}$ and $h_{t(e)}$ respectively, instead of concerning about the gauge transformation local inside the edge. Moreover, under the diffeomorphism action generated by the diffeomorphism constraint H_a, the holonomy transforms

$$g_e[\varphi^* A] = g_{\varphi(e)}[A]\,, \tag{2.2.4}$$

where the $\varphi^* A$ denotes the pull-back action for 1-form field A, and $\varphi(e)$ is the image of e under the diffeomorphism φ. Transforming the connection with the diffeomorphism is therefore equivalent to simply moving the edge with φ.

To equip Cyl_Γ with a scalar product in order to build it into a Hilbert space, the Haar measure $\mathrm{d}g$ on SU(2) is used, which is a unique gauge-invariant and normalized measure for SU(2). Using E copies of the Haar measure, the kinematical scalar product is defined by:

$$\langle \Phi_\Gamma | \Psi_\Gamma \rangle = \int_{\mathrm{SU}(2)} \left(\prod_{e\in\Gamma} \mathrm{d}g_e \right) \overline{\phi(g_1\,, \cdots, g_E)} \psi(g_1\,, \cdots, g_E)\,. \tag{2.2.5}$$

In order to define the scalar product between two functions Ψ_{Γ_1} and Φ_{Γ_2} cylindrical with respect to two different graphs Γ_1 and Γ_2, we note that any cylindrical function Ψ_{Γ_1} based on a graph Γ_1 can be viewed as a cylindrical function Ψ_{Γ_3} based on a larger graph Γ_3 by simply choosing ψ_{Γ_3} to be independent from the edge in Γ_3 but not in Γ_1. Moreover, any edge of a graph can be broken into two edges, separated by a bivalent vertex. This manner actually pushes the Cyl_Γ to the set of all cylindrical functions (with respect to any graph) by Cyl,

$$\mathrm{Cyl} = \bigcup_\Gamma \mathrm{Cyl}_\Gamma\,. \tag{2.2.6}$$

where $\bigcup_\Gamma$ denotes the union on all graphs Γ in Σ. As a consequence the scalar product for two cylindrical functions $\psi_{\Gamma_1}, \psi_{\Gamma_2}$ with respect to graphs Γ_1 and Γ_2 is constructed as follows:

- If Ψ_{Γ_1} and Φ_{Γ_2} share the same graph, i.e. $\Gamma_1 = \Gamma_2$, the definition of the scalar product (2.2.5) immediately applies.
- If $\Gamma_1 \neq \Gamma_2$, then they can be viewed as subgraphs of $\Gamma_3 = \Gamma_1 \cup \Gamma_2$, and $\Psi_{\Gamma_1}\,, \Phi_{\Gamma_2}$ are viewed as cylindrical functions on Γ_3 such that $\psi_{\Gamma_1}\,, \phi_{\Gamma_2}$ are trivially extended on Γ_3, denoted as Ψ_{Γ_1} and Φ_{Γ_2}. The scalar product between the two functions can then be defined as
$$\langle \Psi_{\Gamma_1} | \Phi_{\Gamma_2} \rangle = \left\langle \Psi^{(1)}_{\Gamma_3} \middle| \Phi^{(2)}_{\Gamma_3} \right\rangle\,. \tag{2.2.7}$$

The Eq.(2.2.7) can be interpreted as a scalar product between cylindrical functionals of the connection:

$$\int \mathrm{d}\mu_{AL}[A]\, \overline{\psi_{\Gamma_1}[A]} \phi_{\Gamma_2}[A]\,, \tag{2.2.8}$$

with respect to $\mathrm{d}\mu_{AL}[A]$, the so-called Ashtekar-Lewandowski measure, which is an integration measure over the space of connections [92].

The normalization of the Haar measure guarantees that the value of Eq.(2.2.7) does not depend on how the graph Γ_3 is chosen. Moreover, the transformation laws (2.2.3) and (2.2.4) of holonomies, together with the left and right invariance of the Haar measure, imply that the scalar product defined here is gauge and diffeomorphism invariant.

The kinematical Hilbert space of loop quantum gravity is then defined as the Cauchy completion of Cyl with respect to the norm arising from the scalar product (2.2.5):

$$\mathcal{H}_{\mathrm{kin}} = \overline{\mathrm{Cyl}}\,. \tag{2.2.9}$$

That is, in addition to cylindrical functions, we add to $\mathcal{H}_{\mathrm{kin}}$ the limits of all the Cauchy convergent sequences in the $\mathrm{d}\mu_{AL}$-norm.

It is convenient to introduce an orthonormal basis for $\mathcal{H}_{\mathrm{kin}}$. This can be easily done thanks to the Peter-Weyl theorem, which can be viewed as a generalization of Fourier theorem for functions on circle $\mathcal{S}^1$ [6]. The Peter-Weyl theorem states that, given a function $f \in L_2\left[\mathrm{SU}(2)\right]$ (more general, $L_2(G, \mathrm{d}g_{\mathrm{Haar}})$, with G any compact Lie group), it can be expressed as a sum over irreducible representations of SU(2), i.e.,

$$f(g) = \sum_j d_j\, f^j_{mn} D^j_{mn}(g)\,, \qquad j \in \frac{\mathbb{N}}{2}\,, \quad m = -j\,, \cdots, j\,, \quad d_j = 2j+1\,, \tag{2.2.10}$$

where the Wigner matrices $D^j_{mn}(g)$ give the spin-j irreducible matrix representation of the group element $g \in \mathrm{SU}(2)$, and d_j is the dimension of the spin-j representation. These Wigner matrix elements form a complete set of orthogonal functions of SU(2) via

$$\int_{\mathrm{SU}(2)} \mathrm{d}g\, \overline{D^{j_1}_{m_1 n_1}(g)} D^{j_2}_{m_2 n_2}(g) = \frac{1}{d_j} \delta_{j_1 j_2} \delta_{m_1 m_2} \delta_{n_1 n_2}\,, \tag{2.2.11}$$

where $\mathrm{d}g$ is the SU(2) Haar measure which in fact solves the coefficients f^j_{mn} via

$$f^j_{mn} = \int_{\mathrm{SU}(2)} \mathrm{d}g\, f(g) D^j_{mn}(g)\,. \tag{2.2.12}$$

Since the space Cyl_Γ is essentially a tensor product of the spaces Cyl_e over all the edges $e \in \Gamma$, it follows that an orthonormal basis on Cyl_Γ is formed by products of

$$f_{\Gamma,\{j_e\},\{m_e\},\{n_e\}}(g_1\,, \cdots, g_E) = \prod_{e\in\Gamma} \sqrt{d_{j_e}}\, D^{j_e}_{m_e n_e}(g_e)\,. \tag{2.2.13}$$

This allows a useful generalization: consider a node $v \in \Gamma$ with N inward edges $(e_1\,, \cdots, e_N)$ carrying spins $(j_1\,, \cdots, j_N)$, and N' outward edges $(e'_1\,, \cdots, e'_{N'})$ carrying spins $(j'_1\,, \cdots, j'_{N'})$. We then associate a set of tensors of the form

$$[\mathcal{R}_v]^{n_{e'_1} \cdots n_{e'_{N'}}}_{m_{e_1} \cdots m_{e_N}}$$

to the node v at which forms an orthonormal basis of the space

$$\mathcal{R}_v \in \mathcal{H}^*_{j_1} \otimes \cdots \otimes \mathcal{H}^*_{j_N} \otimes \mathcal{H}_{j'_1} \otimes \cdots \mathcal{H}_{j'_{N'}} \,. \tag{2.2.14}$$

It actually defines a map

$$\mathcal{R}_v : \mathcal{H}_{j_1} \otimes \cdots \otimes \mathcal{H}_{j_N} \longrightarrow \mathcal{H}_{j'_1} \otimes \cdots \mathcal{H}_{j'_{N'}} \,, \tag{2.2.15}$$

i.e. mapping the incoming tensor representation space $\mathcal{H}_{j_1} \otimes \cdots \otimes \mathcal{H}_{j_N}$ to outgoing tensor representation space $\mathcal{H}_{j'_1} \otimes \cdots \mathcal{H}_{j'_{N'}}$. After assigning tensor at each node of the graph, it defines the function in the form of

$$\left[f_{\Gamma,\{j_e\},\{\mathcal{R}_v\}}\right]^{m_{e'_1}\cdots m_{e'_{N'}}}_{n_{e_1}\cdots n_{e_N}} (g_1 \,, \cdots \,, g_E) = \left(\prod_{v\in\Gamma} [\mathcal{R}_v]^{n_{e'_1}\cdots n_{e'_{N'}}}_{m_{e_1}\cdots m_{e_N}}\right) \left(\prod_{e\in\Gamma} \sqrt{d_{j_e}} D^{j_e}_{m_e n_e}(g_e)\right) . \tag{2.2.16}$$

Functions defined so form a subset of Cyl_Γ. As seen later, a set of particular tensors $\mathcal{R}_v$ will solve the quantum Gauss constraints. Before solving them, we are going to introduce the elementary operators in kinematical Hilbert space of loop quantum gravity.

2.3 Operators on Kinematical Hilbert Space

In this section we will introduce the elementary operators on the kinematical Hilbert space $\mathcal{H}_{\text{kin}}$ — the operators corresponding to holonomies and fluxes.

2.3.1 Holonomy Operators

The spin-ℓ holonomy operator acts on cylindrical functions by multiplication

$$\widehat{D}^\ell_{ab}(g_e)\Psi_\Gamma[A] = D^\ell_{ab}(g_e)\psi(g_1 \,, \cdots \,, g_E) \,. \tag{2.3.1}$$

Note that the definition does not depend on whether the edge e belongs to graph Γ or not. If $e \notin \Gamma$, then the right-hand side of Eq.(2.3.1) is a cylindrical function on the graph $\Gamma \cup e$. That is, the holonomy operator $D^j_{mn}(g_e)$ adds a new edge e making the original graph Γ to be the new graph $\Gamma \cup e$. On the other hand, if $e \in \Gamma$, then the function in Eq.(2.3.1) is still an element of Cyl_Γ. In this case, recalling Eq.(2.2.13), the holonomy operator $\widehat{D}^\ell_{ab}(g_e)$ acts on any basic cylindrical function by tensoring the representation, which can be decomposed in terms of recoupling via Clebsch-Gordan coefficients of SU(2):

$$D^\ell_{ab}(g_e) D^{j_e}_{m_e n_e}(g_e) = \sum_{J=|j-\ell|}^{J+\ell} \sum_{M,N=-J}^{J} C^{\ell j_e J}_{a m_e M} C^{\ell j_e J}_{b n_e N} D^J_{MN}(g_e) \,. \tag{2.3.2}$$

Here $|j-\ell| \le J \le j+\ell$ is the triangle condition due to the recoupling $\mathcal{V}_\ell \otimes \mathcal{V}_j = \bigotimes_{J=|j-\ell|}^{j+\ell} \mathcal{V}_J$. The remaining cases that e partially overlaps or multiples edges of Γ, can be legitimized by cutting or gluing the piecewise edges due to the property of composition $g_{e_1}[A] \cdot g_{e_2}[A] = g_{e_1 \circ e_2}[A]$ of holonomies.

2.3.2 Flux Operators

The holonomy operator is defined as a multiplicative operator on $\mathcal{H}_{\text{kin}}$. Correspondingly, the flux operator would be defined as a differential operator on $\mathcal{H}_{\text{kin}}$. Since holonomies are group elements of SU(2), the corresponding differential operators are the so-called left- and right-invariant vector fields,

$$L_i\psi(g) = \mathrm{i}\frac{\mathrm{d}}{\mathrm{d}t}\psi\left(ge^{t\tau_i}\right)\Big|_{t=0}, \qquad R_i\psi(g) = \mathrm{i}\frac{\mathrm{d}}{\mathrm{d}t}\psi\left(e^{-t\tau_i}g\right)\Big|_{t=0}, \tag{2.3.3}$$

where $\{\tau_i\,, i = 1, 2, 3\}$ form an orthonormal basis of $\mathfrak{su}(2)$. Any element $\xi \in \mathfrak{su}(2)$ can be decomposed into $\xi = \xi^i\tau_i$ hence it generalizes above actions via

$$L_\xi\psi(g) = \mathrm{i}\frac{\mathrm{d}}{\mathrm{d}t}\,\psi\left(ge^{t\xi}\right)\Big|_{t=0}, \qquad R_\xi\psi(g) = \mathrm{i}\frac{\mathrm{d}}{\mathrm{d}t}\,\psi\left(e^{-t\xi}g\right)\Big|_{t=0}. \tag{2.3.4}$$

Furthermore, using the left- and right-invariant vector fields, we define the momentum operators on $\mathcal{H}_{\text{kin}}$, which are denoted by $\widehat{J}_i^{(x,e)}$ labeled by a point x and an edge e such that either $x = s(e)$ or $x = t(e)$, together with the $\mathfrak{su}(2)$ vector index i. The action of these operators on cylindrical functions is defined in the following way:

$$\widehat{J}_i^{(x,e)}\Psi_\Gamma[A] = \begin{cases} \mathrm{i}\dfrac{\mathrm{d}}{\mathrm{d}t}\,\psi\left(g_{e_1}\,,\cdots,g_{e_k}e^{t\tau_i}\,,\cdots,g_{e_E}\right)\Big|_{t=0}, & \text{if } e = e_k \text{ and } x = s(e)\,, \\ \mathrm{i}\dfrac{\mathrm{d}}{\mathrm{d}t}\,\psi\left(g_{e_1}\,,\cdots,e^{-t\tau_i}g_{e_k}\,,\cdots,g_{e_E}\right)\Big|_{t=0}, & \text{if } e = e_k \text{ and } x = t(e)\,, \\ 0\,, & \text{if } e \notin \Gamma \text{ or } x \in V(\Gamma)\,, \end{cases} \tag{2.3.5}$$

where $V(\Gamma)$ stands for the set of nodes of Γ. The momentum operator $\widehat{J}_i^{(x,e)}$ form a $\mathfrak{su}(2)$ Lie algebra

$$\left[\widehat{J}_i^{(x,e)}\,,\widehat{J}_j^{(x',e')}\right] = \delta_{x,x'}\delta_{e,e'}\epsilon_{ijk}\widehat{J}_k^{(x,e)}\,. \tag{2.3.6}$$

Therefore it is ready to discuss the flux operator. As mentioned earlier, the flux operator should be represented as the differential operator due to the quantization rule $E_i^a \to -\mathrm{i}\frac{\delta}{\delta A_a^i}$. To be more precise, its action on a cylindrical function is expressed as

$$E_i(S)\psi_\Gamma\left(g_{e_1}\,,\cdots,g_{e_E}\right) = -\mathrm{i}8\pi\beta G\int_S \mathrm{d}^2\sigma\, n_a(\sigma)\frac{\delta}{\delta A_a^i}\psi_\Gamma\left(g_{e_1}\,,\cdots,g_{e_E}\right)\,. \tag{2.3.7}$$

Then the action of flux operator can be formulated as

$$E_i(S)\Psi_\Gamma[A] = 8\pi\beta G\sum_{x\in S}\sum_{e\ni x}\frac{1}{2}\kappa(S,e)\widehat{J}_i^{(x,e)}\Psi_\Gamma[A]\,, \tag{2.3.8}$$

where the factor $\kappa(S,e)$ is defined as

$$\kappa(S,e) = \begin{cases} +1\,, & \text{if } e \text{ lies above } S\,, \\ -1\,, & \text{if } e \text{ lies below } S\,, \\ 0\,, & \text{if } e\cap S = \emptyset \text{ or } e \text{ lies in } S\,, \end{cases} \tag{2.3.9}$$

Since the surface S is oriented with normal n_a, "above" means $n_a \left(\frac{\partial}{\partial t}\right)^a |_x > 0$, and 'below' means $n_a \left(\frac{\partial}{\partial t}\right)^a |_x < 0$, where the $\left(\frac{\partial}{\partial t}\right)^a |_x$ is the tangent vector of e at x.

So Eq.(2.3.8) shows flux operators momentum operators and satisfying (2.3.6), i.e., forming $\mathfrak{su}(2)$ Lie algebra. In meanwhile, the holonomy is naturally viewed as the configuration variables as already known. An interesting question arises from the non-commutativity between the momentum operators since they are viewed as momentum variables and they Poisson bracket should have vanished at first glance. The answer is prescribed by noticing that flux operator is obtained by smearing on a surface instead of $3d$ region. One could think of flux as a $3d$ smearing if consider Gaussian constraint [93]

$$E(S,\Lambda) = \int_{\mathrm{Int}[S]} d_A \Lambda_i \wedge E^i \tag{2.3.10}$$

by some proper extension, where E^i_{ab} is the dual 2-form of vectorial E^a_i. Therefore the Poisson bracket between two fluxes is given by

$$\begin{aligned} & \big\{E(S,X)\,, E(S,Y)\big\} \\ = & \int_{\mathrm{Int}[S]} \int_{\mathrm{Int}[S]} \mathrm{d}^3x \mathrm{d}^3y \left\{ dX_i \wedge E^i + \epsilon_{ijk} A^j \wedge X^j \wedge E^k \,, dY_l \wedge E^l + \epsilon_{lmn} A^m \wedge Y^n \wedge E^n \right\} \\ = & -8\pi\beta G E(S,[X\,,Y])\,, \qquad \text{where} \quad [X\,,Y]_i = \epsilon_{ijk} X_j Y_k\,. \end{aligned} \tag{2.3.11}$$

This prescription provides an interpretation that flux is a kind of 'quasi-local' charge, or called 'gravitational edge mode' [45, 46, 47, 48, 49] arisen from the introduction of non-empty boundary.

2.4 Gauge-Invariant Hilbert Space: Spin Networks

We are now going to solve the quantum Gauss constraint. Given a cylindrical function Ψ_Γ, $\widehat{G}_i(\Lambda^i)$ acts as

$$\widehat{G}_i(\Lambda^i)\Psi_\Gamma[A] = 8\pi\beta G \sum_{v\in\Gamma} \sum_{e\ni v} \frac{1}{2} \Lambda^i(v) \widehat{J}_i^{(x,e)} \Psi_\Gamma[A]\,. \tag{2.4.1}$$

This operator is densely defined and essentially self-adjoint on $\mathcal{H}_{\mathrm{kin}}$. We can first look at the simplest case that the quantum Gauss constraint but defined locally at single node v, and only concern the arguments around the node. Suppose the node $v \in \Gamma$ with N incoming edges $(e_1\,, \cdots, e_N)$ carrying spins $(j_1\,, \cdots, j_N)$, and N' outgoing edges $(e'_1\,, \cdots, e'_{N'})$ carrying spins $(j'_1\,, \cdots, j'_{N'})$. According to the implementation (2.3.6), the quantum Gauss constraint equation $\widehat{G}^{(v)}_i(\Lambda^i)\Psi_v[A] = 0$ amounts to asking the solution for

$$\psi_v(g_{e'_1} e^{t\tau_i}\,, \cdots, g_{e'_{N'}} e^{t\tau_i}\,, e^{-t\tau_i} g_{e_1}\,, \cdots, e^{-t\tau_i} g_{e_N}) = \psi_v(g_{e'_1}\,, \cdots, g_{e'_{N'}}\,, g_{e_1}\,, \cdots, g_{e_N}) \tag{2.4.2}$$

for any value of parameter t, and $e^{-t\tau_i} \in \mathrm{SU}(2)$ could be generalized to arbitrary $h_v \in \mathrm{SU}(2)$. Let us express the gauge invariant transformation by $h_v \triangleright \psi_v$ hence above equation

is in fact $h_v \triangleright \psi_v = \psi_v$. Note that the invariance of Haar measure, which implies

$$\int_{\mathrm{SU}(2)} \mathrm{d}h_v \, \psi_v(h_v g_{e'_1}, \cdots, h_v g_{e'_{N'}}, g_{e_1} h_v^{-1}, \cdots, g_{e_N} h_v^{-1}) = \psi_v(g_{e'_1}, \cdots, g_{e'_{N'}}, g_{e_1}, \cdots, g_{e_N}) \,. \tag{2.4.3}$$

For instance, we suppose a trivalent node v with two incoming edges e_1, e_2 and one outgoing edge e_3. Then we take the basic cylindrical function in the form of Eq.(2.2.13),

$$D^{j_1}_{m_1 n_1}(g_{e_1}) D^{j_2}_{m_2 n_2}(g_{e_2}) D^{j_3}_{m_3 n_3}(g_{e_3}) \,. \tag{2.4.4}$$

The gauge invariant equation is then expressed as

$$\int_{\mathrm{SU}(2)} \mathrm{d}h_v \, D^{j_1}_{m_1 n_1}(h_v g_{e_1}) D^{j_2}_{m_2 n_2}(h_v g_{e_2}) D^{j_3}_{m_3 n_3}(g_{e_3} h_v^{-1}) = D^{j_1}_{m_1 n_1}(g_{e_1}) D^{j_2}_{m_2 n_2}(g_{e_2}) D^{j_3}_{m_3 n_3}(g_{e_3}) \,. \tag{2.4.5}$$

On the left-hand side, the group element h_v contained in every Wigner matrices can be extracted due to the group multiplication

$$D^{j_1}_{m_1 s_1}(h_v) D^{j_2}_{m_2 s_2}(h_v) D^{j_3}_{s_3 n_3}(h_v^{-1}) D^{j_1}_{s_1 n_1}(g_{e_1}) D^{j_2}_{s_2 n_2}(g_{e_2}) D^{j_3}_{m_3 s_3}(g_{e_3}) \,. \tag{2.4.6}$$

All the Wigner matrices with argument h_v turn out to be integrated into two Clebsch-Gordan coefficients

$$\int_{\mathrm{SU}(2)} \mathrm{d}h_v \, D^{j_1}_{m_1 s_1}(h_v) D^{j_2}_{m_2 s_2}(h_v) D^{j_3}_{s_3 n_3}(h_v^{-1}) = \frac{1}{2j_3 + 1} C^{j_1 j_2 j_3}_{m_1 m_2 n_3} C^{j_1 j_2 j_3}_{s_1 s_2 s_3} \,. \tag{2.4.7}$$

By using the following orthogonality for Clebsch-Gordan coefficients

$$\sum_{m_1 = -j_1}^{j_1} \sum_{m_2 = -j_1}^{j_2} C^{j_1 j_2 j_3}_{m_1 m_2 m_3} C^{j_1 j_2 k_3}_{m_1 m_2 n_3} = \delta_{j_3 k_3} \delta_{m_3 n_3} \tag{2.4.8}$$

we solve the basic cylindrical function (2.4.5) for the vertex v with the two incoming edges and one outgoing edge as

$$\sum_{m_1, m_2, n_3} C^{j_1 j_2 j_3}_{m_1 m_2 n_3} D^{j_1}_{m_1 n_1}(g_{e_1}) D^{j_2}_{m_2 n_2}(g_{e_2}) D^{j_3}_{m_3 n_3}(g_{e_3}) \,, \tag{2.4.9}$$

whose gauge invariance can be verified straightforwardly.

The key to solve the quantum Gauss constraint equation is to solve the tensor $\mathcal{R}_v$ defined in Eq.(2.2.15) and Eq.(2.2.16). Now we denote I_v the gauge invariant solutions distinguished from arbitrary tensor $\mathcal{R}_v$. Let us focus on the cylindrical function at node v which amounts to considering a single node graph associated with tensor I_v,

$$\left[f_{v,\{j_e\},I_v}\right]^{m_{e'_1} \cdots m_{e'_{N'}}}_{n_{e_1} \cdots n_{e_N}} (g_1, \cdots, g_E) = [I_v]^{n_{e'_1} \cdots n_{e'_{N'}}}_{m_{e_1} \cdots m_{e_N}} \left(\prod_{e \ni v} \sqrt{d_{j_e}} D^{j_e}_{m_e n_e}(g_e) \right) \,. \tag{2.4.10}$$

A gauge transformation local at node v transforms the function in this way:

$$\begin{aligned}
&\left[f_{v,\{j_e\},I_v}\right]^{m_{e'_1}\cdots m_{e'_{N'}}}_{n_{e_1}\cdots n_{e_N}}\left(\left\{g_e\, h_v^{-1}\right\}_{s(e)=v}, \left\{h_v\, g_{\widetilde{e}}\right\}_{t(\widetilde{e})=v}\right)\\
= \;& [I_v]^{n_{e'_1}\cdots n_{e'_{N'}}}_{m_{e_1}\cdots m_{e_N}}\, D^{j_{e'_1}}_{p_{e'_1}n_{e'_1}}(h_v^{-1})\cdots D^{j_{e'_{N'}}}_{p_{e'_{N'}}n_{e'_{N'}}}(h_v^{-1}) D^{j_{e_1}}_{m_{e_1}p_{e_1}}(h_v)\cdots D^{j_{e_N}}_{m_{e_N}p_{e_1}}(h_v)\\
& \prod_{s(e)=v}\sqrt{d_{j_e}}\, D^{j_e}_{m_e p_e}(g_e)\prod_{t(\widetilde{e})=v}\sqrt{d_{j_{\widetilde{e}}}} D^{j_{\widetilde{e}}}_{p_{\widetilde{e}}n_{\widetilde{e}}}(g_{\widetilde{e}})\,.
\end{aligned} \tag{2.4.11}$$

Then the requirement of gauge invariance implies the equation

$$[I_v]^{p_{e'_1}\cdots p_{e'_{N'}}}_{p_{e_1}\cdots p_{e_N}} = [I_v]^{n_{e'_1}\cdots n_{e'_{N'}}}_{m_{e_1}\cdots m_{e_N}}\, D^{j_{e'_1}}_{p_{e'_1}n_{e'_1}}(h_v^{-1})\cdots D^{j_{e'_{N'}}}_{p_{e'_{N'}}n_{e'_{N'}}}(h_v^{-1}) D^{j_{e_1}}_{m_{e_1}p_{e_1}}(h_v)\cdots D^{j_{e_N}}_{m_{e_N}p_{e_N}}(h_v)\,, \tag{2.4.12}$$

which is rewritten further via multiplying the number of inward many respect $D(h_v)$ from left on both sides

$$D^{j_{e'_1}}_{n_{e'_1}p_{e'_1}}(h_v)\cdots D^{j_{e'_{N'}}}_{n_{e'_{N'}}p_{e'_{N'}}}(h_v)\,[I_v]^{p_{e'_1}\cdots p_{e'_{N'}}}_{p_{e_1}\cdots p_{e_N}} = [I_v]^{n_{e'_1}\cdots n_{e'_{N'}}}_{m_{e_1}\cdots m_{e_N}}\, D^{j_{e_1}}_{m_{e_1}p_{e_1}}(h_v)\cdots D^{j_{e_N}}_{m_{e_N}p_{e_N}}(h_v)\,. \tag{2.4.13}$$

Note that I_v is a linear map as stated in Eq.(2.2.15), i.e. sending N many of inward representations to N' many of outward representations, since the Wigner matrices on both sides form two tensor representations for h_v, Eq.(2.4.13) is essential the definition of intertwining map (or called equivariant) in the language of representation theory

$$h_v\, I_v = I_v\, h_v\,, \qquad \forall\, h_v \in G\,. \tag{2.4.14}$$

The intertwining map satisfies the commutativity is the so-called intertwiner, defining a map

$$I_v : \mathcal{H}_{j_1}\otimes\cdots\otimes\mathcal{H}_{j_N} \longrightarrow \mathcal{H}_{j'_1}\otimes\cdots\mathcal{H}_{j'_{N'}} \tag{2.4.15}$$

commutative between group actions (gauge transformations) and representation transformations. It is free to make the intertwining map as

$$I_v : \mathcal{H}^*_{j_1}\otimes\cdots\otimes\mathcal{H}^*_{j_N}\otimes\mathcal{H}_{j'_1}\otimes\cdots\mathcal{H}_{j'_{N'}} \longrightarrow \mathbb{C}\,, \tag{2.4.16}$$

All intertwines form a SU(2)-invariant space with respect to spins $\{j_e\}_{e\ni v}$

$$\mathcal{H}_{v,\{j_e\}} = \mathrm{Inv}_{\mathrm{SU}(2)}\left[\left(\bigotimes_{s(e)=v}\mathcal{H}_{j_e}\right)\otimes\left(\bigotimes_{t(\widetilde{e})=v}\mathcal{H}^*_{j_{\widetilde{e}}}\right)\right], \tag{2.4.17}$$

and one can allow the spins to be superposed thus define SU(2)-invariant space associated to node v

$$\mathcal{H}_v = \mathrm{Inv}_{\mathrm{SU}(2)}\left[\left(\bigotimes_{s(e)=v}\mathcal{H}_e\right)\otimes\left(\bigotimes_{t(\widetilde{e})=v}\mathcal{H}^*_{\widetilde{e}}\right)\right]. \tag{2.4.18}$$

Moreover, since $\mathbb{C}$ is the trivial representation of SU(2) corresponding to singlet (spin-0 state), one can understand an intertwining map (2.4.16) as a spin-coupling that couples spins $\{j_e\}$ into singlet, or equivalently, interpret intertwining map (2.4.15) as recoupling between spins systems $\{j_e\}_{t(e)=v}$ and $\{j_e\}_{s(e)=v}$.

In general, there are degeneracies in the program of spin-couplings. As Eq.(2.4.16), the input is a reducible tensor product of representations so it allows gauge-invariant subspaces. In the language of spin-coupling, given three spins, say $\{j_1, j_2, j_3\}$, one can couple the first of two spins, then the total spin j_{12} should be bounded by triangle condition $|j_1 - j_2| \leq j_{12} \leq j_1 + j_2$. The next step is to couple j_{12} to the third spin j_3. In order to obtain a singlet, j_{12} has to be j_3. In the case of coupling three spins, there is no degeneracy. While in the cases of coupling four or more spins, there are indeed degeneracy because one can couple j_1, j_2 to j_{12} and j_3, j_4 to j_{34}, then singlet requires $j_{12} = j_{34}$. The only restriction on the value of j_{12} is due to two triangle conditions, i.e. $\max\{|j_1 - j_2|, |j_3 - j_4|\} \leq j_{12} \leq \min\{j_1 + j_2, j_3 + j_4\}$. This four spins coupling corresponds to a four-valent node, so we say the degeneracy results from the high valency (higher than 4) of a node.

It may be useful to present how to obtain the expression of an intertwiner associated with a higher valency node. Let $|j_e, m_e\rangle \in \mathcal{H}_{j_e}$ be the usual SU(2) representation for the edge. The basis $|I_v\rangle$ of intertwiner space can be given in terms of Clebsch–Gordan recoupling,

$$\left|\{j_e\}_{e\ni v}, I_v^{(\{j_e\}_{e\ni v})}\right\rangle = \sum_{m_e=-j_e}^{j_e} \begin{pmatrix} j_{e_1} & j_{e_2} & \cdots & j_{e_n} \\ m_{e_1} & m_{e_2} & \cdots & m_{e_n} \end{pmatrix}^{(I)} \bigotimes_{e\ni v} |j_e, m_e\rangle\,, \quad (2.4.19)$$

where I stands for the alleviation $I \equiv (j_{12}\,, j_{123}\,, \cdots, j_{1\cdots(n-2)})$, and

$$\begin{aligned} &\begin{pmatrix} j_{e_1} & j_{e_2} & \cdots & j_{e_n} \\ m_{e_1} & m_{e_2} & \cdots & m_{e_n} \end{pmatrix}^{(I)} \\ := &\sum_{m_{12}=-j_{12}}^{j_{12}} \cdots \sum_{m_{1\cdots(n-2)}=-j_{1\cdots(n-2)}}^{j_{1\cdots(n-2)}} \begin{pmatrix} j_{e_1} & j_{e_2} & j_{12} \\ m_{e_1} & m_{e_2} & -m_{12} \end{pmatrix} (-1)^{2j_{12}-m_{12}} \\ &\sqrt{2j_{12}+1} \begin{pmatrix} j_{12} & j_{e_3} & j_{123} \\ m_{12} & m_{e_3} & -m_{123} \end{pmatrix} \cdots (-1)^{2j_{1\cdots(n-2)}-m_{1\cdots(n-2)}} \\ &\sqrt{2j_{1\cdots(n-2)}+1} \begin{pmatrix} j_{1\cdots(n-2)} & j_{e_{n-1}} & j_{e_n} \\ m_{1\cdots(n-2)} & m_{e_{n-1}} & m_{e_n} \end{pmatrix}\,, \end{aligned} \quad (2.4.20)$$

where we use Wigner $3j$-symbols to express the recoupling. The simplest cases are bivalent and trivalent intertwiner, both of which is unique when spins are given. For higher valent intertwiner, extra indices are required, here we simply denote them by I, which is actually a series of recoupling spins $j_{12}\,, \cdots, j_{1\cdots(n-2)}$ labeled by intermediate spins (internal, or invisible spins) via unfolding intertwiner in terms of trivalent tree intertwiners, e.g., fig.2.1b.

Following the logic, one is able to solve the quantum Gauss constraint via associating each node v an intertwiner, which defines a spin network state. We can understand a

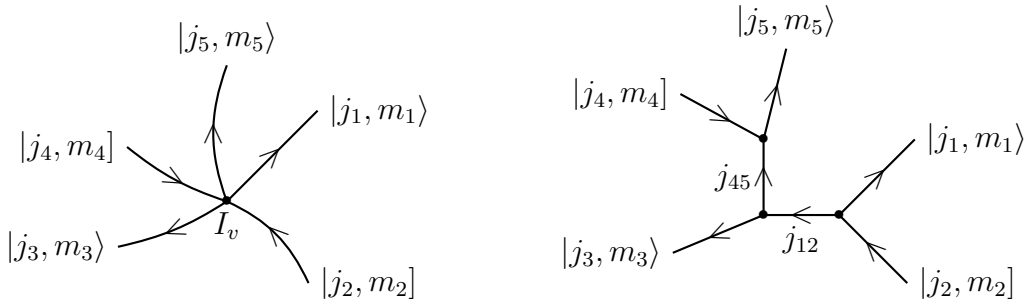

(a) An five-valent intertwiner I_v at vertex v. (b) Unfolding the five-valent intertwiner with trivalent virtual vertices.

Figure 2.1: The notation for a higher valent intertwiner I_v in terms of virtual spins.

spin network as being obtained via gluing intertwiners as illustrated in Fig.2.2 where each intertwiner is viewed as an open spin spin network with single node for the building block of the larger spin network. In particular, a spin network basis state is a spin network state with given spins at every edges and intertwiners at every nodes, i.e. no superposition with respect to spins or intertwiners. More explicitly, a spin network basis state has the form of

$$\psi_{\Gamma,\{j_e\},\{I_v\}}(\{g_{e_i}\}_{e_i\in\Gamma}) = \left(\prod_{v\in\Gamma} I_v\right)\cdot\left(\prod_{e\in\Gamma}\sqrt{d_{j_e}}D^{j_e}_{m_e n_e}(g_e)\right) . \tag{2.4.21}$$

Moreover, the orthogonality between spin network basis states is expressed as

$$\langle\Psi_{\Gamma,\{j_e,I_v\}}|\Psi'_{\Gamma',\{j'_{e'},I'_{v'}\}}\rangle = \delta_{\Gamma,\Gamma'}\delta_{\{j_e\},\{j'_e\}}\delta_{\{I_v\},\{I'_v\}} . \tag{2.4.22}$$

Equivalently, we can also understand that the solution is obtained by gluing the solutions at every individual node by putting holonomies along the interfacing edges. That is, we are going to form a larger spin network by gluing open spin networks -spin network with one node.

2.5 Diffeomorphism Constraint: Abstract Spin Networks

From now on, we note an embedded spin network basis given by the triple $(\Gamma, \{j_e, I_v\})$. It defines a quantum state $|\Gamma, \{j_e, I_v\}\rangle$, represented in terms of the connection by a functional, a spin network state $\Psi_\Gamma[A]$ such that $\psi_\Gamma[A]$ is in $\mathcal{H}^G_{\text{kin}}$, i.e. $\widehat{G}_i\psi_\Gamma[A] = 0$. The next step is to implement the spatial diffeomorphisms, namely $\widehat{V}^a\psi_\Gamma[A] = 0$, constructing $\mathcal{H}_{\text{Diff}}$.

The imposition of the diffeomorphism constraint is a crucial step in the quantization program of loop quantum gravity, since it is at this point that the essential requirement of background independence becomes fully introduced into the formalism. At the technical level, although the process of solving the diffeomorphism constraint contains a couple

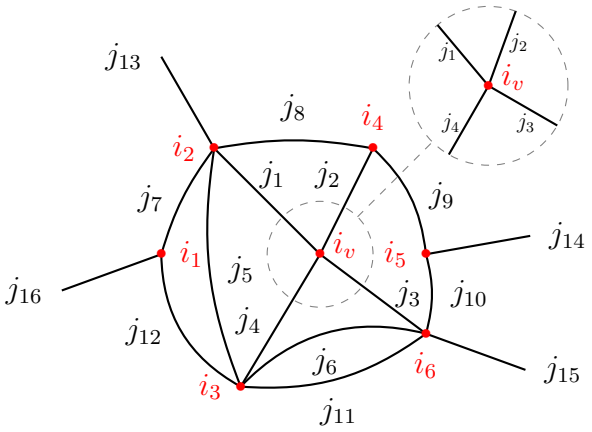

Figure 2.2: A spin network is obtained via gluing intertwiners where each intertwiner is a building block for the spin network.

of complications which were absent in the case of the Gauss constraint, an analogous technique to group averaging — the one used to obtained $\mathcal{H}^G_{\text{kin}}$ can be applied. However, one should bear in mind that the diffeomorphism invariant states are not contained in the original $\mathcal{H}_{\text{kin}}$. They have to be regarded as distribution states.

Let us break the issue down. We first clarify the diffeomorphism operations. Let Γ be any graph, there are three classes of diffeomorphism operations on Γ:

1. The trivial diffeomorphism operations $\mathcal{T}_\Gamma$ that do not change the graph at all (including the orientations of edges). For instance, a re-parameterization of an edge.

2. The slight diffeomorphism operations $\mathcal{D}_\Gamma$ but still mapping Γ into Γ. For instance, reversing the orientation of an edge.

3. The diffeomorphism operations $\text{Diff}/\mathcal{D}_\Gamma$ preserving the relations between edges and vertices. For instance, moving the graph around in Σ.

The first complication is that, due to the nature of the scalar product on the kinematical Hilbert space, the infinitesimal generator of diffeomorphisms does not exist as a well-defined operator on $\mathcal{H}_{\text{kin}}$. If the infinitesimal generator did exist, it could be extracted from the operator of diffeomorphisms by considering a limit of the kind

$$\lim_{\epsilon\to 0} \frac{\widehat{U}(\varphi_\epsilon)|\Psi_\Gamma\rangle - |\Psi_\Gamma\rangle}{\epsilon}\,. \tag{2.5.1}$$

However, this limit does not exist in general, because the states $U(\varphi_\epsilon)|\Psi_\Gamma\rangle$ and $|\Psi_\Gamma\rangle$ are orthogonal to each other if the diffeomorphism φ_ϵ moves the graph Γ even by an infinitesimally small amount. For this reason it is not possible to solve the diffeomorphism constraint by constructing a constraint operator on $\mathcal{H}_{\text{kin}}$ and looking for the states which are annihilated by the operator. Instead, the diffeomorphism invariant states must be sought by using an appropriately constructed group averaging procedure.

The other difficulty is that since diffeomorphisms act on the graph of a cylindrical function, the diffeomorphism invariant states cannot be proper, normalizable elements of the kinematical Hilbert space. In fact, the only diffeomorphism invariant element of $\mathcal{H}_{\rm kin}$ is the constant function (which can be viewed as a cylindrical function on a graph consisting of no edges and no nodes). Therefore non-trivial diffeomorphism invariant states should be searched for in the dual space Cyl* (i.e. the space of linear functionals on Cyl).

After these preliminary remarks, let us move on to the construction of the group averaging map. To get rid of infinity of $\mathcal{T}$, define the quotient group $\mathcal{D}_\Gamma/\mathcal{T}_\Gamma$. Then averaging of a cylindrical function Ψ_Γ with respect to the symmetries of the graph is achieved via projection operator P_Γ in the following way,

$$P_\Gamma|\Psi_\Gamma\rangle = \frac{1}{N_{\mathcal{D}_\Gamma/\mathcal{T}_\Gamma}} \sum_{\varphi\in\mathcal{D}_\Gamma/\mathcal{T}_\Gamma} U(\varphi)|\Psi_\Gamma\rangle\,, \tag{2.5.2}$$

where $N_{\mathcal{D}_\Gamma/\mathcal{T}_\Gamma}$ is the number of members in $\mathcal{D}_\Gamma/\mathcal{T}_\Gamma$.

It is remain to average the state with respect to diffeomorphisms belonging to Diff$/\mathcal{D}_\Gamma$, which move the graph around in the spatial manifold Σ (as illustrated in Fig.2.3). While Diff$/\mathcal{D}_\Gamma$ is an uncountably infinite group, so the result of the averaging will not be a proper cylindrical function, but only an element of Cyl*. Hence we define the averaging $P_{\rm Diff}$ with respect to diffeomorphism operations Diff$/\mathcal{D}_\Gamma$,

$$P_{\rm Diff}:{\rm Cyl}\longrightarrow{\rm Cyl}^*\,,\qquad P_{\rm Diff}\left[\Psi_\Gamma\right]=\sum_{\varphi\in{\rm Diff}/\mathcal{D}_\Gamma}\langle U(\varphi)P_\Gamma\Psi_\Gamma|\,,\qquad\forall\,\Psi_\Gamma\in\mathcal{H}_\Gamma\,. \tag{2.5.3}$$

This is an uncountable sum on the right-hand side, but it is a well-defined element of Cyl*, because when acting on a cylindrical function, only a finite number of terms in the sum will be non-vanishing, due to the graph orthogonality. Note that the operator $P_{\rm Diff}$ is very like a projector, but it is not a true projector, because $P_{\rm Diff}$ maps elements of Cyl into elements of Cyl*. The $P_{\rm Diff}$ is a so-called rigging map.

Along with the same logic as group averaging, it is straightforward to see

$$P_{\rm Diff}\left[U(\varphi)\Psi_\Gamma\right]=P_{\rm Diff}\left[\Psi_\Gamma\right]\,,\qquad\forall\,\varphi\in{\rm Diff}/\mathcal{D}_\Gamma\,. \tag{2.5.4}$$

On the other hand, even though the diffeomorphism invariant state are unnormalizable in the scalar product on $\mathcal{H}_{\rm kin}$, a nature scalar product on $\mathcal{H}_{\rm Diff}$ can be nevertheless defined by

$$\langle P_{\rm Diff}\left[\Psi_\Gamma\right]|P_{\rm Diff}\left[\Psi_{\Gamma'}\right]\rangle:=P_{\rm Diff}\left[\Psi_\Gamma\right]\left(|\Psi'_{\Gamma'}\rangle\right)\,, \tag{2.5.5}$$

where the right-hand side is defined by Eq.(2.5.3) and the scalar product on $\mathcal{H}_{\rm kin}$. The scalar product defined via Eq.(2.5.5) also leads to the definition of diffeomorphism invariant operators. Let $\mathcal{O}_{\rm kin}:\mathcal{H}_{\rm kin}\longrightarrow\mathcal{H}_{\rm kin}$ be any diffeomorphism invariant operator on $\mathcal{H}_{\rm kin}$. Analogous to the construction of intertwiner, it naturally defines a corresponding diffeomorphism invariant operator $\mathcal{O}_{\rm Diff}:\mathcal{H}_{\rm Diff}\longrightarrow\mathcal{H}_{\rm Diff}$ on $\mathcal{H}_{\rm Diff}$ via

$$\mathcal{O}_{\rm Diff}P_{\rm Diff}=P_{\rm Diff}\mathcal{O}_{\rm kin} \tag{2.5.6}$$

Figure 2.3: Diffeomorphism invariance in loop quantum gravity. The graph on right-hand side is obtained by moving the edges on left-hand side. Due to the diffeomorphism invariance, the two spin networks are gauge-equivalent with respect to $\mathcal{H}_{\text{Diff}}$.

in the spirit of Eq.(2.4.14) which means

$$\langle P_{\text{Diff}}[\Psi'_{\Gamma'}]|\mathcal{O}_{\text{Diff}}P_{\text{Diff}}[\Psi_\Gamma]\rangle = \langle P_{\text{Diff}}[\Psi'_{\Gamma'}]|P_{\text{Diff}}\mathcal{O}_{\text{kin}}[\Psi_\Gamma]\rangle = \left(P_{\text{Diff}}[\Psi'_{\Gamma'}]\right)\left(\mathcal{O}_{\text{kin}}|\Psi'_{\Gamma'}\rangle\right). \quad (2.5.7)$$

The definition is consistent with the scalar product on $\mathcal{H}_{\text{Diff}}$ in the sense that the operator O_{Diff} is self-adjoint with respect to $\mathcal{H}_{\text{Diff}}$ if O_{kin} is self-adjoint with respect to $\mathcal{H}_{\text{kin}}$.

It is accessible to apply the operation P_{Diff} to all cylindrical function for the sake of constructing the space of all diffeomorphism invariant cylindrical functionals, i.e. Cyl^*. The simultaneous solutions of the Gauss and diffeomorphism constraints are obtained by restricting the set of initial cylindrical functions to the gauge invariant subspace Cyl_G. Therefore the diffeomorphism invariant Hilbert space of loop quantum gravity is defined as

$$\mathcal{H}_{\text{Diff}} = P_{\text{Diff}}\left(\mathcal{H}^G_{\text{kin}}\right) = \overline{P_{\text{Diff}}\left(\text{Cyl}_G\right)}. \quad (2.5.8)$$

Solving the diffeomorphism constraint is the key step in realizing the crucial requirement of background independence in loop quantum gravity. Loosely speaking, one should think of a state in diffeomorphism invariant Hilbert space as a spin network based on an "abstract" graph, instead of a graph embedded in Σ. Each state has the form of Eq.(2.4.21) and is labeled by an equivalent class of graphs (abstract graph) under diffeomorphisms, which is not localized anywhere in Σ. There are still two points of view to look at the graph: one is the 'semi-abstract graph' perspective that still remains some diffeomorphism invariant information from the original embedded graph (such as the possible knottedness of the graph and the differential structure of the edges at each node), while another one is pure 'abstract graph' perspective that discards the notion of embedded graphs and considers algebraic graphs instead, underlying the foundation of algebraic quantum gravity (AQG) [94, 95, 96, 97]. In the framework of AQG, the graph is treated as an algebraic graph [98], which is simply a labeling set consisting of abstract points (vertices) together with information on how many abstract arrows (edges) point between points. There is no information about the knotting and braiding of those edges or about the location of the points.

The two different perspectives are both legitimate so far, but they diverge significantly when comes to Hamiltonian constraint.

2.6 The Hamiltonian Constraint

So far, the structure that gives the quantum states of the gravitational field at the kinematical level is, therefore, well understood. It then remains to consider the Hamiltonian constraint, which encodes the dynamics. The physical states of loop quantum gravity should lie in the kernel of the quantum Hamiltonian constraint operator. Although the traditional canonical point of view is to attempt to discretize, regularize and quantize the Hamiltonian constraints [99, 100], this often leads to anomalies. Besides, it turns out that there are many candidate constructions for the Hamiltonian constraint operator.

Laying aside these issues, we outline the program as the following three steps: (1) quantizing/constructing the Hamiltonian constraint operator; (2) implementing the quantum Hamiltonian on $\mathcal{H}_{\text{kin}}$; (3) solving the quantum Hamiltonian constraint operator. Additionally, one would check whether the solutions or evolutions admit suitable semi-classical limits, or whether it is anomaly-free or anomalous, etc. The dynamics topic, involved in the Hamiltonian constraint is rather big and is still an open question. Here I will only give a brief review.

As mentioned in the previous section, there are two inequivalent manners to define the implementation of the Hamiltonian constraint operator,

- Graph-changing. For instance, Thiemann's Hamiltonian [101, 99, 14] and Warsaw Hamiltonian [102, 103].
- Graph-preserving. For instance, algebraic quantum gravity (AQG) [94, 95, 96, 97].

In both manners, the Hamiltonian operator is constructed by summing the actions at every individual vertex

$$\widehat{H} = \sum_{v\in V(\Gamma)} \widehat{H}_v \,, \tag{2.6.1}$$

and it can be decomposed into the Euclidean part $\widehat{H}_v^E$ and Lorentzian part $\widehat{H}_v^L$,

$$\widehat{H}_v = \widehat{H}_v^E + \widehat{H}_v^L \,. \tag{2.6.2}$$

Precisely, the $\widehat{H}_v^E$ and $\widehat{H}_v^L$ should be symmetrized because of the requirement of hermiticity. Denote $\widehat{C}(N)$, the operator that is obtained via quantizing Hamiltonian constraint, which is non-hermitian in general. Thus, symmetrization would be necessary. If the adjoint operator $\widehat{C}^\dagger(N)$ is available, then a symmetric Hamiltonian could be constructed as $\frac{1}{2}\left(\widehat{C}(N)+\widehat{C}^\dagger(N)\right)$, or $\sqrt{\widehat{C}(N)^\dagger\widehat{C}(N)}$, or any other symmetric combination of $\widehat{C}(N)$ and its adjoint $\widehat{C}^\dagger(N)$. Moreover, in the cases of quantization in reduced phase space, e.g. gravitational field coupled with matter fields, the suitable symmetrization relies on some extra considerations [104]. For instance, if the gravitational field is coupled to scalar field, then symmetrization $\sqrt{\widehat{C}(N)^\dagger\widehat{C}(N)}$ could be adopted since the reduced Hamiltonian is necessary to be positive definite, while if the gravitational field is coupled to dust field, then symmetrization $\frac{1}{2}\left(\widehat{C}(N)+\widehat{C}^\dagger(N)\right)$ could be adopted since the reduced Hamiltonian can be positive or negative. The symmetrization issue should be considered in both graph-changing and graph-preserving manners.

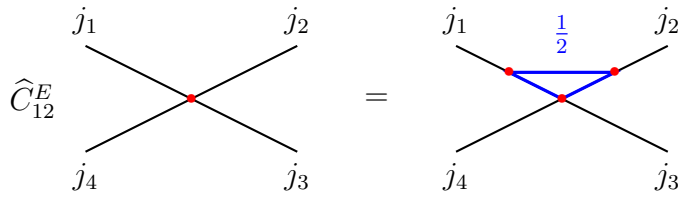

(a) The implementation of Thiemann Euclidean Hamiltonian constraint operator. The Ashtekar-Barbero curvature is represented by the loop holonomy along the path (blue).

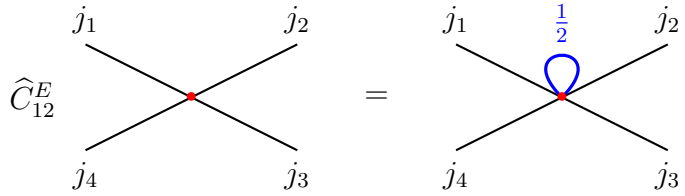

(b) The implementation of Warsaw Euclidean Hamiltonian constraint operator. The Ashtekar-Barbero curvature is represented by the loop holonomy along the loop (blue).

Figure 2.4: The implementations of graph-changing Euclidean Hamiltonian constraint operator.

In Thiemann's Hamiltonian, the Lorentzian part is quantized via alteration extrinsic curvature in terms of commutator

$$K = \frac{1}{\mathrm{i}\hbar}\left[\widehat{C}^E(1)\,,\widehat{V}\right]\,, \tag{2.6.3}$$

where $\widehat{C}^E(1)$ is the operator quantized from the Euclidean part with a fixed lapse function, and $\widehat{V}$ is the volume operator. While in Warsaw Hamiltonian, the Lorentzian part is quantized via $3d$ Regge calculus [105]. One of the remarkable differences is that the Lorentzian part of Thiemann's Hamiltonian changes the graph while the Warsaw Hamiltonian only acts on intertwiner space; hence it does not change the graph. The two programs correspond to semi-classical meanings in a different sense. The Thiemann proposal corresponds to the classical KK-term when one considers Thiemann's coherent state in cube graph. The Warsaw proposal corresponds to Regge calculus with respect to tetrahedron when one considers Livine-Speziale coherent state.

On the other hand, the Euclidean part of the Hamiltonian operator can be constructed as a graph-changing operator, both in Thiemann's Hamiltonian and Warsaw Hamiltonian. The two distinct constructions can be also constructed as a graph-preserving operator.

The reason of the graph-changing versus graph-preserving distinction for the Euclidean part construction, originates from the associative perspectives for the regularization of Ashtekar-Barbero curvature. We first look at the graph-changing manner. If the graph is somehow embedded in the manifold Σ, then the quantization requires some suitable regularization by which the Ashtekar-Barbero curvature could be defined. Loosely speaking, in order to quantize the curvature, one has to consider small loops attaching to

vertex at which the Ashtekar-Barbero curvature F^i_{ab} could be defined. The infinitesimal Ashtekar-Barbero connection A^i_a and its associative curvature F^i_{ab} are expressed in terms of discretized variables as following

$$g_e = 1_2 - \epsilon \dot{e}^a A^i_a \frac{\tau_i}{2} + O(\epsilon^2)\,, \qquad g_\alpha = 1_2 - \epsilon'^2 F^i_{ab} \dot{e}^a \dot{e}^b \frac{\tau_i}{2} + O(\epsilon'^3)\,, \tag{2.6.4}$$

where $\epsilon > 0$ and $\epsilon' > 0$ are respectively the coordinate sizes of a curve e and a closed loop α. The coordinate size will play the role of regulator in quantization: one first introduces a triangulation of the hypersurface Σ into tetrahedra, characterized by a coordinate size ϵ. In Thiemann's Hamiltonian, these loops are realized by adding so-called *extraordinary edges*, and a loop can be defined around a pair of edges at the vertex. In other words, the Euclidean part of Thiemann's Hamiltonian creates extraordinary edges thus changes the graph, as illustrated in Fig. 2.4a. In Warsaw Hamiltonian, the Euclidean part creates self-loop that is attached to vertex and is sandwiched between the pair of edges, as illustrated in Fig. 2.4b.

Along with the graph-changing manner, the last step in defining the operator is to take the limit of regulator $\epsilon \to 0$. The natural regularization of the constraint involves small loops that are attached to the vertices of a given graph which shrink towards the vertex as the regulator is removed. However, the shrinking process can be compensated for by a spatial diffeomorphism, and since the limit is taken in an operator topology that involves spatial diffeomorphism invariant states, the loops actually do not completely shrink to the vertex.

On the other hand, in graph-preserving manner, on a given algebraic graph, the Ashtekar-Barbero curvature is quantized only along the so-called minimal loops [106], where the curvature can be represented by loop holonomy operator. The regularization used in graph-changing manner is then fulfilled by the minimal loops, thus it is needless to create any new edge onto the graph.

As pointed out in [94], for graph-changing operators such as the Hamiltonian constraints, it turns out to be extremely difficult to define coherent (or semi-classical) states [107, 108, 109]. Graph-changing operators add degrees of freedom to the state on which they act, and the fluctuations of those are, therefore, no longer suppressed. In contrast, graph-preserving operators can be defined directly on the kinematical Hilbert space, thus still allowing the existing semi-classical tools for analysis. The graph-preserving Hamiltonian operator would be anomalous, but this problem can be cured by invoking the master constraint method [110, 111, 112, 113, 114].

A promising exploration of the loop quantum gravity's dynamics is to look for the covariant quantization. The Lagrangian formalism based on tetradic Palatini action (1.1.16) naturally evolved towards a path integral formulation. The resulting spin foam models, constructed from (extended) topological quantum field theories (TQFTs) with defects, define transition amplitudes for histories of spin networks [18, 19, 115, 20] (see [23, 24, 25] for reviews). The formalism then evolves in a third quantization, where so-called "group field theories" define non-perturbative sums over random spin network histories in a similar way to matrix model partition functions define sums over random 2d discrete surfaces [28, 116, 29] (see [30, 31, 33] for reviews).

The canonical loop quantum gravity is a quantum theory that follows Dirac's canonical quantization program. Its framework is basically well-established, even though the existing description is incomplete, in particular the aspects of Hamiltonian dynamics. In the later chapters, we will define spin networks as bulk-to-boundary maps, which are, more or less, motivated by the spin form approaches for the sake of tacking loop quantum gravity's dynamics. Moreover, we will define dual boundary Hilbert space comprising the set of bulk-boundary maps, equipping with the scalar product of spin networks, which is, again, more or less, motived by the definition of diffeomorphism invariant Hilbert space. In the context of entanglement, we will also study the action of holonomy operator, which is a basic building block for the quantum Hamiltonian constraint operator.

Chapter 3

Quantum Information Theory

The birth of quantum mechanics at the beginning of the 20th century has shaken many intuitions underlying classical physics. One of its most crucial aspects comes from the fact that quantum mechanical states induce, in general, probabilistic outcomes instead of definite outcomes. Besides this statistical aspect, the superposition principle and entanglement represent more counter-intuitive features of quantum theory than classical physics. With the recent rise of quantum information theory, topics in quantum foundations, such as non-locality, contextuality, and steering, found ways to challenge and advance information theory.

Our current understanding of quantum physics still needs to be completed because of the elusive quantum theory of gravitation. Historically, tentative explorations interfacing quantum information and gravity have been fruitful in exposing internal paradoxes in the standard modern physics framework based on quantum field theory and general relativity. The milestone observation and conjecture between black hole entropy and area questioned the degrees of freedom of gravitation [117, 118]. The surprising study on Rindler observer dug the link between reference frames, entanglement, and horizon [119]. The well-known information loss paradox [120] or the more recent firewall paradox relies [121] on quantum information and entanglement properties. In the quantum gravity community, from the AdS/CFT to the loop quantum gravity approaches, a major research program is to use entanglement to understand the quantum nature of space-time [122, 123], including Ryu-Takayanagi formula that links entanglement entropy and minimal area [124] by AdS/CFT, and the recent EP=EPR proposal [125] that tries to establish a link between wormhole geometry (Einstein-Rosen bridges) and entanglement properties between two regions (Einstein-Podolski-Rosen).

The goal is then to understand the notions of locality and relations between subsystems or reference frames and eventually to reconstruct the space-time as a manifestation of entanglement and correlations of fundamental degrees of freedom. Before embarking on the quantum theory of gravitation, we present a brief overview of quantum information theory containing the concepts that will be encountered later.

This chapter aims to introduce two crucial concepts in quantum information theory. Section 3.1 is dedicated to quantum entanglement, the cornerstone of quantum information theory. We begin the section with a rather general mathematical definition of

quantum entanglement. Then we introduce bipartite entanglement, the most well-studied type of entanglement in physics. Meanwhile, we also pay attention to the notion of purification, i.e., reconstructing the pure state from the mixed state by utilizing the notion of bipartite entanglement. In the following subsection, we go from bipartite entanglement to multipartite entanglement. This is a topic needed to be fully understood, and contains much richer structure than bipartite entanglement. The first section ends with introducing entanglement measures, i.e., the quantities that quantify the entanglement. This subsection starts with the axioms for entanglement measures. Again, this topic is still developing since different entanglement measures are generally inequivalent. We only introduce *geometric measure of entanglement* that quantifies pure state's multipartite entanglement, and *entanglement of formation* that quantifies mixed state's entanglement. Section 3.2.1 of this chapter aims to introduce the formalism of quantum operations, especially the corresponding Choi-Kraus theorem that states that any completely positive map can be realized by a set of Kraus operators. We start this section with classical operations, usually called stochastic processes. Then we give a few mathematical details to show that the convex linear maps (for the space of density operators) can be extended to linear maps (for the space of operators) naturally. This extension is the key to constructing Choi operators as seen immediately. We present a sketch for the proof of the Choi-Kraus theorem, to emphasize the connection between the notion of entanglement and completely positive maps. The second section ends with some examples of quantum operations.

3.1 Quantum Entanglement

In 1935, Einstein, Podolsky, and Rosen (EPR) presented their famous argument against the completeness of quantum mechanics [126]. In this argument, a two-particle state is considered, where one party can measure the position or momentum, and the correlations of the state allow one to predict the results of these measurements on the other party if the same type of measurement is performed there. The argument was considered a philosophical question rather than a physical one for a long time until Bell proposed his famous inequality – Bell inequality [127] based on the assumption that local hidden variables exist and a revised ideal experiment advocated by Bohm and Aharonov [128]. As most (or not) physicists expected, the subsequent experiments disproved Bell's inequality, thus sentencing the local hidden variables out.

From a purely mathematical perspective, the notion of entanglement is rooted in the language of quantum mechanics — it manifests the unfactorizability of quantum entangled states. Let $\mathcal{H}$ be Hilbert space composed of subsystems whose Hilbert spaces are $\mathcal{H}_i$ respectively, i.e.,

$$\mathcal{H} = \bigotimes_i \mathcal{H}_i \,, \tag{3.1.1}$$

then a state ψ is entangled if it can not be factorized with respect to Hilbert spaces of subsystems, i.e.,

$$|\psi\rangle \neq \bigotimes_i |\psi_i\rangle \,. \qquad \forall\, |\psi_i\rangle \in \mathcal{H}_i \,. \tag{3.1.2}$$

A famous example of entangled state is the so-called Bell states for two qubits system. One of four Bell states is

$$\frac{|01\rangle + |10\rangle}{\sqrt{2}},$$

where $|0\rangle$ and $|1\rangle$ could stand for spin-up and spin-down state, respectively. The expression of the Bell state is just one possible decomposition. One can decompose the state along any axis, which implies the correlation between measurements done by Alice and Bob: if Alice measures the first qubit along a certain axis, then the second qubit after Alice's measurement must be along the same axis even though Bob could measure the qubit along other axes! Alice's measurement seems to be able to affect Bob's qubit remotely and instantaneously, which seems to be "spooky" from Einstein's viewpoint.

It should be pointed out that the distant intervention can not transform any instantaneous information according to the no-communication theorem [129].

3.1.1 Bipartite Entanglement and Purification

The most well-known and studied situation in the field of quantum entanglement is bipartite entanglement. The Bell state is the simplest case of bipartite entanglement. In general, a bipartite quantum system is defined as a Hilbert space $\mathcal{H} = \mathcal{H}_A \otimes \mathcal{H}_B$ whose subsystems are described by Hilbert space $\mathcal{H}_A$ and $\mathcal{H}_B$ respectively, in which any pure state is in the form of

$$|\psi\rangle = \sum_{i,j} \psi_{ij} |i_A\rangle \otimes |j_B\rangle \tag{3.1.3}$$

where $\{|i_A\rangle\}$ and $\{|i_B\rangle\}$ are orthonormal basis with respect to $\mathcal{H}_A$ and $\mathcal{H}_B$. Note that it is probable to have $\dim \mathcal{H}_A \neq \dim \mathcal{H}_B$. The correlated coefficients ψ_{ij} characterizes the state $|\psi\rangle$ in terms of a $\dim \mathcal{H}_A \times \dim \mathcal{H}_B$ matrix and thanks to the Schmidt decomposition, one is able to find two unitary matrices U, V such that $\psi_{ij} = \sqrt{p_k} U_{ik} \delta_{kl} V_{lj}$ with non-negative p_k and the $|\psi\rangle$ is rewritten into the form of

$$|\psi\rangle = \sum_k \sqrt{p_k} |\psi_A^k\rangle \otimes |\psi_B^k\rangle\,, \qquad \text{where} \quad |\psi_A^k\rangle = \sum_i U_{ik} |i_A\rangle\,, \quad |\psi_B^k\rangle = \sum_j V_{kj} |j_B\rangle\,. \tag{3.1.4}$$

The $\{|\psi_A^k\rangle\}$ and $\{|\psi_B^l\rangle\}$ are orthogonal basis as U, V are unitary matrices. Note that in this form the correlations between the two subsystems are fully displayed. For example, if $\mathcal{H}_A$ is found in the state $|\psi_A^k\rangle$, then the state of $\mathcal{H}_B$ is $|\psi_B^k\rangle$. The state $|\psi\rangle$ is unfactorized unless only one nonzero $p_i = 1$. The Schmidt rank is defined as the number of nonzero p_i. It is better to describe the entanglement with density matrix

$$\rho = \sum_{k,l} \sqrt{p_k p_l} |\psi_A^k\rangle\langle\psi_A^l| \otimes |\psi_B^k\rangle\langle\psi_B^l|\,. \tag{3.1.5}$$

The reduced density matrix ρ_A for $\mathcal{H}_A$ is induced via partial tracing over $\mathcal{H}_B$,

$$\rho_A = \mathrm{Tr}_B \rho = \sum_l \langle\psi_B^l|\rho|\psi_B^l\rangle = \sum_k p_k |\psi_A^k\rangle\langle\psi_A^k|\,. \tag{3.1.6}$$

The reduced density matrix is in general a mixed state, i.e. rank greater than 1. If $\mathcal{O}_A$ is any operator on $\mathcal{H}_A$, then then the corresponding operator on $\mathcal{H}$ is $\mathcal{O}_A \otimes \mathbb{I}_B$, and its expectation value can be worked out by reduced density matrix $\mathrm{Tr}\,(\rho_A \mathcal{O}_A)$. Furthermore, the partial trace is the unique operation which gives rise to the correct description of observables quantities for subsystems of a composite system [130].

In the formalism of density matrices, the factorizability of bipartite system is translated into the Schmidt rank, or equivalently, the rank of reduced density matrix. But note that reduced density matrix with rank greater than 1 is not sufficient to deduce the bipartite state entangled — the rank criterion only works for reduced density matrix induced from pure state. More general, a state ρ is a separable (unentangled) state if

$$\rho = \sum_k p_k \rho_A^k \otimes \rho_B^k \,, \qquad \text{where} \quad \sum_k p_k = 1 \,, \tag{3.1.7}$$

otherwise ρ is an entangled state.

Given any mixed state, it can be purified into pure state, meaning that the mixed state can be thought as the reduced density matrix of some pure state on certain bipartite system. To be precise, $\forall\, \rho_A \in \mathcal{H}_A$, which allows spectrum decomposition $\rho = \sum_i p_i |i_A\rangle\langle i_A|$, then one can take

$$|\psi_{AB}\rangle = \sum_i \sqrt{p_i} |i_A\rangle \otimes |i_B\rangle \,, \qquad \text{such that} \quad \rho_A = \mathrm{Tr}_B \left(|\psi_{AB}\rangle\langle\psi_{AB}| \right) . \tag{3.1.8}$$

In other words, we reconstruct a pure state from the mixed state. Note that the purification $|\psi_{AB}\rangle$ of a ρ_A is far from unique, even if the auxiliary system $\mathcal{H}_B$ is specified, say, it is free to implement a local unitary U with respect to $\mathcal{H}_B$ such that the $\big(U|i_B\rangle\big)$ are used to purify ρ_A.

The existence of purifications is a nice property of quantum mechanics that has no classical analog: the classical analog of a density matrix is a probability distribution, and there is no notion of purifying a probability distribution [130, 131].

3.1.2 Multipartite Entanglement

Multipartite entanglement has richer structure than bipartite entanglement. Indeed, only rarely multipartite pure states admit the generalized Schmidt decomposition. For instance in tripartite system, one may usually encounter

$$|\psi_{ABC}\rangle \neq (U_A \otimes U_B \otimes U_C) \sum_{i=1}^{d} \sqrt{\lambda_i} |i_A\rangle \otimes |i_B\rangle \otimes |i_C\rangle \,.$$

We take tripartite system as example for the sake of illustration. Let us first look at pure three-qubit states. A pure tripartite state is said to be *fully separable* if it is factorized with respect to the three subsystems, i.e., product state $|\psi^{\mathrm{fs}}\rangle = |\alpha_A\rangle \otimes |\beta\rangle_B \otimes |\gamma\rangle_C$. An entangled three-qubit state is said to be *biseparable*, denote as $|\psi^{\mathrm{bs}}\rangle$, if there is a bipartition in which the two subsystems are unentangled, e.g. $|\alpha_A\rangle \otimes |\delta\rangle_{BC}$ where $|\delta\rangle_{BC}$ is entangled. An entanglement is said to be *genuine tripartite entangled* if is neither full separable or biseparable. Similar to the case of bipartite entanglement, the classification can be generalized to mixed states [132, 133, 134]:

- fully separable: $\rho = \sum_i p_i |\psi_i^{\text{fs}}\rangle\langle\psi_i^{\text{fs}}|$.
- biseparable: $\rho = \sum_i p_i |\psi_i^{\text{bs}}\rangle\langle\psi_i^{\text{bs}}|$.
- genuine tripartite entangled: neither fully unentangled nor biseparable.

The genuine entangled three-qubit states can be further divided into two inequivalent classes, the so-called GHZ state and W state

$$|GHZ_3\rangle = \frac{1}{\sqrt{2}}(|000\rangle + |111\rangle)\,, \qquad |W_3\rangle = \frac{1}{\sqrt{3}}(|100\rangle + |010\rangle + |001\rangle)\,.$$

They can not be transformed into another by stochastic local operations and classical communication (SLOCC). The GHZ state is maximally entangled, while W state is more robust against partial trace [134], that is, if one partition is lost, say C, then reduced state $\text{Tr}_C(|W\rangle\langle W|)$ is separable, while $\text{Tr}_C(|W\rangle\langle W|)$ is still entangled.

For bipartite and multipartite entanglement, it is crucial to quantify how much entanglement is contained in a quantum state. Naturally, one may anticipate that the field of multipartite entanglement permits and has bred various and diverse probable entanglement measures to quantify the entanglement of multipartite states. In the next subsection we will have a closer look.

3.1.3 Entanglement Measures

For the purpose of reconstructing geometry from entanglement and correlations, a crucial question is to quantify the entanglement, especially in multipartite quantum system. The quantity that quantifies entanglement is called entanglement measure. In the case of pure bipartite state, reduced von Neumann entropy quantifies entanglement in a rather information-theoretic way. However, due to the failure of generalized Schmidt decomposition in most of cases of mixed states and multipartite states, the von Neumann entropy of reduced density matrix is not a suitable entanglement measure anymore, meanwhile it is far from unique to quantify entanglement unequivocally [1].

On the other hands, it has been approval that some features should be presented in an entanglement measure [137, 136, 138].

Definition 3.1 (Axioms of entanglement measures)**.** Any good entanglement measure E should, at least, satisfy the following criteria:

- (a) $\mathcal{E}(\rho) \geq 0$; (b) $\mathcal{E}(\rho) = 0$ if ρ is unentangled.
- Local unitary transformations do not change E. That is, for instance for any three-qubit state, the entanglement measure E has to satisfy

$$\mathcal{E}(\rho) = \mathcal{E}\left(U_A \otimes U_B \otimes U_C\, \rho\, U_A^\dagger \otimes U_B^\dagger \otimes U_C^\dagger\right)\,. \tag{3.1.9}$$

[1] It should be noted that the attempts for seeking superior entanglement measure, or asking whether superior entanglement measure exists, has been answered negatively from quantum resource theory [135]. From the perspective of quantum resource theory, entanglement is encoded as a partial-order relation in non-local resource, whereas each entanglement measure is a total-order relation defined by an entanglement monotone [136], thus it is expected that the apparent inequivalence exists.

- Monotonicity under local operation: If either of the parties sharing the pair in the state ρ performs the operation leading to state σ_i with probability p_i, then the expected entanglement cannot increase

$$\mathcal{E}(\rho) \geq \sum_i p_i \mathcal{E}(\sigma_i)\,. \tag{3.1.10}$$

- Convexity (monotonicity under discarding information), i.e.,

$$\sum_i p_i \mathcal{E}(\rho_i) \geq \mathcal{E}\left(\sum_i p_i \rho_i\right)\,. \tag{3.1.11}$$

Around the axioms for entanglement measure, there are many proposals proposed for quantifying the entanglement of mixed states and multipartite states. As expected, they are inequivalent at all. Still, a valid and universal entanglement measure is under exploration.

For the cases of multipartite entanglement, there are many measures to quantify the entanglement. We would like to introduce the *geometric measure of entanglement* (GME), or called geometric entanglement. The definition is based on the Hilbert-Schmidt norm on Hilbert space. For any Hilbert space $\mathcal{H}$, we denote $\{\phi\}$ the set of pure product states (unentangled states). Any product state is in the form of

$$|\phi\rangle = \bigotimes_i |\phi^{(i)}\rangle\,, \qquad \text{where} \quad |\phi^{(i)}\rangle = \sum_{\alpha_i} C^{(i)}_{\alpha_i} |e^{(i)}_{\alpha_i}\rangle\,, \tag{3.1.12}$$

where $\left\{|e^{(i)}_{\alpha_i}\rangle\right\}$ stands for the orthonormal basis associated with Hilbert space $\mathcal{H}_i$, and $C^{(i)}_{\alpha_i}$ are superposition coefficients for state $|\phi^{(i)}\rangle \in \mathcal{H}_i$. Then given any pure state $|\psi\rangle \in \mathcal{H}$, its distance to a product state $|\phi\rangle$ is given by

$$d = \||\psi\rangle - |\phi\rangle\| = \sqrt{2 - \langle\phi|\psi\rangle - \langle\psi|\phi\rangle}\,. \tag{3.1.13}$$

Thus the minimization amounts to maximizing $\langle\phi|\psi\rangle + \langle\psi|\phi\rangle$. One then applies variational method to solve the extreme values problem [139], under the constraints $\langle\phi^{(i)}|\phi^{(i)}\rangle = 1$. Then we obtain two equations as follow:

$$\left(\bigotimes_{j\neq i} \langle\phi^j|\right) |\psi\rangle = \Lambda |\phi^i\rangle\,, \qquad \text{and} \qquad \langle\psi| \left(\bigotimes_{j\neq i} |\phi^j\rangle\right) = \Lambda \langle\phi^i|\,. \tag{3.1.14}$$

The eigenvalue Λ is associated with the Lagrange multiplier enforcing the constraint $\langle\phi^{(i)}|\phi^{(i)}\rangle = 1$. It is clear that Λ is a real number bounded by $[-1, 1]$. Note that asking minimal distance $d_{\min}$ is equivalent to asking maximal Λ, i.e.,

$$\Lambda_{\max} = \max_{\phi} |\langle\phi|\psi\rangle|\,. \tag{3.1.15}$$

Eventually, the *geometric measure of entanglement* is defined as the logarithmic maximal projection [134]:

$$S_g(\psi) = -\ln \max_{\phi} |\langle\phi|\psi\rangle|^2 . \tag{3.1.16}$$

One may realize that the definition coincides with the Hilbert-Schmidt scalar product for density matrices, since

$$|\langle\phi|\psi\rangle|^2 = \mathrm{Tr}\left(\sigma^\dagger \rho\right) , \tag{3.1.17}$$

where $\sigma = |\phi\rangle\langle\phi|$ and $\rho = |\psi\rangle\langle\psi|$ are density matrices.

For the cases of mixed states, we would like to introduce the *entanglement of formation*. The notion is based on the fact that any mixed state is some ensemble of pure states, i.e.,

$$\forall\, \rho \in \mathcal{D}(\mathcal{H}) , \qquad \rho = \sum_n W_n |\psi_n\rangle\langle\psi_n| , \qquad |\psi_n\rangle \in \mathcal{H} , \tag{3.1.18}$$

where $\mathcal{D}(\mathcal{H})$ stands for the space of density operators associated with Hilbert space $\mathcal{H}$. The W_n is the probability distribution with respect to pure states $|\psi_n\rangle\langle\psi_n|$. While note that the decomposition is not unique, namely, there may be many ensembles corresponding to one mixed state. The essence is a minimization over all possible decompositions. The *entanglement of formation* is then defined as

$$E(\rho) = \min_{\{W_n, \psi_n\}} \left\{ \sum_n W_n\, E(|\psi_n\rangle\langle\psi_n|) \right\} , \tag{3.1.19}$$

where the subscript (W_n, ψ_n) under min presents the ensemble to be taken into account. That is to say, one decomposes a mixed state into pure states and then averages the entanglement measure of pure states, and the entanglement of formation is defined as the minimal average of entanglement measure among all possible decompositions. Here we didn't specify which entanglement measure is used on $|\psi_n\rangle\langle\psi_n|$. For the cases of bipartite system, it is nature to adopt reduced von Neumann entropy as the entanglement measure for pure states. For the cases of multipartite entanglement, the entanglement measure can be taken as geometric measure of entanglement S_g [139].

3.2 Mathematical Formalism of Quantum Operations

This section aims to introduce a prevalent framework in the field of quantum information theory — the mathematical formalism of quantum operations. The quantum operation formalism enables us to describe noisy quantum theory and open quantum system. It generalizes the unitary time evolution or symmetry transformations of isolated systems, providing a power set of tools handling the effects of measurement and transient interactions with an environment. Thus it nevertheless has something to do with our goal that aspires to put quantum gravity with non-empty boundaries into a rigorous mathematical framework.

In addition, quantum operation formalism is conventionally used by physicists to describe and address a wide range of physical scenarios, such as quantum Liouvillian equations (or called Lindbladian equations) [140], quantum process tomography, decoherence,

Einselection, and the quantum origins of the classical, quantum reference frames [141, 142], etc.

3.2.1 Classical Operations: Stochastic Process

The formalism of quantum operation is usually viewed as the quantum-mechanical generalization of classical stochastic process that allows a realization of discrete state changes [130]. Suppose a classical system described by states with label $\{n\}$ for which the corresponding probability distribution is described by respect $p(n)$ for the nth state. Then suppose a process $p_1(n) \to p_2(n) \to \cdots \to p_i(n) \to \cdots$ for the nth state where the $i = 1, 2, \cdots$ are adopted for labeling time instants.

We can collect all $p_i(m)$ at ith discrete instant to form a column vector $\vec{p}_i$. The probability distributions at ith and $(i+1)$th instants can be then related $\vec{p}_{i+1} = T^{(i)}\vec{p}_i$ by some matrix T of *transition probabilities* that presents the classical conditional probabilities $T^{(i)}_{nm} := p_i(n \,|\, m)$.

Obviously, the transition matrix M has to satisfies the following conditions $\forall\, i$:

$$\text{positivity:} \qquad T^{(i)}_{nm} \geq 0\,, \quad \forall\, i\,, \tag{3.2.1}$$

$$\text{completeness:} \qquad \sum_n T^{(i)}_{nm} = 1\,, \quad \forall\, i\,. \tag{3.2.2}$$

One could attribute the positivity to the conditional probability. If there were not this condition, the probability of some n for the next step of the process would probably have been negative. The second condition is the normalization of probability due to $\sum_n p_{i+1}(n) = 1$, defining a stochastic matrix. Thus the equation $\vec{p}_{i+1} = T^{(i)}\vec{p}_i$ defines a Markov process. The matrix T is also referred to as the *evolution matrix*, since it relates the probability distributions with respect to adjacent instants. Overall, the final state of the system is linearly related to the initial state.

3.2.2 Quantum Operations: Choi-Kraus Theorem and Kraus Operators

We now move to the concept of quantum operations for which an axiomatic approach is accessible. In order to formulate it, it is better to clarify the following extension from space of density operators to space of arbitrary operators: let $\mathcal{H}_A$ be the Hilbert space to be considered, then

- $\mathcal{D}(\mathcal{H}_A)$: the space of density operators acting on Hilbert space $\mathcal{H}_A$.
- $\mathcal{L}(\mathcal{H}_A)$: the space of square linear operators acting on Hilbert space $\mathcal{H}_A$.
- $\mathcal{L}(\mathcal{H}_A, \mathcal{H}_B)$: the space of linear operators taking a Hilbert space $\mathcal{H}_A$ to a Hilbert space $\mathcal{H}_B$.

Obviously, $\mathcal{D}(\mathcal{H}_A) \subset \mathcal{L}(\mathcal{H}_A)$. The word "quantum operations" is used for density operators, the square operator with three conditions: unit trace, Hermitian, positive semidefinite. But the notion of that quantum operation can be extended to $\mathcal{L}(\mathcal{H}_A)$ by exploiting the *convex linearity* [143] for quantum operations with respect to $\mathcal{D}(\mathcal{H}_A)$. Let $\mathcal{N}$

be any quantum operation with respect to $\mathcal{D}(\mathcal{H}_A)$, then the convex linearity is defined as

$$\mathcal{N}\Big(\lambda\rho+(1-\lambda)\sigma\Big)=\lambda\mathcal{N}_A(\rho)+(1-\lambda)\mathcal{N}_A(\sigma)\ ,\qquad \rho,\sigma\in\mathcal{D}(\mathcal{H}_A)\quad\text{and}\quad\lambda\in[0,1]\,. \tag{3.2.3}$$

Now we are going to promote the domain of $\widetilde{\mathcal{N}}$ from $\mathcal{D}(\mathcal{H}_A)$ to $\mathcal{L}(\mathcal{H}_A)$, which will also promotes the convex linearity to linearity. It turns out that these following rules are required

$$\widetilde{\mathcal{N}}(X_A) := \mathrm{Tr}(X_A)\mathcal{N}\left(\frac{X_A}{\mathrm{Tr}X_A}\right), \tag{3.2.4}$$

$$\widetilde{\mathcal{N}}(X_A) := \widetilde{\mathcal{N}}\left(X_A^+\right)-\widetilde{\mathcal{N}}\left(X_A^-\right), \tag{3.2.5}$$

$$\widetilde{\mathcal{N}}(X_A) := \widetilde{\mathcal{N}}\left(X_A^R\right)+\mathrm{i}\widetilde{\mathcal{N}}\left(X_A^I\right). \tag{3.2.6}$$

The Eq.(3.2.4) requirement works for non-unit trace operators. Indeed it is easy to check that $\widetilde{\mathcal{N}}(sX)=s\widetilde{\mathcal{N}}(X_A)$ for any scaling factor, meanwhile it promotes convex linearity to linearity. The Eq.(3.2.5) aims to extend the domain from positive semi-definite Hermitian to arbitrary Hermitian operator, where both X_A^+ and X_A^- are positive semi-definite Hermitian operator but all nonzero eigenvalues of X_A^- are negative eigenvalues of X_A. The Eq.(3.2.6) extends the domain from Hermitian operators to non-Hermitian operators, since any operator can be decomposed into the combination of two Hermitian operators, i.e. $X_A=X_A^R+\mathrm{i}X_A^I$ where $X_A^R=\frac{1}{2}\left(X_A+X_A^\dagger\right)$ and $X_A^I=\frac{1}{2\mathrm{i}}\left(X_A-X_A^\dagger\right)$.

Therefore, any convex linear map $\mathcal{N}$ for $\mathcal{D}(\mathcal{H}_A)$ can be extended to linear map $\widetilde{\mathcal{N}}$ for $\mathcal{L}(\mathcal{H}_A)$. From now on, we denote the extended linear map by $\mathcal{N}$ instead of $\widetilde{\mathcal{N}}$ for the sake of simplicity.

Quantum operations are defined as linear maps with *complete positivity*, namely, completely positive (CP) maps. We list the axioms for CP maps as follow:

Definition 3.2 (Linearity)**.** Map $\mathcal{N}:\mathcal{L}(\mathcal{H}_A)\longrightarrow\mathcal{L}(\mathcal{H}_B)$ is linear if

$$\mathcal{N}(\alpha X_A+\beta Y_A)=\alpha\mathcal{N}(X_A)+\beta\mathcal{N}(Y_A)\ ,\qquad \forall X_A,Y_A\in\mathcal{L}(\mathcal{H}_A)\ ,\quad\forall\alpha,\beta\in\mathbb{C}\,. \tag{3.2.7}$$

Definition 3.3 (Complete Positivity)**.** A linear map $\mathcal{N}:\mathcal{L}(\mathcal{H}_A)\to\mathcal{L}(\mathcal{H}_B)$ is said to be *positive* if $\mathcal{N}(X_A)$ is positive semi-definite for all positive semi-definite $X_A\in\mathcal{L}(\mathcal{H}_A)$. More restrictive, a linear map $\mathcal{N}:\mathcal{L}(\mathcal{H}_A)\to\mathcal{L}(\mathcal{H}_B)$ is *completely positive* if $\mathbb{I}_R\otimes\mathcal{N}$ is a positive map for an arbitrary reference system R.

It is worth to emphasize the notion of 'complete positivity'. The positivity is to ensure the positivity of density operators. But what about the positivity of any larger quantum system in which the original quantum system is a subsystem? A well-known counterexample for positive map but not completely positive map is presented as follow [130]: consider transpose operation on a single qubit,

$$\begin{pmatrix}a&b\\c&d\end{pmatrix}\overset{T}{\to}\begin{pmatrix}a&c\\b&d\end{pmatrix},$$

which is a linear, positive and trace preserving map. While it is not completely because for entangled state $\frac{|00\rangle+|11\rangle}{2}$, one has

$$\begin{pmatrix} 1 & 0 & 0 & 1 \\ 0 & 0 & 0 & 0 \\ 0 & 0 & 0 & 0 \\ 1 & 0 & 0 & 1 \end{pmatrix} \overset{\mathbb{I}_2 \otimes T}{\to} \begin{pmatrix} \begin{pmatrix} 1 & 0 \\ 0 & 0 \end{pmatrix}^T & \begin{pmatrix} 0 & 1 \\ 0 & 0 \end{pmatrix}^T \\ \begin{pmatrix} 0 & 0 \\ 1 & 0 \end{pmatrix}^T & \begin{pmatrix} 0 & 0 \\ 0 & 1 \end{pmatrix}^T \end{pmatrix} = \begin{pmatrix} 1 & 0 & 0 & 0 \\ 0 & 0 & 1 & 0 \\ 0 & 1 & 0 & 0 \\ 0 & 0 & 0 & 1 \end{pmatrix} .$$

The counterexample is then illustrated by the non-positivity of the matrix on the right-hand side.

Moreover, if a CP map is trace preserving, it is called *complete positivity trace preserving* (CPTP) map. The tracing preserving condition is usually taken into account due to the normalization for probability, unless some situations e.g. the statistic of outcomes is not complete, or the system to be studied is dissipative.

The extension allows to represent any completely positive map in terms of Kraus operators.

Definition 3.4 (Trace Preserving)**.** A linear map $\mathcal{M}$ is trace preserving if $\mathrm{Tr}\left(X_A\right) = \mathrm{Tr}\left(\mathcal{M}\left(X_A\right)\right)$, $\forall\, X_A \in \mathcal{L}\left(\mathcal{H}_A\right)$.

A CP map is a linear, completely positive map. A CPTP Map is a CP map with additional trace preserving condition.

Choi-Kraus theorem states that any linear completely positive map can be realized by some Kraus operators. To be precise, let $\mathcal{N} : \mathcal{L}\left(\mathcal{H}_A\right) \to \mathcal{L}\left(\mathcal{H}_B\right)$ be a CP map, then there exists a Choi-Kraus decomposition as follows [143]:

$$\mathcal{N}_{A\to B}\left(X_A\right) = \sum_{l=1}^{d} K_l\, X_A\, K_l^\dagger\,, \qquad V_l \in \mathcal{L}\left(\mathcal{H}_A\,, \mathcal{H}_B\right)\,, \quad d \leq \dim\left(\mathcal{H}_A\right)\dim\left(\mathcal{H}_B\right)\,, \tag{3.2.8}$$

$\forall\, X_A \in \mathcal{L}\left(\mathcal{H}_A\right)$. Moreover, if the map is a CPTP map, then the set of operators $\{\, K_l \mid l = 1, \cdots, d \,\}$ satisfies

$$\sum_{l=1}^{d} K_l^\dagger\, K_l = \mathbb{I}_A\,. \tag{3.2.9}$$

The proof of Choi-Kraus theorem can be achieved by essentially exploiting the notion of entanglement. Let us first sketch the proof in a short sentence before moving into more details:

- We construct a maximally entangled state on which the Choi operator with respect to CP map can be constructed. The Kraus representation with respect to the Choi operator is then induced from the projection and linearity [143].

Let $\left\{|i_A\rangle\right\}_{i=1}^{d_A}$ be an orthonormal basis for $\mathcal{H}_A$ where d_A the dimension of Hilbert space $\mathcal{H}_A$. Likewise, let $\left\{|i_R\rangle\right\}_{i=1}^{d_R}$ be an orthonormal basis for reference system R. Note that the reference system R is total arbitrary.

For any operator $X_A \in \mathcal{L}(\mathcal{H}_A)$, linear map $\mathcal{N}$ acts on it as following manner:

$$X_A = \sum_{i_A=1}^{d_A}\sum_{j_A=1}^{d_A} X_A^{i_A j_A}\,|i_A\rangle\langle j_A|\,, \qquad \mathcal{N}_{A\to B}(X_A) = \sum_{i_A=1}^{d_A}\sum_{j_A=1}^{d_A} X_A^{i_A j_A}\,\mathcal{N}_{A\to B}\left(|i_A\rangle\langle j_A|\right)\,. \tag{3.2.10}$$

One of key steps is to construct an unnormalized maximally entanglement state

$$|\Gamma_{RA}\rangle = \sum_{i=1}^{d_A} |i_R\rangle\otimes|i_A\rangle\,. \tag{3.2.11}$$

The map $\mathbb{I}_R\otimes\mathcal{N}_{A\to B}: \mathcal{H}_R\otimes\mathcal{H}_A \longrightarrow \mathcal{H}_R\otimes\mathcal{H}_B$ defines a so-called Choi operator [144]

$$\begin{aligned}(\mathbb{I}_R\otimes\mathcal{N}_{A\to B})\left(|\Gamma_{RA}\rangle\langle\Gamma_{RA}|\right) &= \sum_{i=1}^{d_A}\sum_{j=1}^{d_A}|i_R\rangle\langle j_R|\otimes\mathcal{N}_{A\to B}\left(|i_A\rangle\langle j_A|\right) &(3.2.12)\\ &= \sum_{l=1}^{d}|\psi_{RB}^l\rangle\langle\psi_{RB}^l|\,, &(3.2.13)\end{aligned}$$

from which the Kraus representation $\mathcal{N}_{A\to B}\left(|i_A\rangle\langle j_A|\right)$ is derived by projection

$$\mathcal{N}_{A\to B}\left(|i_A\rangle\langle j_A|\right) = \left(\langle i_R|\otimes\mathbb{I}_B\right)\Big[(\mathbb{I}_R\otimes\mathcal{N}_{A\to B})\left(|\Gamma_{RA}\rangle\langle\Gamma_{RA}|\right)\Big]\left(|j_R\rangle\otimes\mathbb{I}_B\right)\,. \tag{3.2.14}$$

This matrix completely describes the action of the map because it describes the action of it on every operator $|i_A\rangle\langle j_A|$, from which we can construct any other operator on which the map acts, due to the fact that $\mathcal{N}_{A\to B}$ is linear. Eventually, the Kraus operator is defined as

$$(K_l)_{A\to B}\,|i_A\rangle := \left(\langle i_R|\otimes\mathbb{I}_B\right)|\psi_{RB}^l\rangle = \sum_{m_B=1}^{d_B}\psi_{m_B,i}^l|m_B\rangle\,, \tag{3.2.15}$$

thus representing

$$\mathcal{N}_{A\to B}\left(|i_A\rangle\langle j_A|\right) = \sum_{l=1}^{d} K_l\,|i_A\rangle\langle j_A|\,K_l^\dagger\,, \tag{3.2.16}$$

and finally the Eq.(3.2.8) is proved.

Therefore, one is able to represent a given CP map via a set of Kraus operators. But note that the set of Kraus operators is not unique. However, it turns out that these different Kraus representations are equivalent up to unitary transformations. To be more precise, let $\{\,K_i \mid i=1,\cdots,d_m\,\}$ and $\{\,F_i \mid i=1,\cdots,d_n\,\}$ be sets of Kraus operators giving rise to quantum operations $\mathcal{N}_1$ and $\mathcal{N}_2$, respectively. By appending zero operators to the shorter list of operators such that $d_m = d_n$, then the following statement is true [130]: $\mathcal{N}_1 = \mathcal{N}_2$ if and only if $\exists\, U_{ij}$ such that

$$K_i = \sum_{j=1}^{d_m} U_{ij}\,F_j\,, \qquad \text{where} \quad \sum_{k=1}^{d_m} U_{ik}\,\overline{U_{jk}} = \delta_{ij}\,, \quad i,\,j=1,\cdots,d_m\,. \tag{3.2.17}$$

3.2.3 Examples of Quantum Operations

Let us look at some concrete examples of quantum operations. The first obvious and trivial example is the unitary transformation or unitary evolution, i.e. the state ρ is manipulated by a unitary operator U,

$$\rho \to U\rho U^{-1}\,. \tag{3.2.18}$$

The U is the single Kraus operator in this CPTP map. An interesting remark is to put a state ρ in $\mathcal{H}$ into a larger system $\mathcal{H}_R \otimes \mathcal{H}$, say if one initializes the extended system with the density matrix $\widetilde{\rho} = |1\rangle\langle 1| \otimes \rho$ in the extended Hilbert space where $|1\rangle$ is an arbitrary referent state, then $\rho' = \mathrm{Tr}_{\mathcal{H}_R}(U\widetilde{\rho}U^\dagger) = \sum_l K_l \rho K_l^\dagger$ is automatically expressed in terms of Choi-Kraus theorem, which illustrates why quantum operation formalism is vital in the topic of open quantum system.

Just formally, another well-known example is the notion of *general measurement*, which formalizes quantum measurements by a collection of $\{M_m\}$ of measure operators labeled with measurement outcomes m, satisfying completeness relation

$$\sum_m M_m^\dagger M_m = \mathbb{I}\,. \tag{3.2.19}$$

It is unnecessary to have $M_m = M_m^\dagger$ and $M_m M_{m'} = 0$ for any $m \neq m'$, otherwise the measurement is said to be a *projective measurement*. However, it should be very careful to view general measurement as a kind of quantum operation for the reason of "collapse of the quantum state". In other words, a post-measurement state with outcome m should be normalized as

$$\frac{M_m \rho M_m^\dagger}{\mathrm{Tr}\left(\rho M_m^\dagger M_m\right)}\,, \tag{3.2.20}$$

instead of summing all possible m. One can still define a quantum operation that would change quantum states in the manner of $\sum_m M_m \rho M_m^\dagger$ without the normalization but the result of the measurement is lost.

A slight different formalism of measurement is the *positive operator-valued measure* (POVM) where the set of measurement operators is $\{F_m\}$ satisfying $\sum_m F_m = 1$ and each F_m positive semi-definite, so one still has the chance to set $\sqrt{F_m}$ as Kraus operators.

In addition, as already mentioned, the Kraus representation can be used to prove the no-communication theorem [129].

The last example slightly departs the framework presented earlier. A G-twirling operation is defined as follow [141, 142]: Let G be a compact Lie group (if G is a finite group, the definition is to be revised slightly), and any state ρ in $\mathcal{H}$, then we define G-twirling operation as following

$$\mathcal{G}[\rho] := \int_G \mathrm{d}g\, T(g)\rho T^\dagger(g) \tag{3.2.21}$$

where $T(g)$ is a unitary representation of g on $\mathcal{H}$, and $\mathrm{d}g$ the Haar measure measure associated with G. Note that $\forall\, g \in \mathrm{SU}(2)$, $T^\dagger(g)T(g) = \mathbb{I}$, so it seems that summing over g will spoil the trace-preserving condition (3.2.9), but one can take into weight $\mathrm{d}g$ into

account and assign it to fulfill the unit-trace condition. For the same reason, if G is a finite group, one can assign $\frac{1}{|G|}$ as the normalized factor to fulfill the unit-trace condition. Due to the group-invariant property of Haar measure $\mathrm{d}g$, $\mathcal{G}[\rho]$ is a G-invariant state in the sense of $\mathcal{G}[\rho] = T(g)\mathcal{G}[\rho]T^{\dagger}(g)$ for any $g \in G$. Since we especially concern about the case $G = \mathrm{SU}(2)$, we will employ following lemma when comes to induced boundary density matrix [142].

Lemma 3.5. *A normalized* SU(2)*-invariant density matrix ρ has the following form:*

$$\rho = \bigoplus_J p(J)\frac{\mathbb{I}_{\mathcal{V}_J}}{2J+1} \otimes \rho_{\mathcal{N}_J}\,, \qquad \mathrm{Tr}\rho_{\mathcal{N}_J} = 1\,, \qquad \mathrm{Tr}\rho = \sum_J p(J) = 1\,. \tag{3.2.22}$$

The coefficients $p(J)$ define the probability distribution over the total spin J. The operator $\mathbb{I}_{\mathcal{V}_J} = \sum_{M=-J}^{J} |J,M\rangle\langle J,M|$ is the identity on $\mathcal{V}_J$ and $\rho_{\mathcal{N}_J}$ is an arbitrary density matrix in the multiplicity space $\mathcal{N}_J$.

Proof. It is always possible to decompose ρ into an ensemble of pure states $\{\psi_1, \psi_2 \cdots\}$

$$\rho = \sum_n W_n |\psi_n\rangle\langle\psi_n|\,, \tag{3.2.23}$$

where W_n is the probability with respect to $|\psi_n\rangle$. For every pure state $\psi_n \in \mathcal{H}$, it admits decomposition

$$|\psi_n\rangle = \sum_{J,M,I^{(J)}} C^{(n)}_{JMI^{(J)}} |J,M\rangle \otimes |J,I^{(J)}\rangle\,. \tag{3.2.24}$$

Here $C^{(n)}_{JMI^{(J)}}$ are the superposition coefficients, $I^{(J)}$ are multiplicity indices. The integration over SU(2) leads to

$$\int_G g\rho g^{-1}\,\mathrm{d}g = \sum_J \frac{\mathbb{I}_J}{2J+1} \otimes \left(\sum_n W_n \sum_M \sum_{I^{(J)},\widetilde{I}^{(J)}} C^{(n)}_{JMI^{(J)}} \overline{C^{(n)}_{JM\widetilde{I}^{(J)}}} |J,I^{(J)}\rangle\langle J,\widetilde{I}^{(J)}| \right)\,, \tag{3.2.25}$$

from which the probability distribution is defined as

$$p(J) = \sum_n W_n \sum_{M,I^{(J)}} |C^{(n)}_{J,M,I^{(J)}}|^2 \tag{3.2.26}$$

and the density matrix for the part of intertwiners as

$$\rho_{\mathcal{N}_J} = \frac{1}{p(J)} \sum_n W_n \sum_M \sum_{I^{(J)},\widetilde{I}^{(J)}} C^{(n)}_{JMI^{(J)}} \overline{C^{(n)}_{JM\widetilde{I}^{(J)}}} |J,I^{(J)}\rangle\langle J,\widetilde{I}^{(J)}|\,. \tag{3.2.27}$$

□

These examples are just a small part of the application of quantum operations and Kraus operators. Retaking the G-twirling operation, it actually defines a quantum reference frame by the randomness of the corresponding unitaries [141, 142]. Moreover, we can restrict the quantum operations on the quantum reference frame: they should preserve the G-invariance property. In this way, implementations such as dynamics are easier to be defined.

At the end of the day, we have looked the topics of entanglement and quantum operations. They are significant in the field of quantum information theory. We can not phrase too much on that, but we want to point out that the two topics relate to each other through the idea of purification that will be encountered in Chapter 6. Moreover, in Chapter 7 and Chapter 8, we will focus on exploring quantum entanglement in the context of loop quantum gravity. In a word, entanglement is the essential cornerstone of quantum information theory. By appealing to entanglement, the relation between Hilbert spaces is established in the sense of unfactorizability, thus providing the non-locality from the perspective of pure algebraic data. In the later chapters, we would like to reveal the manifestation of the connection of non-locality, boundaries, and entanglement.

Chapter 4

Two-body Entanglement in Newtonian Gravity

In this chapter, we look at the quantum theory of Newtonian gravity. Through the well-established but non-relativistic dynamics, we hope the presented study provides hints to future studies on gravitational entanglement in full dynamics of quantum gravity. We restrict ourselves to two-body entanglement, i.e., the bipartite entanglement of two particles, as a prototype for multipartite entanglement between many particles. Furthermore, we investigate how geometry gets reflected in entanglement and correlations.

This chapter starts with the well-known background for the two-body state under Newtonian potential in non-relativistic quantum mechanics. To study two-body entanglement, we present the reduced density matrix from a two-body pure state in subsection 4.2.1 Two-body entanglement depends on both the barycenter and interaction states. We then focus on the entanglement originating from the interaction state by setting the barycenter state as a plane wave. In subsection 4.2.2 we prove a simple relation (Result 4.3) between the dispersion (an entanglement quantifier), and eigen-energy. In subsection 4.3.1 we compute two-body entanglement entropy for particular eigenstates. In the following subsection 4.3.3 we present a discussion about interaction, geometry, and entanglement, from which we show that entanglement can reflect more geometric information, not only relative distance. This discussion motivates further exploration of entanglement-geometry reconstruction in the context of quantum gravity.

4.1 Quantum theory of Newtonian gravity

4.1.1 Two-body states

We start by remembering classical mechanics. Let (x, y, z) be a Cartesian coordinates system. We study two spinless particles A, B, which are coordinated by position vectors $\vec{r}_A \equiv (r_{Ax}, r_{Ay}, r_{Az})$ and $\vec{r}_B \equiv (r_{Bx}, r_{By}, r_{Bz})$, respectively. Correspondingly, $\vec{p}_A \equiv (p_{Ax}, p_{Ay}, p_{Az})$ and $\vec{p}_B \equiv (p_{Bx}, p_{By}, p_{Bz})$ stand for their conjugate momenta. The generalized position of the two-body system is then characterized by six parameters for $(\vec{r}_A, \vec{r}_B)$, and likewise, generalized momentum by $(\vec{p}_A, \vec{p}_B)$. The two-body Hamiltonian is

the sum of kinetic energies plus interaction potential. We only consider central potential which only depend on the distance between two particles, i.e., $V(|\vec{r}_A - \vec{r}_B|)$. So the two-body Hamiltonian is read

$$H = \frac{\vec{p}_A^2}{2m_A} + \frac{\vec{p}_B^2}{2m_B} + V(|\vec{r}_A - \vec{r}_B|)\,. \tag{4.1.1}$$

A more usual way to the study is to work with barycenter-relative coordinates, characterizing the two-body system with the following bijective and linear canonical transformation:

$$\begin{aligned} &\text{barycenter part:} \qquad \vec{R} = \frac{m_A\vec{r}_A + m_B\vec{r}_B}{m_A + m_B}\,, \qquad \vec{P} = \vec{p}_A + \vec{p}_B\,, \\ &\text{relative part:} \qquad \vec{r} = \vec{r}_A - \vec{r}_B\,, \qquad \vec{p} = \frac{m_B\vec{p}_A - m_A\vec{p}_B}{m_A + m_B}\,. \end{aligned} \quad , \tag{4.1.2}$$

where $\vec{R} \equiv (R_x, R_y, R_z)$, $\vec{r}$ are barycenter's position, relative position, respectively, and $\vec{P}$, $\vec{p}$ are barycenter's momentum, relative momentum, respectively. Under the transformation, we rewrite the two-body Hamiltonian as

$$H = \frac{\vec{P}^2}{2M} + \frac{\vec{p}^2}{2\mu} + V(r)\,, \qquad \text{with} \quad M = m_A + m_B\,,\ \mu = \frac{m_A m_B}{m_A + m_B}\,, \tag{4.1.3}$$

where M and μ are total mass and reduced mass of the two particles, respectively, and $r = \sqrt{\vec{r}\cdot\vec{r}} \in (0, \infty)$ is the radial distance. The barycenter only contributes kinematic energy to the two-body Hamiltonian, while relative part is viewed as a one-body Hamiltonian.

We then move to the quantization based on position representation that promotes $\vec{P}$, $\vec{p}$ to vectorial differential operators $-\mathrm{i}\hbar\nabla_{\vec{R}}$, $-\mathrm{i}\hbar\nabla_{\vec{r}}$, defining two-body Hamiltonian operator and Schrödinger equation as

$$\hat{H} = -\frac{\hbar^2}{2M}\nabla_{\vec{R}}^2 - \frac{\hbar^2}{2\mu}\nabla_{\vec{r}}^2 + V(r)\,, \qquad \hat{H}\Psi(\vec{R},\vec{r}) = E_{\mathrm{tol}}\Psi(\vec{R},\vec{r})\,. \tag{4.1.4}$$

The eigenstates $\Psi(\vec{R},\vec{r})$ associated to the Hamiltonian can be solved separately: the barycenter part is easily solved by plane waves, and relative part is to be solved as an one-body problem with reduced mass μ The eigenstate of Schrödinger equation is in the form of

$$\Psi_{\vec{P},Elm}(\vec{R},\vec{r}) = \phi_{\vec{P}}(\vec{R})\,\psi_{Elm}(\vec{r}) = \frac{1}{\sqrt{V_R}} e^{\frac{\mathrm{i}}{\hbar}\vec{P}\cdot\vec{R}}\, R_{El}(r)\, Y_{lm}(\theta,\varphi)\,. \tag{4.1.5}$$

The eigenstate is labeled by six numbers: three $\vec{P} = (P_x, P_y, P_z)$ for barycenter's momentum within continuous spectral, and three E, l, m for relative energy E, orbital angular momentum l, and azimuthal angular momentum m boundeed by $-l \le m \le l$. We denote the basic solution for relative part by $\psi_{Elm}(\vec{r})$, associated to (interaction) eigenenergy E. Moreover, due to the spherical symmetry of the central potential, we have $\psi_{Elm}(\vec{r}) = R_{El}(r)Y_{lm}(\theta,\varphi)$ where $Y_{lm}(\theta,\varphi)$ is spherical harmonic

$$Y_{lm}(\theta,\varphi) = (-1)^m \sqrt{\frac{(2l+1)}{4\pi}\frac{(l-m)!}{(l+m)!}}\, P_l^m(\cos\theta)\, e^{\mathrm{i}m\varphi} \tag{4.1.6}$$

with orbital angular momentum l and azimuthal angular momentum m in terms of polar angle $\theta \in [0, \pi)$ and azimuth angle $\varphi \in [0, 2\pi)$. The $P_l^m(\cos\theta)$ is associated Legendre polynomial. The solution $R_{nl}(r)$ of radial equation (4.1.10) depends on the form of central potential $V(r)$ and asymptotic behavior [145]. The next subsection will focus on the solutions under Coulomb potential.

Notice that plane wave is δ-normalization, but one could introduce the volume of position space

$$V_R = (2\pi\hbar)^3 \delta^{(3)}(\vec{P} - \vec{P}) \tag{4.1.7}$$

to tame the divergence [146, 147, 148]. The taming factor can be understood as the replacement in the manner of Eq.(8.32) in Page 180, [149]

$$\lim_{V_R \to \infty} \sum \frac{(2\pi\hbar)^3}{V_R} f(\vec{P}) = \int_{\mathbb{R}^3} f(\vec{P})\, \mathrm{d}^3\vec{P}\,. \tag{4.1.8}$$

The two-body wave function (4.1.5) is expressed in terms of coordinates $(\vec{R}, \vec{r})$. This expression naturally admits the substitution of variables Eq.(4.1.2). That is, for any wave function in terms of barycenter-relative coordinates $(\vec{R}, \vec{r})$, we can define the wave function in terms of two-body coordinates $(\vec{r}_A, \vec{r}_B)$ via evaluation,

$$\Psi_{AB}(\vec{r}_A, \vec{r}_B) := \Psi_{br}(\vec{R} = \frac{m_A\vec{r}_A + m_B\vec{r}_B}{m_A + m_B}, \vec{r} = \vec{r}_A - \vec{r}_B)\,. \tag{4.1.9}$$

This substitution will reveal the entanglement between the two particles. We will have a closer look in the section 4.2.

4.1.2 Solutions of bound states and SO(4) symmetry

This part offers a brief review of the solutions of Newtonian quantum gravity, which is described by an attractive Coulomb potential $V(r) = -b/r$ with constant $b = Gm_Am_B$. We need to solve the Schrödinger equation to obtain the solutions $R_{El}(r)$ for the relative part. Then due to the Eq.(4.2.11), we also need to know the Fourier transformation for these solutions $R_{El}(r)$, for the sake of having a diagonal reduced state. In fact, for the case of attractive Coulomb potential, the bound state solutions are the representations of SO(4).

We still start by looking at the position representation. The relative part is a one-body problem with reduced mass μ. Call (r, θ, φ) the spherical coordinates for relative position $\vec{r}$. Then the Schrödinger equation via variables separation $\psi_{nlm}(\vec{r}) = R_{nl}(r)\, Y_{lm}(\theta, \varphi)$ presents as follows:

$$\left[-\frac{\hbar^2}{2\mu}\left(\frac{\mathrm{d}^2}{\mathrm{d}r^2} + \frac{2}{r}\frac{\mathrm{d}}{\mathrm{d}r}\right) + \frac{\hbar^2\, l(l+1)}{2\mu\, r^2} - \frac{b}{r}\right] R_{nl}(r) = E_n R_{nl}(r)\,, \tag{4.1.10}$$

$$\Delta_{S^2}\, Y_{lm}(\theta, \varphi) = -l(l+1)\, Y_{lm}(\theta, \varphi)\,, \tag{4.1.11}$$

where Δ_{S^2} is Laplacian operator on S^2, solved by spherical harmonics (4.1.6). Azimuthal m is bounded by $-l \leq m \leq l$. The solution $R_{nl}(r)$ of radial equation (4.1.10) depends

on the asymptotic behavior [145]. The bound states are solved by Laguerre polynomial $L_\mu^\nu(x)$,

$$R_{nl}(r) = \sqrt{\Big(\frac{2}{na}\Big)^3 \frac{(n-l-1)!}{2n\cdot(n+l)!}}\, e^{-\frac{r}{na}} \Big(\frac{2r}{na}\Big)^l L_{n-l-1}^{2l+1}\Big(\frac{2r}{na}\Big)\,, \tag{4.1.12}$$

where $a = \frac{\hbar^2}{\mu b}$ is reduced Bohr radius with respect to reduced mass μ. The energy spectrum $E_n = -\frac{\mu b^2}{2n^2\hbar^2}$ is discrete with integers $n = 1, 2, \cdots$, called principal quantum numbers, which bounds the orbital quantum numbers l with $0 \le l \le n-1$.

The wave function $\psi_{nlm}(\vec{p})$ expressed in terms of momentum coordinates can be obtained via Fourier transformation for $\psi_{nlm}(\vec{r})$ up to a phase [150]:

$$\psi_{nlm}(\vec{p}) = \mathrm{i}^{l-m} 2^{2l+2} \sqrt{\frac{2n^4a^3}{\pi\hbar^3}} \sqrt{\frac{(n-l-1)!}{(n+l)!}}\, \frac{l!\, p^l p_0^{l+4}}{(p^2+p_0^2)^{l+2}}\, C_{n-l-1}^{l+1}\left(\frac{p^2-p_0^2}{p^2+p_0^2}\right) Y_{lm}(\theta,\varphi)\,, \tag{4.1.13}$$

where C_{n-l-1}^{l+1} is Gegenbauer polynomial of degree $n-l-1$, whose definition is presented as following.

Definition 4.1. A Gegenbauer polynomial C_a^ν of degree a (non-negative integer) with parameter $\nu > -1/2\,,\ \nu \neq 0$, is defined by

$$C_a^\nu(s) = \sum_{k=0}^{[\frac{a}{2}]} \frac{\Gamma(a+\nu-k)}{\Gamma(\nu)k!(a-2k)!}(2s)^{a-2k}\,. \tag{4.1.14}$$

It is convenient to define the normalized Gegenbauer polynomial $\tilde{C}_a^\nu(s)$ [151] associated to the measure $w_\nu(s)$,

$$\tilde{C}_a^\nu(s) = \sqrt{\frac{a!(a+\nu)\Gamma(2\nu)}{\nu\Gamma(a+2\nu)}} C_a^\nu(s)\,, \qquad w_\nu(s) = \frac{\Gamma(\nu+1)}{\sqrt{\pi}\Gamma(\nu+\frac{1}{2})}(1-s^2)^{\nu-\frac{1}{2}}\,, \tag{4.1.15}$$

where $0 \le a \in \mathbb{N}$, then the orthogonality is written as

$$\int_{-1}^{1} \tilde{C}_a^\nu(s)\, \tilde{C}_{a'}^\nu(s)\, w_\nu(s)\, \mathrm{d}s = \delta_{aa'}\,. \tag{4.1.16}$$

Remarkably, the solutions $\psi_{nlm}(\vec{p})$ for bound states, belong to the representations of SO(4), i.e., they can be expressed in terms of S^3-spherical harmonics through Fock's method [152]. This additional symmetry - from SO(3) to SO(4), is sometimes called accident symmetry, and it is due to the Laplace-Runge-Lenz vector, a constant of motion particularly given by Coulomb potential.

Fock's method can be extended to scattering solutions [153]. It turns out that the irreducible representation of SO(4, 2) spans the solution space, where SO(4, 1) irreducible representation spans the bound states (varying principal quantum number n), and SO(3, 2) irreducible representation spans scattering states. The SO(4) irreducible representation spans bound states with given binding energy - fixed principal number n.

Let $\mathbb{R}^4 = \mathbb{R}^3 \times \mathbb{R}$ where $\mathbb{R}^3$ is the momentum space, and $\mathbb{R}$ is defined by a unit vector $\vec{n}$ orthogonal to $\mathbb{R}^3$. Every bound state is labeled by 4-vector $(\vec{p}, p_0)$ where $p_0 = \sqrt{-2\mu E_n}$ is the fourth component, presenting binding energy E_n. Here we require n (energy) to be fixed. By means of stereographic projection, one defines a 4-dimensional unit dimensionless vector $\vec{w} = (\vec{u}, u_0)$ by

$$\vec{w} := \vec{u} + u_0\vec{n}\,, \qquad \vec{u} = \frac{2p_0}{p^2+p_0^2}\vec{p}, \qquad u_0 = \frac{p^2-p_0^2}{p^2+p_0^2}\,, \tag{4.1.17}$$

where $p = \sqrt{\vec{p}\cdot\vec{p}}$ the length of $\vec{p}$ and $\vec{w}\cdot\vec{w} := \vec{u}\cdot\vec{u} + u_0^2 = 1$. The unit vector $\vec{w}$ points toward $S^3 \subset \mathbb{R}^4$ from origin and is parameterized by angular coordinates on S^3:

$$\begin{cases} u_x = \frac{1}{p^2+p_0^2}(2p_0p_x) = \sin\alpha\sin\theta\cos\varphi\,, \\ u_y = \frac{1}{p^2+p_0^2}(2p_0p_y) = \sin\alpha\sin\theta\sin\varphi\,, \\ u_z = \frac{1}{p^2+p_0^2}(2p_0p_z) = \sin\alpha\cos\theta\,, \\ u_0 = \frac{1}{p^2+p_0^2}(p^2-p_0^2) = \cos\alpha\,. \end{cases} \tag{4.1.18}$$

Call $\mathrm{d}\Omega_{S^3}$ the measure of S^3, the relation between $\mathrm{d}\Omega_{S^3}$ and $\mathrm{d}^3\vec{p}$ is given by

$$\mathrm{d}\Omega_{S^3} = \sin^2\alpha\sin\theta\,\mathrm{d}\alpha\,\mathrm{d}\theta\,\mathrm{d}\varphi\,, \qquad \mathrm{d}^3\vec{p} = \frac{p_0^3}{(1-\cos\alpha)^3}\,\mathrm{d}\Omega_{S^3} = \frac{(p^2+p_0^2)^3}{8p_0^3}\,\mathrm{d}\Omega_{S^3}\,. \tag{4.1.19}$$

The solutions $\psi(\vec{p})$ are mapped onto wave functions $\widetilde{\psi}(\vec{w})$ on S^3 via the following transformation:

$$\widetilde{\psi}(\vec{w}) = \frac{1}{4}p_0^{-\frac{5}{2}}(p^2+p_0^2)^2\psi(\vec{p})\,, \qquad \psi(\vec{p}) = p_0^{-\frac{3}{2}}(1-\cos\alpha)^2\widetilde{\psi}(\vec{w})\,, \tag{4.1.20}$$

where the relation $\langle\hat{p}^2\rangle = p_0^2$ for Coulomb potential is used [152]. Let us decompose $\psi_{nlm}(\vec{p}) = F_{nl}(p)Y_{lm}(\theta,\varphi)$, then the corresponding $\widetilde{\psi}_{nlm}(\vec{w})$ can be also decomposed into the form

$$\widetilde{\psi}_{nlm}(\vec{w}) = \widetilde{F}_{nl}(\cos\alpha)Y_{lm}(\theta,\varphi)\,. \tag{4.1.21}$$

The coordinate α is supported in interval $[0,\pi]$. Denote $s = \cos\alpha$ bounded by interval $[-1,1]$. The $\widetilde{F}_{nl}$ can be factorized further: a polynomial part and weight function part. The wave function $\widetilde{\psi}(\vec{w})$ turns out to be a S^3-spherical harmonic, built up by Gegenbauer polynomials.

Fock's method shows that the solutions of Coulomb potential are S^3-spherical harmonics $Y_{nlm}(\vec{w})$ (cf. [151, 154]), i.e.,

$$\widetilde{\psi}_{nlm}(\vec{w}) = Y_{nlm}(\vec{w}) = \widetilde{F}_{nl}(\alpha)\,Y_{lm}(\theta,\varphi) \tag{4.1.22}$$

where both functions $\widetilde{F}_{nl}(s)$ and $Y_{lm}(\theta,\varphi)$ can be factorized into normalized Gegenbauer polynomials together with weight function:

$$\widetilde{F}_{nl}(s) = (1-s^2)^{-\frac{1}{4}}\tilde{C}^{l+1}_{n-l-1}(s)\sqrt{w_{l+1}(s)}\,, \tag{4.1.23}$$

$$Y_{lm}(\theta,\varphi)=\sqrt{\frac{1}{2\pi}}e^{\mathrm{i}m\varphi}\cdot\widetilde{C}^{|m|+\frac{1}{2}}_{l-|m|}(\cos\theta)\sqrt{w_{|m|+\frac{1}{2}}(\cos\theta)}\,. \tag{4.1.24}$$

The orthogonality is consistently checked as,

$$\int_0^\pi\overline{\widetilde{F}_{n'l'}(\cos\alpha)}\widetilde{F}_{nl}(\cos\alpha)\sin^2\alpha\,\mathrm{d}\alpha\int_0^\pi\sin\theta\,\mathrm{d}\theta\int_0^{2\pi}\overline{Y_{l'm'}(\theta,\varphi)}Y_{lm}(\theta,\varphi)\,\mathrm{d}\varphi=\delta_{n'n}\delta_{l'l}\delta_{m'm}\,. \tag{4.1.25}$$

To close this part, we have seen the representation of the bound state in momentum space, which gives the diagonal entries of the reduced state, and contains the information for two-body entanglement. Moreover, the SO(4) symmetry reveals a mathematical relation to loop quantum gravity, due to the well-known $\mathrm{SO}(4)\cong\mathrm{SU}(2)_L\times\mathrm{SU}(2)_R$.

4.2 Two-body entanglement in non-relativistic theory

4.2.1 Reduced state for two-body state

Bipartite entanglement is better to be characterized by the formulation of reduced density matrix, in which the entanglement entropy is defined by von Neumann entropy of reduced state. However, there are infinite eigenvalues, which would cause issues involving the volume factor. This subsection will suggest a prescription that emphasizes the difference between the entropies of states rather than the entropy of individual states.

Consider a pure two-body state Ψ. We can express it in terms of variables for $\mathcal{H}_{\mathrm{bcm}}\otimes\mathcal{H}_{\mathrm{rel}}$, for instance, $\Psi(\vec{R},\vec{r})$ in terms of position representation, but it is free to use momentum representation by means of Fourier transformation. Now the wave function admits bijective substitution $(\vec{R},\vec{r})\to(\vec{r}_A,\vec{r}_B)$ in the manner of Eq.(4.1.5), supported by Eq.(4.1.2). Now we view the barycenter coordinates $\vec{R}$ and $\vec{r}$, or two-body coordinates $\vec{r}_A$, $\vec{r}_B$ as the resemblance of matrix indices. That is, recalling a pure state density matrix, whose entry at mth row nth column can be expressed by $\rho_{mn}=v_m\overline{v_n}$, the pure state density matrix entry of two-body state, is expressed as

$$\rho_{br}(\vec{R},\vec{r};\vec{\tilde{R}},\vec{\tilde{r}})=\Psi_{br}(\vec{R},\vec{r})\overline{\Psi_{cr}(\vec{\tilde{R}},\vec{\tilde{r}})}=\Psi_{AB}(\vec{r}_A,\vec{r}_B)\overline{\Psi_{AB}(\vec{\tilde{r}}_A,\vec{\tilde{r}}_B)}=\rho_{AB}(\vec{r}_A,\vec{r}_B;\vec{\tilde{r}}_A,\vec{\tilde{r}}_B)\,, \tag{4.2.1}$$

where the variables without '$\sim$' over head are analogies to row indices, and the variables with '$\sim$' over head analogies to column indices. The second step is done by $(\vec{R},\vec{r})\to(\vec{r}_A,\vec{r}_B)$ and $(\vec{\tilde{R}},\vec{\tilde{r}})\to(\vec{\tilde{r}}_A,\vec{\tilde{r}}_B)$ with respect to Eq.(4.1.2). Overall, this $\Psi\overline{\Psi}$ is a continuous analogy to finite dimensional matrix, and the semicolon ';' in ρ is designed to separate the 'row' and 'column' indices. The reduced state ρ_A for $\mathcal{H}_A$ is then defined by partial trace over $\mathcal{H}_B$, that is, integrating $\vec{r}_B$ and $\vec{\tilde{r}}_B$ with delta function $\delta^{(3)}(\vec{r}_B-\vec{\tilde{r}}_B)$:

$$\rho_A(\vec{r}_A;\vec{\tilde{r}}_A) = \int_{\mathbb{R}^3}\rho_{AB}(\vec{r}_A,\vec{r}_B;\vec{\tilde{r}}_A,\vec{\tilde{r}}_B)\mathrm{d}^3r_B=\int_{\mathbb{R}^3}\Psi_{br}(\vec{R},\vec{r})\,\overline{\Psi_{br}(\vec{\tilde{R}},\vec{\tilde{r}})}\mathrm{d}^3r_B \tag{4.2.2}$$

$$= \int_{\mathbb{R}^3}\Psi_{br}\Big(\frac{m_A}{M}\vec{r}_A+\frac{m_B}{M}\vec{r}_B,\vec{r}_A-\vec{r}_B\Big)\overline{\Psi_{br}\Big(\frac{m_A}{M}\vec{\tilde{r}}_A+\frac{m_B}{M}\vec{r}_B,\vec{\tilde{r}}_A-\vec{r}_B\Big)}\,\mathrm{d}^3r_B\,, \tag{4.2.3}$$

In general, the $\rho_A(\vec{r}_A, \vec{r}'_A)$ is not diagonal. Diagonalization for the ρ_A amounts to asking the solutions of Fredholm integral equation [146, 148]:

$$\int_{\mathbb{R}^3} \rho_A(\vec{r}_A; \tilde{\vec{r}}_A)\psi_{\lambda,m}(\tilde{\vec{r}}_A)\,\mathrm{d}^3\tilde{r}_A = \lambda\,\psi_{\lambda,m}(\vec{r}_A)\,. \tag{4.2.4}$$

Here m labels the multiplicity in case various linear-independent solutions have common eigenvalue λ.

Similarly to the situations in finite-dimensional density matrix, the entanglement is encoded in the eigenvalues of the reduced state. To be more precise, if the solution space of non-zero $\lambda\,\psi_{\lambda,m}$ has dimension greater than 1, then the two-body state is entangled. Moreover, the entropy is computed based on non-zero eigenvalues λ.

It turns out that the barycenter state matters to the diagonalization of the reduced density matrix, then it does matter to the two-body entanglement. However, finding a general formulation for diagonalization is a formidable task.

In this work, we focus on the case whose barycenter state has a definite momentum $\vec{P}$, and we can solve the diagonalization easily. Another easy diagonalization case is that barycenter state has a definite position $\vec{R}$. In this work, we do not consider the case with a definite position since its barycenter state is not an eigenstate of the free Schrödinger equation.

The barycenter state with definite momentum $\vec{P}_0$ is given by delta function

$$\phi(\vec{P}) = \frac{(2\pi\hbar)^{\frac{3}{2}}}{\sqrt{V_R}}\delta^{(3)}(\vec{P} - \vec{P}_0) \tag{4.2.5}$$

where V_R is the volume factor for position space [146, 147, 148]. The solution for diagonalization is easier done in momentum representation than in position representation. To do this, we start by two-body state in terms of momenta coordinates $(\vec{P}, \vec{p})$,

$$\Psi_{br}(\vec{P}, \vec{p}) = \phi(\vec{P})\psi(\vec{p}) = \frac{(2\pi\hbar)^{\frac{3}{2}}}{\sqrt{V_R}}\delta^{(3)}(\vec{p}_A + \vec{p}_B - \vec{P}_0)\psi(\frac{m_B\vec{p}_A - m_A\vec{p}_B}{m_A + m_B})\,, \tag{4.2.6}$$

where the wave function $\psi(\vec{p})$ is obtained from Fourier transformation from $\psi(\vec{r})$,

$$\psi(\vec{p}) = \frac{1}{(2\pi\hbar)^{\frac{3}{2}}}\int_{\mathbb{R}^3} e^{-\frac{\mathrm{i}}{\hbar}\vec{p}\cdot\vec{r}}\psi(\vec{r})\,\mathrm{d}^3r\,. \tag{4.2.7}$$

Now, the two-body pure state density matrix ρ_{AB} is expressed in terms of momenta coordinates $(\vec{P}, \vec{p})$ as below,

$$\begin{aligned} &\rho_{AB}(\vec{p}_A, \vec{p}_B; \tilde{\vec{p}}_A, \tilde{\vec{p}}_B) \\ = \;& \frac{(2\pi\hbar)^3}{V_R}\delta^{(3)}(\vec{p}_A + \vec{p}_B - \vec{P}_0)\delta^{(3)}(\tilde{\vec{p}}_A + \tilde{\vec{p}}_B - \vec{P}_0)\psi\Big(\frac{m_B}{M}\vec{p}_A - \frac{m_A}{M}\vec{p}_B\Big)\overline{\psi\Big(\frac{m_B}{M}\tilde{\vec{p}}_A - \frac{m_A}{M}\tilde{\vec{p}}_B\Big)}\,, \end{aligned} \tag{4.2.8}$$

then as the similar procedure in Eq.(4.2.3), it is straightforward to show the reduced state ρ_A obtained from partial tracing $\mathcal{H}_B$,

$$\rho_A(\vec{p}_A; \tilde{\vec{p}}_A) = \int_{\mathbb{R}^3} \rho_{AB}(\vec{p}_A, \vec{p}_B; \tilde{\vec{p}}_A, \vec{p}_B)\,\mathrm{d}^3p_B = \frac{(2\pi\hbar)^3}{V_R}\Big|\psi\Big(\vec{p}_A - \frac{m_A}{M}\vec{P}_0\Big)\Big|^2\delta^{(3)}(\vec{p}_A - \tilde{\vec{p}}_A)\,. \tag{4.2.9}$$

It is clear a diagonal reduced state with respect to coordinates $\vec{p}_A$ and $\vec{\tilde{p}}_A$, since the entries vanish whenever $\vec{p}_A \neq \vec{\tilde{p}}_A$. However, the diagonal matrix admits infinite number of diagonal elements. The diagonal entries are just the probabilities in the distribution $|\psi(\vec{p})|^2$ up to a translation. In accord with Eq.(4.1.8), we verify the normalization of $\psi(\vec{r})$,

$$\lim_{V_R\to\infty}\sum_{\vec{p}}\frac{(2\pi\hbar)^3}{V_R}|\psi(\vec{p})|^2=\int_{\mathbb{R}^3}|\psi(\vec{p})|^2\,\mathrm{d}^3p=1\,. \tag{4.2.10}$$

Hence, for simplicity, we write the reduced state by

$$\rho_A(\vec{p};\vec{\tilde{p}})=\frac{(2\pi\hbar)^3}{V_R}|\psi(\vec{p})|^2\delta^{(3)}(\vec{p}-\vec{\tilde{p}})\,. \tag{4.2.11}$$

The Fredholm equation (4.2.4) is solved automatically. The entanglement gets reflected on the probability distribution $|\psi(\vec{p})|^2$. The two-body state is entangled provided that $|\psi(\vec{p})|^2$ has multiply numbers of $\vec{p}$ that $|\psi(\vec{p})|^2\neq 0$. In particular, we conclude:

Proposition 4.2. *If the barycenter state of a two-body state is a plane wave*

$$\phi_{\vec{P}}(\vec{R})=\frac{1}{\sqrt{V_R}}e^{\frac{\mathrm{i}}{\hbar}\vec{P}\cdot\vec{R}}\,,\qquad \textit{or equivalently}\quad \phi(\vec{P})=\frac{(2\pi\hbar)^{\frac{3}{2}}}{\sqrt{V_R}}\delta^{(3)}(\vec{P}-\vec{P}_0)\,, \tag{4.2.12}$$

then the two-body state is unentangled if and only if the relative state has the form

$$\psi(\vec{p})=\frac{(2\pi\hbar)^{\frac{3}{2}}}{\sqrt{V_r}}\delta^{(3)}(\vec{p}-\vec{p}_0) \tag{4.2.13}$$

up to some global phase, where V_r is the volume factor like V_R. That is to say, the relative part of an unentangled two-body state has to be a plane wave, which is the solution for Hamiltonian with free potential $V=0$.

This is not surprising, and the proposition means that the entanglement emanates from the interaction potential. What we want to emphasize here, is the converse statement, namely, the logic that the interaction could be deduced from entanglement. This is one of main motivations of the thesis since the purpose is to reconstruct gravitational interaction from entanglement in case the description of dynamics is incomplete, so we wish the study on Newtonian gravity could provide some hints.

To do so, we emphasize that the entanglement-interaction deduction holds under the precondition that barycenter state is a plane wave. For the cases that barycenter state is not a plane wave, the two-body state is entangled even though the interaction $V=0$. For instance, consider the relative state $|\psi\rangle$ to be a momentum eigenstate $|\vec{q}\rangle=e^{\frac{\mathrm{i}}{\hbar}\vec{q}\cdot\vec{r}}$, and the barycenter state being in superposition $\frac{1}{\sqrt{2}}(|\vec{P}_0\rangle+e^{\mathrm{i}\gamma}|\vec{Q}_0\rangle)$ where $\vec{P}_0$ and $\vec{Q}_0$ are two plane waves in different directions with same kinetic energy. So the normalized two-body state reads $\frac{1}{\sqrt{2V_RV_r}}(|\vec{P}_0\rangle+e^{\mathrm{i}\gamma}|\vec{Q}_0\rangle\otimes|\vec{q}\rangle$, giving the density matrix of two-body state:

$$\sigma_q=\frac{1}{2V_RV_r}(|\vec{P}_0\rangle+e^{\mathrm{i}\gamma}|\vec{Q}_0\rangle)(\langle\vec{P}_0|+e^{-\mathrm{i}\gamma}\langle\vec{Q}_0|)\otimes|\vec{q}\rangle\langle\vec{q}|\,. \tag{4.2.14}$$

The reduced state of $\mathcal{H}_A$ reads:

$$\sigma_{qA}(\vec{p}_A;\vec{\tilde{p}}_A)=\frac{\delta^{(3)}(\vec{p}_A-\vec{\tilde{p}}_A)}{2V_RV_r}\delta^{(3)}\Big(\vec{p}_A-\frac{m_A\vec{P}_0}{M}-\vec{q}\Big)^2+\frac{\delta^{(3)}(\vec{p}_A-\vec{\tilde{p}}_A)}{2V_RV_r}\delta^{(3)}\Big(\vec{p}_A-\frac{m_A\vec{Q}_0}{M}-\vec{q}\Big)^2. \tag{4.2.15}$$

The normalization reads $\mathrm{Tr}(\sigma_{qA})=1$, and it exhibits two nonzero eigenvalues when $\vec{p}_A=\vec{q}+m_A\vec{P}_0/M$ and $\vec{p}_A=\vec{q}+m_A\vec{Q}_0/M$. Thus σ_q is entangled, which shows that the two-body entanglement could exist due to the superposition in barycenter part even though the interaction vanishes. A similar situation would happen in the case that relative part is in superposition such that free Hamiltonian admits entanglement again. But recall that the propose is to reconstruct the relational information from entanglement, this superposition still encodes these information such as relative distance and relative angles with respect to axes.

4.2.2 Correlation functions of two-body operators

We define the correlation function of operator $\hat{O}_1\hat{O}_2$ with respect to two-body state $|\Psi\rangle$ as following,

$$\Delta(\hat{O}_1\hat{O}_2)=\frac{\langle\Psi|\hat{O}_1\hat{O}_2|\Psi\rangle}{\langle\Psi|\Psi\rangle}-\frac{\langle\Psi|\hat{O}_1|\Psi\rangle}{\langle\Psi|\Psi\rangle}\frac{\langle\Psi|\hat{O}_2|\Psi\rangle}{\langle\Psi|\Psi\rangle}\,. \tag{4.2.16}$$

This definition coms from the variation or dispersion. The denominator $|\Psi\rangle$ is meant to remove the δ-normalizable from barycenter part. Let us look at the correlation functions of fundamental momentum and position operators,

$$\begin{cases}\hat{\vec{p}}_A=\dfrac{m_A}{M}\hat{\vec{P}}+\hat{\vec{p}}=-\mathrm{i}\hbar\dfrac{m_A}{M}\nabla_{\vec{R}}-\mathrm{i}\hbar\nabla_{\vec{r}}\,,\\ \hat{\vec{p}}_B=\dfrac{m_B}{M}\hat{\vec{P}}-\hat{\vec{p}}=-\mathrm{i}\hbar\dfrac{m_B}{M}\nabla_{\vec{R}}+\mathrm{i}\hbar\nabla_{\vec{r}}\,,\end{cases}\qquad\begin{cases}\hat{\vec{r}}_A=\hat{\vec{R}}+\dfrac{m_B}{M}\hat{\vec{r}},\\ \hat{\vec{r}}_B=\hat{\vec{R}}-\dfrac{m_A}{M}\hat{\vec{r}},\end{cases} \tag{4.2.17}$$

for any one of probable directions i chosen from $i=x,y,z$. Consider the correlations of two-body momentum operator and position operator with respect to direction i,

$$\Delta(\hat{p}_{Ai}\hat{p}_{Bi})=\frac{\mu}{M}\Delta(\hat{P}_i^2)-\Delta(\hat{p}_i^2)+\frac{m_B-m_A}{M}\Big(\langle\hat{p}_i\hat{P}_i\rangle-\langle\hat{p}_i\rangle\langle\hat{P}_i\rangle\Big)\,, \tag{4.2.18}$$

$$\Delta(\hat{r}_{Ai}\hat{r}_{Bi})=\Delta(\hat{R}_i^2)-\frac{\mu}{M}\Delta(\hat{r}_i^2)+\frac{m_B-m_A}{M}\Big(\langle\hat{r}_i\hat{R}_i\rangle-\langle\hat{r}_i\rangle\langle\hat{R}_i\rangle\Big)\,, \tag{4.2.19}$$

where the $\Delta(\hat{R}_i^2)$, $\Delta(\hat{r}_i^2)$, $\Delta(\hat{P}_i^2)$ and $\Delta(\hat{p}_i^2)$ are correlation functions defined by Eq.(4.2.16), by viewing them as particular $\hat{O}_1\hat{O}_2$ with $\hat{O}_1=\hat{O}_2$, which return to the definition of dispersion. Since wave function is assumed to be factorized by $\Psi(\vec{R},\vec{r})=\phi(\vec{R})\psi(\vec{r})$, the last terms on right hand side vanish, i.e., $\langle\hat{p}_i\hat{P}_i\rangle-\langle\hat{p}_i\rangle\langle\hat{P}_i\rangle=\langle\hat{r}_i\hat{R}_i\rangle-\langle\hat{r}_i\rangle\langle\hat{R}_i\rangle=0$. If a two-body state is unentangled, then above correlation functions vanish.

Both two correlation functions have translation invariance in the sense of, for instance $\Delta[(\hat{p}_{Ai}+a_i)(\hat{p}_{Bi}+a_i)]=\Delta(\hat{p}_{Ai}\hat{p}_{Bi})$, where a_i is the i-component of an arbitrary vector $\vec{a}$ for the translation. The correlation function of individual component, e.g. $\Delta(\hat{p}_{Ai}\hat{p}_{Bi})$, is

not rotational invariance, but we can construct rotational invariant correlation functions via dot product:

$$\Delta(\hat{\vec{p}}_A \cdot \hat{\vec{p}}_B) = \frac{\mu}{M}\Delta(\hat{P}^2) - \Delta(\hat{p}^2)\,, \qquad \Delta(\hat{\vec{r}}_A \cdot \hat{\vec{r}}_B) = \Delta(\hat{R}^2) - \frac{\mu}{M}\Delta(\hat{r}^2)\,, \tag{4.2.20}$$

i.e., summing $\Delta(\hat{p}_{Ai}\hat{p}_{Bi})$ and $\Delta(\hat{r}_{Ai}\hat{r}_{Bi})$ over $i = x, y, z$. In addition, the corresponding components $\Delta(\hat{p}_i^2)$ and $\Delta(\hat{r}_i^2)$ can be computed: since the relative wave function is factorized by $\psi(\vec{r}) = R_{nl}(r)\,Y_{lm}(\theta,\varphi)$ or $\psi(\vec{p}) = F_{nl}(r)\,Y_{lm}(\theta,\varphi)$, the dispersions of these components can be computed as follows:

$$\begin{aligned}
\langle\psi_{nlm}|\hat{p}_x^2|\psi_{nlm}\rangle &= \langle\psi_{nlm}|\hat{p}_y^2|\psi_{nlm}\rangle = \frac{l^2+l+m^2-1}{(2l-1)(2l+3)}\langle\psi_{nlm}|\hat{p}^2|\psi_{nlm}\rangle\,,\\
\langle\psi_{nlm}|\hat{p}_z^2|\psi_{nlm}\rangle &= \frac{2l^2+2l-2m^2-1}{(2l-1)(2l+3)}\langle\psi_{nlm}|\hat{p}^2|\psi_{nlm}\rangle\,,\\
\langle\hat{r}_x^2\rangle = \langle\psi_{nlm}|\hat{r}_y^2|\psi_{nlm}\rangle &= \frac{l^2+l+m^2-1}{(2l-1)(2l+3)}\langle\psi_{nlm}|\hat{r}^2|\psi_{nlm}\rangle\,,\\
\langle\psi_{nlm}|\hat{r}_z^2|\psi_{nlm}\rangle &= \frac{2l^2+2l-2m^2-1}{(2l-1)(2l+3)}\langle\psi_{nlm}|\psi_{nlm}|\hat{r}^2|\psi_{nlm}\rangle\,.
\end{aligned} \tag{4.2.21}$$

That is, knowing $\langle p^2\rangle$ and (l,m) is enough to know $\langle\hat{p}_i^2\rangle$, because the expectations of the spherical harmonics only depend on the angular quantum numbers (l,m) [148]

$$\begin{aligned}
\langle Y_{lm}|\sin^2\theta\cos^2\varphi|Y_{lm}\rangle = \langle Y_{lm}|\sin^2\theta\sin^2\varphi|Y_{lm}\rangle &= \frac{l^2+l+m^2-1}{(2l-1)(2l+3)}\,,\\
\langle Y_{lm}|\cos^2\theta|Y_{lm}\rangle &= \frac{2l^2+2l-2m^2-1}{(2l-1)(2l+3)}\,,
\end{aligned} \tag{4.2.22}$$

then we only need to compute the dispersion $\langle\hat{p}^2\rangle$. In fact, it is easy to compute if the interaction potential is a monomial potential ($d \neq 2$).

Result 4.3. *Given any $d \neq -2$ monomial potential $V(r) = -b\,r^d$ where b is a coupling constant, consider energy eigenstate $|\psi_n\rangle$ satisfy $\hat{H}|\psi_n\rangle = E|\psi_n\rangle$ and normalization $\langle\psi_n|\psi_n\rangle = 1$, then $\langle\psi_n|\hat{p}^2|\psi_n\rangle$ only depends on the energy eigenvalue, i.e.,*

$$V(r) = -b\,r^d\,(d \neq -2)\,: \qquad \langle\psi_n|\hat{p}^2|\psi_n\rangle = \frac{2\mu d}{d+2}E\,. \tag{4.2.23}$$

The proof is easy by applying virial theorem:

$$2\langle T\rangle = \langle\vec{r}\cdot\nabla V(\vec{r})\rangle\,. \tag{4.2.24}$$

For a monomial potential, it implies $\langle V\rangle = 2\langle T\rangle/d$. Due to $\langle T\rangle + \langle V\rangle = E$, one can solve the $\langle\psi_n|\hat{p}^2|\psi_n\rangle$ in terms of eigen-energy when $d \neq -2$.

The dispersion $\langle\hat{p}^2\rangle$ can be used as an entanglement quantifier in [146], portraying the 'width' of probability distribution with respect to the reduced state. We re-explain the entanglement quantifier in terms of correlation function associated to two-body momentum operator $\hat{p}_A \cdot \hat{p}_B$, and give the relation (4.2.23) that extends the entanglement quantifier [146] to any monomial potential $d \neq -2$ and any energy eigenstate.

Whereas for the viewpoint of correlation functions, one should keep in mind about which two-body operators and barycenter states are to be considered. To be more specific, for the case that barycenter state is a plane wave, the correlation function $\Delta(\hat{\vec{p}}_A \cdot \hat{\vec{p}}_B) = -\langle \hat{p}^2 \rangle$ since $\Delta(\hat{P}^2) = 0$, while the correlation function $\Delta(\hat{\vec{r}}_A \cdot \hat{\vec{r}}_B)$ is divergent because of $\Delta(\hat{R}^2) = \infty$. So in this case we do not say $\Delta(\hat{\vec{r}}_A \cdot \hat{\vec{r}}_B)$ a proper entanglement quantifier. The divergence could be explained by Heisenberg uncertainty principle: $\Delta(\hat{P}^2) = 0$ implies $\Delta(\hat{R}^2) = \infty$.

It is remarkable that Result 4.3 shows a simple relation between the entanglement quantifier $\langle \psi_n | \hat{p}^2 | \psi_n \rangle$ and eigen-energy. This is an encouragement for the project that relates gravitational dynamics and entanglement. On the other hand, the entanglement quantifier $\langle \psi_n | \hat{p}^2 | \psi_n \rangle$ does not look the angular quantum number at all. While the angular quantum numbers indeed make some difference in the two-body entanglement as to be seen in the next subsection.

4.2.3 Expectations of relative momentum and relative distance for Newtonian gravity

The expectation values for suitable powers α of $\hat{p}$ and $\hat{r}$ are presented as following. But note that $\hat{\vec{p}}$ and $\hat{\vec{r}}$ are vectorial operators, the expectation value of odd exponent always vanishes due to the parity. In order to include the odd exponent, we define and give the expectations as follows [155, 156]:

$$\begin{aligned}
&\langle \psi_{nlm} | p^\alpha | \psi_{nlm} \rangle = \int_{\mathbb{R}^3} p^\alpha |\psi_{nlm}(\vec{p})|^2 \, \mathrm{d}^3 p \\
=& \left(\frac{\mu b}{n\hbar}\right)^\alpha \frac{\sqrt{\pi} n \Gamma(n+l+1)}{2^{2l+1}(n-l-1)!} \frac{\Gamma(l+\frac{\alpha+3}{2})\Gamma(l+\frac{5-\alpha}{2})}{\Gamma(l+2)\Gamma(l+\frac{5}{2})\Gamma^2(l+\frac{3}{2})} \\
&\times {}_5F_4\left(\begin{matrix} -n+l+1, & n+l+1, & l+1, & l+\frac{\alpha+3}{2}, & l+\frac{5-\alpha}{2} \\ & 2l+2, & l+\frac{3}{2}, & l+2, & l+\frac{5}{2} \end{matrix} \middle| 1 \right)
\end{aligned} \tag{4.2.25}$$

converges for $-2l-3 < \alpha < 2l+5$, and

$$\begin{aligned}
&\langle \psi_{nlm} | r^\alpha | \psi_{nlm} \rangle = \int_{\mathbb{R}^3} r^\alpha |\psi_{nlm}(\vec{r})|^2 \, \mathrm{d}^3 r \\
=& \frac{1}{2n} \left(\frac{n\hbar}{\mu b}\right)^\alpha \frac{\Gamma(2l+\alpha+3)}{2^\alpha \Gamma(2l+2)} {}_3F_2\left(\begin{matrix} -n+l+1, & -\alpha-1, & \alpha+2 \\ & 2l+2, & 1 \end{matrix} \middle| 1 \right)
\end{aligned} \tag{4.2.26}$$

converges for $\alpha > -2l-3$. In particular, the expectations $\langle \psi_{nlm} | r^\alpha | \psi_{nlm} \rangle$ for integer α can be also computed by Kramers-Pasternack relations (c.f. [157])

$$\frac{4(\alpha+1)}{n^2} \langle \psi_{nlm} | r^\alpha | \psi_{nlm} \rangle + a^2 \alpha [(2l+1)^2 - \alpha^2] \langle \psi_{nlm} | r^{\alpha-2} | \psi_{nlm} \rangle = 4a(2\alpha+1) \langle \psi_{nlm} | r^{\alpha-1} | \psi_{nlm} \rangle \tag{4.2.27}$$

In particular, the dispersions of relative momentum and distance, are related to correlation functions of two-body operators $\hat{p}_{Ai}\hat{p}_{Bi}$ and $\hat{r}_{Ai}\hat{r}_{Bi}$ respectively,

$$\langle\psi_{nlm}|\hat{p}^2|\psi_{nlm}\rangle = -2\mu E_n = \frac{\mu^2 b^2}{n^2\hbar^2} = \frac{\hbar^2}{n^2 a^2}\,, \tag{4.2.28}$$

and the dispersion of relative distance, we have

$$\langle\psi_{nlm}|\hat{r}^2|\psi_{nlm}\rangle = a^2\frac{n^2(5n^2 - 3l(l+1)+1)}{2}\,. \tag{4.2.29}$$

where $a = \frac{\hbar^2}{\mu b}$ is the reduced Bohr radius. The dispersion of relative momentum can be also computed easily by Proposition 4.3, and it does not depend on orbital angular momentum l. As the argument is subsection 4.2.2, the dispersion of relative momentum is an entanglement quantifier with respect to the well-defined correlation function $\hat{p}_{Ai}\hat{p}_{Bi}$, while the dispersion of relative position corresponding to the two-body operator $\hat{r}_{Ai}\hat{r}_{Bi}$ diverges due to the spreading-out of barycenter position $\hat{R}$. Note that the dispersion $\langle\psi_{nlm}|\hat{r}^2|\psi_{nlm}\rangle$ still makes sense since it is convergent and characterizes the relative distance between two particles, with dependency on both principal quantum number n and angular quantum number l.

An obvious question is whether the relative distance gets reflected on two-body entanglement. Indeed, the entanglement is weakened as the principal number n increases. In turn, the relative distance increases as principal number n increases, which seems to be explained by the weakening entanglement. In fact, Eq.(4.2.29) shows the negative dependency between relative distance and orbital momentum l. If we followed the logic that relative distance implies the strength of two-body entanglement, we would have deduced that the higher l state is more entangled than the lower l state. However, as we will see later, this deduction is incorrect when we look at the entanglement entropy in Section 4.3.2. Therefore, the answer should be that relative distance is reflected in two-body entanglement, but two-body entanglement contains more relative information than relative distance. In other words, entanglement allows us to read more geometric information, not just distance.

4.3 Two-body entanglement entropy

4.3.1 Two-body momentum entropy

The reduced state (4.2.11) gives von Neumann entropy

$$\begin{aligned} S_{V_R}(\rho_A) &= -\lim_{V_R\to\infty}\sum_{\vec{p}}\frac{(2\pi\hbar)^3|\psi(\vec{p})|^2}{V_R}\ln\frac{(2\pi\hbar)^3|\psi(\vec{p})|^2}{V_R} \\ &= \ln\frac{V_R}{(2\pi\hbar)^3} - \int_{\mathbb{R}^3}|\psi(\vec{p})|^2\ln|\psi(\vec{p})|^2\,\mathrm{d}^3p\,. \end{aligned} \tag{4.3.1}$$

When $V_R\to\infty$, the von Neumann entropy entails logarithmic divergence. But the integral

$$S = -\int_{\mathbb{R}^3}|\psi(\vec{p})|^2\ln|\psi(\vec{p})|^2\,\mathrm{d}^3p \tag{4.3.2}$$

can be finite. The S is the Shannon entropy associated with the probability distribution $|\psi(\vec{p})|^2$, and is called momentum entropy [158]. Note that the momentum entropy could be negative because the probability distribution admits $|\psi(\vec{p})|^2 > 1$ at some points. In the rest of this part, we will focus on momentum entropy.

Usually, the momentum entropy S is finite. Then the von Neumann entropy will ineluctably diverge as $V_R \to \infty$, which means that the volume divergence will suppress any other contributions. We can not see eigenstates from the diverging entropy. A similar argument was shown in [148], where they computed the linear entropy of reduced state that turned out to be trivial due to the volume divergence.

We consider the difference between entropies: given two reduced states ρ_A and ρ'_A, the difference between von Neumann entropies equals the difference between Shannon entropies

$$S_{V_R}(\rho_A) - S_{V_R}(\rho'_A) = S(\rho_A) - S(\rho'_A) \tag{4.3.3}$$

since V_R is a constant. For instance, we could set ρ_A and ρ'_A as reduced states from two eigenstates. In this prescription, we no longer have volume divergence; meanwhile, the triviality disappears.

The diverging volume factor is because the barycenter state is δ-normalizable. It is possible to avoid the divergence by considering a Gaussian wave-packet [159, 148]. However, such a barycenter state is not an eigen-solution for the free Schrödinger equation. Moreover, the two-body state can get entangled due to the barycenter state, as the example in Eq.(4.2.14), which has nothing to do with two-body interaction. Since we want to reconstruct gravitational interaction from entanglement, it is natural to pay immediate attention to the contribution from the relative part. Thus we are only interested in the plane wave barycenter state.

4.3.2 Momentum entropy for Newtonian gravity bound states

We now look at the entanglement entropy of the two-body Newtonian gravity state. In this part, we express the integral (4.3.2) for momentum entropy in terms of quantum numbers (n, l, m) as explicitly as possible. The expression will contain two Gegenbauer entropies. However, we do not have an effective expression for them, in the cases of arbitrary (n, l, m). But it is enough for us to consider two particular cases, i.e., $l = m = 0$ and $l = m = n - 1$. By means of analyzing the two particulars, we can re-inspect the question in the previous subsection.

Let us start with arbitrary eigenstate $\psi_{nlm}(\vec{p}) = F_{nl}(p)Y_{lm}(\theta, \varphi)$, then the momentum entropy (4.3.2) can be factorized further

$$S_{nlm} = -\int_0^\infty p^2 |F_{nl}(p)|^2 \ln |F_{nl}(p)|^2 \, \mathrm{d}p - \int_{S^2} |Y_{lm}(\theta, \varphi)|^2 \ln |Y_{lm}(\theta, \varphi)|^2 \, \mathrm{d}\Omega_{S^2} \,. \tag{4.3.4}$$

Calling the transformation (4.1.20), the momentum entropy (4.3.4) is factorized further

$$S_{nlm} = \frac{3}{2} \ln(-2\mu E_n) + S^T_{nl} + S^R_{nl} + S^Y_{lm} \,, \tag{4.3.5}$$

where S^T_{nl}, S^R_{nl} and S^Y_{lm} are integrals

$$S^T_{nl} = -\int_{-1}^{1} 4|\widetilde{F}_{nl}(s)|^2(1-s^2)^{\frac{1}{2}}\ln(1-s)\,\mathrm{d}s\,, \tag{4.3.6}$$

$$S^R_{nl} = -\int_{-1}^{1} (1-s^2)^{\frac{1}{2}}|\widetilde{F}_{nl}(s)|^2\ln|\widetilde{F}_{nl}(s)|^2\,\mathrm{d}s\,, \tag{4.3.7}$$

$$S^Y_{lm} = -\int_{S^2} |Y_{lm}(\theta,\varphi)|^2\ln|Y_{lm}(\theta,\varphi)|^2\,\mathrm{d}\Omega_{S^2}\,, \tag{4.3.8}$$

where we have used the fact that Gegenbauer polynomial has parity — is either odd or even function, thus $|\widetilde{F}_{nl}(s)|^2$ must be an even function. The S^T_{nl} is given by Theorem 4 in [155]. The integrals S^R_{nl} and S^Y_{nl} consist of two parts, expressed as follows:

$$S^G_{a\nu} = -\int_{-1}^{1} w_\nu(s)[\tilde{C}^\nu_a(s)]^2\ln[\tilde{C}^\nu_a(s)w_\nu(s)]^2\,\mathrm{d}s = S(\tilde{C}^\nu_a) + I(\tilde{C}^\nu_a)\,. \tag{4.3.9}$$

The $S(\tilde{C}^\nu_a)$ is the so-called Gegenbauer entropy,

$$S(\tilde{C}^\nu_a) = -\int_{-1}^{1} w_\nu(s)[\tilde{C}^\nu_a(s)]^2\ln[\tilde{C}^\nu_a(s)]^2\,\mathrm{d}s\,, \tag{4.3.10}$$

which is formidable to compute [160, 161, 162, 163, 164, 165, 166]. A practical expression for generic Gegenbauer entropies with respect to arbitrary a and ν is still under investigation. It is known to compute particular Gegenbauer entropies [158]

$$S(\tilde{C}^\nu_0) = 0\,, \qquad \text{and} \quad S(\tilde{C}^1_a) = \frac{1}{a+1} - 1\,. \tag{4.3.11}$$

Even the expression $S(\tilde{C}^2_a)$ is rather complicated and lengthy [163]. As for the integral $I(\tilde{C}^\nu_a)$, it is computed by Theorem 3 in [155],

$$\begin{aligned} I(\tilde{C}^\nu_a) =& -\int_{-1}^{1} w_\nu(s)[\tilde{C}^\nu_a(s)]^2\ln w_\nu(s)\,\mathrm{d}s \\ =&(\nu-\frac{1}{2})\left(2\ln 2 + \frac{1}{a+\nu} + 2\Gamma^{(1)}(a+\nu) - 2\Gamma^{(1)}(a+2\nu)\right) + \ln\frac{\sqrt{\pi}\Gamma(\nu+\frac{1}{2})}{\Gamma(\nu+1)}\,. \end{aligned} \tag{4.3.12}$$

Now, S^T_{nl}, S^R_{nl} and S^Y_{lm} are listed as follows:

$$S^T_{nl} = -2n\left(\frac{2}{n}\big[1-\ln 2+\Gamma^{(1)}(n+l+1)-\Gamma^{(1)}(n)\big] - \frac{4(2l+1)}{4n^2-1} - \frac{1}{n^2}\right)\,, \tag{4.3.13}$$

$$S^R_{nl} = S(\tilde{C}^{l+1}_{n-l-1}) + l\left(2\ln 2 + \frac{1}{n} + 2\Gamma^{(1)}(n) - 2\Gamma^{(1)}(n+l+1)\right) + \ln\frac{\sqrt{\pi}\Gamma(l+\frac{3}{2})}{\Gamma(l+2)}\,, \tag{4.3.14}$$

$$S^Y_{lm} = S(\tilde{C}^{|m|+\frac{1}{2}}_{l-|m|}) + |m|\left(2\ln 2 + \frac{1}{l+\frac{1}{2}} + 2\Gamma^{(1)}(l+\frac{1}{2}) - 2\Gamma^{(1)}(l+|m|+1)\right)$$

$$+\ln\frac{\sqrt{\pi}\Gamma(|m|+1)}{\Gamma(|m|+\frac{3}{2})}+\ln 2\pi\,, \tag{4.3.15}$$

where $\Gamma^{(1)}(z)=\Gamma'(z)/\Gamma(z)$ denotes digamma function. Putting them together, the momentum entropy (4.3.5) is determined except for two Gegenbauer entropies

$$\begin{aligned}S_{nlm}=&\frac{3}{2}\ln(-2\mu E_n)+\left(4\big[\ln 2-1+\Gamma^{(1)}(n)-\Gamma^{(1)}(n+l+1)\big]+\frac{8n(2l+1)}{4n^2-1}+\frac{2}{n}\right)\\&+l\left(2\ln 2+\frac{1}{n}+2\Gamma^{(1)}(n)-2\Gamma^{(1)}(n+l+1)\right)+\ln\frac{\sqrt{\pi}\Gamma(l+\frac{3}{2})}{\Gamma(l+2)}\\&+|m|\left(2\ln 2+\frac{1}{l+\frac{1}{2}}+2\Gamma^{(1)}(l+\frac{1}{2})-2\Gamma^{(1)}(l+|m|+1)\right)\\&+\ln\frac{\sqrt{\pi}\Gamma(|m|+1)}{\Gamma(|m|+\frac{3}{2})}+\ln 2\pi+S(\tilde{C}^{l+1}_{n-l-1})+S(\tilde{C}^{|m|+\frac{1}{2}}_{l-|m|})\,.\end{aligned} \tag{4.3.16}$$

4.3.3 An observation about entanglement reconstruction for interaction and geometry

Now we consider the two particular cases $l=m=0$ and $l=m=n-1$, their momentum entropies are given as the following:

$$S_{n00}=\frac{3}{2}\ln(-2\mu E_n)+\frac{2}{n(4n^2-1)}-\frac{n-1}{n}+4(\ln 2-1)+\ln(2\pi^2)\,, \tag{4.3.17}$$

$$S_{n,n-1,n-1}=\frac{3}{2}\ln(-2\mu E_n)-\ln n-\frac{4}{2n+1}+\frac{n+1}{n}+2\Big(\Gamma^{(1)}(n)-\Gamma^{(1)}(n+\frac{1}{2})\Big)+\ln(2\pi^2)\,. \tag{4.3.18}$$

Here S_{n00} and $S_{n,n-1,n-1}$ are expressed exactly, due to the exact expressions (4.3.11) for Gegenbauer entropy.

From the two expressions, we compare them by fixing the principle quantum number n, then, we do not need to look at the first term, but the rest of the terms make a difference. When $n\to 0$, the $S_{n,n-1,n-1}$ has negative logarithmic divergence, so $S_{n,0,0}>S_{n,n-1,n-1}$, which means $\psi_{n00}(\vec{r})$ is more entangled than $\psi_{n,n-1,n-1}(\vec{r})$. However, recall the dispersion (4.2.29), the state $\psi_{n00}(\vec{r})$ has longer relative distance than $\psi_{n,n-1,n-1}(\vec{r})$, which goes against the naive intuition that more entangled state implies a shorter relative distance. Meanwhile, the relative distance reflects the strength of the central interaction between the two particles, so gravitational interaction behaves differently from two-body entanglement in this case.

A reasonable explanation will be: that the two-body entanglement reflects more information about the geometry, such as distance, shape, etc. Due to the result, the relative distance only reflects part of the information of two-body entanglement. Although the gravitational interaction is considered the entanglement source, the entanglement contains more information. For instance, entanglement reflects the shape information about wave function: the quantum number m does not matter to the relative distance at all, but it does matter to the projective dispersions (4.2.21). In particular, when $l=m$,

the azimuthal quantum number m minimizes the projection on the z-axis, which clearly outlines the information about the shape of spherical harmonic Y_{ll}. The spherical harmonics and quantum angular momenta are the manifestations of space quantization. Hence this information reveals more quantum properties of geometry than the crude picture of aligning interaction of gravitational force.

This chapter is to study the two-body entanglement in Newtonian gravity and, more important, sees the possibility of entanglement-geometry reconstruction in the context of quantum gravity. Since Newtonian gravity is believed to be a limit for general relativity, and the dynamics of the non-relativistic quantum theory are well-known, we embarked on the study to seek some hints.

One of the hints is that the entanglement can be partially encoded in the correlation function of the two-body local operator $\hat{\vec{p}}_A \cdot \hat{\vec{p}}_B$, and more important, this correlation function can be simply expressed in terms of eigen-energy. That means energy gets reflected in the entanglement of quantum gravity. At the same time, it is well-known that the energy is defined quasi-locally in general relativity instead of being defined as a local energy density. Does it imply that quantum gravity entanglement can get reflected entirely on the boundary?

Another hint is about the possibility of entanglement-geometry reconstruction. We have encountered a case in which some correlation operator goes again the usual intuition about geometry and entanglement. In there, for instance, we considered the correlation function of two-body $\hat{\vec{r}}_A \cdot \hat{\vec{r}}_B$, which turns out to be reflected in the dispersion of relative distance. Moreover, we show that the relative distance sometimes goes against the strength of two-body entanglement, i.e., the higher orbital l bound state has a shorter relative distance. However, it is less entangled than the lower orbital l bound state. In other words, one kind of geometric notion only reflects partial information from entanglement, and conversely, entanglement includes various geometric notions. In this Newtonian gravity case, the classical picture is that the relative distance reflects the most important data for the gravitational interaction, which was believed to be the source of entanglement. However, entanglement tells us more: two-body entanglement not just reflects the relative distance for determining gravitational force but also other information about geometry, e.g., the geometric distribution of quantum state, which is relevant to space quantization.

In Chapter 6, we will explore quantum information on boundary Hilbert space. Moreover, in later Chapter 7, we will explore the entanglement-geometry reconstruction further, beyond the distance-reconstruction (c.f. [167]), and embark on the reconstruction for curvature.

Part II

Entanglement and Bulk-Boundary Map in Quantum Gravity

Chapter 5

Bulk-Boundary Maps

In this chapter, we take a trip back to the foundations of loop quantum gravity to describe (spatial) boundaries. In spin foam approaches, the transition amplitude is defined for initial and final spin network states, which are boundary states in the sense of histories of spin networks. Inspired by the spin foam approaches, given boundary Hilbert spaces, the spin network wave-functions can be viewed as maps from inward states to outward states or equivalently as maps from bulk to the boundary. Following the logic, our program can be understood as studying 'spatial' spin foam in some sense [168]. Moreover, as we will see, the bulk holonomies resemble the topological defects in extended topological field theories [169].

This chapter is based on [52] and some supplements in [54]. It is organized as follows: Section 5.1 starts with the setting of space-time corner. The following subsection is to define boundary Hilbert space corresponding to the space-time corner. Based on the boundary Hilbert space, we define bulk-boundary map with spin network wave-function. Section 5.2 introduces a coarse-graining procedure implemented by gauge-fixing bulk holonomies. By this coarse-graining procedure, we define coarse-grained states obtained via gauge-fixing. Moreover, the scalar product associated with the boundary Hilbert space can give the bulk probability. We then show in Proposition 5.2 that the configuration of flat bulk holonomies is always a stationary point for the bulk probability function. Section 5.3 introduces recoupled spin basis for boundary Hilbert space, decomposing tensor product state in terms of total spin and multiplicity. It turns out to be useful in Chapter 6. We also refer to it as *closure defect*. In Section 5.4, we equip the dual boundary Hilbert space with the scalar product of spin network Hilbert space, meaning that we can compute spin network scalar product from the viewpoint of dual boundary Hilbert space. This viewpoint does not construct anything new, but it allows us to define the unitary transformation with respect to the entire spin network, as presented in Proposition 5.4, which will be helpful in Chapter 7 and Chapter 8.

5.1 Spin Networks as Bulk-Boundary Maps

5.1.1 Corners

To be more concrete, the geometrical setting we wish to study is a cylinder in space-time: we consider a bounded region of space $\mathcal{R}$, with the topology of a 3-ball, whose boundary $\mathcal{S} = \partial\mathcal{R}$ has the topology of a 2-sphere; the space-time structure is then the cylinder $\mathcal{R} \times [t_i, t_f]$ whose time-like boundary is the 2+1-dimensional $\mathcal{S}_T = \mathcal{S} \times [t_i, t_f]$, such that the space boundary can be considered as the corner of space-time $\mathcal{S} = \mathcal{S}_T \cap \mathcal{R}$, as illustrated on fig.5.1. A canonical framework describes the evolution in time of the state of the 3d geometry of the space slice $\mathcal{R}$. In this context, the question of holography amounts to identify the degrees of freedom of the boundary geometry on the corner $\mathcal{S}$ - the gravitational edge modes[1] - which will generate the boundary conditions on $\mathcal{S}_T$ for the bulk geometry, study how the dynamics of those edge modes propagate into the bulk and, as a consequence, understand to which extent boundary observables reflect the bulk geometry's evolution and fluctuations. From this perspective, the study of holography is intimately intertwined with the renormalization flow à la Wilson, where the coarse-graining of the dynamics of the bulk geometry in $\mathcal{R}$ induces effective dynamics and boundary theory on $\mathcal{S}$, in a bulk-to-boundary process which should ultimately be dual to the boundary-to-bulk reconstruction intended by holography (see e.g. [44] for an early attempt to realize this scenario in loop quantum gravity).

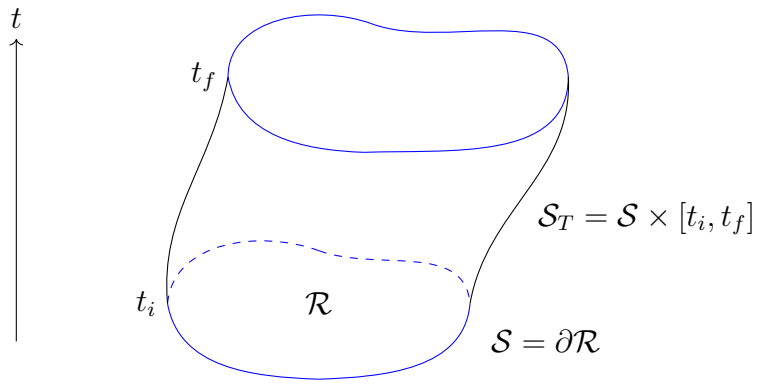

Figure 5.1: Boundary and corner: we consider the evolution in time of a bounded region of space $\mathcal{R}$ whose spatial boundary $\mathcal{S} = \partial\mathcal{R}$ defines what is called the two-dimensional corner of space-time; the evolution of the corner defines the 2+1-d boundary of the region of space-time, $\mathcal{S}_T = \mathcal{S} \times [t_i, t_f]$.

To implement this in quantum gravity, we follow a logic paralleling the hierarchy of 4d/3d/2d/1d defects and their algebraic description in a 4d TQFT, the introduction of quantum states on the boundary forces to go one level higher algebraically and define bulk states as operators (linear forms) acting on boundary states: bulk states will not

[1]For recent works on classical edge modes for general relativity in its first order formulation in terms of connection-vierbein variables, the interested reader can see [46, 47, 48, 49].

simply be wave-functions valued in $\mathbb{C}$ but valued in Hilbert space of boundary states. To make things explicit, we call the boundary Hilbert space $\mathcal{H}_\mathcal{B}$ with boundary states $|\Phi_\mathcal{B}\rangle$ living on the space-time corner $\mathcal{S} = \partial\mathcal{R}$. A wave-function ψ is a function of the bulk fields φ_{bulk} valued in the (dual of the) boundary Hilbert space, $\psi[\varphi_{bulk}] \in \mathcal{H}^*_\mathcal{B}$, and thus defines a linear form on the boundary Hilbert space:

$$\psi : \varphi_{bulk} \mapsto \Psi[\varphi_{bulk}] \in \mathcal{H}^*_\mathcal{B}\,, \qquad \langle \psi[\varphi_{bulk}] \,|\, \Phi_\mathcal{B}\rangle \in \mathbb{C}\,. \tag{5.1.1}$$

We interpret these bulk wave-functions as defining a probability distribution for the bulk observables dependant on the choice of boundary states (i.e. quantum boundary conditions): once $\Phi_\mathcal{B}$ is fixed, the function

$$\langle \Phi_\mathcal{B} | \psi[\cdot]\rangle \,:\, \varphi_{bulk} \mapsto \langle \Phi_\mathcal{B} | \psi[\varphi_{bulk}]\rangle \in \mathbb{C} \tag{5.1.2}$$

is a standard $\mathbb{C}$-valued wave-function for the bulk fields. As we explain in the present chapter, this can done in a natural way in loop quantum gravity since spin networks can be geometrically interpreted as aggregates of area quanta, glued together to create 3d spaces from 2d excitations, and can thus be naturally extended to include the area quanta on the 2d boundary $\mathcal{S}$. A spin network wave-function on an open graph then naturally defines a linear form on the Hilbert space of spin states living on the open edges of the graph, as illustrated on fig.5.3 and thus induces a boundary density matrix.

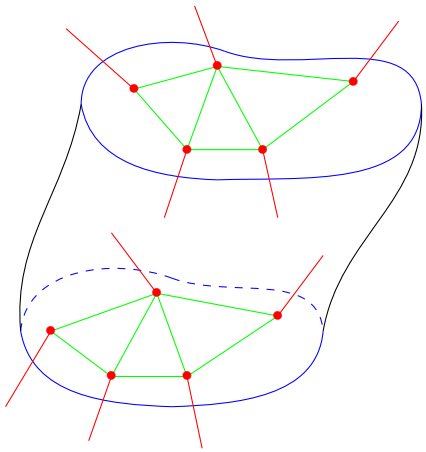

Figure 5.2: Spin network with a boundary: on each spatial slice, the embedded graph Γ punctures the boundary surface of the bounded region of space $\mathcal{R}$; we distinguish the boundary edges $e \in \partial\Gamma$ in red and the bulk edges $e \in \Gamma^o$ in green; the spin network defines a wave-function for the holonomies living on the bulk edges valued in the Hilbert space attached to the open ends of the boundary edges.

5.1.2 Boundary States and Maps

We consider introducing spin networks on a bounded spatial slice similar to taking a bounded subset of a spin network state. As illustrated on fig.5.3, this means considering

a graph Γ with open edges $e \in \partial\Gamma$ puncturing the boundary surface. We do not endow the boundary with extra structure, representing the 2d boundary intrinsic geometry as in [170, 171, 46] or locality on the boundary as in [172], but discuss the minimal boundary structure.

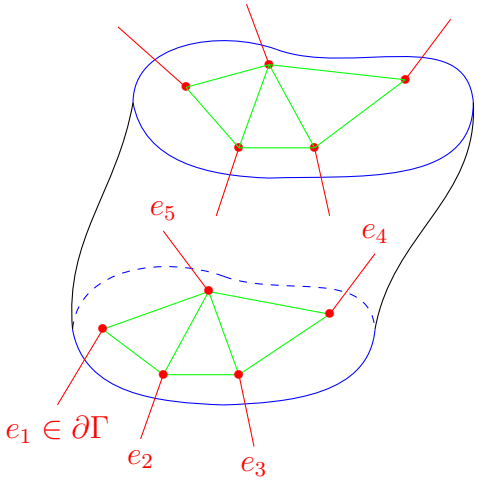

Figure 5.3: On each spatial slice, the boundary states consist in the tensor product of spin states living on the boundary edges of the spin network: $\mathcal{H}_{\partial\Gamma} = \bigotimes_{e\in\partial\Gamma} \bigoplus_{j_e} \mathcal{V}_{j_e}$.

Each boundary edge $e \in \partial\Gamma$ carries a spin j_e and a vector in the corresponding representation $v_e \in \mathcal{V}_{j_e}$. This defines the boundary Hilbert space as:

$$\mathcal{H}_{\partial\Gamma}^{\{j_e\}_{e\in\partial\Gamma}} = \bigotimes_{e\in\partial\Gamma} \mathcal{V}_{j_e} \,. \tag{5.1.3}$$

One does not need to fix the spins carried by the boundary edges and can consider the larger boundary Hilbert space [2]:

$$\mathcal{H}_{\partial\Gamma} = \bigoplus_{\{j_e\}} \mathcal{H}_{\partial\Gamma}^{\{j_e\}_{e\in\partial\Gamma}} = \bigotimes_{e\in\partial\Gamma} \mathcal{V}_e \qquad \text{with} \quad \mathcal{V} = \bigoplus_j \mathcal{V}_j \,. \tag{5.1.4}$$

Using the Schwinger realization of the $\mathfrak{su}(2)$ Lie algebra in terms of a pair of quantum oscillators, the Hilbert space $\mathcal{V}$ is the tensor product of two copies of the harmonic oscillator Hilbert space, which can be understood as (holomorphic) wave-functions of a spinor, i.e. a complex 2-vector [173, 174, 175, 176, 177, 178, 179, 180].

Calling $\Gamma^o = \Gamma \setminus \partial\Gamma$ the bulk or interior of the graph Γ, a spin network wave-function on the graph Γ with boundary is still a function of group elements living on bulk edges $e \in \Gamma \setminus \partial\Gamma$, but is not anymore valued in the field $\mathbb{C}$ but into the boundary Hilbert space $\mathcal{H}_{\partial\Gamma}$:

$$\psi(\{g_e\}_{e\in\Gamma^o}) \in \mathcal{H}_{\partial\Gamma} \,. \tag{5.1.5}$$

[2] In fact, $\partial\Gamma = \mathcal{B}$, so $\mathcal{H}_{\partial\Gamma} \cong \mathcal{H}_{\mathcal{B}}$. But we sometimes adopt $\partial\Gamma$ to accent that we are considering the boundary of graph Γ. We use $\mathcal{B}$ usually for the cases that the bulk of the graph is unspecified or unnecessary to be specified.

The scalar product between wave-functions is inherited from the inner product between boundary states:

$$\langle\psi|\widetilde{\psi}\rangle = \int \prod_{e\in\Gamma^o} \mathrm{d}g_e \, \langle\psi(\{g_e\}_{e\in\Gamma^o})|\widetilde{\psi}(\{g_e\}_{e\in\Gamma^o})\rangle \,, \tag{5.1.6}$$

with the normalization of wave-functions reading as:

$$\langle\psi|\psi\rangle = \int \prod_{e\in\Gamma^o} \mathrm{d}g_e \, \langle\psi(\{g_e\}_{e\in\Gamma^o})|\psi(\{g_e\}_{e\in\Gamma^o})\rangle = 1 \,. \tag{5.1.7}$$

To be more precise, it should actually be considered as a linear form on the boundary Hilbert space and thus live in the dual Hilbert space, $\psi(\{g_e\}_{e\in\Gamma^o}) \in (\mathcal{H}_{\partial\Gamma})^*$. This means that it defines a distribution on boundary states depending on the group elements, or holonomies, living in the bulk:

$$\forall\Phi \in \mathcal{H}_{\partial\Gamma} \,, \quad \langle\psi(\{g_e\}_{e\in\Gamma^o}) \,|\, \Phi\rangle \ \in \mathbb{C} \,. \tag{5.1.8}$$

In simpler words, a spin network state is now a map on boundary states (or corner states), which we will loosely refer to as a boundary map.

The statement of gauge invariance also has to take into account the boundary: the wave-function will be invariant with respect to bulk gauge transformations while it will be covariant under gauge transformations on the boundary. More precisely, we distinguish bulk vertices $v \in V^o$ that are not connected to any boundary edge and boundary vertices $v \in V_\partial$ that are attached to at least one boundary edge. The wave-function is assumed to be invariant under SU(2) transformations acting at bulk vertices, while SU(2) transformations acting at boundary vertices will act on the spin states dressing the boundary edges:

$$|\psi(\{h_{t(e)} g_e h_{s(e)}^{-1}\})\rangle = \left(\bigotimes_{e\partial\Gamma} h_{v(e)}^{\epsilon_e^v}\right) |\psi(\{g_e\})\rangle \tag{5.1.9}$$

where $v(e)$ for $e \in \partial\Gamma$ denotes the vertex to which the boundary edge is attached and $\epsilon_e^v = 1$ is the boundary edge is outgoing ($v(e) = s(e)$) while $\epsilon_e^v = -1$ is the boundary edge is incoming ($v(e) = t(e)$).

The definition of the spin network basis states can then be adapted to the case with boundary:

$$\begin{aligned}
&\Psi_{\{j_e,I_v\}}(\{g_e\}_{e\in\Gamma^o}) \\
=&\sum_{m_e^{t,s}} \prod_{e\in\Gamma^o} \sqrt{2j_e+1}\, \langle j_e m_e^t|g_e|j_e m_e^s\rangle \prod_v \langle \bigotimes_{e\in\Gamma^o|\, v=s(e)} j_e m_e^s| \, I_v \, | \bigotimes_{e\in\Gamma^o|\, v=t(e)} j_e m_e^t\rangle \\
\in& \bigotimes_{\substack{e\in\partial\Gamma \\ t(e)\in\Gamma}} \mathcal{V}_{j_e}^* \otimes \bigotimes_{\substack{e\in\partial\Gamma \\ s(e)\in\Gamma}} \mathcal{V}_{j_e} \,.
\end{aligned} \tag{5.1.10}$$

We sum over the magnetic indices m's only for the bulk edges, in contrast to what (**??**) does, where boundary magnetic indices had been summed. One might analogously think

above formalism as components of a vector with boundary magnetic indices, meanwhile chooses a basis in boundary Hilbert space (amounts to choose a boundary condition) thence puts vector components into a true "vector" in geometrical sense. To be more precise, the spin states on the boundary edges are not contracted, so that the wave-function $\Psi_{\{j_e,I_v\}}$ is valued in the boundary Hilbert space $\mathcal{H}_{\partial\Gamma}$. This can be made more explicit by writing the wave-function ψ as a tensor by evaluating on a basis of boundary states,

$$\psi^{\{j_e,m_e\}_{e\in\partial\Gamma}} = \langle \otimes_{e\in\partial\Gamma} j_e, m_e \,|\, \psi\rangle \,. \tag{5.1.11}$$

Assuming that boundary edges are outgoing for the sake of simplicity, this gives for spin network basis states:

$$\begin{aligned} & \Psi_{\{j_e,I_v\}}(\{g_e\})^{\{j_e,m_e^s\}_{e\in\partial\Gamma}} \\ = \;& \langle \otimes_{e\in\partial\Gamma} j_e, m_e^s \,|\, \Psi_{\{j_e,I_v\}}(\{g_e\})\rangle \\ = \;& \sum_{m_e^{t,s}} \prod_{e\in\Gamma^o} \sqrt{2j_e+1}\, \langle j_e m_e^t | g_e | j_e m_e^s\rangle \prod_v \langle \bigotimes_{e\in\Gamma|\, v=s(e)} j_e m_e^s |\, I_v \,|\, \bigotimes_{e\in\Gamma^o|\, v=t(e)} j_e m_e^t\rangle \end{aligned} \tag{5.1.12}$$

The scalar product between those wave-functions is given by the scalar product of the bulk intertwiner as for the no-boundary case:

$$\begin{aligned} \langle \Psi_{\{j_e,I_v\}} | \Psi_{\{\tilde{j}_e,\tilde{I}_v\}}\rangle &= \sum_{\{k_e,m_e\}} \overline{\Psi_{\{j_e,I_v\}}(\{g_e\})^{\{k_e,m_e\}}}\, \Psi_{\{\tilde{j}_e,\tilde{I}_v\}}(\{g_e\})^{\{k_e,m_e\}_{e\in\partial\Gamma}} \\ &= \prod_e \delta_{j_e,\tilde{j}_e} \prod_v \langle I_v | \tilde{I}_v\rangle \,. \end{aligned} \tag{5.1.13}$$

5.1.3 Spin Network Maps as Quantum Circuits

We would like to build on the interpretation of spin network wave-functions as valued in the space of linear forms on the boundary Hilbert space, or boundary maps. This can be translated operationally as spin networks defining quantum circuits on the boundary data.

Let us fix the spins on the boundary edges and distinguish their orientation. Then a spin network wave-function for the bulk graph defines a family of maps, between the spins on the incoming boundary edges to the spins on the outgoing boundary edges, labeled by the holonomies living on the bulk links:

$$\psi(\{g_e\}_{e\in\Gamma^o}) \,:\, \bigotimes_{\substack{e\in\partial\Gamma \\ t(e)\in\Gamma}} \mathcal{V}_{j_e} \longmapsto \bigotimes_{\substack{e\in\partial\Gamma \\ s(e)\in\Gamma}} \mathcal{V}_{j_e} \,. \tag{5.1.14}$$

Of course, we could unfix the boundary spins and more generally attach the larger Hilbert space $\mathcal{V} = \bigoplus_j \mathcal{V}_j$ to each boundary edge. As illustrated on fig.5.4, the spin network graph, with its link and node structure, already carries the natural structure of a circuit. The holonomies, or SU(2) group elements, on the graph links are interpreted as unitary one-spin gates, while the intertwiners, or SU(2)-invariant maps, naturally define multi-spins gates.

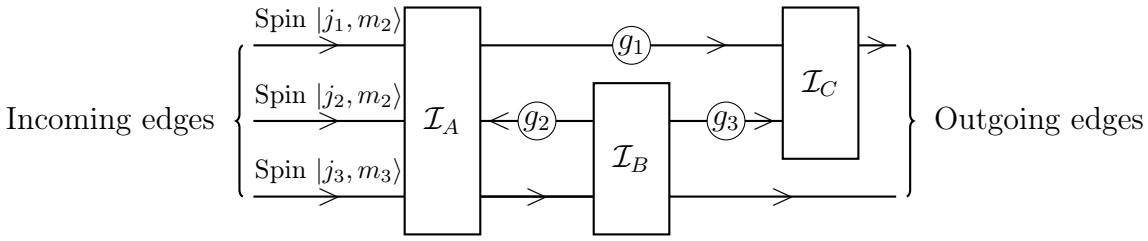

Figure 5.4: Spin network as a quantum circuit: holonomies become unitary one-spin gates while intertwiners are multi-spin gates; the circuit can contains loops.

The spin network state is not a process in itself. There are two important points to keep in mind. First, a spin network is a spatial construct, and not directly a space-time structure. A spin network is not a (quantum) causal history (see e.g. [181, 182] for a presentation and discussion on quantum causal histories). The maps that it defines between the boundary spins are thus possible processes that might occur if the spin network state itself (i.e. the quantum state of 3D geometry) does not evolve. In that sense, it is truly a circuit, to which we haven't yet sent an input and on which we can still adjust some parameters. Indeed, the second important remark is that the holonomies are not fixed. The spin network defines a whole family of boundary maps, which vary in the individual one-spin gates defined by the holonomies $\{g_e\}_{e\in\Gamma^o}$ along the bulk edges. From the point of view of the boundary, these holonomies are not fixed, they should either be averaged over or some other criteria should be found to determine them. For instance, the holonomies, or more precisely their quantum probability distribution, should ultimately be determined by the dynamics of quantum gravity. Nevertheless, even without exploring the issue of defining the dynamics of loop quantum gravity, either by a Hamiltonian constraint operator or by spinfoam transition amplitudes, this quantum circuit perspective allows to formulate interesting questions:

- Working with a given spin network state, with a fixed graph, fixed spins and intertwiners, can we characterize the resulting subset of boundary maps induced by allowing for arbitrary holonomies along the edges? Or vice-versa, how much does a boundary state (for both incoming and outgoing boundary spins) fixes the holonomies in the bulk? Could this be used to formulate a holographic principle for loop quantum gravity?

- Going further, looking at the spin network state as a black box, with access solely to the boundary spins, if we know the subset of boundary maps that it defines, how much of the bulk graph and intertwiners can we re-construct? Could one think of the diffeomorphism constraints of loop quantum gravity as identifying spin network states which lead to same set of boundary maps? This would be an holographic implementation of the dynamics through bulk-to-boundary coarse-graining, along the lines of [44].

- The issue of defining the dynamics or the coarse-graining of the theory is actually equivalent to the problem of defining a physical inner product or a flow of

inner products from the microscopic theory to a coarse-grained macroscopic theory. The quantum circuit perspective offers a possible approach. The microscopic inner product between quantum circuit is defined as the loop quantum gravity kinematical inner product, reflecting the scalar product between intertwiners, i.e. the basic multi-spin gates. As we coarse-grain or sparsify the quantum circuit (while possibly not affecting the boundary maps), we reduce the bulk structure of the circuit by encompassing subsets of holonomies and intertwiners into single larger multi-spin gates, thus leading to a scalar product between those multi-spin gates. The ultimate stage is the fully coarse-grained state, directly provided with the inner product between boundary maps. Studying this in more details would reveal the coarse-graining flow of spin network states in loop quantum gravity.

Although these topics are very likely essential to the understanding of the renormalization flow, holographic behavior and semi-classical regime of loop quantum gravity, they are broad questions out of the scope of the present work and are postponed to future investigation.

5.2 Coarse-graining via Gauge-fixing

5.2.1 Coarse-grained States

This part shows how the gauge invariance takes into account the boundary: the gauge invariance of wave-function with respect to bulk gauge transformations leads to covariant gauge transformations on the boundary. This leads to the definition of coarse-graining via gauge-fixing.

Consider local gauge transformations at vertices, which leads to gauge transformation along bulk edges in this way: $g_e \mapsto h_{t(e)} g_e h_{s(e)}^{-1}$. The boundary state determined by wave-function transformed covariantly via dressing the boundary edges with boundary holonomies [52]:

$$|\psi_{\partial\Gamma}(\{h_{t(e)} g_e h_{s(e)}^{-1}\}_{e\in\Gamma^o})\rangle = \left(\bigotimes_{e\in\partial\Gamma} h_{v(e)}^{\epsilon_e^v}\right) |\psi_{\partial\Gamma}(\{g_e\}_{e\in\Gamma^o})\rangle\,, \tag{5.2.1}$$

where $v(e)$ for $e \in \partial\Gamma$ denotes the vertex to which the boundary edge is attached, and $\epsilon_e^v = -1$ is for the outward boundary edge $v(e) = s(e)$ while $\epsilon_e^v = 1$ is for the inward boundary edge $v(e) = t(e)$.

The gauge-fixing is based on the covariance. Following the earlier work on spin networks [183] and subsequent works [38, 184, 169, 52, 40, 43, 185], we choose an arbitrary root vertex $u \in \Gamma$ and a maximal tree in the bulk graph $T \subset \Gamma^o$. A tree is a set of edges that never form any cycle (or loop). A maximal tree T has $(V-1)$ edges. Furthermore, for any vertex $v \in \Gamma$, it defines a unique path of edges $P[u \to v] \subset T$ along the tree linking the root vertex u to the vertex v. This allows to gauge-fix all the group elements along tree edges to the identity, $g_{e\in T} \mapsto \mathbb{I}$, by choosing gauge transformations h_v at every

vertex but the root vertex as:

$$h_v = \left(\overleftarrow{\prod_{\ell \in P[u \to v]}} g_\ell \right)^{-1} , \tag{5.2.2}$$

where the product of group elements is taken from right to left over g_ℓ if the edge ℓ is oriented in the same direction than the path $P[u \to v]$ and over its inverse g_ℓ^{-1} otherwise. This maps all the group elements on tree edges to the identity, $h_{t(e)} g_e h_{s(e)}^{-1} = \mathbb{I}$ for $e \in T$. The remaining edges, which do not belong the tree actually correspond to a minimal generating set of loops (or cycles) on the bulk graph Γ^o. Indeed, each non-tree edge defines a loop from the root vertex to the edge and back,

$$\mathcal{L} = \{e | e \in \Gamma^o \setminus T\} , \qquad e \in \mathcal{L} : u \underset{T}{\to} s(e) \underset{e}{\to} t(e) \underset{T}{\to} v_0 .$$

The number of loops is $L = E^o - V + 1$ where E^o is the number of bulk edges. One can show that every cycle on the bulk graph Γ^o can generate from those cycles. For $e \in \mathcal{L}$, the gauge transformation built above does not map the group element g_e to the identity anymore but maps it to the holonomy around the corresponding loop,

$$\forall e \in \mathcal{L} , \qquad h_{t(e)} g_e h_{s(e)}^{-1} = \overleftarrow{\prod_{\ell \in \mathcal{L}_e}} g_\ell \equiv G_e .$$

As a consequence, we obtain the gauge-fixed boundary state in line with eq.(5.2.1)

$$|\psi_{\partial\Gamma}(\{g_e\}_{e \in \Gamma^o})\rangle = \left(\bigotimes_{e \in \partial\Gamma} h_{v(e)}^{\epsilon_e^v} \right) |\psi_{\partial\Gamma}(\{G_e\}_{e \in \mathcal{L}}, \{\mathbb{I}\}_{e \in T})\rangle . \tag{5.2.3}$$

That is, we glue boundary edges along the maximal tree T such that the spin network transforms to a loopy spin network Υ to which L of loops are attached, i.e.,

$$\Upsilon = \partial\Gamma \sqcup \mathcal{L} \sqcup u , \qquad \partial\Upsilon = \partial\Gamma , \qquad \Upsilon^o = \mathcal{L} \sqcup u . \tag{5.2.4}$$

This is one of definitions for coarse-graining procedure [38]. The graph after the coarse-graining procedure is visualized as a vertex plus boundary edges and self-loops. We refer to the single vertex as *loop vertex* (even there is not self-loop at all), since it likely has some self-loop. We also refer to the graph with single loopy vertex as *loop spin network*, even though the work 'network' was usually phrased the cases of multi-node.

Note that nothing is changed by the gauge-fixing procedure, since every vertex is assumed to be gauge invariant. Then it is free for us to think of the $|\psi_{\partial\Gamma}(\{G_e\}_{e \in \mathcal{L}}, \{\mathbb{I}\}_{e \in T})\rangle$ in Eq.(5.2.3) providing an identical bulk-boundary map as a loopy spin network based on Υ. That is to mean, a bulk-boundary is actually defined by an equivalent class whose members can be related by gauge-fixings.

Conversely, we can consider the transformation between the members within equivalent class. We will explain this point more in Section 5.4. Before it, let us look at the notion of bulk probability.

5.2.2 Bulk Probability

Now that the bulk wave-function has been promoted to a map from bulk degrees of freedom to boundary state, in a logic following topological field theories, the corresponding probability distribution for the bulk fields is given by the boundary space scalar product instead of the mere squared modulus:

$$\psi(\{g_e\}_{e\in\Gamma^o}) \in \mathcal{H}_{\partial\Gamma}\,, \qquad \mathcal{P}(\{g_e\}_{e\in\Gamma^o}) = {}_\partial\langle\psi(\{g_e\}_{e\in\Gamma^o})|\psi(\{g_e\}_{e\in\Gamma^o})\rangle_\partial\,, \tag{5.2.5}$$

where we use '${}_\partial\langle\ |\ \rangle_\partial$' to denote the scalar product for boundary Hilbert space $\mathcal{H}_{\partial\Gamma}$, which is the nature extension of usual SU(2) scalar product to tensor product Hilbert space, i.e., $\mathcal{P}(\{g_e\}_{e\in\Gamma^o})$ is evaluated by usual SU(2) scalar product for spin states $|\{j,m\}\rangle \in \mathcal{H}_{\partial\Gamma}$.

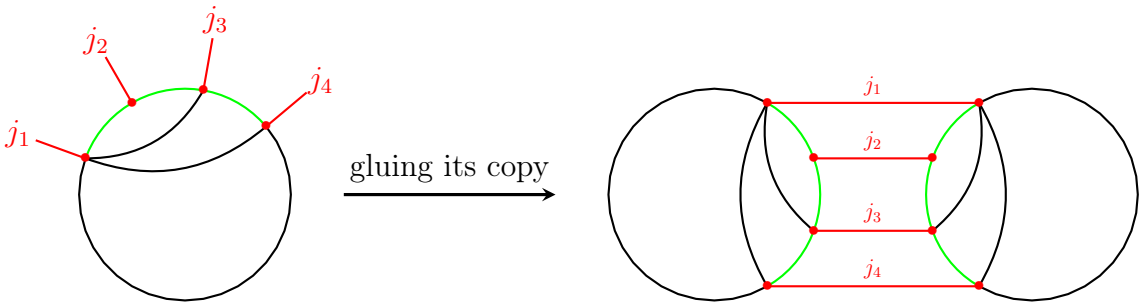

Figure 5.5: Gluing the two copies of the spin network into the boundary density matrix: boundary edges (red lines) are glued together using the boundary space scalar product, and for each copy; the maximal tree for the bulk gauge fixing consist in the green edges, while the remaining edges, in black, define the independent loops of the bulk graph .

To have wave-function's squared modulus, we are gluing two copies of the spin network with trivial holonomies along the open edges on the boundary, for instance, as illustrated in fig.5.5. This yields a totally gauge-invariant probability distribution, despite the gauge covariance of the wave-function under boundary gauge transformations:

$$\mathcal{P}(\{g_e\}_{e\in\Gamma}) = \mathcal{P}(\{h_{t(e)}g_e h_{s(e)}^{-1}\}_{e\in\Gamma}) \quad \forall h_v \in \mathrm{SU}(2)^V\,, \tag{5.2.6}$$

with no difference between bulk and boundary vertices or edges.

With the gauge-fixing technique, we can prove below proposition:

Proposition 5.1. *Let ψ_Γ and ϕ_Γ be any two spin networks on same graph Γ. The corresponding boundary states are $|\psi_{\partial\Gamma}(\{g_e\}_{e\in\Gamma^o})\rangle$ and $|\phi_{\partial\Gamma}(\{g_e\}_{e\in\Gamma^o})\rangle$, respectively. Then the scalar product for boundary Hilbert space is a function depending only on L of group elements, i.e.,*

$${}_\partial\langle\psi_{\partial\Gamma}(\{g_e\}_{e\in\Gamma^o})|\phi_{\partial\Gamma}(\{g_e\}_{e\in\Gamma^o})\rangle_\partial = F_{\psi\phi}(G_1,\cdots,G_L)\,. \tag{5.2.7}$$

Moreover, the function is invariant under conjugation:

$$F_{\psi\phi}(G_1,..,G_L) = F_{\psi\phi}(h\,G_1\,h^{-1},\cdots,h\,G_L\,h^{-1})\,, \quad \forall\, h\in\mathrm{SU}(2)\,. \tag{5.2.8}$$

Proof. Since spin networks ψ_Γ and ϕ_Γ based on same graph Γ, we repeat the gauge-fixing implementation for ψ_Γ to ϕ_Γ. The gauge-fixing leads to identical boundary holonomies with respect to eq.(5.2.3). As a consequence, the scalar product for $\mathcal{H}_{\partial\Gamma}$ depends only on these L of group elements,

$$\begin{aligned}{}_\partial\langle\psi_{\partial\Gamma}(\{g_e\}_{e\in\Gamma^o})|\phi_{\partial\Gamma}(\{g_e\}_{e\in\Gamma^o})\rangle_\partial =&{}_\partial\langle\psi_{\partial\Gamma}(\{G_e\}_{e\in\mathcal{L}},\{\mathbb{I}\}_{e\in T})|\phi_{\partial\Gamma}(\{G_e\}_{e\in\mathcal{L}},\{\mathbb{I}\}_{e\in T})\rangle_\partial\\ \equiv&F_{\psi\phi}(G_1,\cdots,G_L)\,,\end{aligned} \tag{5.2.9}$$

since for every boundary edges, the boundary holonomies are undone by the scalar product for $\mathcal{H}_{\partial\Gamma}$: ${}_\partial\langle j_e m_e|h^\dagger h|j'_e m'_e\rangle_\partial = {}_\partial\langle j_e m_e|j'_e m'_e\rangle_\partial = \delta_{j_e j'_e}\delta_{m_e m'_e}$. □

For spin networks ψ_Γ, $\phi_{\tilde{\Gamma}}$ based on different graphs, the boundary holonomies cannot be undone by scalar product ${}_\partial\langle\ |\ \rangle_\partial$. But thanks for graph orthogonality, the scalar product for $(\mathcal{H}_\mathcal{B})^*$ simply vanishes after integrating holonomies.

Particularly, for the cases that $\psi_\Gamma = \phi_\Gamma$, one could define the probability with respect to bulk holonomies,

$$\mathcal{P}(\{g_e\}_{e\in\Gamma}) := {}_\partial\langle\psi_{\partial\Gamma}(\{g_e\}_{e\in\Gamma^o})|\psi_{\partial\Gamma}(\{g_e\}_{e\in\Gamma^o})\rangle_\partial = F_{\psi\psi}(G_1,\cdots,G_L)\,. \tag{5.2.10}$$

As a consequence of Proposition 5.1, the bulk probability distribution depends only on those L group elements:

$$\mathcal{P}(\{g_e\}_{e\in\Gamma}) = \mathcal{P}(\{G_e\}_{e\notin T},\{\mathbb{I}\}_{e\in T}) \equiv \mathcal{P}_{GF}(G_1,..,G_L)\,. \tag{5.2.11}$$

Putting aside the gauge-fixed group elements living on the tree edges and focusing on the non-trivial loop holonomies, this gauge-fixed bulk probability $\mathcal{P}_{GF}$ is still invariant under gauge transformation at the root vertex v_0:

$$\mathcal{P}_{GF}(G_1,..,G_L) = \mathcal{P}_{GF}(h\,G_1\,h^{-1},\cdots,h\,G_L\,h^{-1})\,,\quad \forall\, h\in\mathrm{SU}(2)\,. \tag{5.2.12}$$

This directly implies two simple results:

Proposition 5.2. *The configuration $G_1 = \cdots = G_L = \mathbb{I}$, representing a flat* SU(2) *connection, is always a stationary point for the bulk probability function $\mathcal{P}(\{g_e\}) = \langle\psi(\{g_e\}_{e\in\Gamma^o})|\psi(\{g_e\}_{e\in\Gamma^o})\rangle$.*

We leave the proof in Appendix B. According to the proposition, we can interpret SU(2) Ponzano-Regge model (c.f. [186]) as a particular configuration with flat holonomies.

Proposition 5.3. *If the bulk graph Γ^o is a tree, i.e. does not contain any loop, then the bulk probability function $\mathcal{P}(\{g_e\})$ is constant and does not depend on the bulk holonomies g_e.*

Proof. If bulk graph Γ^o doesn't contain loop, the bulk probability function $\mathcal{P}(\{g_e\})$ doesn't have dependency on G_i as (5.2.11), thus it is a constant. □

5.3 The closure defect basis

In the framework of the coarse-graining of spin networks introduced in [43], the total spin J is the tag and the multiplicity states $I \in \mathcal{N}_J^{\{j_e\}}$ are tagged intertwiners. We would like to introduce the closure defect basis for boundary states, which amounts to decompose them according to the total boundary spin, since the SU(2) gauge invariance is enforced by the closure constraint, which is a discretization of the Gauss law of the first order formulation of general relativity [40, 187]. Assuming that the boundary edges are all outward (or all inward) to simplify the orientation conventions, we recouple all the boundary spins j_e into their total spin J:

$$\mathcal{H}_{\partial\Gamma} = \bigoplus_{\{j_e\}_{e\in\partial\Gamma}} \bigotimes_e \mathcal{V}_{j_e} = \bigoplus_{\{j_e\}_{e\in\partial\Gamma}} \bigoplus_J \mathcal{V}_J \otimes \mathcal{N}_J^{\{j_e\}}\,, \tag{5.3.1}$$

where the multiplicity spaces (or degeneracy spaces) $\mathcal{N}_J^{\{j_e\}}$ consist in the spaces of intertwiners (i.e. SU(2)-invariant states) in the tensor product of the total spin Hilbert space $\mathcal{V}^J$ with the individual spins $\bigotimes_e \mathcal{V}_{j_e}$,

$$\mathcal{N}_J^{\{j_e\}} := \mathrm{Inv}_{\mathrm{SU}(2)}\left[\mathcal{V}_J \otimes \bigotimes_{e\in\partial\Gamma} \mathcal{V}_{j_e}\right]. \tag{5.3.2}$$

Here, due to the bulk spin network structure, the total spin J is necessary an integer. Instead of the decoupled basis $|\{j_e, m_e\}_e\rangle$, we use the recoupled basis, as illustrated on fig.5.6:

$$\mathcal{H}_{\partial\Gamma} = \bigoplus_{\{j_e\}_{e\in\partial\Gamma}} \bigoplus_{J,M} \bigoplus_{I^{(J,\{j_e\})}} \mathbb{C}|J,M\rangle \otimes |(J,\{j_e\}),I\rangle = \bigoplus_{J,M} \bigoplus_{\{j_e\}} \bigoplus_{I^{(J,\{j_e\})}} \mathbb{C}|J,M\rangle \otimes |(J,\{j_e\}),I\rangle\,, \tag{5.3.3}$$

where the $I^{(J,\{j_e\})} = |(J,\{j_e\}),I\rangle$'s are a basis of intertwiners in the multiplicity space $\mathcal{N}_J^{\{j_e\}}$. We might write $I^{(J)}$ instead of $I^{(J,\{j_e\})}$ whenever we don't need to explicitly specify the value of the boundary spins. These intertwiner states not only encode the recoupled total spin J, but also how the individual spins j_e are weaved together.

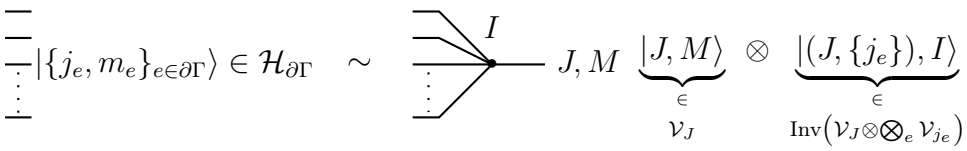

Figure 5.6: Recoupled basis for boundary states in terms of the total boundary spin (or closure defect) J.

5.4 Boundary Hilbert Space and Dual Boundary Hilbert Space

5.4.1 Scalar Products of Dual Boundary Hilbert Space

In principle, it is free to view bulk-boundary maps as spin network wave-functions. This subsection is meant to clarify some details for establishing the Hilbert space of bulk-boundary maps. We especially deal with the scalar products of boundary Hilbert space and bulk Hilbert space separately.

We first clarify the scalar product for boundary Hilbert space $\mathcal{H}_{\partial\Gamma}$ or $\mathcal{H}_{\mathcal{B}}$. Now $\mathcal{H}_{\partial\Gamma}$ is the tensor product of spin states living on the boundary edges. Suppose $\{|j_e m_e\rangle\}$ basis states for a $\mathcal{V}_{j_e}$, then ${}_\partial\langle j_e m_e | j'_e m'_e\rangle_\partial = \delta_{j_e j'_e}\delta_{m_e m'_e}$. We adopt '${}_\partial\langle\ |\ \rangle_\partial$' to denote the scalar product for the $\mathcal{H}_{\mathcal{B}}$ as in subsection 5.2.2.

Bulk-boundary maps are considered as linear form living in dual Hilbert space $(\mathcal{H}_{\partial\Gamma})^*$. To see this, consider any boundary state $|\Phi_{\mathcal{B}}\rangle$. The boundary Hilbert space's scalar product for $|\Phi_{\mathcal{B}}\rangle$ and $|\psi_{\partial\Gamma}(\{g_e\}_{e\in\Gamma^o})\rangle$ defines a distribution on boundary states depending on the group elements, or holonomies,

$$\forall\, |\Phi_{\mathcal{B}}\rangle \in \mathcal{H}_{\mathcal{B}}\,, \qquad {}_\partial\langle \Phi_{\mathcal{B}} | \psi_{\partial\Gamma}(\{g_e\}_{e\in\Gamma^o})\rangle_\partial \in \mathbb{C}\,. \tag{5.4.1}$$

One does not need to integrate any bulk holonomies. The complex number is evaluated by assigning every g_e. To illustrate, there are three situations:

- Assume $|\Phi_{\mathcal{B}}\rangle$ does not depend on any holonomies at all (i.e. quantum boundary condition). That is, $|\Phi_{\mathcal{B}}\rangle$ allows for a linear combination in terms of the basis vectors $\mathcal{H}_{\mathcal{B}}$. In that case, the coefficients of the linear combination are complex numbers without dependency of holonomies, thus

$$|\Phi_{\mathcal{B}}\rangle = \bigotimes_{e\in\partial\Gamma} |j_e m_e\rangle\,, \qquad {}_\partial\langle \Phi_{\mathcal{B}} | \psi_{\partial\Gamma}(\{g_e\}_{e\in\Gamma^o})\rangle_\partial \in \mathcal{F}\big[\mathrm{SU}(2)^{\{e\in\Gamma^o\}}\big]\,, \tag{5.4.2}$$

  i.e., the dependency of holonomies are all due to $|\psi_{\partial\Gamma}(\{g_e\}_{e\in\Gamma^o})\rangle$.

- Assume $|\Phi_{\mathcal{B}}\rangle = |\phi_{\partial\Gamma}(\{g_e\}_{e\in\Gamma^o})\rangle$ is a boundary state that corresponds to another spin network wave-function ϕ_Γ based on the same graph. Again, the $|\Phi_{\mathcal{B}}\rangle$ allows for a linear combination in terms of the basis vectors $\mathcal{H}_{\mathcal{B}}$. In that case, the linear combination coefficients depend on holonomies, thus

$$|\Phi_{\mathcal{B}}\rangle = |\phi_{\partial\Gamma}(\{g_e\}_{e\in\Gamma^o})\rangle\,, \qquad {}_\partial\langle \phi_{\partial\Gamma}(\{g_e\}_{e\in\Gamma^o}) | \psi_{\partial\Gamma}(\{g_e\}_{e\in\Gamma^o})\rangle_\partial \in \mathcal{F}\big[\mathrm{SU}(2)^{\{e\in\mathcal{L}\}}\big]\,, \tag{5.4.3}$$

  where the $\mathcal{L}$ is the set of loop edges, with less number of holonomies than the number of bulk edges. We will explain this in the next subsection.

- Assume $|\Phi_{\mathcal{B}}\rangle = |\phi_{\partial\widetilde{\Gamma}}(\{g_{\widetilde{e}}\}_{\widetilde{e}\in\widetilde{\Gamma}^o})\rangle$ is a boundary state that corresponds to spin network wave-function $\phi_{\widetilde{\Gamma}}$ based on a different graph $\widetilde{\Gamma}$, i.e., $\widetilde{\Gamma} \neq \Gamma$. The number of holonomies is more than the number of Γ^o or $\widetilde{\Gamma}^o$, i.e.,

$$|\Phi_{\mathcal{B}}\rangle = |\phi_{\partial\widetilde{\Gamma}}(\{g_{\widetilde{e}}\}_{\widetilde{e}\in\widetilde{\Gamma}^o})\rangle\,, \qquad {}_\partial\langle \phi_{\partial\widetilde{\Gamma}}(\{g_{\widetilde{e}}\}_{\widetilde{e}\in\widetilde{\Gamma}^o}) | \psi_{\partial\Gamma}(\{g_e\}_{e\in\Gamma^o})\rangle_\partial \in \mathcal{F}\big[\mathrm{SU}(2)^{\{e\in\Gamma^o\cup\widetilde{\Gamma}^o\}}\big]\,. \tag{5.4.4}$$

The quantum boundary condition $|\Phi_{\mathcal{B}}\rangle$ in the first situation is considered as 'no bulk degree of freedom at all', while the $|\Phi_{\mathcal{B}}\rangle$ in the second and third situations are considered as carrying bulk degrees of freedom.

Overall, the scalar product for $\mathcal{H}_{\mathcal{B}}$ gives a distribution depending on holonomies. We can define the scalar product thus to establish the dual boundary Hilbert space $(\mathcal{H}_{\mathcal{B}})^*$ via integration over holonomies. We denote $|\psi_{\partial\Gamma}\rangle$ the member of $(\mathcal{H}_{\mathcal{B}})^*$. A $|\psi_{\partial\Gamma}\rangle$ corresponds to a boundary state $|\psi_{\partial\Gamma}(\{g_e\}_{e\in\Gamma^o})\rangle \in \mathcal{H}_{\partial\Gamma}$ depending on holonomies, or equivalently, corresponds to spin network wave-function $\psi_\Gamma(\{g_e\}_{e\in\Gamma^o})$. For any two $|\phi_{\partial\widetilde{\Gamma}}\rangle, |\psi_{\partial\Gamma}\rangle \in (\mathcal{H}_{\mathcal{B}})^*$, the scalar product for the dual boundary Hilbert space $(\mathcal{H}_{\mathcal{B}})^*$ is:

$$\langle\phi_{\partial\widetilde{\Gamma}}|\psi_{\partial\Gamma}\rangle = \begin{cases} \int \prod_{e\in\Gamma^o} \mathrm{d}g_e \; {}_\partial\langle\phi_{\partial\Gamma}(\{g_e\}_{e\in\Gamma^o})|\psi_{\partial\Gamma}(\{g_e\}_{e\in\Gamma^o})\rangle_\partial\,, & \Gamma = \widetilde{\Gamma}\,, \\ 0\,, & \partial\Gamma = \partial\widetilde{\Gamma}\,, \quad \Gamma^o \neq \widetilde{\Gamma}^o\,. \end{cases} \tag{5.4.5}$$

The first equation of eq.(5.4.5) is equivalent to the scalar product for $\mathcal{H}_\Gamma$ defined by eq.(2.2.5)

$$\begin{aligned} \langle\phi_{\partial\Gamma}|\psi_{\partial\Gamma}\rangle &= \int \prod_{e\in\Gamma^o} \mathrm{d}g_e \; {}_\partial\langle\phi_{\partial\Gamma}(\{g_e\}_{e\in\Gamma^o})|\psi_{\partial\Gamma}(\{g_e\}_{e\in\Gamma^o})\rangle_\partial \\ &= \int \prod_{e\in\Gamma} \mathrm{d}g_e \; \overline{\phi_\Gamma(\{g_e\}_{e\in\Gamma})}\,\psi_\Gamma(\{g_e\}_{e\in\Gamma}) = \langle\phi_\Gamma|\psi_\Gamma\rangle\ . \end{aligned} \tag{5.4.6}$$

Note that the integrals for boundary holonomies in the second line are equivalent to the scalar product for $\mathcal{H}_{\partial\Gamma}$ in the first line. In fact, it does not matter to add boundary holonomies for the first line since they are boundary unitary transformations and ${}_\partial\langle jm|g^\dagger g|j'm'\rangle_\partial = {}_\partial\langle jm|j'm'\rangle_\partial = \delta_{jj'}\delta_{mm'}$. The second equation of eq.(5.4.5) is due to the graph orthogonality in LQG. One could confirm this orthogonality from spin network wave-function form Eq.(2.4.21) or Eq.(2.2.16): If $\Gamma^o \neq \widetilde{\Gamma}^o$, and let us suppose $e \in \Gamma^o$ but $e \notin \widetilde{\Gamma}^o$, then g_e appears only once in the integration. Due to Peter-Weyl theorem (2.2.11), the spin carried by e must be $j = 0$, meaning that the edge e is degenerate.

Therefore, we define dual boundary Hilbert space $(\mathcal{H}_{\mathcal{B}})^*$ via decomposition

$$(\mathcal{H}_{\mathcal{B}})^* = \bigoplus_{\Gamma|\,\partial\Gamma=\mathcal{B}} (\mathcal{H}_{\partial\Gamma})^*\,. \tag{5.4.7}$$

The normalization of $|\psi_{\partial\Gamma}\rangle$ is expressed as

$$\langle\psi_{\partial\Gamma}|\psi_{\partial\Gamma}\rangle = \int \prod_{e\in\Gamma^o} \mathrm{d}g_e \; {}_\partial\langle\psi_\Gamma(\{g_e\}_{e\in\Gamma^o})|\psi_\Gamma(\{g_e\}_{e\in\Gamma^o})\rangle_\partial = 1\,. \tag{5.4.8}$$

Up to now, we have defined the scalar product for dual boundary Hilbert space $(\mathcal{H}_{\mathcal{B}})^*$. Let us close this subsection by summing up the three scalar products:

- The scalar product '${}_\partial\langle\ |\ \rangle_\partial$' for boundary Hilbert space $\mathcal{H}_{\partial\Gamma}$ does not integrate bulk holonomies, so insensitive to the bulk's graph structure.

- The scalar product '$\langle \phi_{\widetilde{\Gamma}} | \psi_{\Gamma} \rangle$' for spin network Hilbert space and scalar product '$\langle \phi_{\partial\widetilde{\Gamma}} | \psi_{\partial\Gamma} \rangle$' for dual boundary Hilbert space are always equal, i.e.,

$$\langle \phi_{\widetilde{\Gamma}} | \psi_{\Gamma} \rangle = \langle \phi_{\partial\widetilde{\Gamma}} | \psi_{\partial\Gamma} \rangle \ . \tag{5.4.9}$$

In principle, the scalar product for $\mathcal{H}_{\partial\Gamma}$ can also be defined by the scalar product for $\mathcal{H}_{\Gamma}$ by considering boundary holonomies [188]. The advantage of using bulk-boundary maps method is that we analyze the boundary holonomies and bulk holonomies separately. For instance, evaluating $\langle \phi_{\partial\Gamma} | \psi_{\partial\Gamma} \rangle$ requires less number of integrals to holonomies, leading to coarse-graining. Let us explain in more details.

5.4.2 Unitary transformations underlying dual boundary Hilbert spaces

This subsection is to read the boundary holonomies and channel transformations as unitary maps for $(\mathcal{H}_{\mathcal{B}})^*$. Thus the coarse-graining via gauge-fixing is viewed as a consequence of the unitarity of $(\mathcal{H}_{\mathcal{B}})^*$. It will be useful when comes to entanglement topic.

Following the analysis below eq.(5.2.3), there exists a loopy spin network state mapping identically as the gauge-fixed spin network state, i.e.

$$|\psi_{\partial\Gamma}(\{G_e\}_{e\in\mathcal{L}}, \{\mathbb{I}\}_{e\in T})\rangle = |\psi_{\partial\Upsilon}(\{G_e\}_{e\in\mathcal{L}})\rangle \, . \tag{5.4.10}$$

So eq.(5.2.9) can be written as

$${}_{\partial}\langle \psi_{\partial\Gamma}(\{g_e\}_{e\in\Gamma^o}) | \phi_{\partial\Gamma}(\{g_e\}_{e\in\Gamma^o})\rangle_{\partial} = {}_{\partial}\langle \psi_{\partial\Upsilon}(\{G_e\}_{e\in\mathcal{L}}) | \phi_{\partial\Upsilon}(\{G_e\}_{e\in\mathcal{L}})\rangle_{\partial} \, , \tag{5.4.11}$$

and the scalar product for $(\mathcal{H}_{\partial\Gamma})^* \subset (\mathcal{H}_{\mathcal{B}})^*$,

$$\begin{aligned} \langle \psi_{\partial\Gamma} | \phi_{\partial\Gamma} \rangle &= \int \prod_{e\in\Gamma^o} \mathrm{d}g_e \, {}_{\partial}\langle \psi_{\partial\Gamma}(\{g_e\}_{e\in\Gamma^o}) | \phi_{\partial\Gamma}(\{g_e\}_{e\in\Gamma^o})\rangle_{\partial} \\ &= \int \prod_{e\in\Upsilon^o} \mathrm{d}G_e \, {}_{\partial}\langle \psi_{\partial\Upsilon}(\{G_e\}_{e\in\mathcal{L}}) \, | \, \phi_{\partial\Upsilon}(\{G_e\}_{e\in\mathcal{L}})\rangle_{\partial} = \langle \psi_{\partial\Upsilon} | \phi_{\partial\Upsilon} \rangle \, . \end{aligned} \tag{5.4.12}$$

From the second equality to the third, only L number of integrals will be taken account, since the rest of integrals are trivial $\int_{\mathrm{SU}(2)} \mathrm{d}g_e = 1$.

Notably, the correspondence between $|\psi_{\partial\Gamma}(\{g_e\}_{e\in\Gamma^o})\rangle$ and $|\psi_{\partial\Upsilon}(\{G_e\}_{e\in\mathcal{L}})\rangle$ is one-to-many, since there are many doable implementations for gauge-fixing. But the wanted relation $\langle \psi_{\partial\Gamma} | \phi_{\partial\Gamma} \rangle = \langle \psi_{\partial\Upsilon} | \phi_{\partial\Upsilon} \rangle$ is not affected by how to gauge-fix.

Eq.(5.4.12) sheds light on the unitary maps for $(\mathcal{H}_{\mathcal{B}})^*$. Given a spin network state, we implement gauge-fix to obtain a loopy spin network state such that the two states provides identical bulk-boundary maps up to boundary holonomies, i.e., from $|\psi_{\partial\Gamma}\rangle$ to $|\psi_{\partial\Upsilon}\rangle$,

$$|\psi_{\partial\Gamma}(\{g_e\}_{e\in\Gamma^o})\rangle = \left(\bigotimes_{e\in\partial\Gamma} h_{v(e)}^{\epsilon_e^v} \right) |\psi_{\partial\Upsilon}(\{G_e\}_{e\in\Gamma^o})\rangle \equiv \mathcal{G}_{\mathcal{B}} \triangleright |\psi_{\partial\Upsilon}(\{G_e\}_{e\in\Upsilon^o})\rangle \, , \tag{5.4.13}$$

where $\mathcal{G}_{\mathcal{B}}$ denotes the operation of boundary holonomies. The reverse problem, i.e., how to recover $|\psi_{\partial\Gamma}\rangle$ from $|\psi_{\partial\Upsilon}\rangle$ is worth studying, which may appear elsewhere. At the present stage, one should remember that the reverse procedure is doable and related to manipulating boundary holonomies.

In the present work, we also consider another type of unitary transformation. The $\mathcal{H}_{\Upsilon}$ is the intertwiner space for the loopy vertex, and is defined according to (2.4.18),

$$\mathcal{H}_{\Upsilon} := \mathrm{Inv}_{\mathrm{SU}(2)}\left[\bigotimes_{e\in\partial\Upsilon|\, u=s(e)} \mathcal{V}_{j_e} \otimes \bigotimes_{e\in\partial\Upsilon|\, u=t(e)} \mathcal{V}_{j_e}^{*} \otimes \bigotimes_{e'\in\mathcal{L}} \left(\mathcal{V}_{j_{e'}} \otimes \mathcal{V}_{j_{e'}}^{*}\right)\right] . \tag{5.4.14}$$

Then we denote $\mathcal{U}_{\Upsilon}$, the channel transformation for the loopy intertwiner. $\mathcal{U}_{\Upsilon}$ is just for redefinition of internal labels for the intertwiner (e.g. Fig.5.7). To see this more specifically, for instance in Fig.5.7b, we can gauge fix the holonomy g_5. After the gauge-fixing, the nontrivial holonomies are either along boundary edges or loop edges in bulk. For the next, we temporarily disregard the boundary holonomies, since one can counterbalance them with boundary holonomies. For holonomy along the loop edge (here is the edge associated to j_6), we can cut it into three piecewise edges, where the middle of the three is carrying the nontrivial loop holonomy $g_5^{-1}g_6$, and the other two (the two ends of the original edge) are carrying trivial holonomies. Now we temporarily do not look at the piecewise edge carrying nontrivial holonomy. The remain spin network (without loop) turns out to be represented by a $3nj$-symbol, which is a unitary transformation in the loopy intertwiner space. Finally, we retrieve back the piecewise edge carrying nontrivial holonomies $g_5^{-1}g_6$, and acquire the right-hand side in Fig.5.7b. The analysis can be generalized straightforwardly to the cases with many loop edges.

In order to study the coarse-graining via gauge-fixing in later chapters, we list the two classes of unitary transformations for the dual boundary Hilbert space $(\mathcal{H}_{\mathcal{B}})^*$:

(a) Boundary holonomies for boundary unitary transformation $\mathcal{G}_{\mathcal{B}} : \mathcal{H}_{\mathcal{B}} \longrightarrow \mathcal{H}_{\mathcal{B}}$.

(b) Channel transformation for loopy intertwiner unitary transformation $\mathcal{U}_{\Upsilon} : \mathcal{H}_{\Upsilon} \longrightarrow \mathcal{H}_{\Upsilon}$.

Both particular $\mathcal{G}_{\mathcal{B}}$ and $\mathcal{U}_{\Upsilon}$ never change the boundary representations, i.e. change the boundary spins. Moreover, they are mutually commutative, i.e., $\mathcal{G}_{\mathcal{B}} \circ \mathcal{U}_{\Upsilon} = \mathcal{U}_{\Upsilon} \circ \mathcal{G}_{\mathcal{B}}$.

Let us close the subsection by summing up the above discussions:

Proposition 5.4. *Let $\mathcal{B}$ be boundary of spin network and $\mathcal{H}_{\mathcal{B}}$ be the boundary Hilbert space associated to $\mathcal{B}$, a unitary map for the dual boundary Hilbert space $(\mathcal{H}_{\mathcal{B}})^*$ preserves the scalar product*

$$\left\langle \phi_{\partial\widetilde{\Gamma}} \middle| \psi_{\partial\Gamma} \right\rangle = \begin{cases} \langle \phi_{\partial\Upsilon} | \psi_{\partial\Upsilon} \rangle \ , & \Gamma = \widetilde{\Gamma} \, , \\ 0 \, , & \Gamma \neq \widetilde{\Gamma} \, . \end{cases} \tag{5.4.15}$$

Here Υ is the coarse-grained graph (loopy spin network) induced from Γ. We can compose boundary holonomies $\mathcal{G}_{\mathcal{B}} : \mathcal{H}_{\mathcal{B}} \longrightarrow \mathcal{H}_{\mathcal{B}}$ and channel transformation $\mathcal{U}_{\Upsilon} : \mathcal{H}_{\Upsilon} \longrightarrow \mathcal{H}_{\Upsilon}$ to define the unitary map $\mathcal{U}_{\mathcal{B}} : (\mathcal{H}_{\mathcal{B}})^* \longrightarrow (\mathcal{H}_{\mathcal{B}})^*$ via $\mathcal{U}_{\mathcal{B}} = \mathcal{G}_{\mathcal{B}} \circ \mathcal{U}_{\Upsilon}$.

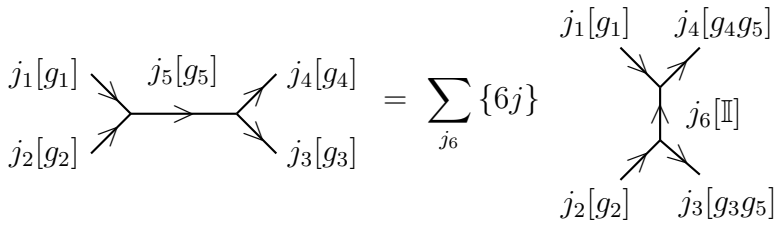

(a) The $6j$-symbol represents the unitary matrix for the channel transformation.

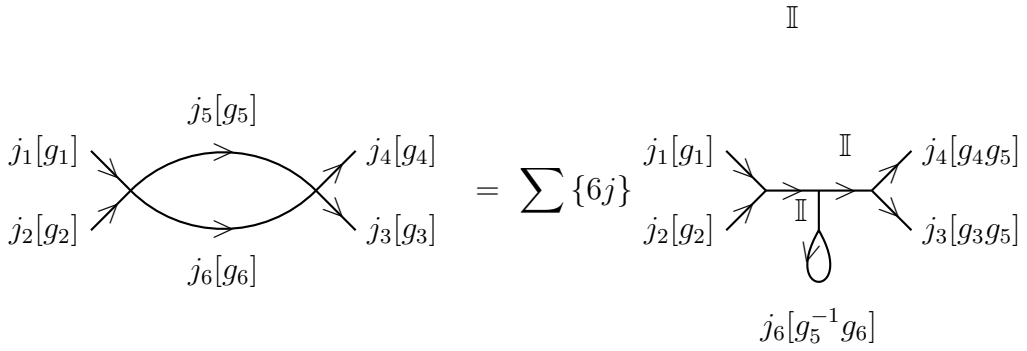

(b) The $6j$-symbol represents the unitary matrix for the channel transformation. The right hand side is equivalent to a loopy spin network in the sense of bulk-boundary map.

Figure 5.7: Channel transformations for spin networks with tree and loop.

In particular, suppose $|\psi_{\partial\Gamma}(\{g_e\}_{e\in\Gamma^o})\rangle \in (\mathcal{H}_{\partial\Gamma})^*$ *and* $|\psi_{\partial\Upsilon}(\{G_e\}_{e\in\Upsilon^o})\rangle \in (\mathcal{H}_{\partial\Upsilon})^*$. *Let* $\left\{|\Psi_{\Gamma,\{I_v\}}\rangle\right\}$ *be orthonormal basis for* $\mathcal{H}_\Gamma$ *and* $\left\{|\Psi_{\Upsilon,I_u}\rangle\right\}$ *be orthonormal basis for* $\mathcal{H}_\Upsilon$. *Then according to eq.(5.4.10), they are related by:*

$$|\psi_{\partial\Gamma}(\{g_e\}_{e\in\Gamma^o})\rangle = \Big[\mathcal{U}_{\mathcal{B}}\Big]^\dagger \triangleright |\psi_{\partial\Upsilon}(\{G_e\}_{e\in\Upsilon^o})\rangle\,, \tag{5.4.16}$$

$$|\Psi_{\partial\Gamma,\{I_v\}}(\{g_e\}_{e\in\Gamma^o})\rangle = \sum_{I_u} \Big[\mathcal{U}_{\mathcal{B}}\Big]^{I_u}_{\{I_v\}_{v\in\Gamma}} \triangleright |\Psi_{\partial\Upsilon,I_u}(\{G_e\}_{e\in\Upsilon^o})\rangle\,. \tag{5.4.17}$$

The first line expresses the Schrödinger picture for the unitary transformation, and the second line expresses the Heisenberg picture for the unitary transformation.

We have clarified the unitary transformation for dual boundary Hilbert space. It is beneficial in clarifying the local unitary transformation with respect to loop spin network, as in Chapter 8.

In the quest to understand the holographic nature of gravitational interaction and quantum gravity, it is essential to investigate the bulk-boundary relation and interplay. It goes both ways: on the one hand, we need to understand the boundary modes and dynamics induced by the bulk degrees of freedom, and on the other hand, we need to understand how boundary conditions propagate within and throughout the bulk at both classical and quantum levels. Such holographic mapping between bulk and boundary theories needs to be achieved at multiple levels: the symmetry groups, the dynamics, the quantum states, and the algebra of observables.

In this chapter, to start analyzing the potential holographic behavior of loop quantum gravity, we introduced explicit 2d boundaries to the 3d space, i.e., space-time corners. This 2d boundary admits a Hilbert space of boundary states, understood as quantum boundary conditions. Then loop quantum gravity's spin network states for the bulk geometry become *bulk-boundary maps*, wave-functions still depending on bulk fields or degrees of freedom but valued in the boundary Hilbert space (instead of $\mathbb{C}$ for standard quantum mechanics). In some sense, bulk wave-functions can be interpreted as quantum circuits acting on the boundary states. In other words, bulk-boundary map emphasizes the relation between input and output, defining a coarse-graining in the sense that the bulk graph structure is now behind the scenes. Via gauge-fixing, the coarse-graining meaning is illustrated further. The bulk degrees of freedom for spin network states are the SU(2) holonomies of the Ashtekar-Barbero connection along the graph links. In contrast, the boundary states are the spin states living on the spin network open edges puncturing the 2d boundary surface. As expected, the squared norm of the bulk wave-function using the scalar product of the boundary Hilbert space gives the probability distribution for the bulk holonomies.

At the end of the chapter, we define dual boundary Hilbert space by equipping it with the scalar product of spin network Hilbert space. We claim that the definition is analogous to the manner for solving diffeomorphism. The advantage of defining dual boundary Hilbert space is two-fold: (i) in Chapter 6 it gives induced boundary density matrix via tracing over bulk holonomies, which is another coarse-graining procedure beside via gauge-fixing; (ii) In Chapter 8 it facilitates the partial trace for spin sub-networks.

Chapter 6

Boundary Density Matrices and Reconstructed Bulk States

In Chapter 5, Eq.(5.1.1) and Eq.(5.1.2) are interpreted as probability distribution for the bulk observables dependent on the choice of boundary states, i.e. quantum boundary conditions: once $\Phi_{\mathcal{B}}$ is fixed, the function

$$\langle \Phi_{\mathcal{B}} | \psi[\cdot] \rangle : \varphi_{bulk} \mapsto \langle \Phi_{\mathcal{B}} | \psi[\varphi_{bulk}] \rangle \in \mathbb{C}$$

is a standard $\mathbb{C}$-valued wave-function for the bulk fields. In this chapter, we reverse this logic and look at the probability distribution for the boundary observables after integration over the bulk fields. In that case,

$$\rho_{\partial}[\psi] = \int [\mathcal{D}\varphi_{bulk}] \, |\psi[\varphi_{bulk}]\rangle\langle\psi[\varphi_{bulk}]| \in \mathrm{End}[\mathcal{H}_{\mathcal{B}}] \tag{6.0.1}$$

is the density matrix induced on the boundary by the bulk state ψ. The goal of this chapter is to study the latter case in the framework of loop quantum gravity and clearly define this bulk-to-boundary coarse-graining (via tracing-bulk) from bulk spin networks to boundary density matrix. This entails extending the spin network states of the 3d bulk geometry in $\mathcal{R}$ to include the boundary degrees of freedom on the corner $\mathcal{S}$. As we will explain in the present chapter, this can be done in a natural way in loop quantum gravity since spin networks can be geometrically interpreted as aggregates of area quanta, glued together to create 3d spaces from 2d excitations, and can thus be naturally extended to include the area quanta on the 2d boundary $\mathcal{S}$. A spin network wave-function on an open graph then naturally defines a linear form on the Hilbert space of spin states living on the open edges of the graph, as illustrated on fig.5.3 and thus induces a boundary density matrix.

This chapter is based on [52]. Section 6.1 starts with the definition of the coarse-graining procedure via tracing-bulk from which an induced boundary density matrix is obtained. The most important result in this chapter is presented in Result 6.2 in Section 6.2. It states a universal bulk reconstruction procedure: starting from a gauge-invariant density matrix on the boundary Hilbert space, we show that one can always obtain it as the induced boundary density matrix of a spin network state on the bulk graph with a

single vertex connected to all the boundary edges and to a single bulk loop. This can be understood as a purification result since it shows how an arbitrary gauge-invariant mixed state on the boundary can be lifted to a pure bulk spin network state. In Section 6.3, we investigate the finer structure of the induced boundary density matrices in terms of boundary vertices and bouquets of boundary edges. Section 6.4 finally presents explicit examples with the candy graphs, made of two vertices connected with bulk links, with four boundary edges, and then with six boundary edges. This illustrates the various levels of mixed states one can obtain on the boundary in loop quantum gravity.

6.1 Boundary Density Matrices: Coarse-Graining via Tracing-Bulk

We would like to shift the focus from the bulk to the boundary and investigate in more details the boundary state induced by the bulk spin network state defined as the density matrix obtained by integrating over the group elements, or in other words, taking the partial trace over bulk holonomies:

$$\rho_{\partial\Gamma}[\psi] = \int \prod_{e\in\Gamma^o} \mathrm{d}g_e \, |\psi(\{g_e\}_{e\in\Gamma^o})\rangle\langle\psi(\{g_e\}_{e\in\Gamma^o})| \, \in \mathrm{End}(\mathcal{H}_{\partial\Gamma}) \,, \tag{6.1.1}$$

$$\mathrm{Tr}\, \rho_{\partial\Gamma}[\psi] = \int [\mathrm{d}g_e] \, \langle\psi(\{g_e\}_{e\in\Gamma^o})|\psi(\{g_e\}_{e\in\Gamma^o})\rangle = \int [\mathrm{d}g_e] \, \mathcal{P}(\{g_e\}_{e\in\Gamma^o}) \,.$$

This mixed state on the boundary can be considered as a coarse-graining of the bulk spin network state [38, 189]. For this reason, we particularly refer it as *coarse-graining via tracing-bulk*, in order to distinguish the procedure *coarse-graining via gauge-fixing*. The goal of this paper is to compare the data encoded in the bulk wave-function ψ_Γ and in the induced boundary density matrix $\rho_{\partial\Gamma}$.

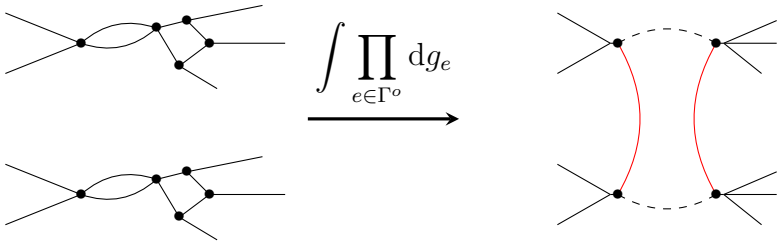

Figure 6.1: Boundary density matrix for spin network basis states. The two copies of the spin networks are the bra $\langle\psi|$ and ket $|\psi\rangle$ which are glued together by the Haar integration over the bulk holonomies $\int \prod \mathrm{d}g_{e\in\Gamma^o}$.

Let us start by looking at normalized pure spin network basis states, i.e. with fixed spins j_e and fixed normalized intertwiners I_v. They are factorized states in the sense that the intertwiners are decoupled so that there is no intertwiner entanglement as discussed in [190]. As a result, the boundary state only depends on the intertwiners living on the

boundary vertices (i.e. the vertices with at least one boundary edge) and not on the bulk intertwiners. Let us insist that "boundary vertices" are still in the bulk, the adjective "boundary" refers to the fact that they are connected to boundary edges. Indeed, the orthonormality of the Wigner matrices implies that that each bulk edge is cut in half and both half-edges are glued with their counterparts on the second copy of the wave-function, as illustrated on fig.6.1. We get the norm of every bulk intertwiner, normalized to 1, times the contribution from boundary intertwiners which gives the boundary density matrix:

$$\begin{aligned}
&\langle\{\tilde{k}_e,\tilde{m}_e\}\,|\rho_{\partial\Gamma}[\Psi_{\{j_e,I_v\}}]|\{k_e,m_e\}\rangle \\
&= \prod_e \delta_{k_e,j_e}\delta_{\tilde{k}_e,j_e} \prod_{v\in\partial\Gamma} \langle \bigotimes_{\substack{e\in\partial\Gamma\\ v\in e}} j_e\tilde{m}_e \otimes \bigotimes_{\substack{e\in\Gamma^o\\ v=s(e)}} j_e m_e^s|\, I_v \,|\bigotimes_{\substack{e\in\Gamma^o\\ v=t(e)}} j_e m_e^t\rangle \\
&\overline{\langle \bigotimes_{\substack{e\in\partial\Gamma\\ v\in e}} j_e m_e \otimes \bigotimes_{\substack{e\in\Gamma^o\\ v=s(e)}} j_e m_e^s|\, I_v \,|\bigotimes_{\substack{e\in\Gamma^o\\ v=t(e)}} j_e m_e^t\rangle}\,.
\end{aligned} \tag{6.1.2}$$

Assuming that each boundary edge is attached to a different vertex, i.e. each boundary vertex connects to a single boundary edge, this tremendously simplifies. Indeed, as illustrated on fig. 6.2, the self-gluing of an intertwiner on itself leads to the identity matrix on the open edge. As a consequence, the density matrix is the totally mixed state with fixed spin on each boundary edge:

$$\rho_{\partial\Gamma}[\Psi_{\{j_e,I_v\}}] = \bigotimes_{e\in\partial\Gamma} \frac{\mathbb{I}_{j_e}}{(2j_e+1)}\,. \tag{6.1.3}$$

This boundary density matrix, for a spin network basis state, clearly does not allow to see the bulk structure!

In the slightly more general case of boundary vertices connected to several boundary edges, the boundary density matrix reflects the first layer of the bulk and "sees" the total recoupled spin of the boundary edges for each boundary edge. We will analyze this case in more details in the later section 6.3.

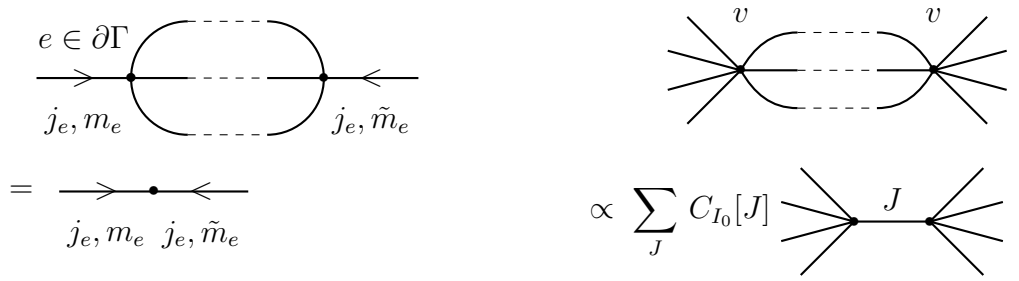

Figure 6.2: Boundary vertex contribution to the boundary density matrix from the self-gluing of intertwiners: single boundary edge vs many boundary edges.

Spin network basis states are actually very peculiar and are a very special case for the bulk quantum geometry. They are eigenstates for geometrical observables, such as areas

and volumes, but there are not coherent states with minimal spread on both connection and triad (i.e. on parallel transport and metric) and they do not commute with the Hamiltonian constraints. More generally, physically relevant states will be superposition of such spin network basis states, thus superposition of spins and intertwiners, leading to correlation and entanglement between bulk vertices, in which case the boundary density matrix will become non-trivial. Before analyzing in more details the structure of the boundary density matrix, let us underline the main two features of the boundary state as compared to the bulk state:

- The boundary state $\rho_{\partial\Gamma}$ is typically mixed even if the bulk spin network state is pure [38, 189]. Thus a coarse-graining via tracing-bulk procedure trading the bulk states for the boundary state irremediably creates entropy. In particular, endowing the bulk states with a unitary dynamics would naturally lead to a decoherence process (and possibly re-coherence) for the boundary states [191, 172].

- The boundary state $\rho_{\partial\Gamma}$ does not decompose onto intertwiners between the boundary spins, even though the bulk spin network is made out of individual intertwiners, as pointed out in [38, 40, 44]. Indeed, the density matrix is invariant under the action by conjugation of the SU(2) group,

$$\forall h \in \mathrm{SU}(2)\,, \quad \langle \{\tilde{k}_e, \tilde{m}_e\} \,|\, h^{-1}\rho_{\partial\Gamma}[\psi]h \,|\, \{k_e, m_e\}\rangle = \langle \{\tilde{k}_e, \tilde{m}_e\} \,|\rho_{\partial\Gamma}[\psi]|\{k_e, m_e\}\rangle \tag{6.1.4}$$

  where the SU(2) transformation acts simultaneously on all the boundary edges. It is however not invariant under gauge transformations acting on left or right, $\rho_{\partial\Gamma} \mapsto h^{-1}\rho_{\partial\Gamma}$ or $\rho_{\partial\Gamma} \mapsto \rho_{\partial\Gamma}h$. This means that the total spin of the boundary state does not vanish. In fact the boundary defines an intertwiner between the two copies of the wave-function, the bra $\langle\psi(\{g_e\}_{e\in\Gamma^\circ})|$ and the ket $|\psi(\{g_e\}_{e\in\Gamma^\circ})\rangle$, as illustrated on fig.6.1. The recoupled spin (closure defect) J between the boundary edges defines the overall channel between the bra and the ket. The $J = 0$ component is the component with vanishing total boundary spin - in usual jargon, the intertwiner component. It represents the "closed" or flat component, while the components with $J \neq 0$ can be interpreted as bulk curvature. From the viewpoint of coarse-graining, it reflects that curvature builds up when gluing flat blocks -the intertwiners- together [40]. The gauge symmetry breaking at the boundary, due to allowing $J \neq 0$, can be also understood as responsible for the entropy of isolated horizon (and thus black holes) in the loop quantum gravity framework [192, 193, 190] (see [194, 45] for a more general discussion of gauge symmetry and symmetry breaking on the boundary of gauge field theories). At the end of the day, the closure defect, or total spin, provides a very useful basis to study the structure of boundary states and of induced boundary density matrices.

6.1.1 Bulk state to boundary density matrix

6.1.2 SU(2)-invariance of the boundary density matrix

As introduced in Section 5.3, in the framework of the coarse-graining of spin networks introduced in [43], the total spin J is the tag and the multiplicity states $I \in \mathcal{N}_J^{\{j_e\}}$ are

tagged intertwiners. From a physical standpoint, the multiplicity spaces $\mathcal{N}_J^{\{j_e\}}$ for spin recoupling give the black hole horizon micro-states in a naïve leading order approach to black hole (micro-canonical) entropy and holography in loop quantum gravity, e.g. [195, 196, 197, 198, 199, 200].

Let us focus on the case with fixed boundary spins $\{j_e\}$, although this is a mere alleviation of the notations, since the spins j_e can be implicitly absorbed in the definition of the recoupling intertwiner $I^{(J,\{j_e\})}$. The bulk wave-function evaluated on bulk holonomies is a boundary state and can thus be decomposed onto the recoupled basis:

$$|\psi(\{g_e\}_{e\in\Gamma^o})\rangle = \sum_J \sum_M \sum_{I^{(J)}} C_{JMI}(\{g_e\}_{e\in\Gamma^o})|J,M\rangle \otimes |J,I^{(J)}\rangle\,, \tag{6.1.5}$$

where the coefficients $C_{JMI}(\{g_e\}_{e\in\Gamma^o})$ reflect the internal bulk structure of the wave-functions and depend on the bulk spins and intertwiners. SU(2) gauge transformations act non-trivially on the wave-function by the group action on the boundary spins. Now, as we have seen earlier, the density matrix $\rho_\partial = \int \mathrm{d}g_e\, |\psi(g_e)\rangle\langle\psi(g_e)|$ is invariant under conjugation by the simultaneous SU(2) action on all the boundary spins $\bigotimes_e D^{j_e}(h)$. This is a direct consequence of the bulk SU(2) gauge invariance,

$$\begin{aligned}
\forall\, h\in \mathrm{SU}(2)\,, \qquad \rho_{\partial\Gamma}[\psi] &= \int \prod_e \mathrm{d}g_e\, |\psi(\{g_e\}_{e\in\Gamma^o})\rangle\langle\psi(\{g_e\}_{e\in\Gamma^o})| \\
&= \int \prod_e \mathrm{d}g_e\, |\psi(\{h\, g_e\, h^{-1}\}_{e\in\Gamma^o})\rangle\langle\psi(\{h\, g_e\, h^{-1}\}_{e\in\Gamma^o})| \\
&= \int \prod_e \mathrm{d}g_e\, h|\psi(\{g_e\}_{e\in\Gamma^o})\rangle\langle\psi(\{g_e\}_{e\in\Gamma^o})|h^{-1} \qquad (6.1.6)\\
&= h\,\rho_{\partial\Gamma}[\psi]\,h^{-1}\,. \qquad (6.1.7)
\end{aligned}$$

This SU(2) action on the boundary boils down to the SU(2) action on the recoupled spin $D^J(h)$ and does not touch the multiplicity sector,

$$h \triangleright |\psi(\{g_e\}_{e\in\Gamma^o})\rangle = \sum_J \sum_{M,N} \sum_{I^{(J)}} C_{JMI}(\{g_e\}_{e\in\Gamma^o})\, D^J_{\tilde{M}M}(h)\, |J,\tilde{M}\rangle \otimes |J,I\rangle\,. \tag{6.1.8}$$

This means that the invariance of the boundary density matrix, $h\,\rho_\partial\, h^\dagger = \rho_\partial$ for all group elements $h\in\mathrm{SU}(2)$ implies it is necessarily totally mixed on each subspace at fixed total spin J and that all the information is encoded in the multiplicity subspaces. Recalling Lemma 3.5, the case here is expressed more precisely by the following lemma (here J must be integer):

Lemma 6.1. *A normalized* SU(2)*-invariant density matrix ρ, thus satisfying $h\,\rho\, h^\dagger = \rho\,, \forall\, h\in\mathrm{SU}(2)$, has the following form:*

$$\rho = \bigoplus_{J\in\mathbb{N}} p(J)\frac{\mathbb{I}_{\mathcal{V}_J}}{2J+1}\otimes\rho_{\mathcal{N}_J}\,, \qquad \mathrm{Tr}\rho = \sum_J p(J) = 1\,. \tag{6.1.9}$$

The coefficients $p(J)$ define the probability distribution over the total spin J. The operator $\mathbb{I}_{\mathcal{V}_J} = \sum_M |J,M\rangle\langle J,M|$ is the identity on $\mathcal{V}_J$ and $\rho_{\mathcal{N}_J}$ is an arbitrary density matrix in the multiplicity space $\mathcal{N}_J$.

The SU(2) invariance is a key property of the boundary density matrix, which descends directly from the gauge invariance of the bulk wave-functions under local SU(2) transformations. Let us stress the important point that this is a statistical invariance under the SU(2) action, at the level of the density matrix. This does not amount to the invariance of pure quantum states on the boundary. Indeed strict SU(2) invariance of the wave-function (i.e. $h\,\rho = \rho\,h^\dagger = \rho$) would require $J = 0$, while we can have here an arbitrary distribution over all (allowed) values of the total spin J.

6.2 Universal bulk reconstruction from the boundary density matrix

The natural question is how much can we know about the bulk structure from the boundary density matrix. For instance, does the combinatorial structure of the bulk graph deeply affect the type of boundary density matrix one gets? Here, we show a universal reconstruction procedure. As hinted by the work in [44], a single bulk loop is enough to get arbitrary boundary density matrices. More precisely, any arbitrary SU(2)-invariant density matrix on the boundary Hilbert space can be induced from a pure bulk state on the single loop bulk graph. We prove this powerful result below. This can be understood as a boundary-to-bulk purification theorem.

Result 6.2. *A mixed state ρ on the boundary Hilbert space $\mathcal{H}_\mathcal{B}$ is* SU(2)*-invariant, $h\,\rho\,h^\dagger = \rho$, if and only if it is an induced boundary density matrix (IBDM) from a pure (gauge-invariant) bulk state $|\psi(\{g_e\}_{e\in\Gamma^o})\rangle$ for some bulk graph Γ^o connecting the boundary edges.*

Proof. We already know that induced boundary density matrices are SU(2)-invariant. We have to show the reverse statement. Let us consider an arbitrary SU(2)-invariant density matrix,

$$\rho = \bigoplus_J p(J)\frac{\mathbb{I}_{\mathcal{V}_J}}{2J+1}\otimes\rho_{\mathcal{N}_J}\,,$$

and let us diagonalize the density matrices for each multiplicity subsector,

$$\rho_{\mathcal{N}_J} = \sum_{r=1}^{R_J} W_{I_r}^{(J)}\,|J, I_r^{(J)}\rangle\langle J, I_r^{(J)}|\,, \tag{6.2.1}$$

where R_J is the rank of $\rho_{\mathcal{N}_J}$ and the intertwiners $I_r^{(J)}$ are orthonormal states in the multiplicity space $\mathcal{N}_J$.

Let us consider the bulk graph, as [44], with a single vertex tying all the boundary edges to a single loop as drawn on fig 7.8. Then a spin network state is a superposition of intertwiners between the boundary spins and the (pair of) spin(s) carried by the loop. We can unfold this intertwiner with a (virtual) link between the boundary edge and the loop. This (virtual) intermediate link carries the total boundary spin J. For each value of J, we need to specify the spin k carried by the loop and the two intertwiners at the nodes. The three-valent intertwiner recoupling the loop spin k to the total spin J is unique (when it

exists), while the intertwiner recoupling the boundary spins $\{j_e\}$ into J will naturally be the intertwiners $I_r^{(J)}$.

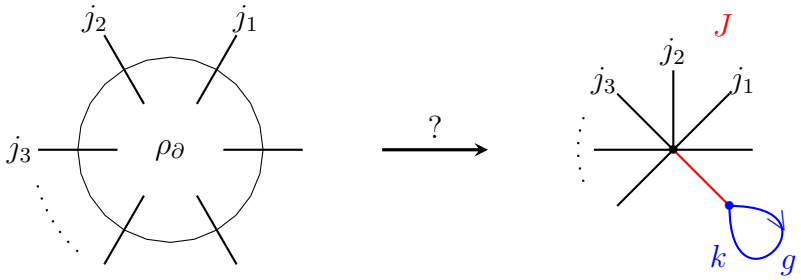

Figure 6.3: The universal reconstruction procedure purifying a SU(2)-invariant boundary density matrix into a pure spin network superposition for a bulk made of a single vertex and single loop.

Indeed, for each value of the total spin J, we choose R_J distinct spins $k_r^{(J)}$ for the loop with $J \leq 2k_{r(J)}$, so that $\mathcal{V}_J \subset \mathcal{V}_k \otimes \mathcal{V}_k$, i.e. the loop spin can recouple to J, i.e. there exists a 3-valent intertwiner (given by the corresponding Clebsh-Gordan coefficients). We then define the following pure spin network for the 1-loop graph, in terms of a single bulk holonomy g on the loop,

$$|\psi(g)\rangle = \sum_{J,M} \sqrt{p(J)} |J,M\rangle \otimes \sum_{r}^{R_J} \sum_{m,n}^{k_r^{(J)}} (-1)^{k_r^{(J)}+m} \sqrt{2k_r^{(J)}+1}\, D^{k_r^{(J)}}_{nm}(g) \times \begin{pmatrix} J & k_r^{(J)} & k_r^{(J)} \\ M & -m & n \end{pmatrix} \sqrt{W_{I_r}^{(J)}}\, |J, I_r^{(J)}\rangle \,. \tag{6.2.2}$$

It is straightforward to check this boundary pure state leads back to the wanted SU(2)-invariant density matrix (6.2.1) upon integration over the bulk holonomy g.

□

It is quite remarkable that the superposition of loop spins and bulk intertwiners naturally leads to mixed boundary density matrices.

6.3 Probing the first layer of the bulk: bouquets of boundary edges

Up to now, we have defined the boundary density matrix induced by a bulk spin network state, underlined the fact that the resulting boundary density matrix is typically mixed for a pure spin network state and showed how to construct such a pure bulk state on a graph with at least one loop given a (suitably gauge invariant) boundary density matrix. This universal reconstruction procedure, given above in the proof of Result 6.2,

with a bulk graph made of a single vertex and a single bulk loop, should be understood as a purification of the boundary density matrix into a bulk state. There are nevertheless many possible bulk states on possibly complicated graphs inducing the same boundary state, leading to many ways to purify a given mixed boundary state. In light of this fact, we wish to understand better how the bulk graph structure and potential correlations between the spins and intertwiners within the bulk possibly get reflected in the boundary density matrix.

In this section, we would like to start diving into the bulk, or at least start probing the first layer of the bulk beyond the boundary edges. More precisely, we would like to see the "boundary vertices", i.e. the vertices to which are attached boundary edges, and understand if a finer study of the boundary density matrix allows to extract the information about whether bunches of boundary edges are attached to the same boundary vertex. Indeed, although a rather natural assumption is that each boundary edge connected to a different vertex in the bulk, this is not a generic configuration. A more general configuration involves boundary edges regrouped into bouquets, each attached to a vertex, as illustrated on Fig.6.4.

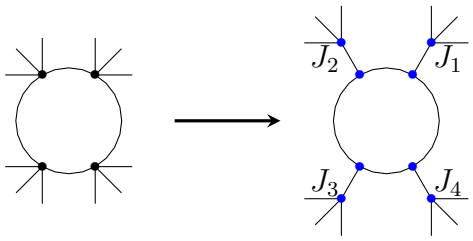

Figure 6.4: Bouquets of boundary edges attached to boundary vertices $v \in V^\partial$ and the chicken feet basis labeled by the recoupled spin J_v for each bouquet.

This leads us to introduce a "chicken feet" basis where we recouple the spin of the boundary edges of each bouquet separately instead of only considering the total recoupled spin J. We thus introduce the bouquet spin J_v for each boundary vertex v. Writing V^∂ for the set of boundary vertices, the boundary Hilbert space decomposes as:

$$\mathcal{H}_\mathcal{B} = \bigoplus_{\{j_e\}_{e\in\partial}} \bigotimes_{e\in\partial} \mathcal{V}_{j_e} = \bigoplus_{\{J_v\}_{v\in V^\partial}} \bigotimes_{v\in V^\partial} \mathcal{V}_{J_v} \otimes \mathcal{N}_{\{J_v\}}\,, \tag{6.3.1}$$

$$\mathcal{N}_{\{J_v\}} = \bigotimes_{v\in V^\partial} \bigoplus_{\{j_e\}_{e\,|\,v\in\partial e}} \mathrm{Inv}\Big[\mathcal{V}_{J_v} \otimes \bigotimes_{e\,|\,v\in\partial e} \mathcal{V}_{j_e}\Big]\,, \tag{6.3.2}$$

leading to the chicken feet basis states $|\{J_v\}_{v\in V^\partial}, \{j_e\}_{e\in\partial}, \{\mathcal{I}^{J_v}_{\{j_e\}}\}_{v\in V^\partial}\rangle$ labelled by the boundary edge spins j_e, the boundary bouquet spins J_v and the intertwiners recoupling them, as depicted on fig.6.4.

As for the bulk, we similarly unfold the intertwiner states living on the boundary vertices and decompose them into two intertwiners, one "boundary" component which recouples all the boundary spins into J_v and one "bulk" component which recouples the spins on the remaining bulk edges attached to the vertex to J_v, as illustrated on fig.6.5.

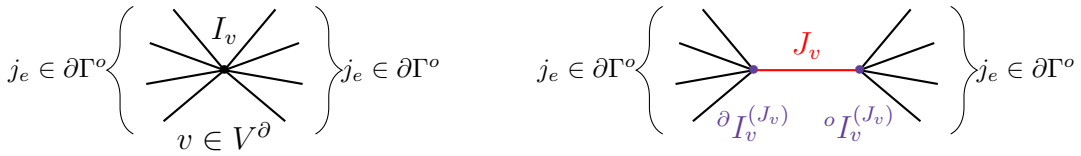

Figure 6.5: Unfolding intertwiners on boundary vertices: the decomposition into boundary and bulk intertwiner components.

Decomposed intertwiner basis states are then labeled by the boundary and bulk spins attached to the (boundary) vertex, the bouquet spin J_v and the two boundary and bulk intertwiner, $|\{j_e\}_{e\in\partial}, J_v, {}^\partial I_v^{(J_v)}, {}^o I_v^{(J_v)}\rangle$.

The reconstruction of the first layer of the bulk from the boundary density matrix simply reflects the fact that the boundary component of the intertwiners I_v at a vertex attached to some boundary edges matches the boundary intertwiner recoupling the boundary spins to their bouquet spins, i.e. $\mathcal{I}^{J_v}_{\{j_e\}} = {}^\partial I_v^{(J_v)}$ for a boundary vertex $v \in V^\partial$ and for all values of the bouquet spin J_v. Let us see more precisely how this gets encoded into the boundary density matrix.

To alleviate the notations, let us fix the spins j_e on the boundary edges $e \in \partial\Gamma$, although it is straightforward to allow arbitrary superpositions of the boundary spins. In light of the SU(2) gauge transformations at the vertices and the resulting SU(2) gauge invariance of the boundary density matrix at each boundary vertex, a boundary density matrix necessarily reads:

$$\rho_\partial = \sum_{\{J_v\}_{v\in V^\partial}} \bigotimes_{v\in V^\partial} \frac{\mathbb{I}_{J_v}}{(2J_v+1)} \otimes \rho_{\{J_v\}}\,, \tag{6.3.3}$$

where, for each value of the bouquet spins $\{J_v\}$, we have the totally mixed state on the spin states and a possibly non-trivial density matrix $\rho_{\{J_v\}}$ on the corresponding multiplicity space,

$$\rho_{\{J_v\}} \in \mathrm{End}[\mathcal{N}_{\{J_v\}}]\,, \qquad \mathcal{N}_{\{J_v\}} = \bigotimes_{v\in V^\partial} \mathrm{Inv}\Big[\mathcal{V}_{J_v} \otimes \bigotimes_{e\,|v\in\partial e} \mathcal{V}_{j_e}\Big]\,, \tag{6.3.4}$$

since we are working at fixed boundary spins $j_{e\in\partial}$.

For spin network basis state, a straightforward calculation leads to the multiplicity matrices $\rho_{\{J_v\}}$ simply given by the boundary components of the intertwiners living at the boundary vertices:

Lemma 6.3. *For a spin network basis state $\Psi_{\{j_e,I_v\}}$ with given spins j_e on all bulk and boundary edges, as well as chosen intertwiner states I_v at each vertex, we decompose the intertwiner states living on boundary vertices in the bouquet spin basis separating their "boundary" component from their "bulk" component,*

$$\forall v \in V^\partial\,, \quad I_v = \sum_{J_v} C_v(J_v)\,|J_v, {}^\partial I_v^{(J_v)}, {}^o I_v^{(J_v)}\rangle\,, \tag{6.3.5}$$

with normalized intertwiners ${}^{\partial}I_v^{(J_v)}$ *and* ${}^{\partial}I_v^{(J_v)}$*, respectively between the boundary spins and the bouquet spin, then between the bouquet spin and the bulk spins attached to the vertex* v*. Then the induced boundary density matrix reads:*

$$\rho_\partial[\Psi_{\{j_e,I_v\}}] = \sum_{\{J_v\}_{v\in V^\partial}} \bigotimes_{v\in V^\partial} \frac{\mathbb{I}_{J_v}}{(2J_v+1)} \otimes \rho_{\{J_v\}}\,, \qquad \textit{where} \quad |{}^{\partial}I_v^{(J_v)}\rangle \in \mathrm{Inv}\Big[\mathcal{V}_{J_v} \otimes \bigotimes_{e\,|v\in\partial e} \mathcal{V}_{j_e}\Big]\,. \tag{6.3.6}$$

The multiplicity matrices $\rho_{\{J_v\}}$ *have rank-one:*

$$\rho_{\{J_v\}} = |\iota_{\{J_v\}}\rangle\langle\iota_{\{J_v\}}|\,, \quad \iota_{\{J_v\}} = \bigotimes_{v\in V^\partial} C_v(J_v)|{}^{\partial}I_v^{(J_v)}\rangle \;\in \mathcal{N}_{\{J_v\}}\,. \tag{6.3.7}$$

This rank-one property obviously extends to possible spin network superposition states with correlation between bouquet spins, i.e. with coefficients $C(\{J_v\})$ generalizing the factorized ansatz $\prod_v C_v(J_v)$ of basis states, but is ruined as soon as there is non-trivial superpositions of the bulk components of the boundary intertwiners or more generally non-trivial intertwiner correlations between the bulk vertices. Indeed, let us consider a generic spin network state:

$$\psi = \sum_{\{j_e\},\{I_v\}} C^{\{j_e\}_{e\in\partial\Gamma},\{j_e\}_{e\in\Gamma^o}}_{\{J_v\}_{v\in V^\partial}}(\{{}^{\partial}I_v^{(J_v)}, {}^{o}I_v^{(J_v)}\}_{v\in V^\partial}, \{I_w\}_{w\notin V^\partial}) \bigotimes_{v\in V^\partial} \Big({}^{\partial}I_v^{(J_v)} \otimes {}^{o}I_v^{(J_v)}\Big) \otimes \bigotimes_{w\notin V^\partial} I_w \\ \in \mathcal{H}_\Gamma\,, \tag{6.3.8}$$

where we use the notation v for the boundary vertices and w for the remaining vertices of the bulk graph. We have chosen an arbitrary orthonormal basis of intertwiners I_w for bulk vertices while using explicitly the bouquet spin basis for the boundary vertices. A straightforward calculation yields the following induced boundary density matrix:

$$\rho_\partial[\psi] \;=\; \sum_{\{J_v\}_{v\in V^\partial}} \bigotimes_{v\in V^\partial} \frac{\mathbb{I}_{J_v}}{(2J_v+1)} \otimes \rho_{\{J_v\}}\,, \tag{6.3.9}$$

$$\rho_{\{J_v\}} \;=\; \sum_{\partial I_v, \widetilde{\partial I_v}} \sum_{j_e, {}^{o}I_v, I_w} C^{\{j_e\}}_{\{J_v\}}(\{\widetilde{{}^{\partial}I_v^{(J_v)}}, {}^{o}I_v^{(J_v)}\}, \{I_w\})\, \overline{C^{\{j_e\}}_{\{J_v\}}(\{{}^{\partial}I_v^{(J_v)}, {}^{o}I_v^{(J_v)}\}, \{I_w\})} \\ \bigotimes_{v\in V^\partial} |\widetilde{{}^{\partial}I_v^{(J_v)}}\rangle\langle {}^{\partial}I_v^{(J_v)}|\,. \tag{6.3.10}$$

The integration over the bulk holonomies amounts in the end to the partial trace over the bulk intertwiners (i.e. the intertwiner states at the vertices not connected to any boundary edge), over the bulk component of the intertwiners at the boundary vertices, and over the spins of the graph edges. This partial trace naturally leads to mixed states on the multiplicity spaces $\mathcal{N}_{\{J_v\}}$ with higher rank multiplicity matrices $\rho_{\{J_v\}}$. This means that non-trivial bulk correlations (between bulk intertwiners and bulk spins) get reflected in the rank of the multiplicity matrices $\rho_{\{J_v\}}$. This is a much finer witness of the bulk structure than the overall closure defect.

This hints towards a natural layer-by-layer reconstruction of the bulk from the boundary density matrix. Starting from ρ_∂, one can try the various partitions of the boundary,

grouping the boundary edges, and check which partition leads to a multiplicity matrix with the lowest rank, and thus with the least correlation between boundary vertices. Once the first layer of the bulk graph, one would thank follow the same logic to reconstruct the second layer of the bulk, grouping the bouquets together so that the second layer intertwiners are the least correlated possible. We would pursue this onion-like reconstruction until we reach the inner loop of the universal reconstruction procedure described in the previous section. It would be enlightening if one could translate this idea of a bulk with the least correlation between graph vertices into an action principle whose extrema would determine the bulk structure from the quantum boundary data fixed by the chosen boundary density matrix.

6.4 Examples: Boundary Density Matrix for Candy Graphs

We would like to conclude this paper with explicit examples of the bulk-to-boundary procedure, from bulk spin networks to boundary density matrices. We will consider the case of a bulk graph with two boundary vertices. The deeper bulk structure does not matter and it is enough to consider a single loop to which the bulk edges connect. We consider the two examples of boundary vertices each with two boundary edges, and then each with three boundary edges, as drawn on fig.6.6.

Figure 6.6: Candy graphs.

6.4.1 The four-qubit candy graph

Let us describe the graph with two vertices linked by a single loop and each with two boundary edges, as drawn on fig.6.7. We assume that the spin on the four boundary edges are fixed to $j_1 = j_2 = j_3 = j_4 = \frac{1}{2}$ and we also fix the spin around the loop to an arbitrary value k. The bulk Hilbert space thus consists in the tensor product of the spaces of intertwiners living at the two vertices α and β:

$$\mathcal{H}_{bulk} = \mathcal{H}_\alpha \otimes \mathcal{H}_\beta \,, \qquad \mathcal{H}_\alpha = \mathcal{H}_\beta = \mathrm{Inv}[\mathcal{V}_{\frac{1}{2}} \otimes \mathcal{V}_{\frac{1}{2}} \otimes \mathcal{V}_k \otimes \mathcal{V}_k] \,. \tag{6.4.1}$$

For each vertex, $v = \alpha$ or $v = \beta$, we recouple the two boundary spins, leading to the bouquet spin basis. Here the bouquet spin J_v can take two values, 0 or 1, and entirely determines the intertwiner state:

$$\mathcal{H}_v = \mathrm{Inv}[\mathcal{V}_{\frac{1}{2}} \otimes \mathcal{V}_{\frac{1}{2}} \otimes \mathcal{V}_k \otimes \mathcal{V}_k] = \mathbb{C}|J=0\rangle \oplus \mathbb{C}|J=1\rangle \,, \quad \dim \mathcal{H}_v = 2 \,, \tag{6.4.2}$$

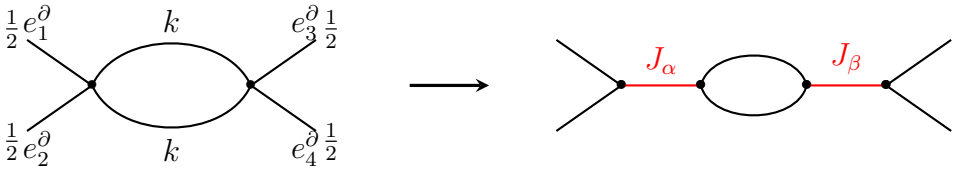

Figure 6.7: 4-qubit candy graph: spin and intertwiner decomposition.

so that bulk spin network basis states are labelled by the two bouquet spins[1]:

$$\mathcal{H}_{bulk} = \bigoplus_{J_\alpha, J_\beta \in \{0,1\}} \mathbb{C}|J_\alpha, J_\beta\rangle\,, \quad \dim \mathcal{H}_{bulk} = 4\,. \tag{6.4.3}$$

The boundary Hilbert space consists in the tensor product of the four spin-$\frac{1}{2}$ spaces, i.e. it is made of four qubits,

$$\mathcal{H}_\partial = \left(\mathcal{V}_{\frac{1}{2}}\right)^{\otimes 4}\,, \qquad \dim \mathcal{H}_\partial = 2^4\,. \tag{6.4.4}$$

Let us consider an arbitrary spin network state,

$$\psi = \sum_{J_\alpha, J_\beta} C_{J_\alpha, J_\beta} |J_\alpha, J_\beta\rangle \in \mathcal{H}_{bulk}\,. \tag{6.4.5}$$

The corresponding wave-function defines a boundary map, mapping the bulk holonomy along the two links of the inner loop to a boundary state in $\mathcal{H}_\partial$:

$$\begin{aligned} & |\psi(g_1, g_2)\rangle \\ = & \sum_{a_i, b_i} (-1)^{k-a_1}(-1)^{k-a_2} D^k_{a_1 b_1}(g_1) D^k_{a_2 b_2}(g_2) \langle (k,-a_1)(k,-a_2)|J_\alpha\rangle\langle (k,b_1)(k,b_2)|J_\beta\rangle \\ \in & \ \mathcal{H}_\partial\,. \end{aligned} \tag{6.4.6}$$

The boundary density matrix is obtained by integrating over the bulk holonomy:

$$\rho_\partial[\psi] = \int \mathrm{d}g_1 \mathrm{d}g_2\, |\psi(g_1, g_2)\rangle\langle\psi(g_1, g_2)| \in \mathrm{End}[\mathcal{H}_\partial]\,. \tag{6.4.7}$$

The integration over the SU(2) group elements is straightforward to compute and yields:

$$\rho_\partial[\psi] = \sum_{J_\alpha, J_\beta} |C_{J_\alpha, J_\beta}|^2 \frac{\mathbb{I}_{J_\alpha}}{2J_\alpha + 1} \otimes \frac{\mathbb{I}_{J_\beta}}{2J_\beta + 1}\,, \tag{6.4.8}$$

[1]It might seem awkward that the dimension of the bulk Hilbert space is here (much) smaller than the dimension of the boundary Hilbert space: it would be weird to talk about a bulk-to-boundary coarse-graining in that situation. This is due to the extremely simple structure of the bulk graph. In fact, the dimension of the bulk Hilbert space increases exponentially with the number of bulk vertices (actually, more precisely, the number of independent cycles in the bulk graph as shown in [184]). For instance, merely pinching the loop to create an extra bulk vertices would increase the dimension of the bulk Hilbert space to $\dim \mathcal{H}_{bulk} = 2 \times (2k+1) \times 2$, which would be larger from $\dim \mathcal{H}_\partial = 2^4$ as soon as the spin j around the loop is larger than 2.

where $\mathbb{I}_J$, for $J = 0$ and $J = 1$, is the projector on the subspace of total spin J in the tensor product of two qubits $(V_{\frac{1}{2}})^{\otimes 2}$. This confirms that a pure bulk spin network state leads naturally to a mixed boundary state, indicating bulk-boundary entanglement. Moreover, due to the simple structure of the boundary in the present example, multiplicity matrix only has rank one for each J_α, J_β, the induced boundary density matrix carries no entanglement between the pair of boundary edges attached to the vertex α and the pair attached to the vertex β. A bit more complicated case will be given latter, which has higher rank for multiplicity matrix.

6.4.2 The six-qubit candy graph

We can upgrade the previous example by enriching the structure of the boundary intertwiner thereby allowing for the possibility of non-trivial entanglement between the boundary edges attached to the two vertices. Instead of attaching two boundary edges to each vertex, we now connect three boundary edges to each vertex. We still fix the spins on the boundary edges to $j_1 = .. = j_6 = \frac{1}{2}$, as well as on the inner loop to k and $k + \frac{1}{2}$ (with the half-integer shift to account for the extra half-spin on the boundary) for $k > 0$.

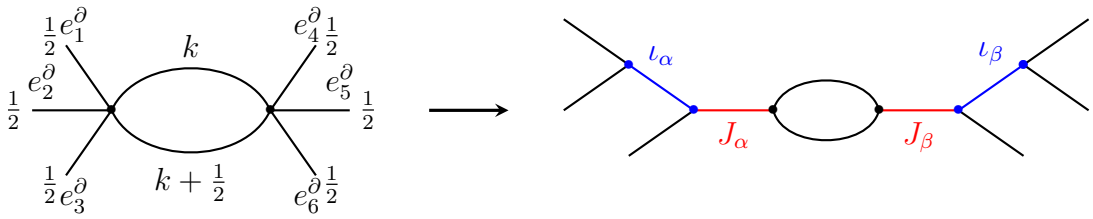

Figure 6.8: The one-loop 6-qubit candy graph and intertwiner basis.

The bulk Hilbert space thus consists in the tensor product of the spaces of intertwiners living at the two vertices α and β:

$$\mathcal{H}_{bulk} = \mathcal{H}_\alpha \otimes \mathcal{H}_\beta\,, \qquad \mathcal{H}_\alpha = \mathcal{H}_\beta = \mathrm{Inv}\big[(\mathcal{V}_{\frac{1}{2}})^{\otimes 3} \otimes \mathcal{V}_k \otimes \mathcal{V}_{k+\frac{1}{2}}\big]\,. \tag{6.4.9}$$

For each vertex, $v = \alpha$ and $v = \beta$, we unfold the intertwiner space by recoupling the three spins $\frac{1}{2}$ together into the bouquet spin J_v, as drawn on fig.6.8. Since the 3-valent intertwiner between the spins k, $k + \frac{1}{2}$ and $\frac{1}{2}$ is unique (and given by the corresponding Clebsh-Gordan coefficients), we can put aside this bulk component of the intertwiner and focus on the boundary component of the intertwiner. Then, since the tensor product of three spins $\frac{1}{2}$ decomposes as

$$(\mathcal{V}_{\frac{1}{2}})^{\otimes 3} = \mathcal{V}_{\frac{3}{2}} \otimes 2\mathcal{V}_{\frac{1}{2}}\,, \tag{6.4.10}$$

the intertwiner space is three-dimensional:

$$\mathcal{H}_v = \mathbb{C}|J_v = \frac{3}{2}\rangle \oplus \mathbb{C}|J_v = \frac{1}{2}, \iota_v = 0\rangle \oplus \mathbb{C}|J_v = \frac{1}{2}, \iota_v = 1\rangle\,. \tag{6.4.11}$$

The extra index $\iota \in \{0, 1\}$ when the three qubits recouple to the bouquet spin $J = \frac{1}{2}$ label the degeneracy in the decomposition of the tensor product. As depicted on fig.6.8,

we can simply take it as the spin recoupling for the first two qubits (boundary edges 1 and 2 for the vertex α and boundary edges 4 and 5 for the vertex β). In that case, we can extend the convention for the intertwiner basis state $|J,\iota\rangle$ even to $J=\frac{3}{2}$, in which case the extra label is allowed to take a single value $\iota=1$.

Bulk spin network basis states are then defined by the choice of the two intertwiner basis states at $v=\alpha$ and $v=\beta$:

$$\mathcal{H}_{bulk}=\bigoplus_{\{J_v,\iota_v\}}\mathbb{C}|J_v,\iota_v\rangle\,,\quad \dim\mathcal{H}_{bulk}=3\times 3=9\,. \tag{6.4.12}$$

The boundary Hilbert space simply consists in 6 qubits, from which we also use the bouquet spin basis:

$$\mathcal{H}_{\mathcal{B}}=\big(\mathcal{V}_{\frac{1}{2}}\big)^{\otimes 6}=\mathcal{H}^{\partial}_{\alpha}\otimes\mathcal{H}^{\partial}_{\beta}\,,\quad \mathcal{H}^{\partial}_{\alpha}=\mathcal{H}^{\partial}_{\beta}=\big(\mathcal{V}_{\frac{1}{2}}\big)^{\otimes 3}=\bigoplus_{J=\frac{1}{2},\frac{3}{2}}\mathcal{V}_J\otimes\mathcal{N}_J\,, \tag{6.4.13}$$

with $\mathcal{N}_J=\mathrm{Inv}\Big[\mathcal{V}_J\otimes\big(\mathcal{V}_{\frac{1}{2}}\big)^{\otimes 3}\Big]$, where $\dim\mathcal{N}_{\frac{1}{2}}=2$, $\dim\mathcal{N}_{\frac{3}{2}}=1$, $\dim\mathcal{H}^{\partial}_{\alpha}=\dim\mathcal{H}^{\partial}_{\beta}=2\times 2+4\times 1=2^3$. Let us consider a general spin network state (with fixed spins as we have assumed so far) on this candy graph with six boundary edges:

$$\psi=\sum_{\{J_v,\iota_v\}_{v=\alpha,\beta}}C^{J_\alpha,J_\beta}_{\iota_\alpha,\iota_\beta}\,|(J_\alpha,\iota_\alpha)\,(J_\beta,\iota_\beta)\rangle\,. \tag{6.4.14}$$

The induced boundary density matrix, obtained after integration over the bulk holonomies, is:

$$\rho_\partial[\psi]=\sum_{J_\alpha,J_\beta}\frac{\mathbb{I}_{J_\alpha}}{2J_\alpha+1}\otimes\frac{\mathbb{I}_{J_\beta}}{2J_\beta+1}\otimes\rho_{J_\alpha,J_\beta}\,, \tag{6.4.15}$$

where the multiplicity matrix encodes the data about the intertwiners:

$$\rho_{J_\alpha,J_\beta}\;=\;\sum_{\{\iota_v,\widetilde{\iota}_v\}}C^{J_\alpha,J_\beta}_{\widetilde{\iota}_\alpha,\widetilde{\iota}_\beta}\overline{C^{J_\alpha,J_\beta}_{\iota_\alpha,\iota_\beta}}\Big|(J_\alpha,\widetilde{\iota}_\alpha)(J_\beta,\widetilde{\iota}_\beta)\Big\rangle\Big\langle(J_\alpha,\iota_\alpha)(J_\beta,\iota_\beta)\Big|\quad\in\;\mathrm{End}\big[\mathcal{N}_{J_\alpha}\otimes\mathcal{N}_{J_\beta}\big]\,. \tag{6.4.16}$$

This is always a rank-one matrix and does not lead to entanglement between the boundary edges (1,2,3) and (4,5,6).

If we want to obtain non-trivial multiplicity matrices, i.e. of higher rank, one has to allow for non-trivial bulk components of the intertwiners. To this purpose, we must consider a (slightly) more complicated bulk graph with three bulk edges connecting the two vertices. We can assume that the spins on all the edges, both on the boundary and in the bulk, are fixed to, say, $j_1=..=j_9=\frac{1}{2}$. If we look at the vertex v, which can be α or β, the 6-valent intertwiner can be unfolded into the bouquet spin basis. As depicted on fig.6.9, an intertwiner basis state is now labeled by the bouquet spin J_v, a multiplicity index $\iota^{\partial}_v\in\{0,1\}$ for the boundary component of the intertwiner (which can be taken as the recoupled spin of the edges 1 and 2) and a multiplicity index $\iota^{o}_v\in\{0,1\}$ for the bulk component of the intertwiner (which can be taken as the recoupled spin of the edges 4 and 5).

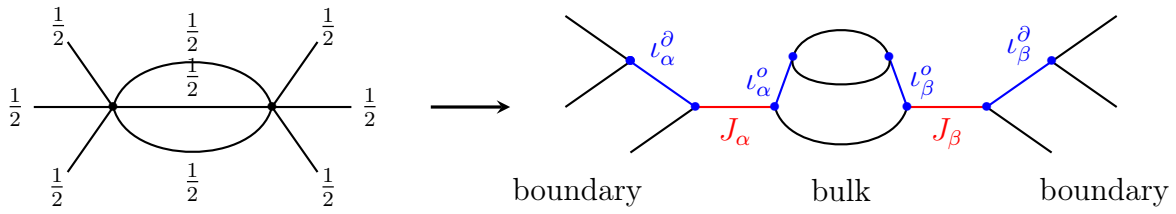

Figure 6.9: The triple link 6-qubit candy graph and intertwiner basis.

The main consequence of adding bulk structure is to increase the dimension of the bulk Hilbert space:

$$\mathcal{H}_{bulk} = \mathcal{H}_\alpha \otimes \mathcal{H}_\beta \,, \quad \mathcal{H}_v = \mathrm{Inv}\big[(\mathcal{V}_{\frac{1}{2}})^{\otimes 6}\big] = \bigoplus_{J_v, \iota_v^\partial, \iota_v^o} \mathbb{C}|J_v, \iota_v^\partial, \iota_v^o\rangle \quad \dim \mathcal{H}_{bulk} = (1{+}2{\times}2)^2 = 25 \,. \tag{6.4.17}$$

On the other hand, the boundary Hilbert space is left unchanged. This much higher dimensionality of the bulk Hilbert space allows for finer structure of the bulk state and induced entanglement on the boundary. Indeed, a generic spin network state decomposes as:

$$\psi = \sum_{\{J_v, \iota_v\}_{v=\alpha,\beta}} C^{J_\alpha, J_\beta}_{\iota_\alpha^\partial, \iota_\alpha^o, \iota_\beta^\partial, \iota_\beta^o} \Big| (J_\alpha, \iota_\alpha^\partial, \iota_\alpha^o)\, (J_\beta, \iota_\beta^\partial, \iota_\beta^o) \Big\rangle \,. \tag{6.4.18}$$

Compared to the previous case of the one-loop candy graph, the bulk part of the intertwiners ι_v^o is not seen by the boundary state. This bulk data "hidden" from the boundary creates entanglement between the two bouquets of boundary edges. Indeed the induced boundary density matrix can be computed as:

$$\rho_\partial[\psi] = \sum_{J_\alpha, J_\beta} \frac{\mathbb{I}_{J_\alpha}}{2J_\alpha + 1} \otimes \frac{\mathbb{I}_{J_\beta}}{2J_\beta + 1} \otimes \rho_{J_\alpha, J_\beta} \,, \tag{6.4.19}$$

where the multiplicity matrix encodes the data about the intertwiners:

$$\begin{aligned} \rho_{J_\alpha, J_\beta} = \sum_{\{\iota_v^\partial, \tilde{\iota}_v^\partial\}} \left(\sum_{\{\iota_v^o\}} C^{J_\alpha, J_\beta}_{\tilde{\iota}_\alpha^\partial, \iota_\alpha^o, \tilde{\iota}_\beta^\partial, \iota_\beta^o} \overline{C^{J_\alpha, J_\beta}_{\iota_\alpha^\partial, \iota_\alpha^o, \iota_\beta^\partial, \iota_\beta^o}} \right) \Big| (J_\alpha, \tilde{\iota}_\alpha^\partial)(J_\beta, \tilde{\iota}_\beta^\partial) \Big\rangle \Big\langle (J_\alpha, \iota_\alpha^\partial)(J_\beta, \iota_\beta^\partial) \Big| \\ \in \mathrm{End}\big[\mathcal{N}_{J_\alpha} \otimes \mathcal{N}_{J_\beta}\big] \,. \end{aligned} \tag{6.4.20}$$

The partial trace over the bulk components of the intertwiners lead to a higher rank of the multiplicity matrix, reflecting the induced entanglement between the boundary edges attached to α and the ones attached to the vertex β. A simple example is, choosing that both intertwiners have support exclusively on the bouquet spins $J_\alpha = J_\beta = \frac{1}{2}$, and form a Bell-like state:

$$\psi_{Bell} = \frac{1}{\sqrt{2}} \left(|(\tfrac{1}{2}, 0, 0)(\tfrac{1}{2}, 1, 1)\rangle - |(\tfrac{1}{2}, 1, 1)(\tfrac{1}{2}, 0, 0)\rangle \right) , \tag{6.4.21}$$

leading to the induced density matrix:

$$\rho_\partial[\psi_{Bell}] = \frac{\mathbb{I}_{\frac{1}{2}}}{2} \otimes \frac{\mathbb{I}_{\frac{1}{2}}}{2} \otimes \rho_{\mathcal{N}}\,, \quad \rho_{\mathcal{N}} = |(\frac{1}{2},0)(\frac{1}{2},1)\rangle\langle(\frac{1}{2},0)(\frac{1}{2},1)| + |(\frac{1}{2},1)(\frac{1}{2},0)\rangle\langle(\frac{1}{2},1)(\frac{1}{2},0)|\,, \tag{6.4.22}$$

where the multiplicity matrix now has rank two. Then it is clear to see the ensemble of pure states as the definition of Eq.(3.1.18), and to read the entanglement of formation $E(\rho_\partial[\psi_{Bell}]) = \ln 2$ as defined by (3.1.19) where we take the ensemble of pure states as

$$\rho_\partial[\psi_{Bell}] = \sum_{+,-} \sum_{m_A,m_B} p(m_A,m_B)|\psi_{m_A,m_B},\pm\rangle\langle\psi_{m_A,m_B},\pm| \tag{6.4.23}$$

for magnetic quantum numbers $m_A = \pm\frac{1}{2}$ and $m_B = \pm\frac{1}{2}$ with probability $p(m_A,m_B) = \frac{1}{4}$ and

$$|\psi_{m_A,m_B},+\rangle = |m_A m_B\rangle \otimes \frac{|(\frac{1}{2},0)(\frac{1}{2},1)\rangle + |(\frac{1}{2},1)(\frac{1}{2},0)\rangle}{\sqrt{2}}\,, \tag{6.4.24}$$

$$|\psi_{m_A,m_B},-\rangle = |m_A m_B\rangle \otimes \frac{|(\frac{1}{2},0)(\frac{1}{2},1)\rangle - |(\frac{1}{2},1)(\frac{1}{2},0)\rangle}{\sqrt{2}}\,. \tag{6.4.25}$$

This perfectly illustrates how tracing out the bulk degrees of freedom leads to a mixed state on the boundary, or in more physical terms, how correlations between bulk intertwiners leads to entanglements between boundary edges.

In this chapter, the new feature is that one can trace over the bulk by integrating over the bulk holonomies and obtaining a density matrix for the boundary states. This boundary density matrix encodes all that we can know about the quantum state of geometry from probing the boundary if we do not have access to any bulk observable. For a pure bulk state, we typically obtain a mixed boundary state. This realizes a bulk-to-boundary coarse-graining via tracing-bulk.

Our main result 6.2 is proof that any gauge-covariant boundary density matrix for an arbitrary number of boundary edges can be induced from a pure spin network state on a simple bulk graph consisting from a single vertex connecting all the boundary edges to a single bulk loop. In quantum information jargon, this universal reconstruction process purifies arbitrary mixed boundary states into pure bulk states. This purification process is, of course, not unique, and one can build infinitely many pure bulk spin networks on more complicated graphs, which still lead to the same boundary density matrix. The relevant question is whether these bulk states could be understood as physically equivalent under to-be-determined gauge transformations. Such gauge transformations, deeply intertwined with the refinement and coarse-graining of the quantum geometry, would immediately be at the heart of loop quantum gravity and have to be compared to a concept of spacetime diffeomorphisms at the discrete quantum level.

We further analyzed the algebraic structure of induced boundary density matrices, more precisely, how intertwiner correlations, i.e., entanglement between bulk volume excitations, get reflected by the boundary density matrix. This should be considered part of the larger program of bulk tomography through boundary observables in loop quantum gravity. Hopefully, the basic tools introduced here should allow a more systematic study of how far one can see into the bulk and how much one observer on the boundary can know about the bulk spin network graph. For instance, we would like to study in more detail the relation between boundary edge entanglement and bulk intertwiner entanglement and quantify their difference in a precise and explicit manner.

These questions are at the kinematical level. We want to tackle the spin network dynamics and reformulate it in light of the bulk-boundary relation. This means projecting the bulk dynamics onto the boundary and writing it in terms of boundary evolution operators. Loop quantum gravity's dynamics would then read in terms of completely positive maps (CP map) already mentioned in Chapter 3 [143], which admits an operator-sum representation in terms of Kraus operators $\{E_k,\, k = 1, 2, \cdots\}$, which leave invariant the trace of quantum states. We wish to describe boundary evolution and measurements in loop quantum gravity in terms of CPTP maps, taking Kraus operators as representations for boundary dynamics.

Furthermore, the induced boundary density matrix can also be understood as obtained via G-twirling operation defined by Eq.(3.2.21), meaning that the boundary Hilbert defines a quantum reference frame for loop quantum gravity. In this sense, the measurements are accessible quasi-locally. A more promising picture may be realized by assigning an induced boundary matrix to each vertex. The advantage is that the assignment has considered coarse-graining automatically. The SU(2)-invariance holds but in the sense of $\rho = g\rho g^{-1}$, with probable nontrivial closure defect.

Chapter 7

Intertwiner Entanglement Excitation

In this chapter, we focus on intertwiner entanglement[1] carried by a spin network state, and study the entanglement created by the holonomy operator, which is recognized as a discretized measure of curvature in loop quantum gravity and as the basic building block of the Hamiltonian operator. We wish to understand how the excitation of curvature is related to the excitation of entanglement on spin network states. This is part of the larger line of research toward answering the question: what is the relation between geometry and entanglement? Can one understand the dynamics of quantum geometry directly in terms of the evolution of entanglement and quantum information?

Furthermore, since the spin network is viewed as a many-body quantum system, it is necessary to introduce the notion of multipartite entanglement (c.f. Chapter 3.1, or [139, 201, 134]). It is still an ongoing topic in the field of quantum information. There are many candidates for quantifying the entanglement of multipartite system. These entanglement measures generally are not equivalent. In order to explore the entanglement structure for LQG, it is required to find a suitable entanglement measure. Our work shows that the notion of the geometric measure of entanglement may be a good one, and justify the geometric measure since it admits a straightforward generalization from bipartite to multipartite spin network.

This chapter is based on [53] and is organized as follows: Section 7.1 starts with an introduction to a gauge-invariant holonomy operator defined on a loop that acts on all the intertwiner states living at the nodes of the spin network. We represent its action in Proposition 7.1. At the end of the section, Corollary 7.2, we give its behavior in a semi-classical regime. Section 7.2 views spin network states as many-body quantum systems living in the tensor product of the space of intertwiners attached to each node of the network. We classify the entangled and separable spin network states in Result 7.7. In particular, spin network basis states, with fixed spins on the links and fixed intertwiners on the nodes, are separable and carry no entanglement. We explore the notion of multipartite entanglement [139, 201, 134] and define the notion of geometric

[1] As shown in [190], boundary state entanglement typically involves the gauge symmetry breaking and is defined with respect to gauge-variant physical measurements and the corresponding choice of boundary reference frame. On the other hand, intertwiner entanglement is gauge-invariant, and can be argued to quantify genuine spin network entanglement.

entanglement for spin networks. Our main result of this chapter is presented in Result 7.9 in subsection 7.2.3, giving the computation of the growth of entanglement due to the action of the holonomy on a spin network basis state. Finally, sections 7.3 and 7.4 apply this general result to the simplest network structures: the 2-vertex graph with boundary -or candy graph- consisting of two nodes and a triangular graph consisting of three nodes. These simple settings allow for explicit computations of the evolution (generated by the holonomy operator) of both the bipartite entanglement and the geometric multipartite entanglement, showing that they match in the leading order.

7.1 Loop holonomy operator on spin networks

The dynamics of spin network states implement the flow generated by the Hamiltonian constraints on the embedded geometry of the canonical hypersurface. At the quantum level, the Hamiltonian constraint operators involve the holonomy operator and geometric observables, such as areas and volumes. The holonomy operator is analogous to the Wilson-loop in QCD. It corresponds to the quantization of the curvature in the polymer quantization scheme used in loop quantum gravity, where one does not access to point-like excitations, but only to gauge-invariant observables smeared along 1d structures. Let us analyze the action of the holonomy operator on spin network basis states, along the lines of [202, 203].

Let us look at the holonomy operator with spin ℓ acting on a single edge e. This operator takes the tensor product of the spin-ℓ with the spin k_e carried by the edge, and its action can be expressed in terms of Clebsch-Gordan coefficients decomposing this tensor product $\ell \otimes k_e$ into irreducible representations. Indeed the Wigner matrices for the SU(2) group element g_e carrying the holonomy along the edge e satisfies the following algebraic relations:

$$\widehat{D^{\ell}_{a_e b_e}} \triangleright \left[D^{k_e}_{m_e n_e}(g_e) \right] = D^{\ell}_{a_e b_e}(g_e)\, D^{k_e}_{m_e n_e}(g_e)\,, \qquad D^{\ell} \otimes D^{k_e} = \bigoplus_{K_e=|k_e-\ell|}^{k_e+\ell} D^{K_e}\,, \tag{7.1.1}$$

$$D^{\ell}_{a_e b_e}(g_e)\, D^{k_e}_{m_e n_e}(g_e) = \sum_{K_e=|k_e-\ell|}^{k_e+\ell} \sum_{M_e,N_e=-K_e}^{K_e} (-1)^{M_e-N_e}(2K_e+1) \begin{pmatrix} \ell & k_e & K_e \\ a_e & m_e & -M_e \end{pmatrix} \overline{\begin{pmatrix} \ell & k_e & K_e \\ b_e & n_e & -N_e \end{pmatrix}}\, D^{K_e}_{M_e N_e}(g_e)\,, \tag{7.1.2}$$

where the recoupled spin K_e is bounded by the triangular inequalities $|k_e-\ell| \leq K_e \leq k_e+\ell$.

The holonomy operator along a single edge spoils the gauge invariance. In order to produce a gauge-invariant holonomy operator, one must consider a closed loop on the graph Γ underlying the spin network state. Consider a loop $W \subseteq \Gamma$ with n edges, and assume the simplifying condition that it does not go through a vertex more than that once. The oriented loop W can be described as the path $W[v_1 \overset{e_1}{\to} \cdots \overset{e_{n-1}}{\to} v_n \overset{e_n}{\to} v_1]$ such

that the edge e_i links the vertex v_i to v_{i+1}, with $i = 1, \cdots, n$ and the implicit convention $n+1 \equiv 1$. The loop holonomy operator is defined as a multiplicative operator on the wave-functions:

$$(\widehat{\chi_\ell} \triangleright_W \psi_\Gamma)(\{g_e\}_{e\in\Gamma}) = \chi_\ell(G_W)\psi_\Gamma(\{g_e\}_{e\in\Gamma}), \qquad \text{with} \quad G_W = \overleftarrow{\prod_{e_i\in W}} g_{e_i}, \tag{7.1.3}$$

where $\chi_\ell(g) = \mathrm{Tr}D^\ell(g)$ is the character of the spin-ℓ representation. The notation "$\overleftarrow{\ }$" is assigned to indicate the order of group multiplication. We take the inverse of a group element if the edge is oriented in the opposite direction than the loop. Since the factor $\chi_\ell(G_W)$ is a gauge invariant function, the resulting wave-function is still gauge-invariant. Thus the map $\widehat{\chi_\ell}\triangleright_W$ acts legitimately on the Hilbert space $\mathcal{H}_\Gamma$ and we can write its action on the spin network basis:

$$\widehat{\chi_\ell} \triangleright_W |\Psi_{\Gamma,\{I_v\}}\rangle = \sum_{\{I'_v\}} \left[Z(\Gamma)_{\chi_\ell\triangleright_W}\right]^{\{I'_v\}}_{\{I_v\}} |\Psi_{\Gamma,\{I'_v\}}\rangle, \tag{7.1.4}$$

where the matrix elements $Z(\Gamma)_{\chi_\ell\triangleright_W}$ are given by the following integrals:

$$\left[Z(\Gamma)_{\chi_\ell\triangleright_W}\right]^{\{I'_v\}}_{\{I_v\}} = \int \prod_{e\in\Gamma} \mathrm{d}g_e\, \overline{\Psi_{\Gamma,\{I'_v\}}(\{g_e\}_{e\in\Gamma})}\, \chi_\ell(G_W)\, \Psi_{\Gamma,\{I_v\}}(\{g_e\}_{e\in\Gamma}). \tag{7.1.5}$$

This matrix $Z(\Gamma)_{\chi_\ell\triangleright_W}$ satisfies a composition rule:

$$\sum_{\{I'_v\}} \left[Z(\Gamma)_{\chi_{\ell_1}\triangleright_W}\right]^{\{I''_v\}}_{\{I'_v\}} \left[Z(\Gamma)_{\chi_{\ell_2}\triangleright_W}\right]^{\{I'_v\}}_{\{I_v\}} = \sum_{s=|\ell_1-\ell_2|}^{\ell_1+\ell_2} \left[Z(\Gamma)_{\chi_s\triangleright_W}\right]^{\{I''_v\}}_{\{I_v\}} \tag{7.1.6}$$

$$= \left[Z(\Gamma)_{(\chi_{\ell_1}\cdot\chi_{\ell_2})\triangleright_W}\right]^{\{I''_v\}}_{\{I_v\}}, \tag{7.1.7}$$

which is inherited from the character recoupling formula $\chi_{\ell_1}\chi_{\ell_2} = \sum_{s=|\ell_1-\ell_2|}^{\ell_1+\ell_2} \chi_s$. An interesting fact to keep in mind is that the matrices $Z(\Gamma)_{\chi_{\ell_1}\triangleright_W}$ and $Z(\Gamma)_{\chi_{\ell_2}\triangleright_W}$ commute with each other with arbitrary spins ℓ_1 and ℓ_2.

The transition matrix Z can be expressed in terms of the $\{6j\}$ symbols of spin recoupling. To this purpose, we recall bouquet spins for the vertices along the loop W following the previous Chapter 6 as Fig.6.4. The bouquet spin is a recoupled spin used to define a convenient intertwiner basis. As illustrated on Fig.7.1, we distinguish at each vertex v the two edges belonging to the loop $\{e \in W\}$ and we recouple all the spins carried by the other edges $\{e \notin W\}$ into a spin J_v. If a vertex around the loop is 3-valent, then the bouquet spin is obvious simply the spin carried by the third edge, not belonging to the loop. In general, the definition of the bouquet spin allows to consider all the intertwiners around the loop as 3-valent for all matters of operators acting on the loop edges. This convenient unfolding of the intertwiners allows to write the action of the holonomy operator in terms of the spins along the loop and the bouquet spins:

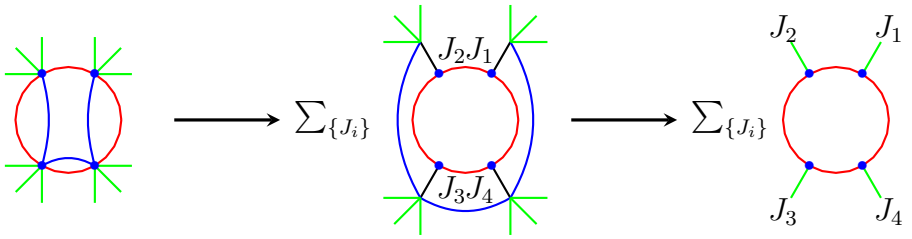

Figure 7.1: The red circle is the path W to be acted by holonomy operator (left). The boundary edges green recouple with bulk edges blue into bouquet spins J_1, J_2, J_3, J_4 at respect vertices (middle). Note that bouquet spins have superposition due to recoupling. The consequence of the loop holonomy operator amounts to acting on a trivalent graph (right).

Proposition 7.1. *Given an oriented loop $W[v_1 \overset{e_1}{\to} \cdots \overset{e_{n-1}}{\to} v_n \overset{e_n}{\to} v_1]$ on the graph Γ, the loop holonomy operator $\widehat{\chi_\ell}_{\triangleright W}$ acts on the spin network basis, labeled by the spins k_i on the loop edges and the bouquet spins J_i on the loop vertices (e.g. Fig.7.2), by the following transition matrix:*

$$\left[Z(\Gamma)^{\{J_i\}}_{\chi_\ell \triangleright W}\right]^{\{K_i\}}_{\{k_i\}} = (-1)^{\sum_{i=1}^n (J_i+k_i+K_i+\ell)} \prod_{i=1}^n \begin{Bmatrix} J_i & K_i & K_{i+1} \\ \ell & k_{i+1} & k_i \end{Bmatrix} \prod_{i=1}^n \sqrt{(2K_i+1)(2k_i+1)}\,. \tag{7.1.8}$$

Proof. The proof is a straightforward spin recoupling computation. One can use graphical calculus to establish the expressions [204, 205, 206, 207]. We split the character $\chi_\ell(G_W)$ into local Wigner D-matrices for each edge of the loop,

$$\chi_\ell(G_W) = \overleftarrow{\prod_{i=1}^n} D^\ell_{m_i m_{i+1}}(g_i)\,, \qquad \text{cycling} \quad n+1 \equiv 1\,, \tag{7.1.9}$$

then apply the formula (7.1.2) for the holonomy operators. As illustrated on fig.7.2, the bulk spins k_i undergo a spin shift $k_i \to K_i$ with the output spins K_i are bounded by triangular inequalities $|k_i - \ell| \leq K_i \leq k_i + \ell$, while the boundary spins j_i and thus the recouped bouquet spins J_i are left unchanged. Hence we use spins the $\{j_i, J_i\}, \{k_i\}$ to label the initial intertwiners $\{I_v\}$ and $\{j_i, J_i\}, \{K_i\}$ to label the final intertwiners $\{I'_v\}$,

$$\left[Z(\Gamma)^{\{j_i,J_i\}}_{\chi_\ell \triangleright W}\right]^{\{K_i\}}_{\{k_i\}} \equiv \left[Z(\Gamma)_{\chi_\ell \triangleright W}\right]^{\{I'_v\}}_{\{I_v\}}\,.$$

As drawn on fig.7.2a, the action of a holonomy operator on an edge amounts to creating two open edges with weight factor $(2K_i+1)$. Summing over the magnetic indices of the character formula (7.1.9) amounts to linking those open edges and closing the corners all around the loop. This leads to a $6j$-symbol factor for each corner/vertex as shown on fig.7.2d, leading to the overall amplitude for the loop holonomy operator $\widehat{\chi_\ell}_{\triangleright W}$ given by

$$\left[\mathcal{W}(\Gamma)^{\{j_i,J_i\}}_{\chi_\ell \triangleright W}\right]^{\{K_i\}}_{\{k_i\}} = (-1)^{\sum_{i=1}^n (J_i+k_i+K_i+\ell)} \prod_{i=1}^n \begin{Bmatrix} J_i & K_i & K_{i+1} \\ \ell & k_{i+1} & k_i \end{Bmatrix} \prod_{i=1}^n (2K_i+1)\,, \tag{7.1.10}$$

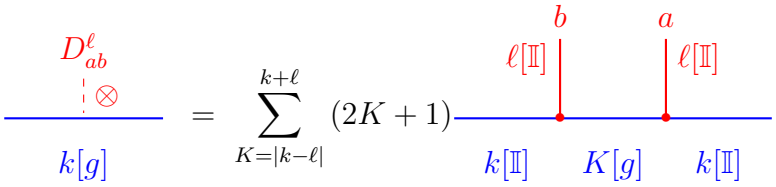

(a) The graphical illustration for the operation of holonomy operator. The red nodes are virtual vertices introduced by D^ℓ.

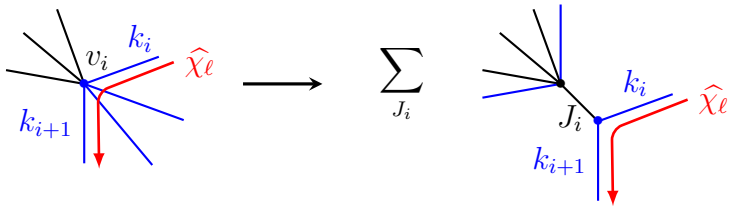

(b) For a vertex v_i living along the W, its attached spins around either acted by, or not acted by the loop holonomy operator. For the spins which are not acted, they recouple into spin-J_i attached to the vertex v_i.

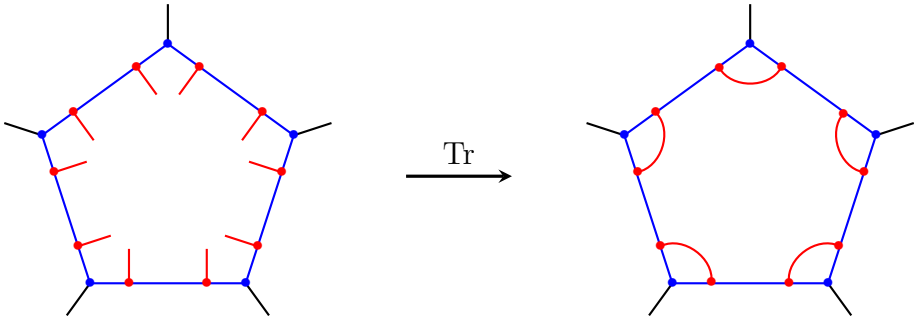

(c) The graphical illustration for loop holonomy operator. The D^ℓ amounts to generates bubbles around the corners.

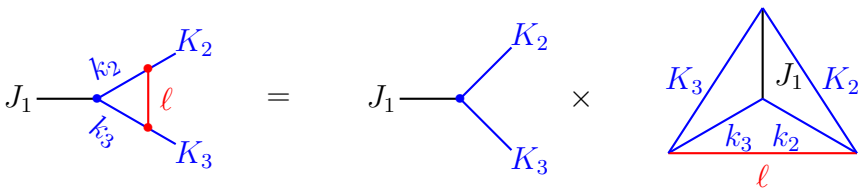

(d) Each corner brings a $6j$-symbol to wave function.

Figure 7.2: The graphical representations for holonomy and loop holonomy operator respectively.

with $n+1 \equiv 1$, which leads to the desired Z's representation (7.1.8). □

The proposition shows that the dynamics generated by the loop holonomy operator depends at each vertex on three spins: the two spins living on the edges attached to the

vertex on the loop and the bouquet spin encoding the recoupling of the spin living on all the other edges attached to the considered vertex.

We can provide the action of the loop holonomy operator with geometrical meaning in the semi-classical regime at the large spin limit. This is provided by the asymptotic behavior of Z, which can be expressed in terms of the angles of the triangles dual to the spin network graph, as shown on figure 7.3a. More precisely, considering that the spins $\{j_i, k_i\}$ of spin network are much larger than the spin-ℓ of holonomy operator, we employ Edmonds's asymptotic formula and get the following corollary of the previous proposition:

Corollary 7.2. *If the bulk spins $\{k_i\}$ and boundary spins $\{j_i\}$ much larger than ℓ, i.e., $\{j_i\,, k_i\} \gg \ell$, matrix Z has following asymptotic formula in terms of Wigner d-matrices:*

$$\left[Z(\Gamma)^{\{j_i\}}_{\chi_\ell \triangleright W}\right]^{\{K_i\}}_{\{k_i\}} \approx \overleftarrow{\prod_{i=1}^{n}} d^{\ell}_{\varepsilon_i\varepsilon_{i+1}}(\theta_i)\,, \quad \textit{with} \quad \varepsilon_i = K_i - k_i\,, \tag{7.1.11}$$

$$\textit{and} \qquad \cos\theta_i = \frac{k_i(k_i+1) + k_{i+1}(k_{i+1}+1) - j_i(j_i+1)}{2\sqrt{k_i(k_i+1)k_{i+1}(k_{i+1}+1)}}\,.$$

Proof. Using Edmonds's asymptotic formula (see equations (3.6) and (3.7) in [208]) for $6j$-symbols,

$$\begin{Bmatrix} c & a & b \\ \ell & b+\varepsilon_2 & a+\varepsilon_1 \end{Bmatrix} \approx \frac{(-1)^{a+b+c+\ell+\varepsilon_2}}{\sqrt{(2a+1)(2b+1)}} d^{\ell}_{\varepsilon_2\varepsilon_1}(\theta)\,, \tag{7.1.12}$$

$$\text{with} \quad \cos\theta = \frac{a(a+1)+b(b+1)-c(c+1)}{2\sqrt{a(a+1)b(b+1)}}\,,$$

where d^ℓ is the reduced Wigner d-matrix for spin-ℓ,

$$d^{\ell}_{mn}(\theta) = \sqrt{(\ell+m)!(\ell-m)!(\ell+n)!(\ell-n)!}\sum_s \frac{(-1)^{m-n+s}\big(\cos\frac{\theta}{2}\big)^{2\ell-m+n-2s}\big(\sin\frac{\theta}{2}\big)^{m-n-2s}}{(\ell+n-s)!s!(m-n+s)!(\ell-m-s)!}\,. \tag{7.1.13}$$

Inserting this asymptotic approximation of the Wigner d-matrices in the expression (7.1.8) of the $6j$-symbols, we get the wanted formula (7.1.11) up to a pre-factor $\sqrt{\frac{2K_i+1}{2k_i+1}}$, which actually goes to 1 when k_i, K_i are large compared to ℓ.

□

This approximation expresses the arguments $\{j_i\, k_i, K_i\}$ in terms of corner angles θ_i and spin shiftings $\varepsilon_i = K_i - k_i$, as illustrated in fig. 7.3b. In addition, one can check the large spin approximation (7.1.11) inherits the same exact composition rule as the exact amplitude (7.1.6).

For instance, in the case $n = 2$, to ease the notations, the composition rule (7.1.6) for the Z-matrix elements reads

$$\sum_{K_1,K_2} (-1)^{k_1+k_2-\tilde{k}_1-\tilde{k}_2+2\ell_1-2\ell_2} \begin{Bmatrix} j_1 & k_1 & k_2 \\ \ell_1 & K_2 & K_1 \end{Bmatrix} \begin{Bmatrix} j_2 & k_1 & k_2 \\ \ell_1 & K_2 & K_1 \end{Bmatrix} \begin{Bmatrix} j_1 & \tilde{k}_1 & \tilde{k}_2 \\ \ell_2 & K_2 & K_1 \end{Bmatrix}$$

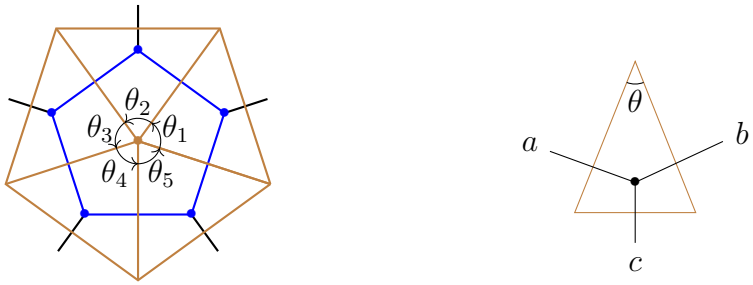

(a) The brown lines portray the dual triangulation of spin network. The angles θ_i are arguments of Wigner d-matrices d^ℓ in asymptotic formula (7.1.11).

(b) The angle variable in Edmonds's asymptotic formula (7.1.12), where a, b, c are spins.

Figure 7.3: The illustration for asymptotic formula.

$$\times \begin{Bmatrix} j_2 & \tilde{k}_1 & \tilde{k}_2 \\ \ell_2 & K_2 & K_1 \end{Bmatrix} \sqrt{(2k_1+1)(2k_2+1)(2\tilde{k}_1+1)(2\tilde{k}_2+1)}(2K_1+1)(2K_2+1)$$

$$= \sum_{s=|\ell_1-\ell_2|}^{\ell_1+\ell_2} (-1)^{j_1+j_2+\tilde{k}_1+\tilde{k}_2+k_1+k_2+2s} \begin{Bmatrix} j_1 & k_1 & k_2 \\ s & \tilde{k}_2 & \tilde{k}_1 \end{Bmatrix} \begin{Bmatrix} j_2 & k_1 & k_2 \\ s & \tilde{k}_2 & \tilde{k}_1 \end{Bmatrix}$$

$$\times \sqrt{(2k_1+1)(2k_2+1)(2\tilde{k}_1+1)(2\tilde{k}_2+1)}\,, \tag{7.1.14}$$

which is equivalent to Biedenharn–Elliott identity (see e.g. [202]). For large spins $\{j_i\,, k_i\} \gg \ell$, one can apply Edmonds's asymptotic formula for $6j$-symbols to get:

$$\sum_{\varepsilon_1,\varepsilon_2} d^{\ell_1}_{\varepsilon_1\varepsilon_2}(\theta_1)\, d^{\ell_1}_{\varepsilon_2\varepsilon_1}(\theta_2)\, d^{\ell_2}_{\varepsilon_1+\Delta_1,\varepsilon_2+\Delta_2}(\theta_1)\, d^{\ell_2}_{\varepsilon_2+\Delta_2,\varepsilon_1+\Delta_1}(\theta_2) \approx \sum_{s=|\ell_1-\ell_2|}^{\ell_1+\ell_2} d^{s}_{\Delta_1,\Delta_2}(\theta_1)\, d^{s}_{\Delta_2,\Delta_1}(\theta_2)\,. \tag{7.1.15}$$

Below we show that this approximative composition rule actually holds exctaly.

Proposition 7.3. *Suppose there is n vertices along loop W, then the composite rule for eqn.(7.1.11) is*

$$\sum_{\{\varepsilon_i\}} \prod_{i=1}^{\overleftarrow{n}} d^{\ell_1}_{\varepsilon_i,\varepsilon_{i+1}}(\theta_i)\, d^{\ell_2}_{\varepsilon_i+\Delta_i,\varepsilon_{i+1}+\Delta_{i+1}}(\theta_i) = \sum_{s=|\ell_1-\ell_2|}^{\ell_1+\ell_2} \prod_{i=1}^{\overleftarrow{n}} d^{s}_{\Delta_i,\Delta_{i+1}}(\theta_i)\,, \qquad \textit{cycling} \quad n+1 \equiv 1\,. \tag{7.1.16}$$

Proof. Let us consider the simplest case $n = 2$. The proof is straightforward to generalize to arbitrary n. We would like to prove the following composition rule:

$$\sum_{\varepsilon_1,\varepsilon_2} d^{\ell_1}_{\varepsilon_1\varepsilon_2}(\theta_1)\, d^{\ell_1}_{\varepsilon_2\varepsilon_1}(\theta_2)\, d^{\ell_2}_{\varepsilon_1+\Delta_1,\varepsilon_2+\Delta_2}(\theta_1)\, d^{\ell_2}_{\varepsilon_2+\Delta_2,\varepsilon_1+\Delta_1}(\theta_2) = \sum_{s=|\ell_1-\ell_2|}^{\ell_1+\ell_2} d^{s}_{\Delta_1,\Delta_2}(\theta_1)\, d^{s}_{\Delta_2,\Delta_1}(\theta_2)\,. \tag{7.1.17}$$

This equation can be proven by means of recoupling Wigner d-matrices. Firstly, we flip the sign of magnetic indices in d^{ℓ_1} by equation $d^j_{mn}(\theta) = (-1)^{m-n} d^j_{-m,-n}(\theta)$. The overall phase has to be 1 because every ε_i appears twice. We then recouple Wigner d-matrices d^{ℓ_1} and d^{ℓ_2} with argument θ_1

$$\begin{aligned} d^{\ell_1}_{-\varepsilon_1,-\varepsilon_2}(\theta_1)\, d^{\ell_2}_{\varepsilon_1+\Delta_1,\varepsilon_2+\Delta_2}(\theta_1) &= \sum_{s=|\ell_1-\ell_2|}^{\ell_1+\ell_2} (-1)^{\Delta_1-\Delta_2}(2s+1) \begin{pmatrix} \ell_1 & \ell_2 & s \\ -\varepsilon_1 & \varepsilon_1+\Delta_1 & -\Delta_1 \end{pmatrix} \\ &\quad \times \begin{pmatrix} \ell_1 & \ell_2 & s \\ -\varepsilon_2 & \varepsilon_2+\Delta_2 & -\Delta_2 \end{pmatrix} d^s_{\Delta_1,\Delta_2}(\theta_1)\,, \end{aligned} \tag{7.1.18}$$

where tensor product $d^{\ell_1} \otimes d^{\ell_2}$ are decomposed into Wigner d-matrices labeled by s. Repeat the step $d^{\ell_1} \otimes d^{\ell_2}$ for argument θ_2, and label the Wigner d-matrices by $d^{s'}$. Now fixing s and s', we take all $3j$-symbols into account, and deal with them by orthogonality of $3j$-symbols so

$$\begin{aligned} \frac{\delta_{ss'}}{(2s+1)(2s'+1)} &= \sum_{\varepsilon_1,\varepsilon_2} \begin{pmatrix} \ell_1 & \ell_2 & s \\ -\varepsilon_1 & \varepsilon_1+\Delta_1 & -\Delta_1 \end{pmatrix} \begin{pmatrix} \ell_1 & \ell_2 & s \\ -\varepsilon_2 & \varepsilon_2+\Delta_2 & -\Delta_2 \end{pmatrix} \\ &\quad \times \begin{pmatrix} \ell_1 & \ell_2 & s' \\ -\varepsilon_2 & \varepsilon_2+\Delta_2 & -\Delta_2 \end{pmatrix} \begin{pmatrix} \ell_1 & \ell_2 & s' \\ -\varepsilon_1 & \varepsilon_1+\Delta_1 & -\Delta_1 \end{pmatrix}. \end{aligned} \tag{7.1.19}$$

The orthogonality eliminates all the $3j$-symbols appearing in the spin recoupling, and we finally we recover composite rule (7.1.17). □

The sum of corner angles defines a deficit angle around a dual vertex in triangulation by $\delta = 2\pi - \sum_i \theta_i$, which is interpreted as the discretization of Ashtekar-Barbero curvature [6]. At the end of the day, we have shown how to define and represent the action of loop holonomy operator on spin networks. The dynamics of the operator is encoded in the spins along loop and bouquet spins around. In the semi-classical regime defined in the large spin limit, the operator relates to the corner angles along the loop.

Now that we have clarified the geometrical interpretation of the loop holonomy operator, we are interested in the entanglement it creates, in the purpose of exploring the relation between quantum geometry and quantum information in the framework of loop quantum gravity.

7.2 Multipartite entanglement and geometric measure of entanglement

In order to investigate and quantify the entanglement structure in loop quantum gravity, the notion of multipartite entanglement is required. Indeed, bipartite entanglement, such as the entanglement between two vertices, is understood to reflect the distance between parts of the quantum state of geometry [167]. General operators, such the loop holonomy, will inevitably create multipartite entanglement between the vertices it acts upon. Since the loop holonomy operator creates curvature excitations, we wish to shed

light on the relation between geometric curvature and multipartite entanglement, in order to open the door to the possibility of defining curvature at the quantum level directly in quantum information terms.

7.2.1 Separable and entangled spin network states

The quantum entanglement between spin sub-networks, is quantified as the *intertwiner entanglement* [190] where spin networks are understood as a many-body quantum system. In order to study multipartite entanglement, we employ the geometric measure of entanglement, which requires us to classify the set of states and distinguish fully separable states [134], i.e., product states as for instance $\rho_{ABC} = \rho_A \otimes \rho_B \otimes \rho_C$. In a fully separable state, subsystems are unentangled.

The present work's purpose is to investigate bulk entanglement on spin network and not to focus on the boundary structures. The difference between bulk and boundary entanglement is described in [190]. We thus look at the Hilbert space of bulk spin network states $\mathcal{H}_{\Gamma^o}$ as the tensor product of the intertwiner Hilbert spaces at every vertex,

$$\mathcal{H}_{\Gamma^o} = \bigoplus_{\{j_e\}_{e\in\Gamma}} \bigotimes_{v\in\Gamma} \mathcal{H}_v^{\{j_e\}_{e\ni v}} \subset \bigotimes_{v\in\Gamma} \mathcal{H}_v \,, \tag{7.2.1}$$

where the vertex Hilbert spaces are defined as

$$\mathcal{H}_v^{\{j_e\}_{e\ni v}} = \mathrm{Inv}_{\mathrm{SU}(2)}\Big[\bigotimes_{e|\, v=s(e)} \mathcal{V}_{j_e} \otimes \bigotimes_{e|\, v=t(e)} \mathcal{V}_{j_e}^* \Big] \quad \text{and} \quad \mathcal{H}_v = \bigoplus_{\{j_e\}_{e\ni v}} \mathcal{H}_v^{\{j_e\}_{e\ni v}} \,. \tag{7.2.2}$$

We consider spin networks as states in the larger Hilbert space $\bigotimes_{v\in\Gamma} \mathcal{H}_v$ of tensor products of intertwiners without imposing the spin matching constraints along the bulk edges $e \in \Gamma^o$. The advantage with this starting point is that we are directly looking at correlations and entanglement between SU(2)-gauge invariant excitations -the intertwiners- and that we do not have to worry about gauge breaking and correlations between non-gauge invariant observables (see e.g. [192, 45, 190] for a discussion on this issue).

A general spin network state can be decomposed as a superposition over spin network basis states:

$$|\psi_\Gamma\rangle \;=\; \sum_{\{I_v\}} C_\Gamma(\{I_v\}) \bigotimes_{v\in\Gamma} |\Psi_{v,I_v}\rangle \,, \qquad \text{where} \quad |\Psi_{\Gamma,\{I_v\}}\rangle = \bigotimes_{v\in\Gamma} |\Psi_{v,I_v}\rangle \,. \tag{7.2.3}$$

Here the intertwiner basis state $|\Psi_{v,I_v}\rangle \in \mathcal{H}_v$ have definite spins and intertwiner, with spins and internal intertwiner indices packaged in the labels I_v. Then the coefficients $C_\Gamma(\{I_v\})$ for a general state allows for superpositions of both spins and intertwiners, thus leading to correlation between intertwiner states located at different vertices.

To define multipartite entanglement and understand how spin sub-networks are entangled, we need to identify the set of fully separable spin network state. Then we will define the geometric entanglement carried by a state as its distance to the set of separable states. Let us thus describe the hierarchy of potential ways to entangle a spin network state. To start with, fully separable (pure) states are states with definite values

of spins and intertwiners, that is spin network basis states (up to the choice of a local basis of intertwiner at each vertex). Then entanglement amounts to non-locally factorizable coefficients $C_\Gamma(\{I_v\})$. We distinguish three sources of entanglement:

1. Entanglement resulting from the correlation between intertwiner states at different vertices for fixed spins on the edges;

2. Entanglement resulting from spin superpositions on edges and thereby creating entanglement between the intertwiners living at the vertices linked by edges carrying such spin superpositions;

3. Entanglement resulting from spin correlations between different edges.

Below, we characterize these three levels in more details.

Let us start by considering two adjacent vertices linked by a certain number of edges. We assume no spin-superposition over these edges. As long as the intertwiners at the two vertices remain uncorrelated (i.e. the coefficient $C(I_{v_1}, I_{v_2}) = C(I_{v_1})C(I_{v_2})$ factorizes), no matter the intertwine superposition at each vertex, the state remains unentangled. Explicitly, this type of uncorrelated but superposed v_1, v_2 state (with no spin-superposition) reads as:

$$\begin{aligned} |\psi\rangle \;=\; \cdots \Bigg(\sum_{I_{v_1}^{(\{j_e\}_{e\ni v_1})}} C(I_{v_1}^{(\{j_e\}_{e\ni v_1})}) |\{j_e\}_{e\ni v_1}, I_{v_1}^{(\{j_e\}_{e\ni v_1})}\rangle \Bigg) \\ \otimes \Bigg(\sum_{I_{v_2}^{(\{j_e\}_{e\ni v_2})}} C(I_{v_2}^{(\{j_e\}_{e\ni v_2})}) |\{j_e\}_{e\ni v_2}, I_{v_2}^{(\{j_e\}_{e\ni v_2})}\rangle \Bigg) \cdots . \end{aligned} \tag{7.2.4}$$

In other words, the uncorrelated intertwiner superposition is simply a change of local intertwiner basis at each vertex.

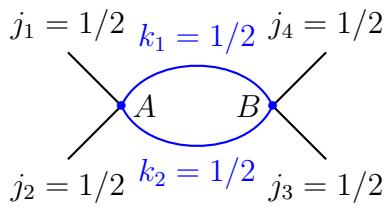

Figure 7.4: Labeling by internal indices, spin network state is written as $\sum_{I_A,I_B} C(I_A, I_B)|I_A, I_B\rangle$. It has intertwiner-correlation via internal indices through nontrivial correlation coefficient $C(I_A, I_B)$, for example, $C(j_{12} = 0, j_{34} = 0) = C(j_{12} = 1, j_{34} = 1) = 1/\sqrt{2}$ and $C(j_{12} = 0, j_{34} = 1) = C(j_{12} = 1, j_{34} = 0) = 0$.

On the other hand, if we still keep spins fixed but consider non-factorizable coefficients $C(I_{v_1}, I_{v_2}) \neq C(I_{v_1})C(I_{v_2})$, then v_1 and v_2 are automatically entangled. A simple example

is shown in fig. 7.4. Note that the cases only happen when v_1 and v_2 both have higher valency than three. This is encapsulated by the following definition:

Definition 7.4 (Entangled states of intertwiner-correlation via internal indices)**.** A spin network state is said to carry intertwiner correlation between vertices v_1 and v_2 via internal indices if the correlation coefficient of internal indices is nontrivial (i.e., unfactorizable). That is,

$$|\psi\rangle = \cdots \Bigg(\sum_{I_{v_1}^{(\{je\}_{e\ni v_1})}, I_{v_2}^{(\{je\}_{e\ni v_2})}} C(I_{v_1}^{(\{j_e\}_{e\ni v_1})}, I_{v_2}^{(\{j_e\}_{e\ni v_2})}) |\{j_e\}_{e\ni v_1}, I_{v_1}^{(\{j_e\}_{e\ni v_1})}\rangle \otimes |\{j_e\}_{e\ni v_2}, I_{v_2}^{(\{j_e\}_{e\ni v_2})}\rangle \Bigg) \cdots . \tag{7.2.5}$$

The set of such states is denoted by $\mathcal{S}_{C_I(\Gamma^o)}$.

This type of intertwiner correlation is only possible due to the non-trivial structure of the intertwiner space for vertices with valence strictly larger than 3. Nevertheless, it turns out possible to correlate two adjacent vertices, even 3-valent ones, and create entanglement by unfreezing the spins and allowing for spin superpositions on the edges linking the two vertices :

Definition 7.5 (Entangled states of bulk spin-superposition)**.** A spin network state has intertwiner-correlation between vertices v_1 and v_2 via bulk spin-superposition if there exists at least one edge $e \in \Gamma^o$ that links two distinct vertices v_1 and v_2 ($v_1 \neq v_2$), the associated spin k_e has spin-superposition. Let $e' \in \{e\}_{e\ni v_1} \cap \{\widetilde{e}\}_{\widetilde{e}\ni v_2}$ be a common edge linked v_1 and v_2, and $C(k_{e'})$ be the spin-superposition coefficient, then any state in the form of

$$|\psi\rangle = \cdots \left(\sum_{k_{e'}} C(k_{e'}) \, |\{j_e\}_{e\ni v_1}, I_{v_1}^{(\{j_e\}_{e\ni v_1})}\rangle \otimes |\{j_{\widetilde{e}}\}_{e\ni v_2}, I_{v_2}^{(\{j_{\widetilde{e}}\}_{\widetilde{e}\ni v_2})}\rangle \right) \cdots \tag{7.2.6}$$

is entangled. Then we denote the set of such states by $\mathcal{S}_{S_j(\Gamma^o)}$.

A simple example is shown in fig. 7.5. Indeed, as long as two vertices have one common edge with spin-superposition, their intertwiners are entangled, since the spin is a common index for intertwiners at v_1 and v_2.

Finally, the vertices v_1 and v_2 can be entangled if their have spin-correlation, i.e., there exists nontrivial correlation coefficient $C(j_1, j_2, \cdots)$ for spins where j_1 and j_2 are two spins attached to two different vertices.

Definition 7.6 (Entangled states of spin-correlation)**.** A spin network state has intertwiner-correlation between vertices v_1 and v_2 via spin-correlation if there exists spin-correlation

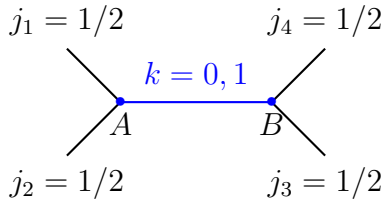

Figure 7.5: Spin network state is written as $\sum_k C(k)|j_1, j_2, k\rangle \otimes |j_3, j_4, k\rangle$. The intertwiners $|j_1, j_2, k\rangle$ and $|j_3, j_4, k\rangle$ are entangled if k has superposition, e.g., $C(k = 0) = C(k = 1) = 1/\sqrt{2}$.

between two edges e_1, e_2 that $e_1 \ni v_1$, $e_2 \ni v_2$ and $v_1 \neq v_2$. Let $C(j_{e_1}, j_{e_2})$ be the correlation coefficient, then any state in the form of

$$|\psi\rangle = \cdots \left(\sum_{j_{e_1}, j_{e_2}} C(j_{e_1}, j_{e_2}) \, |\{j_e\}_{e\ni v_1}, I_{v_1}^{(\{j_e\}_{e\ni v_1})}\rangle \otimes |\{j_{\tilde{e}}\}_{e\ni v_2}, I_{v_2}^{(\{j_{\tilde{e}}\}_{\tilde{e}\ni v_2})}\rangle \right) \cdots \tag{7.2.7}$$

is entangled. The set of such states is denoted by $\mathcal{S}_{C_j(\Gamma)}$.

We look at an example shown in fig. 7.6. Consider below two spin network states

$$|\phi\rangle = \left(\sum_{j_1} C(j_1) \, |j_1, k_1, k_2\rangle \right) \otimes \left(\sum_{j_2} C(j_2) \, |j_2, k_1, k_2\rangle \right) , \tag{7.2.8}$$

$$|\psi\rangle = \sum_{j_1, j_2} C(j_1, j_2) \, |j_1, k_1, k_2\rangle \otimes |j_2, k_1, k_2\rangle \, . \tag{7.2.9}$$

Both states have boundary spin-superposition. The distinction is that $|\psi\rangle$ has spin-correlation while $|\phi\rangle$ has not, thus $|\psi\rangle$ is entangled (e.g., fig.7.6) while $|\phi\rangle$ is unentangled.

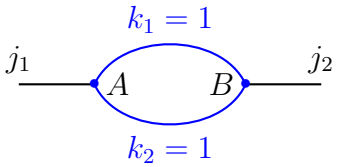

Figure 7.6: Spin network state is written as $\sum_{j_1,j_2} C(j_1, j_2)|j_1, k_1, k_2\rangle \otimes |j_2, k_1, k_2\rangle$ which has boundary spin correlation via unfactorizable correlation coefficient $C(j_1, j_2)$, for example, $C(j_1 = 1, j_2 = 1) = C(j_1 = 2, j_2 = 2) = 1/\sqrt{2}$ and $C(j_1 = 1, j = 2) = C(j_1 = 2, j_1 = 1) = 0$.

Let us summarize the structures described above in the following statement:

(a) Illustration for spin network state whose boundary spins are in superposition but intertwiners are still uncorrelated.

(b) Illustration for spin network state whose loop spins are in superposition but intertwiners are still uncorrelated.

Figure 7.7: The examples for separable states which are not spin network basis states.

Result 7.7. *In the spin network Hilbert space $\mathcal{H}_\Gamma$ for a graph, possibly with a boundary, the set of fully separable states is defined as the set of states which do not carry intertwiner correlation, bulk spin superposition or spin correlations:*

$$\mathcal{S}_{separable(\Gamma)} = \mathcal{H}_\Gamma \setminus \left(\mathcal{S}_{C_I(\Gamma^o)} \cup \mathcal{S}_{S_j(\Gamma^o)} \cup \mathcal{S}_{C_j(\Gamma)}\right). \tag{7.2.10}$$

Separable states are thus states which might have boundary spin superpositions, as long as the boundary spins remain uncorrelated, and that for each set of boundary spins, the bulk spins and intertwiners are fixed.

In particular, spin network basis states are unentangled,

$$\mathcal{S}_{basis(\Gamma)} \subset \mathcal{S}_{separable(\Gamma)}. \tag{7.2.11}$$

It is interesting to characterize the separable states which are not spin network basis states. First, we put aside the possibility of uncorrelated intertwiner superpositions, since these are still spin network basis states up to a mere change of intertwiner basis locally at each vertex. We are then left with two possibilities:

- (uncorrelated) superpositions of boundary spins;
- (uncorrelated) superpositions of spins on a self-loop, i.e. an edge linking a vertex to itself.

Result 7.8 (Unentangled states on trivalent spin network)**.** *For spin network states on trivalent graphs without any self-loop, if we restrict to study a subspace of spin network with fixed boundary spins, then the set of fully separable states is the set of spin network basis states (with fixed spins on every bulk edges).*

In the present work, for the sake of simplicity, we focus on the entanglement carried by trivalent spin networks, in which the above result 7.8 applies. In fact, we could easily extend the analysis to higher valent vertices since the loop holonomy operator does not affect the internal space of intertwiner and can be understood as acting as on 3-valent

vertices obtained by unfolding the vertices in terms of bouquet spins, as explained earlier. This would simply complicate notations.

Knowing what fully separable states are in loop quantum gravity, we are able to adopt the geometric measure of entanglement (c.f. Chapter 3 [139, 201]) as a witness of multipartite entanglement. It quantifies entanglement of a pure state through the minimal distance of the state from the set of pure fully separable states

$$S_g(\Psi) = -\ln \max_{\Phi} |\langle \Phi|\Psi\rangle|^2 \,, \tag{7.2.12}$$

where the maximum is on the set of fully separable states Φ. Via variational method, it turns out that $\langle\Phi|\Psi\rangle$ is a real number when it reaches the extremal value [139]. The maximal value of $|\langle\Phi|\Psi\rangle|^2$ is called *entanglement eigenvalue*. In particular for bipartite system, the entanglement eigenvalue is the maximal Schmidt eigenvalue of reduced density matrix, and moreover, each Schmidt eigenvalue is an extremal value for $|\langle\Phi|\Psi\rangle|^2$.

Usually, the maximal projection is probably not easy to find. For the situation the Proposition 7.8 concerns, to obtain the maximum, what we need to do is to project the considered possibly entangled state onto the spin network basis states, then identify the most probable basis state. The projection determines the entanglement eigenvalue, so determines the geometric measure of entanglement.

So far we have discussed the classification of unentangled spin networks and entangled spin networks, and definition of geometrical measure of entanglement. The next question is how the entanglement evolves under dynamics, for instance generated by a loop holonomy operator.

7.2.2 The leading order evolution of geometric entanglement

In this part, we investigate how geometrical measure of entanglement evolves under dynamics driven by a given hamiltonian. Assume that $|\Psi_0\rangle$ is the initial state and that the evolution is generated by the exponential map $e^{-\mathrm{i}\widehat{H}t}$ with respect to a hermitian operator $\widehat{H}$. We will show that at least the 1st- and 2nd- order derivative of geometric measure of entanglement with respect to time parameter t can be expressed in a simple fashion in terms of the hermitian operator.

The state $|\Psi_0\rangle$ evolves as $|\Psi(t)\rangle = e^{-\mathrm{i}\widehat{H}t}|\Psi_0\rangle$ with $|\Psi(t=0)\rangle = |\Psi_0\rangle$. Expanding it up to the 2nd order around the initial time reads

$$|\Psi(t)\rangle = e^{-\mathrm{i}\widehat{H}t}|\Psi_0\rangle = |\Psi_0\rangle - \mathrm{i}t\widehat{H}|\Psi_0\rangle - \frac{t^2}{2}\widehat{H}^2|\Psi_0\rangle + \mathcal{O}(t^3)\,. \tag{7.2.13}$$

The definition of the geometric measure of entanglement involves the fully separable state $|\Phi(t)\rangle$ corresponding to $|\Psi(t)\rangle$, which maximizes the probability $|\langle\Phi(t)|\Psi(t)\rangle|^2$ at every instant t, i.e., $|\langle\Phi(t)|\Psi(t)\rangle|^2 = \max_{\Phi'} |\langle\Phi'|\Psi(t)\rangle|^2$ for any t where $|\Phi'\rangle$ runs over the set of fully separable states. As we are not dealing with a rigged Hilbert space which may allow diverging distribution, the scalar product reamins bounded, $0 \leq |\langle\Phi'|\Psi(t)\rangle|^2 \leq 1$.

However, notice that the definition of the optimal separable state $\{|\Phi(t)\rangle\}$ might be ambiguous. We provide two simple, hopefully helpful, examples A.1 and A.2 in appendix.

Nevertheless, the geometric entanglement value is always continuous. This follows from the continuity of dynamics. For instance, thinking of a bipartite system, the dynamics of the Schmidt eigenvalues $\lambda(t)$ of the reduced density matrix can be described by a master equation, which relates the 1st-order derivative of the Schmidt eigenvalues with respect to t, to the commutator $[\widehat{H}, \rho]$. Since $\widehat{H}$ and ρ are assumed to be well-behaved operators, the $\mathrm{d}\lambda(t)/\mathrm{d}t$ is also well-behaved. One possible concern is that entanglement eigenvalue $\lambda_{\max}$ might be discontinuous. Indeed starting with the maximal eigenvalue $\lambda_1(t)$ at time t_1, it is possible that it is not anymore the maximal eigenvalue at a later time t_2. Namely, such a discontinuity happens when the order of the eigenvalues switches, i.e. if $\lambda_1(t) > \lambda_2(t)$ when $t \leq t_2$ while $\lambda_1(t) < \lambda_2(t)$ when $t > t_2$: the maximal eigenvalue would jump from the branch λ_1 to the branch λ_2. However, even in that case, the entanglement eigenvalue is still continuous: since $\lambda_1(t)$ and $\lambda_2(t)$ are both continuous, there exists a transition time t such that $\lambda_1(t) = \lambda_2(t)$. The example A.1 is an example for the case where the entanglement eigenvalue switches the branches at $t = \pi/4$ while remaining continuous.

Let us look more closely at the evolution of the entanglement close to the initial time (keeping in mind that one can arbitrarily swift the initial choice). Let us expand the scalar product $|\langle\Phi(t)|\Psi(t)\rangle|^2$ in a Taylor series in t:

$$\begin{aligned} |\langle\Phi(t)|\Psi(t)\rangle|^2 &= |\langle\Phi(t)|e^{-it\widehat{H}}|\Psi_0\rangle|^2 \qquad (7.2.14)\\ &= \big|\langle\Phi(t)|\Psi_0\rangle\big|^2 + it\Big[\langle\Phi(t)|\Psi_0\rangle\langle\Psi_0|\widehat{H}|\Phi(t)\rangle - \langle\Phi(t)|\widehat{H}|\Psi_0\rangle\langle\Psi_0|\Phi(t)\rangle\Big] \\ &\quad + \frac{t^2}{2}\Big[2\langle\Phi(t)|\widehat{H}|\Psi_0\rangle\langle\Psi_0|\widehat{H}|\Phi(t)\rangle - \langle\Phi(t)|\widehat{H}^2|\Psi_0\rangle\langle\Psi_0|\Phi(t)\rangle \\ &\quad - \langle\Phi(t)|\Psi_0\rangle\langle\Psi_0|\widehat{H}^2|\Phi(t)\rangle\Big] + \mathcal{O}(t^3)\,. \qquad (7.2.15)\end{aligned}$$

This is not exactly a full Taylor expansion since $\Phi(t)$ still depends on time. The first term $\big|\langle\Phi(t)|\Psi_0\rangle\big|^2$ actually reaches its maximal value at $t = 0$, by definition of the state $\Phi(t)$, and thus has vanishing first derivative:

$$\big|\langle\Phi(t)|\Psi_0\rangle\big|^2 = \big|\langle\Phi_0|\Psi_0\rangle\big|^2 + \mathcal{O}(t^2)\,. \qquad (7.2.16)$$

But there is a priori no obvious further simplification.

Let us make a first assumption:

- The initial state is separable, thus $\Phi_0 = \Psi_0$.

We can then prove that the first derivative of $|\langle\Phi(t)|\Psi(t)\rangle|^2$ vanishes and that the leading order of the geometric entanglement $\ln|\langle\Phi(t)|\Psi(t)\rangle|^2$ is in $\mathcal{O}(t^2)$. Let us assume that the separable projection is smooth in a neighbourhood of the initial time and expand it in a Taylor series up to second order for $t > 0$:

$$\Phi(t) = \Psi_0 + t\Phi^{(1)} + t^2\Phi^{(2)} + \ldots \qquad (7.2.17)$$

The normalization condition on that state reads:

$$1 = \langle\Phi(t)|\Phi(t)\rangle$$

$$= 1 + t\underbrace{\Big[\langle\Psi_0|\Phi^{(1)}\rangle + \langle\Phi^{(1)}|\Psi_0\rangle\Big]}_{=0} + t^2\underbrace{\Big[\langle\Phi^{(1)}|\Phi^{(1)}\rangle + \langle\Psi_0|\Phi^{(2)}\rangle + \langle\Phi^{(2)}|\Psi_0\rangle\Big]}_{=0} + \dots \tag{7.2.18}$$

This allows us to expand the terms in the scalar product $|\langle\Phi(t)|\Psi(t)\rangle|^2$:

$$\begin{aligned}\big|\langle\Phi(t)|\Psi_0\rangle\big|^2 &= 1 + t\underbrace{\Big[\langle\Psi_0|\Phi^{(1)}\rangle + \langle\Phi^{(1)}|\Psi_0\rangle\Big]}_{=0} \\ &\quad + t^2\underbrace{\Big[\langle\Psi_0|\Phi^{(1)}\rangle\langle\Phi^{(1)}|\Psi_0\rangle + \langle\Psi_0|\Phi^{(2)}\rangle + \langle\Phi^{(2)}|\Psi_0\rangle\Big]}_{=\langle\Psi_0|\Phi^{(1)}\rangle\langle\Phi^{(1)}|\Psi_0\rangle - \langle\Phi^{(1)}|\Phi^{(1)}\rangle} + \mathcal{O}(t^3)\,.\end{aligned} \tag{7.2.19}$$

Similarly, the second term, $\Big[\langle\Phi(t)|\Psi_0\rangle\langle\Psi_0|\widehat{H}|\Phi(t)\rangle - \langle\Phi(t)|\widehat{H}|\Psi_0\rangle\langle\Psi_0|\Phi(t)\rangle\Big]$, vanishes at $t = 0$ and its first order depends on Ψ_0 and $\Phi^{(1)}$. As a consequence, the scalar product has a vanishing first derivative and is trivial up to second order, $|\langle\Phi(t)|\Psi(t)\rangle|^2 = 1 + \mathcal{O}(t^2)$, thus

$$\begin{aligned}S_g &= -\ln|\langle\Phi(t)|\Psi(t)\rangle|^2 \\ &= t^2\Big[\langle\Psi_0|\widehat{H}^2|\Psi_0\rangle - \langle\Psi_0|\widehat{H}|\Psi_0\rangle^2 + \langle\Phi^{(1)}|\Phi^{(1)}\rangle - \langle\Psi_0|\Phi^{(1)}\rangle\langle\Phi^{(1)}|\Psi_0\rangle + \mathrm{i}(\langle\Psi_0|\Phi^{(1)}\rangle \\ &\quad -\langle\Phi^{(1)}|\Psi_0\rangle)\langle\Psi_0|\widehat{H}|\Psi_0\rangle + \mathrm{i}(\langle\Phi^{(1)}|\widehat{H}|\Psi_0\rangle - \langle\Psi_0|\widehat{H}|\Phi^{(1)}\rangle)\Big] + \mathcal{O}(t^3)\,,\end{aligned} \tag{7.2.20}$$

with the t^2-coefficient depending explicitly on the linear deviation $\Phi^{(1)}$ of the separable projection.

Let us then make a further assumption, which is tailor-suited to the present case of study and allows us to determine exactly $\Phi^{(1)}$:

- the set of separable states is discrete, i.e. separable states are isolated points in the Hilbert space.

This happens for trivalent spin networks, since the spin network basis states are entirely determined by the spin labels on the edges and there is no local degrees of freedom at the vertices once the spins are fixed. This leads to a countable set of isolated separable states. The deep consequence is that $\Phi(t)$ is a step function, jumping from separable state to separable state. Let us keep in mind that, although $\Phi(t)$ is discontinuous, the scalar product $|\langle\Phi(t)|\Psi(t)\rangle|^2$ and resulting entanglement remain continuous functions of the time t. Therefore, $\Phi(t)$ is constant in a neighbourhood of the initial time, it is equal to the initial state Ψ_0 and its first derivative $\Phi^{(1)}$ vanishes. The scalar product,

$$|\langle\Phi(t)|\Psi(t)\rangle|^2 \underset{t\sim 0}{=} |\langle\Psi_0|\Psi(t)\rangle|^2\,, \tag{7.2.21}$$

reduces to the projection of the evolving state $\Psi(t)$ onto the initial set and geometric entanglement's leading order is simply given by the dispersion of the Hamiltonian operator:

$$S_g(t) = t^2\Big[\langle\Psi_0|\widehat{H}^2|\Psi_0\rangle - \langle\Psi_0|\widehat{H}|\Psi_0\rangle^2\Big] + \mathcal{O}(t^3) \tag{7.2.22}$$

This will simplify all the entanglement calculations, as we will see in explicit examples in the next sections. It will be validated to the comparison to the linear entanglement entropy (for bipartitions), which will give exactly the same leading order in t^2. One should nevertheless remember that, if we consider spin networks with four-valent or higher-valent vertices, the leading order will remain in t^2 but the precise factor will probably acquire corrections to the $\widetilde{H}$-dispersion depending on the precise dynamics of the separable projection and its linear deviation $\Phi^{(1)}$.

7.2.3 Entanglement excitation and closure defect distribution

Let us apply the results from the previous section to the action of the loop holonomy operator. We consider an unentangled initial state $|\Psi_0\rangle$, given by a spin network basis state. Its separable projection is itself, $|\Phi(t=0)\rangle = |\Psi_0\rangle$. We would like to know the entanglement excitation created by the loop holonomy operator. Applying the formula (7.2.22) derived above to the holonomy operator leads to the following result:

Result 7.9. *Let $|\Psi_0\rangle$ be any trivalent spin network basis state, and $\widehat{\chi_\ell} \triangleright_W$ be a loop holonomy operator where W is loop through more than one vertex (i.e., W is not a self-loop). The $|\Psi(t)\rangle$ is the state driven by $\widehat{\chi_\ell} \triangleright_W$ from initial state $|\Psi_0\rangle$. Then the 1st-order and 2nd-order derivative of geometric measure of entanglement at $t = 0$ are given by*

$$\frac{\mathrm{d}S_g[\Psi(t)]}{\mathrm{d}t}\Big|_{t=0} = 0\,, \qquad \frac{1}{2}\frac{\mathrm{d}^2 S_g[\Psi(t)]}{\mathrm{d}t^2}\Big|_{t=0} = \langle\Psi_0|\left(\widehat{\chi_\ell} \triangleright_W\right)^2|\Psi_0\rangle - \langle\Psi_0|\widehat{\chi_\ell} \triangleright_W|\Psi_0\rangle^2\,. \quad (7.2.23)$$

Let us apply this to a spin network made of a single loop with boundary edge insertions, as drawn in fig.7.8. This case illustrates an interesting relation between the leading order entanglement evolution, as given by equation (7.2.23), and the closure defect, defined as the recoupled spin of the boundary spins . This relation is realized by relating the dispersion of loop holonomy operator $\widehat{\chi_\ell} \triangleright_W$, which gives the 2nd-order derivative of the entanglement, to the probability distribution of the closure defect.

We use the techniques introduced in Chapter 5. The wave-function of spin network (on left hand side of fig.7.8) can be thought as a bulk-boundary map mapping bulk holonomies (on the edges along the loop) to vectors in the boundary Hilbert space $\bigotimes_{e\in\partial\Gamma}\mathcal{V}_{j_e}$. Using the gauge-invariance property of spin networks and proceeding to a gauge-fixing of all but one edges around the loop, we can reduce the the one-loop spin network to its gauge-fixed counterpart, drawn on the right hand side of fig.7.8). This allows to write the spin network functional as a function of a single group element G, representing the holonomy around the loop:

$$|\psi_{\partial\Gamma}(G)\rangle = \sum_J e^{\mathrm{i}\varphi_k(J)}\sqrt{p_k(J)}\sum_{a,b=-k}^{k}\sqrt{2k+1}(-1)^{k-a}D^k_{ab}(G)\begin{pmatrix} J & k & k \\ M & b & -a\end{pmatrix}|J,M\rangle \quad (7.2.24)$$

$$\in \bigotimes_{e\in\partial\Gamma}\mathcal{V}_{j_e}\,.$$

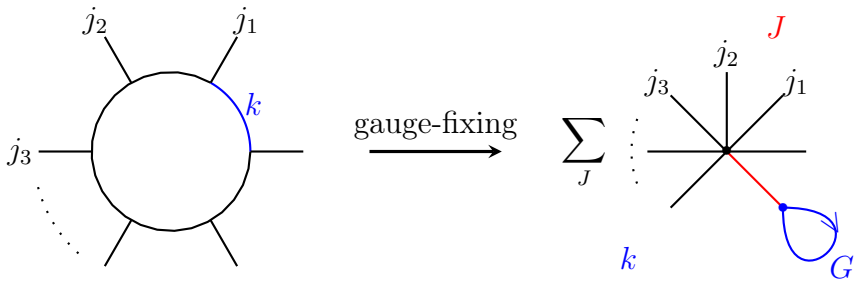

Figure 7.8: The left hand side is a trivalent spin network where all bulk edges lie along a circle. We can choose a maximal tree such that all of bulk edges except the blue one form a path where all the holonomies can be set into identity element of SU(2). By means of contracting the maximal tree, the blue edge with spin-k becomes a loopy edge with same spin-k and holonomy G. The spin-J is recoupled from boundary spins

The spin-J is the recoupled spin of all the boundary spins and is called the closure defect. The probability amplitude $\sqrt{p_k(J)}\, e^{\mathrm{i}\varphi_k(J)}$ is a function of the spin k living on the gauge-fixed loop (the blue edge on fig.7.8). It fully characterizes the gauge-fixed spin network state and reflects the spins dressing the edges around the loop before gauge-fixing. In particular, if one were to choose another edge as the loopy edge, the resulting probability amplitude would be a priori different, though gauge equivalent. The modulus square of the probability amplitude gives the probability distribution $p_k(J)$ for the closure defect, which satisfies the normalization $\sum_J p_k(J) = 1$.

Now let us look at the loop holonomy operator. It acts on the spin network state. But since the operator and state are both gauge invariant, one can legitimately look at the holonomy operator acting on gauge-fixed spin network states. One should be careful: the entanglement structures are totally different on the two graphs, because the gauge-fixing procedure involves the procedure of contracting vertices, thus changes the number of vertices on graph. Nevertheless, if one is interested in the dispersion of the loop holonomy operator, then the gauge-fixing does not change anything. So let us apply the loop holonomy operator on the self-loop of the gauge-fixed state, depicted on the right hand side of fig.7.8. Its action involves both spins k and J. Applying the general formula (7.1.8) to this simple setting yields the following wave-function:

$$\begin{aligned}
&\widehat{\chi}_\ell \triangleright_W |\psi_{\partial\Gamma}(G)\rangle = \chi_\ell(G)\, |\psi_{\partial\Gamma}(G)\rangle \qquad (7.2.25)\\
= &\sum_J e^{\mathrm{i}\varphi_k(J)} \sqrt{p_k(J)} \sum_{K=|k-\ell|}^{k+\ell} (2K+1)(-1)^{J+\ell+k+K} \begin{Bmatrix} J & K & K \\ \ell & k & k \end{Bmatrix}\\
&\times \sum_{a,b=-K}^{K} \sqrt{2k+1}(-1)^{K-a} D^K_{ab}(G) \begin{pmatrix} J & K & K \\ M & b & -a \end{pmatrix} |J, M\rangle\,.
\end{aligned}$$

We compute the mean value and deviation of the operator on the quantum state:

$$\begin{aligned}
\langle\, (\widehat{\chi}_\ell \triangleright_W)^2 \,\rangle &= \int_{\mathrm{SU}(2)^E} \prod_{e\in E} \mathrm{d}g_e \, \langle \psi_{\partial\Gamma}(G) | (\widehat{\chi}_\ell \triangleright_W)^2 | \psi_{\partial\Gamma}(G)\rangle \\
&= \sum_J p_k(J) \sum_{s=0(1)}^{2\ell} (-1)^{J+s+2k} \begin{Bmatrix} J & k & k \\ s & k & k \end{Bmatrix} (2k+1)\,, \qquad (7.2.26) \\
\langle\, \widehat{\chi}_\ell \triangleright_W \,\rangle &= \int_{\mathrm{SU}(2)^E} \prod_{e\in E} \mathrm{d}g_e \, \langle \psi_{\partial\Gamma}(G) | \widehat{\chi}_\ell \triangleright_W | \psi_{\partial\Gamma}(G)\rangle \\
&= \sum_J p_k(J) (-1)^{J+\ell+2k} \begin{Bmatrix} J & k & k \\ \ell & k & k \end{Bmatrix} (2k+1)\,. \qquad (7.2.27)
\end{aligned}$$

Here the notation $s = 0(1)$ below the summation means the spin s starts from 0 ascending with step 1. The expectation $\langle\, \widehat{\chi}_\ell \triangleright_W \,\rangle$ automatically vanishes when $\ell \in \mathbb{N} + \frac{1}{2}$, due to the triangle condition on $6j$-symbol. Here we have employed the recoupling formula $\widehat{\chi}_\ell \triangleright_W \circ \widehat{\chi}_\ell \triangleright_W = \sum_{s=0}^{2\ell} \widehat{\chi}_s \triangleright_W$ to compute the expectation $\langle\, (\widehat{\chi}_\ell \triangleright_W)^2 \,\rangle$. This gives the 2nd-order derivative of the geometric entanglement at the initial time:

$$\begin{aligned}
\frac{1}{2}\frac{\mathrm{d}^2 S_g}{\mathrm{d}t^2}\Big|_{t=0} &= \sum_J p_k(J) \sum_{s=0(1)}^{2\ell} (-1)^{J+s+2k} \begin{Bmatrix} J & k & k \\ s & k & k \end{Bmatrix} (2k+1) \\
&\quad - \left(\sum_J p_k(J) (-1)^{J+\ell+2k} \begin{Bmatrix} J & k & k \\ \ell & k & k \end{Bmatrix} (2k+1) \right)^2 . \qquad (7.2.28)
\end{aligned}$$

This gives the excitation of entanglement created by the loop holonomy operator. We should emphasize that eventhough the probability the $p_k(J)$ might depend on the choice of gauge-fixing (through the choice of the loopy edge), these averages are gauge invariant and do not depend on the gauge-fixing.

Recalling the triangle condition on $6j$-symbols, there are two points observed from above expression: (i) if $\ell \in \mathbb{N} + \frac{1}{2}$, the second term vanishes. (ii) if $s > 2k$, then the contribution from $\begin{Bmatrix} J & k & k \\ s & k & k \end{Bmatrix}$ vanishes. So there is a critical value $\ell_c = 2k + \frac{1}{2}$ such that once ℓ grows beyond this critical value ℓ_c, the 2nd-order derivative is a constant with respect to ℓ. The plateau value is easily computed using a standard identity on the $\{6j\}$-symbols[2] and is a simple averaging of the probability distribution of the closure defect:

$$\ell \geq 2k + \frac{1}{2} : \qquad \frac{1}{2}\frac{\mathrm{d}^2 S_g}{\mathrm{d}t^2}\Big|_{t=0} = \sum_J \frac{p_k(J)}{2J+1}(2k+1)\,. \qquad (7.2.29)$$

This quantifies the amount of multibody entanglement created by the action of loop holonomy operator when acting on a pure spin network basis state. The holonomy operator

[2]We employ $\sum_{s=0(1)}^{2k} (-1)^{J+s+2k} \begin{Bmatrix} J & k & k \\ s & k & k \end{Bmatrix} = \frac{1}{2J+1}$.

entangles all the vertices around the loop with an entanglement growing in t^2 and its acceleration is directly related to the distribution of the closure defect -or, in other words, the recoupled boundary spin.

7.3 Example: Bipartite entanglement on candy graph

In this section we look at the example of entanglement excitation on candy graph as fig.7.9. This is a graph with a single loop and a pair of boundary spin insertions. The very simple structure of the graph allows us to study in full details the entanglement between the two vertices of the graph.

7.3.1 Entanglement entropy excitation on candy graph with truncated dynamics

We consider the holonomy operator acting on the loop of the candy graph. We compute explicitly the bipartite entanglement between the two vertices, defined as the entropy of the reduced density matrix after tracing over one of the two vertices. Actually, we compute both the von Neumann entropy and the linear entropy, but we prefer to use the linear entropy as measure of entanglement due to the non-differentiability of the von Neumann entropy at initial time for an initial separable state. Then we show that this measure of bipartite entanglement fits exactly with the geometric entanglement formula derived in the previous section up to 2nd order, thereby providing a relevant consistency check of that previous analysis.

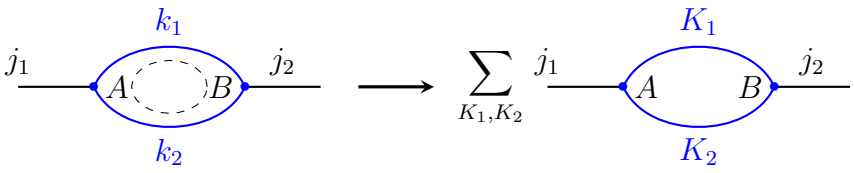

Figure 7.9: Loop holonomy operator acts on candy graph spin network, which leads to the spin-superposition over bulk spins.

As illustrated on fig.7.9, the Hilbert space of spin networks on the candy graph for fixed boundary spins j_1 and j_2 is the tensor poroduct of the two intertwiner spaces sitting at the graph vertices:

$$\mathcal{H}_A = \bigoplus_{K_1,K_2} \mathrm{Inv}_{\mathrm{SU}(2)}\Big(\mathcal{V}_{j_1}\otimes\mathcal{V}_{K_1}\otimes\mathcal{V}_{K_2}\Big)\,, \qquad \mathcal{H}_B = \bigoplus_{K_1,K_2} \mathrm{Inv}_{\mathrm{SU}(2)}\Big(\mathcal{V}_{j_2}\otimes\mathcal{V}_{K_1}\otimes\mathcal{V}_{K_2}\Big)\,. \quad (7.3.1)$$

Spin network states can involve superpositions of the bulk spins K_1 and K_2 (while keeping the boundary spins j_1 and j_2 fixed). Such bulk spin superposition naturally induces a superposition of intertwiners. If this superposition carries correlations between the two vertices, this will be reflected in the entanglement between the two vertices.

Starting with an initial spin network basis state $|\Psi_{can,\{j_i,k_i\}}\rangle = |j_i, k_1, k_2\rangle_A \otimes |j_2, k_1, k_2\rangle_B$, we consider the evolution generated by the loop holonomy operator $\widehat{\chi}_\ell$,

$$\begin{aligned}\widehat{\chi}_\ell : \quad & \mathrm{Inv}_{\mathrm{SU}(2)}\Big(\mathcal{V}_{j_1}\otimes\mathcal{V}_{k_1}\otimes\mathcal{V}_{k_2}\Big)\otimes\mathrm{Inv}_{\mathrm{SU}(2)}\Big(\mathcal{V}_{j_2}\otimes\mathcal{V}_{k_1}\otimes\mathcal{V}_{k_2}\Big)\\ & \longrightarrow \bigoplus_{K_1,K_2}\mathrm{Inv}_{\mathrm{SU}(2)}\Big(\mathcal{V}_{j_1}\otimes\mathcal{V}_{K_1}\otimes\mathcal{V}_{K_2}\Big)\otimes\mathrm{Inv}_{\mathrm{SU}(2)}\Big(\mathcal{V}_{j_2}\otimes\mathcal{V}_{K_1}\otimes\mathcal{V}_{K_2}\Big),\end{aligned}$$

For infinitesimal time $t \to 0$, the unitarity evolution operator is $e^{-\mathrm{i}t\,\widehat{\chi}_\ell} = \mathbb{I} - \mathrm{i}t\,\widehat{\chi}_\ell - \frac{1}{2}t^2\widehat{\chi}_\ell\,\widehat{\chi}_\ell + \mathcal{O}(t^3)$, which acts as

$$\begin{aligned}& e^{-\mathrm{i}t\,\widehat{\chi}_\ell}|\Psi_{can,\{j_i,k_i\}}\rangle = e^{-\mathrm{i}t\,\widehat{\chi}_\ell}|j_1,k_1,k_2\rangle_A\otimes|j_2,k_1,k_2\rangle_B\\ = & \sum_{K_i=|k_i-\ell|}^{k_i+\ell}\left(\delta^{K_1}_{k_1}\delta^{K_2}_{k_2} - \mathrm{i}t[Z(can)^{j_1,j_2}_\ell]^{K_1,K_2}{}_{k_1,k_2} - \frac{1}{2}t^2[Z(can)_\ell Z(can)^{j_1,j_2}_\ell]^{K_1,K_2}{}_{k_1,k_2}\right)\\ & \underbrace{|j_1,K_1,K_2\rangle_A\otimes|j_2,K_1,K_2\rangle_B}_{|\Psi_{can,\{j_i,K_i\}}\rangle} + \mathcal{O}(t^3)\,, \end{aligned} \tag{7.3.2}$$

where $|j_i, K_1, K_2\rangle_A \in \mathcal{H}_A$ and $|j_2, K_1, K_2\rangle_B \in \mathcal{H}_B$ denote the intertwiners living at respect trivalent vertex. According to equation (7.1.8), the transition matrix $Z(can)_\ell$ is given by

$$\begin{aligned}[Z(can)^{j_1,j_2}_\ell]^{K_1,K_2}{}_{k_1,k_2} &= (-1)^{j_1+j_2+k_1+k_2+K_1+K_2+2\ell}\begin{Bmatrix} j_1 & k_1 & k_2\\ \ell & K_2 & K_1\end{Bmatrix}\begin{Bmatrix} j_2 & k_1 & k_2\\ \ell & K_2 & K_1\end{Bmatrix}\\ &\quad\times\prod_{i=1}^{2}\sqrt{(2k_i+1)(2K_i+1)}\,.\end{aligned} \tag{7.3.3}$$

The matrix elements are all real numbers. We take special care in properly normalizing the truncated state:

$$\begin{aligned}& |\Psi_{can,\{j_i,k_i\}}(\ell,t)\rangle\\ = & \Big(|j_1,k_1,k_2\rangle_A\otimes|j_2,k_1,k_2\rangle_B - \mathrm{i}t\sum_{\{K_i\}}[Z(can)^{j_1,j_2}_\ell]^{K_1,K_2}{}_{k_1,k_2}|j_1,K_1,K_2\rangle_A\otimes|j_2,K_1,K_2\rangle_B\\ & -\frac{1}{2}t^2\sum_{s=0}^{2\ell}\sum_{\{K_i\}}[Z(can)^{j_1,j_2}_s]^{K_1,K_2}{}_{k_1,k_2}|j_1,K_1,K_2\rangle_A\otimes|j_2,K_1,K_2\rangle_B\Big)\times\frac{1}{\sqrt{N_{can,\{j_i,k_i\}}(\ell,t)}}\,.\end{aligned} \tag{7.3.4}$$

where the normalization factor is computed up to fourth order

$$N_{can,\{j_i,k_i\}}(\ell,t) = 1 + \mathcal{O}(t^4)\,. \tag{7.3.5}$$

We now compute the entanglement entropy from the truncated state (7.3.4). Since the initial state is unentangled, this entanglement entropy is entirely created by the process.

The reduced density matrix $\rho_{can_A} \in \mathrm{End}(\mathcal{H}_A)$ is obtained via partial tracing over $\mathcal{H}_B$, the reduced density matrix $\rho_{can_A}(t)$ then reads:

$$\begin{aligned}
&\rho_{can_A}(t) \\
= \;& \frac{1}{N_{can,\{j_i,k_i\}}(\ell,t)}\Bigg(\Big(1-t^2\sum_{s=0}^{2\ell}[Z(can)_s^{j_1,j_2}]^{k_1,k_2}{}_{k_1,k_2}\Big)|j_1,k_1,k_2\rangle\langle j_1,k_1,k_2|_A \\
& +t^2\sum_{\{K_i\}}\Big([Z(can)_\ell^{j_1,j_2}]^{K_1,K_2}{}_{k_1,k_2}\Big)^2|j_1,K_1,K_2\rangle\langle j_1,K_1,K_2|_A+\mathcal{O}(t^4)\Bigg)\,. \qquad (7.3.6)
\end{aligned}$$

The eigenvalues of $\rho_{can_A}(t)$ can be read off directly from this formula since the reduced density matrix is diagonal in the $|j_1,K_1,K_2\rangle_A$ basis,

$$\begin{aligned}
\lambda_{\rho_{can_A}}[K_1,K_2] \;=\; & \Big(1-t^2\sum_{s=0}^{2\ell}[Z(can)_s^{j_1,j_2}]^{k_1,k_2}{}_{k_1,k_2}\Big)\delta_{k_1}^{K_1}\,\delta_{k_2}^{K_2} \\
& +t^2\begin{Bmatrix} j_1 & k_1 & k_2 \\ \ell & K_2 & K_1\end{Bmatrix}^2\begin{Bmatrix} j_2 & k_1 & k_2 \\ \ell & K_2 & K_1\end{Bmatrix}^2\prod_{i=1}^{2}(2k_i+1)(2K_i+1)+\mathcal{O}(t^4)\,.
\end{aligned} \qquad (7.3.7)$$

We have a diagonal reduced density matrix of the type:

$$\rho_A \approx \mathrm{diag}\big[(1-\Lambda\epsilon),\,a_1\epsilon,\,a_2\epsilon,\,\ldots\big]+\mathcal{O}(\epsilon^2)\,,\qquad \mathrm{Tr}\rho_A=1\Rightarrow\Lambda=\sum_{m\geq 1}a_m\,, \qquad (7.3.8)$$

at linear order in the infinitesimal parameter ϵ, which is to be identified to the squared time, $\epsilon=t^2$. If one considers the von Neumann entropy as the measure of entanglement, one gets:

$$S_{vN}(\rho_A)=-\mathrm{Tr}(\rho_A\ln\rho_A)\approx-\Lambda\epsilon\ln\epsilon+\epsilon(\Lambda-\sum_{m\geq 1}a_m\ln a_m)\,, \qquad (7.3.9)$$

which looks regular at first glance but actually has a divergent derivative at $\epsilon=0$ due to the $\epsilon\ln\epsilon$ term. This is simply traced back to the vanishing eigenvalues at initial time, i.e. our choice of initial separable state. Although we could go on working with the von Neumann entropy, it appears simpler to turn to the linear entropy (or quadratic Tsallis entropy), which is one minus the fidelity:

$$S_{lin}(\rho_A)=1-\mathrm{Tr}(\rho_A^2)\approx 2\Lambda\epsilon\,. \qquad (7.3.10)$$

The leading order coefficient is the same as the coefficient in front of the divergent derivative term $\epsilon\ln\epsilon$ of the von Neumann entropy, so they are understood to reflect the same growth rate of entanglement. Furthermore, one should realize that the largest eigenvalue is actually the projection of the the density matrix onto the initial separable state, which gives directly, in our case, the geometric entanglement at leading order:

$$S_g\approx-\ln(1-\Lambda\epsilon)\approx\Lambda\epsilon, \qquad (7.3.11)$$

which once again gives the coefficient Λ as the growth factor of the entanglement at leading order in $\epsilon = t^2$.

Coming back to the expression of the eigenvalues $\lambda_{\rho_{can_A}}[K_1, K_2]$ in terms of $6j$-symbols, one extract the growth factor Λ from the Taylor expansion of the largest eigenvalue, obtained for $(K_1, K_2) = (k_1, k_2)$,

$$\lambda_{\rho_{can_A}}[k_1, k_2] \approx 1 - \Lambda t^2 + \mathcal{O}(t^3)\,, \tag{7.3.12}$$

which gives the leading order linear entropy:

$$\begin{aligned}\frac{1}{2}S_{lin}(\rho_{can_A}, t) &= t^2 \prod_{i=1}^{2}(2k_i+1)\sum_{s=0}^{2\ell}(-1)^{j_1+j_2+2k_1+2k_2+2s}\begin{Bmatrix} j_1 & k_1 & k_2 \\ s & k_2 & k_1\end{Bmatrix}\begin{Bmatrix} j_2 & k_1 & k_2 \\ s & k_2 & k_1\end{Bmatrix} \\ &\quad -t^2\begin{Bmatrix} j_1 & k_1 & k_2 \\ \ell & k_2 & k_1\end{Bmatrix}^2\begin{Bmatrix} j_2 & k_1 & k_2 \\ \ell & k_2 & k_1\end{Bmatrix}^2\prod_{i=1}^{2}(2k_i+1)^2 + \mathcal{O}(t^4)\,. \end{aligned}\tag{7.3.13}$$

Let us first point out that the second term vanishes automatically when the holonomy operator spin is not an integer, $\ell \in \mathbb{N} + \frac{1}{2}$. Then this bipartite entanglement exhibits the same plateau behavior as the geometric entanglement studied in the previous section: beyond the critical value $\ell_c = \min\{2k_1, 2k_2\} + \frac{1}{2}$, the entropy $S(\rho_{can_A}, t)$ (at second order) does not depend on $\ell \geq \ell_c$. The origin of this plateau is simply the triangle condition of the spins: the $\{6j\}$-symbols do not vanish only if $s \leq 2k_1$ and $s \leq 2k_2$. A consequence is that the factor of the first term becomes constant (with respect to ℓ) as soon as $\ell \geq \min\{k_1, k_2\}$ while the second term similarly does not depend on ℓ as soon as $\ell > \min\{2k_1, 2k_2\}$. Hence this confirms the critical value analysis for the geometric entanglement as given by equation (7.2.29) in the previous section.

To conclude this section, we remark that, on top of this similar plateau behavior of the linear entropy for large spins ℓ, this entanglement entropy looks also very close to the geometric entanglement (7.2.28) computed previously. Indeed, comparing the formulas, it appears that the geometric entanglement at 2nd order in t corresponds to the eigenvalue $\lambda_{\rho_{can_A}}[K_1, K_2]$ with no spin shift, $(K_1, K_2) = (k_1, k_2)$. We look into the relation between these two measures of entanglement in more details below and show that they are indeed equal at 2nd order.

7.3.2 Geometric entanglement and holonomy operator dispersion

In this subsection we compare the holonomy operator dispersion (7.2.28), which gives the 2nd term coefficient of the geometric entanglement, with the reduced density matrix entropy computed above. It turns out that the geometric entanglement and the bipartite entanglement entropy are equal at 2nd-order of t, which is a neat consistency check of our approach in the simple example of the candy graph.

In order to compute the geometric entanglement via the holonomy operator dispersion formula (7.2.28), we first need to gauge-fix the bulk spin network and derive the closure defect distribution. Here, in the case of the candy graph, there are two possible gauge-fixing choices: either we gauge-fix the holonomy along the second egde k_2 to the identity

as in fig.7.10a, or we gauge-fix the first edge k_1 to a trivial holonomy as in fig.7.10b. These two gauge-fixings lead to different closure defect probability distributions $p_{k_1}(J)$

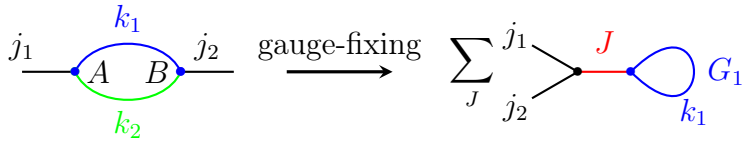

(a)

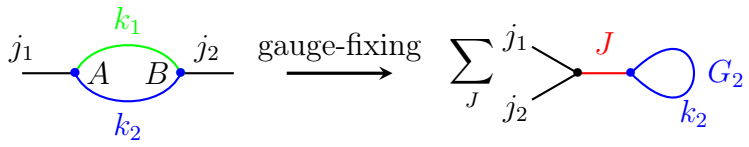

(b)

Figure 7.10: The gauge-fixings on candy graph. The green labels the maximal tree.

and $p_{k_2}(J)$, explicitly given by

$$p_{k_1}(J) = (2k_2+1)(2J+1)\begin{Bmatrix} J & k_1 & k_1 \\ k_2 & j_1 & j_2 \end{Bmatrix}^2, \qquad p_{k_2}(J) = (2k_1+1)(2J+1)\begin{Bmatrix} J & k_2 & k_2 \\ k_1 & j_1 & j_2 \end{Bmatrix}^2. \tag{7.3.14}$$

Both distributions are normalized, $\sum_J p_{k_1}(J) = \sum_J p_{k_2}(J) = 1$. The inequality $p_{k_1}(J) \neq p_{k_2}(J)$ reflects the fact that different choices of gauge-fixing path translate into different boundary maps from bulk holonomies onto boundary states.

Although the closure defect probability distribution depends on the gauge-fixing, the loop holonomy operator is gauge-invariant, and thus its dispersion computed from either gauge-fixing choice turns out to be the same. Using $p_{k_1}(J)$ we have explicitly:

$$\begin{aligned} &\frac{1}{2}\frac{\mathrm{d}^2 S_g}{\mathrm{d}t^2}\Big|_{t=0} \\ =\ &\sum_J (2k_2+1)(2J+1)\begin{Bmatrix} J & k_1 & k_1 \\ k_2 & j_1 & j_2 \end{Bmatrix}^2 \sum_{s=0(1)}^{2\ell} (-1)^{J+s+2k_1}\begin{Bmatrix} J & k_1 & k_1 \\ s & k_1 & k_1 \end{Bmatrix}(2k_1+1) \\ &- \left(\sum_J (2k_2+1)(2J+1)\begin{Bmatrix} J & k_1 & k_1 \\ k_2 & j_1 & j_2 \end{Bmatrix}^2 (-1)^{J+\ell+2k_1}\begin{Bmatrix} J & k_1 & k_1 \\ \ell & k_1 & k_1 \end{Bmatrix}(2k_1+1)\right)^2. \end{aligned} \tag{7.3.15}$$

We can prove that the formula above is actually equal to the linear entropy (7.3.13). More

precisely, what we need to prove is:

$$\begin{Bmatrix} j_1 & k_1 & k_2 \\ s & k_2 & k_1 \end{Bmatrix} \begin{Bmatrix} j_2 & k_1 & k_2 \\ s & k_2 & k_1 \end{Bmatrix} \tag{7.3.16}$$
$$= (-1)^{j_1+j_2+2k_1+2k_2+2s} \sum_J (2J+1) \begin{Bmatrix} J & k_1 & k_1 \\ k_2 & j_1 & j_2 \end{Bmatrix}^2 (-1)^{J+s+2k_1} \begin{Bmatrix} J & k_1 & k_1 \\ s & k_1 & k_1 \end{Bmatrix},$$

which is simply a particular case of the general Biedenharn-Elliot identity (see e.g. [202])

$$\begin{Bmatrix} j & h & g \\ k & a & b \end{Bmatrix} \begin{Bmatrix} j & h & g \\ f & d & c \end{Bmatrix} \tag{7.3.17}$$
$$= \sum_l (-1)^{a+b+c+d+f+k+h+g+j+l} (2l+1) \begin{Bmatrix} k & f & l \\ d & a & g \end{Bmatrix} \begin{Bmatrix} a & d & l \\ c & b & j \end{Bmatrix} \begin{Bmatrix} b & c & l \\ f & k & h \end{Bmatrix}.$$

Summing over the spin J, one recovers exactly the formula for the 2nd order coefficient of the reduced density matrix linear entropy (7.3.13). This is not only a check that the two measures of entanglements -the bipartite entanglement between the two candy graph vertices and the multipartite geometric entanglement- are equal at leading order in the time t, but it also confirms that the geometric entanglement does not depend on the choice of gauge-fixing tree.

7.3.3 Geometric interpretation of the entanglement in the semi-classical regime

We would like to provide the entanglement calculations with a geometric interpretation, for instance understand the extrema of the entanglement in terms of the geometry represented by the spin network states. To this purpose, we work in the semi-classical regime of spin networks at large spins, $j_i, k_i \gg 1$. The spin network geometry can be interpreted in terms of the dual triangulation as illustrated on fig.7.11a. It turns out the entanglement excitation can be described in terms of the dual triangulation angles. Moreover, we find the maximal growth rates of the entanglement corresponds either to flat bulk geometry or maximally curved bulk geometry.

We will look at two cases: small loop holonomy operator spin ℓ and large loop holonomy operator spin ℓ. Let us first look into the case of small loop holonomy operator spin, for which we have $\ell \ll \{j_i, k_i\}$. We use the Racah's approximation for $s \in \mathbb{N}$ and $s \ll a, b, c$ (cf. [208]):

$$\begin{Bmatrix} c & a & b \\ s & b & a \end{Bmatrix} \approx \frac{(-1)^{a+b+s+\ell}}{\sqrt{(2a+1)(2b+1)}} P_s(\cos\theta), \quad \text{with} \quad \cos\theta = \frac{a(a+1)+b(b+1)-c(c+1)}{2\sqrt{a(a+1)b(b+1)}}. \tag{7.3.18}$$

At the large spins a, b, c regime, the θ ranges from 0 to π. The P_s's are the Legendre polynomials, while θ is the angle opposite of the edge of length c in the triangle with edge lenghts a, b, c, as drawn in fig.7.11b. By plugging the Racah's approximation into

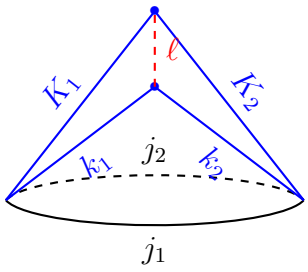

(a) The triangulation for the candy graph. The two triangles of respect length j_1, k_1, k_2 and j_2, k_1, k_2 are glued by matching bulk spins k_1, k_2. Loop holonomy operator changes the height of the cone. The bulk geometry can be viewed from the shape of the cone.

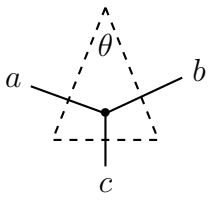

(b) The triangle given by three spins. The spin-c opposes to angle θ.

Figure 7.11: The triangulation for candy graph spin network.

the linear entropy formula (7.3.13), we derive an approximation in terms of the triangle angles:

$$\begin{aligned}
\ell \in \mathbb{N} + \frac{1}{2}: \qquad & \frac{1}{2} S_{lin}(\rho_{can_A}, t) \\
\approx \; & \frac{1}{2} S_{lin}(\rho^{\theta}_{can_A}, t) = t^2 \sum_{s=0}^{2\ell} P_s(\cos\theta_1) P_s(\cos\theta_2) + \mathcal{O}(t^4) \qquad (7.3.19) \\
\ell \in \mathbb{N}: \qquad & \frac{1}{2} S_{lin}(\rho_{can_A}, t) \\
\approx \; & \frac{1}{2} S_{lin}(\rho^{\theta}_{can_A}, t) = t^2 \sum_{s=0}^{2\ell} P_s(\cos\theta_1) P_s(\cos\theta_2) \\
& - t^2 [P_\ell(\cos\theta_1) P_\ell(\cos\theta_2)]^2 + \mathcal{O}(t^4)\,. \qquad (7.3.20)
\end{aligned}$$

The trivial case with vanishing spin $\ell = 0$ excites no entanglement as expected. The two expressions for half-integer spins and integer-spins would be exactly the same if one assumed the convention that half-integer Legendre polynomials vanish. The plots fig.7.12 show the growth rate of intertwiner entanglement provided by the approximation. The fig.7.13 compares above approximation with entropy (7.3.13).

The approximation $S_{lin}(\rho^{\theta}_{can_A}, t)$ now allows us to study how the entanglement excitation depends on the initial state $|\{j_i, k_i\}\rangle$. More precisely, the angles $\theta_{1,2}$ encapsulates the relevant initial data and we would like to determine the extremal initial configurations, i.e. that maximize or minimize the leading order entanglement entropy given by the 2nd order coefficient. It turns out that:

- (i) the balanced configurations $\theta_1 = \theta_2$ are stationary points of the entanglement excitation with respect to variations of the difference $(\theta_1 - \theta_2)$;

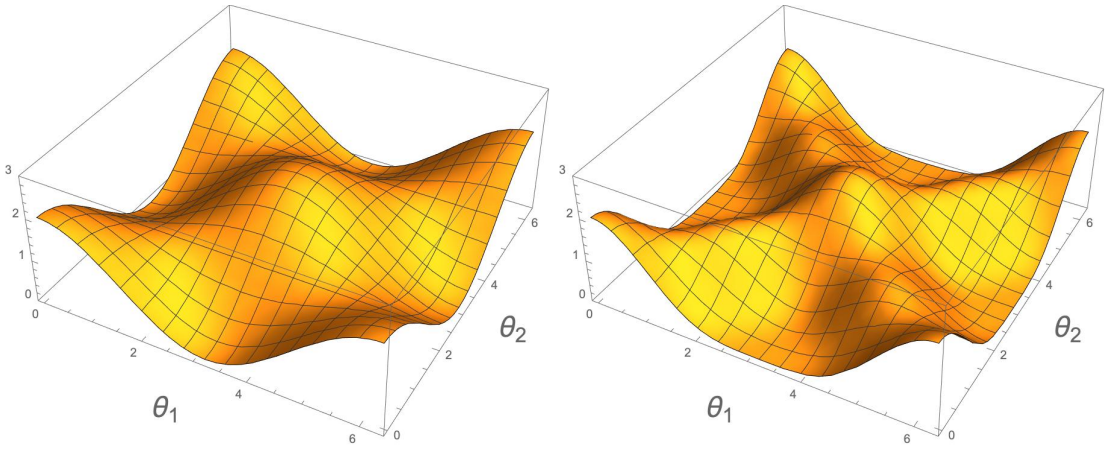

(a) $\ell = \frac{1}{2}$.

(b) $\ell = 1$.

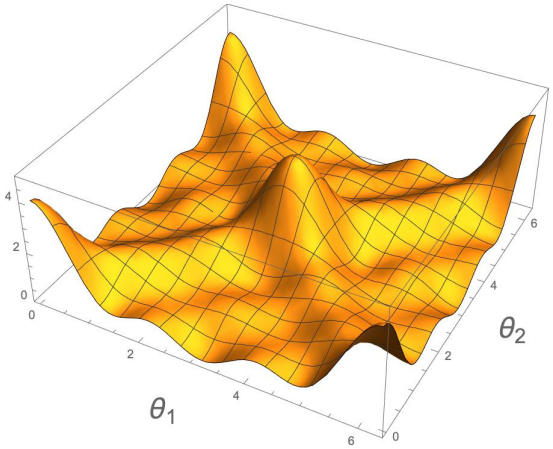

(c) $\ell = \frac{3}{2}$.

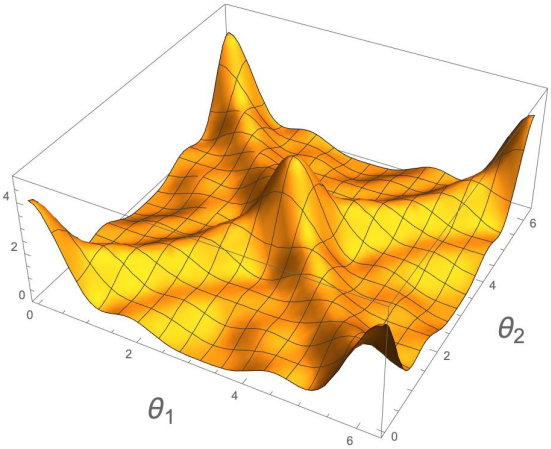

(d) $\ell = 2$.

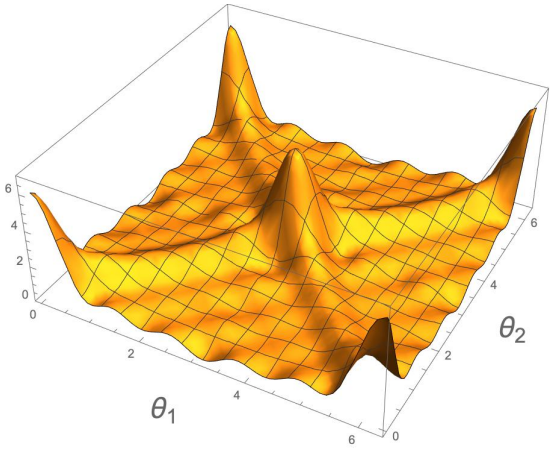

(e) $\ell = \frac{5}{2}$.

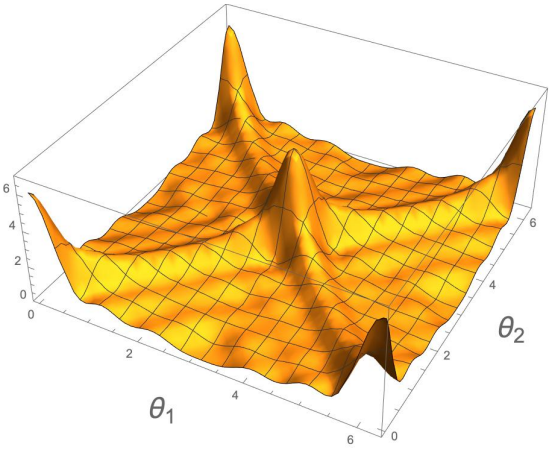

(f) $\ell = 3$.

Figure 7.12: The plots of approximation (7.3.19,7.3.20) with low spin-ℓ. The x and y axis presents corner angle θ_1 and θ_2 respectively. Here we have extended the θ_1, θ_2 domains from $[0, \pi]$ to $[0, 2\pi]$ for the sake of illustrating the shape.

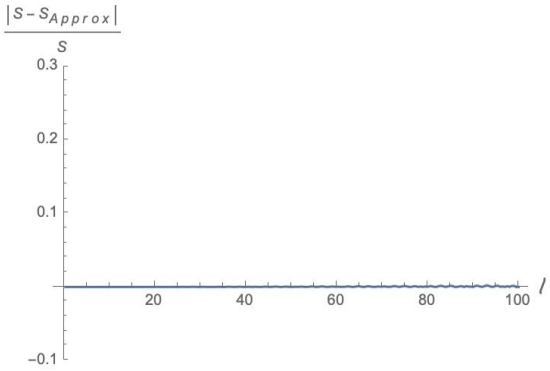

(a) Spins $j_1 = 500, j_2 = 400, k_1 = 700, k_2 = 600$, corner angles $\cos\theta_1 = 1502\sqrt{\frac{2}{8847321}}$ and $\cos\theta_2 = \frac{329}{2}\sqrt{\frac{21}{842602}}$.

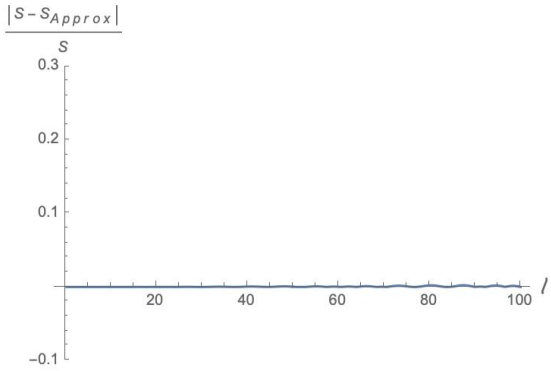

(b) Spins $j_1 = 100, j_2 = 120, k_1 = 500, k_2 = 510$, corner angles $\cos\theta_1 = \frac{50101}{30\sqrt{2901458}}$ and $\cos\theta_2 = \frac{16553}{10\sqrt{2901458}}$.

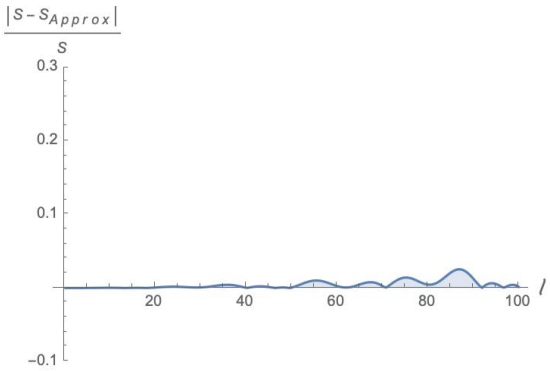

(c) Spins $j_1 = 20, j_2 = 30, k_1 = 200, k_2 = 190$, corner angles $\cos\theta_1 = \frac{7607}{4\sqrt{3647145}}$ and $\cos\theta_2 = \frac{1889}{\sqrt{3647145}}$.

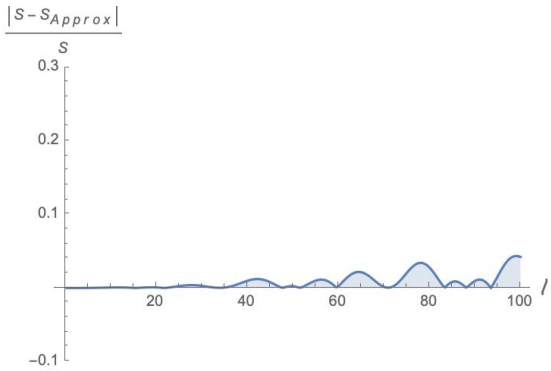

(d) Spins $j_1 = 11, j_2 = 17, k_1 = 141, k_2 = 142$, corner angles $\cos\theta_1 = \frac{773\sqrt{13/1551}}{71}$ and $\cos\theta_2 = \frac{20011}{142\sqrt{20163}}$.

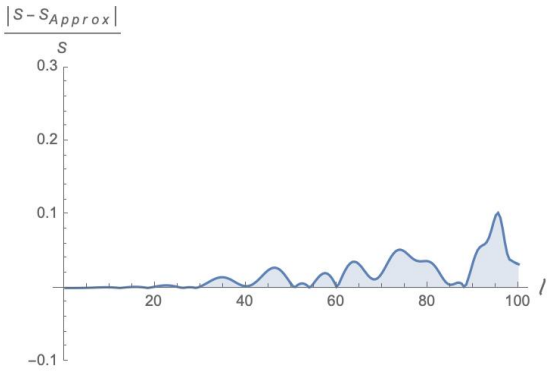

(e) Spins $j_1 = 10, j_2 = 14, k_1 = 100, k_2 = 98$, corner angles $\cos\theta_1 = \frac{1641}{35\sqrt{2222}}$ and $\cos\theta_2 = \frac{2449\sqrt{2/1111}}{105}$.

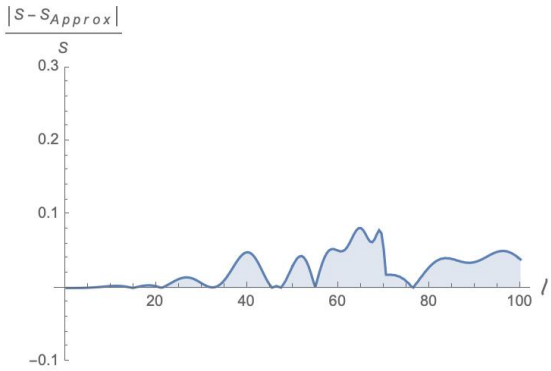

(f) Spins $j_1 = 5.5, j_2 = 8.5, k_1 = 70.5, k_2 = 71$, corner angles $\cos\theta_1 = 0.996503$ and $\cos\theta_2 = 0.992071$.

Figure 7.13: The relative difference $\frac{|S-S_{approx}|}{S}$ between eq.(7.3.13) and eqs.(7.3.19), (7.3.20) for showing the accuracy of the approximation. The spin ℓ ranges from 0 to 100 with step $\frac{1}{2}$. The approximation behaves well if ℓ is sufficiently smaller than $\{j, k\}$, otherwise it behaves not so good.

- (ii) both extremally curved and totally flat geometry maximize the entanglement excitation.

Let us start with (i). We introduce the total angle $\alpha = \theta_1 + \theta_2$ and relative angle $\beta = \theta_1 - \theta_2$. Let us keep α fixed and let the entanglement vary in terms of the difference β. Differentiating[3] $P_s(\cos\theta_1)P_s(\cos\theta_2) = P_s(\cos\frac{\alpha+\beta}{2})P_s(\cos\frac{\alpha-\beta}{2})$ with respect to β gives the stationarity equation:

$$\begin{aligned} 0 &= \frac{\partial}{\partial\beta}\Big(P_s(\cos\frac{\alpha+\beta}{2})P_s(\cos\frac{\alpha-\beta}{2})\Big) \\ &= \frac{s}{2}\frac{-\sin\beta}{\sin\frac{\alpha+\beta}{2}\sin\frac{\alpha-\beta}{2}}P_s(\cos\frac{\alpha+\beta}{2})P_s(\cos\frac{\alpha-\beta}{2}) \\ &\quad + \frac{s}{2\sin\frac{\alpha-\beta}{2}}P_s(\cos\frac{\alpha+\beta}{2})P_{s-1}(\cos\frac{\alpha-\beta}{2}) \\ &\quad - \frac{s}{2\sin\frac{\alpha+\beta}{2}}P_{s-1}(\cos\frac{\alpha+\beta}{2})P_s(\cos\frac{\alpha-\beta}{2})\,, \qquad 0\leq\alpha,\beta\leq 2\pi\,. \end{aligned}$$

The extremal angles $\beta = 0$ and $\beta = \pi$ are both clear solutions. Similarly differentiating with respect to α, we get stationary points $\alpha = 0$ and $\alpha = \pi$ when β is kept fixed.

The configurations $\theta_1 = \theta_2 = 0$ and $\theta_1 = \theta_2 = \pi$, in the $\beta = 0$ branch, give the maximal entanglement excitation. A vanishing relative angle $\beta = 0$ corresponds to equal triangle angles $\theta_1 = \theta_2$, which means that the boundary spins are equal $j_1 = j_2$. This is interpreted as the flat connection configuration. Indeed, the flat constraint operator $\delta(g) = \sum_\ell (2\ell+1)\chi_\ell(g)$, imposing that the loop holonomy be trivial, annihilates initial spin network state $|\Psi_{can,\{j_i,k_i\}}\rangle = |j_1,k_1,k_2\rangle_A \otimes |j_2,k_1,k_2\rangle_B$ as soon as $j_1 \neq j_2$. Thus imposing the flatness of the connection imposes that $j_1 = j_2$. For such $\beta = 0$ configurations, the entanglement evaluates to:

$$\beta = 0 \quad \Rightarrow \quad \frac{1}{2}S_{lin}(\rho^\theta_{can_A}, t) = t^2\sum_{s=0}^{2\ell}\left[P_s(\cos\frac{\alpha}{2})\right]^2 - t^2\left[P_\ell(\cos\frac{\alpha}{2})\right]^4 + \mathcal{O}(t^4) \quad (7.3.21)$$

with $\alpha = \theta_1 + \theta_2$. As plotted on fig.7.14, the entanglement first decreases then increases but it never vanishes. Recalling that the deficit angle given by $\delta = 2\pi - \theta_1 - \theta_2 = 2\pi - \alpha$ at the cone summit provides a measure of the bulk curvature in fig.7.11a, we can interpret the optimal angle confugirations in terms of discrete bulk geometry. The two maximal points correspond to dramatically different bulk geometries. Indeed, the angular-configuration $\theta_1 = \theta_2 = 0$ has a maximal deficit angle; it corresponds to the spin configurations $j_1, j_2 \ll k_1, k_2$ and $k_1 \approx k_2$, with extremely elongated triangles, creating an extremely spiky bulk with maximal bulk curvature. On the other hand, the angle configuration $\theta_1 = \theta_2 = \pi$ has a vanishing deficit angle; it corresponds to spin configuratiosn $j_1 \approx k_1 + k_2 \approx j_2$, with flatten triangles and flat bulk geometry.

[3]The derivative on Legendre polynomial is given by the recursion relation:

$$\frac{\mathrm{d}P_n(x)}{\mathrm{d}x} = \frac{n}{x^2-1}[xP_n(x) - P_{n-1}(x)]\,.$$

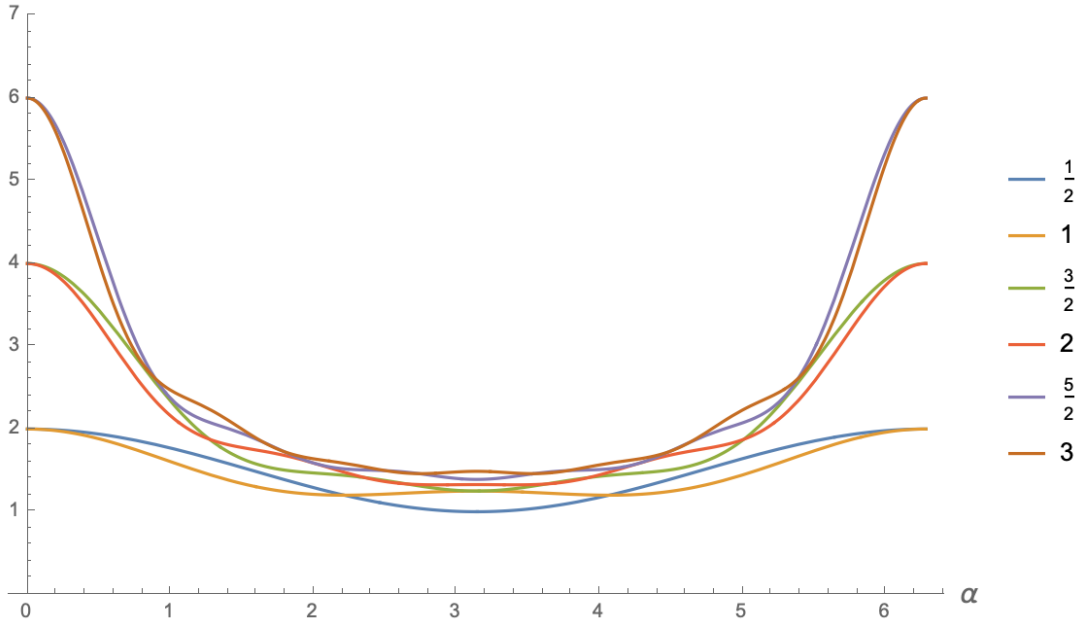

Figure 7.14: When $\theta_1 = \theta_2$, the entanglement (7.3.21) for various spin valuesℓ plotted in terms of the total angle $\alpha = \theta_1 + \theta_2 \in [0, 2\pi]$. Each color corresponds to a value of spin-ℓ.

The $\beta = \pi$ branch lead to a minimal entanglement, with a vanishing leading order in t^2, $S_{lin}(\rho^{\theta}_{can_A}, t) = \mathcal{O}(t^4)$. It corresponds to the maximal difference between the two triangle angles θ_1 and θ_2.Geometrically, this corresponds to unbalanced configuration, with $j_1 \ll j_2$ or $j_2 \ll j_1$, with one flatten triangle and one elongated triangle.

Now that we have looked into the small holonomy operator spin $\ell \ll \{j_i, k_i\}$, let us investigate the large spin regime, $\ell \sim \{j_i, k_i\}$. Since all the spins are assumed of the same order of magnitude, one can use the Ponzano-Regge asymptotic formula in terms of the Regge action for a tetrahedron[208, 209, 6]:

$$\begin{Bmatrix} j_1 & k_1 & k_2 \\ \ell & K_2 & K_1 \end{Bmatrix} \approx \frac{1}{\sqrt{12\pi V}} \cos\left(\sum_{ab}(j_{ab}+\frac{1}{2})\theta_{ab} + \frac{\pi}{4}\right) = \frac{1}{2\sqrt{-12\mathrm{i}\pi V}} e^{\mathrm{i}I} + \frac{1}{2\sqrt{12\mathrm{i}\pi V}} e^{-\mathrm{i}I}\,. \tag{7.3.22}$$

The tetrahedron's edge lengths are given by the spins $\ell, j_1, k_1, k_2, K_1, K_2$. Its volume is V and θ_{ab} is the dihedral angle along the edge of length j_{ab}, where a, b label the tetrahedron's vertices and then every ab presents the segment linking a and b. The Regge action is given by $I = \sum_{ab}(j_{ab} + \frac{1}{2})\theta_{ab}$, which is understood to be the discretization of Einstein-Hilbert action (or more precisely of the Hartle-Hawking boundary term when the bulk curvature vanishes on-shell). This allows to rewrite (7.3.13) as:

$$\ell \in \mathbb{N} + \frac{1}{2}: \qquad \frac{1}{2} S_{lin}(\rho_{can_A}, t) \approx \frac{1}{2} S_{lin}(\rho^{(\mathrm{Regge})}_{can_A}, t)$$

$$= t^2(-1)^{\varphi}\sum_{s=0}^{2\ell}\frac{\cos(I_A[s]-I_B[s])-\sin(I_A[s]+I_B[s])}{24\pi\sqrt{V_A[s]V_B[s]}}\prod_{i=1}^{2}(2k_i+1) + \mathcal{O}(t^4)\,, \tag{7.3.23}$$

$$\ell\in\mathbb{N}: \quad \frac{1}{2}S_{lin}(\rho_{can_A},t)\approx\frac{1}{2}S_{lin}(\rho^{(\text{Regge})}_{can_A},t)$$

$$= t^2(-1)^{\varphi}\sum_{s=0}^{2\ell}\frac{\cos(I_A[s]-I_B[s])-\sin(I_A[s]+I_B[s])}{24\pi\sqrt{V_A[s]V_B[s]}}\prod_{i=1}^{2}(2k_i+1) - t^2\frac{[1-\sin(2I_A[\ell])][1-\sin(2I_B[\ell])]}{576\pi^2V_A[\ell]V_B[\ell]}\prod_{i=1}^{2}(2k_i+1)^2+\mathcal{O}(t^4) \tag{7.3.24}$$

The Regge actions $I_A[s]$ and $I_B[s]$ corresponds respectively to the two tetrahedra dual to the vertices A and B, with edge lengths (j_i,k_1,k_2,s,k_2,k_1) respectivelk with $i=1$ and $i=2$. The phase $\varphi=j_1+j_2+2k_1+2k_2$ and face amplitude factor $(2k_1+1)(2k_2+1)$ both depend on the bulk spins.

Let us conclude this section with a brief summary of our results on the example of the candy graph. The candy graph is the simplest graph with a non-trivial bulk. It is a special case of the 2-vertex graph [203, 174, 210, 211] where the two vertices are linked by a couple of edges forming a loop in the bulk. This configuration allows to define non-trivial dynamical operators acting on the bulk geometry, for instance the loop holonomy operator, and to study the entanglement between the two bulk vertices generated by such dynamics.

In this context, we have explicitly computed the entanglement excitation created by the loop holoonomy operator acting on a pure spin network basis state at leading order in time, that is in t^2. We have considered and compared two measures of entanglement: the geometric entanglement studied in the the previous section and the bipartite entanglement entropy shared between the two vertices (given by the linear entropy of the reduced density matrix). We have shown that these two notions of entanglement match exactly a leading order, thus leading to a consistent picture of the entanglement excitation on the spin network state. Furthermore, in the semi-classical regime at large spins where spin networks can be provided with a discrete geometry interpretation in terms of dual triangulations, we have identified the initial configurations that optimize the excitation of entanglement by the loop operator as the (discrete) geometries with either maximal curvature or vanishing curvature.

7.4 Example: Tripartite entanglement on triangle graph

The triangle graph, as drawn on fig.7.15, is the direct extension of the candy graph to a bulk made of three vertices arranged around a single loop. The spin network Hilbert space on this triangle graph consists in the tensor product of three 3-valent intertwiner spaces, similarly to the candy graph,

$$\mathcal{H}_{tri}=\bigotimes_{v\in tri}\mathcal{H}_v=\mathcal{H}_A\otimes\mathcal{H}_B\otimes\mathcal{H}_C\,,\qquad \mathcal{H}_A=\bigoplus_{K_2,K_3}\text{Inv}_{\text{SU(2)}}\Big(\mathcal{V}_{j_1}\otimes\mathcal{V}_{K_2}\otimes\mathcal{V}_{K_3}\Big)\,,$$

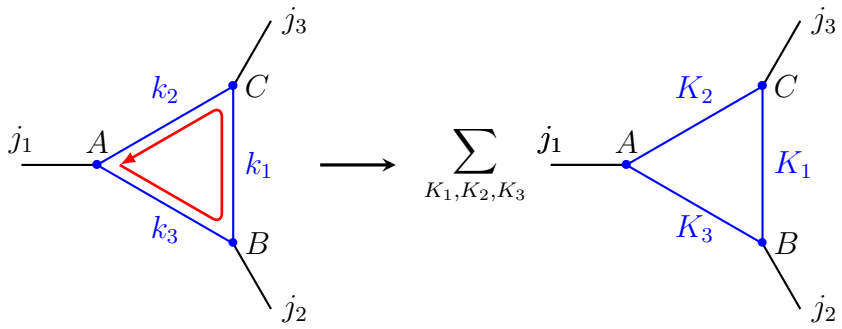

Figure 7.15: The action of loop holonomy operator on triangle graph: it endows spin-superposition along the bulk edges.

and similarly for $\mathcal{H}_B$ and $\mathcal{H}_C$.

We wish to study the action of the loop holonomy operator on an arbitrary spin network basis state chosen as our initial state,

$$|\Psi_{tri,\{j_i,k_i\}}\rangle = |j_1,k_2,k_3\rangle_A \otimes |j_2,k_3,k_1\rangle_B \otimes |j_3,k_1,k_2\rangle_C \quad \in \mathcal{H}_A \otimes \mathcal{H}_B \otimes \mathcal{H}_C\,.$$

The loop holonomy operator affects the bulk spins $\{K_i\}$, but not boundary spins $\{j_i\}$,

$$\begin{aligned}\widehat{\chi}_\ell : \quad & \mathrm{Inv}_{\mathrm{SU}(2)}\Big(\mathcal{V}_{j_1}\otimes\mathcal{V}_{k_2}\otimes\mathcal{V}_{k_3}\Big)\otimes \mathrm{Inv}_{\mathrm{SU}(2)}\Big(\mathcal{V}_{j_2}\otimes\mathcal{V}_{k_3}\otimes\mathcal{V}_{k_1}\Big)\otimes \mathrm{Inv}_{\mathrm{SU}(2)}\Big(\mathcal{V}_{j_3}\otimes\mathcal{V}_{k_1}\otimes\mathcal{V}_{k_2}\Big)\\ \longrightarrow & \bigoplus_{K_1,K_2,K_3} \mathrm{Inv}_{\mathrm{SU}(2)}\Big(\mathcal{V}_{j_1}\otimes\mathcal{V}_{K_2}\otimes\mathcal{V}_{K_3}\Big)\otimes \mathrm{Inv}_{\mathrm{SU}(2)}\Big(\mathcal{V}_{j_2}\otimes\mathcal{V}_{K_3}\otimes\mathcal{V}_{K_1}\Big)\\ & \otimes \mathrm{Inv}_{\mathrm{SU}(2)}\Big(\mathcal{V}_{j_3}\otimes\mathcal{V}_{K_1}\otimes\mathcal{V}_{K_2}\Big)\,.\end{aligned}$$

Following the same logic as with the candy graph, we compute the evolution of the state, truncated to leading order and properly normalized,

$$\begin{aligned}|\Psi_{tri,\{j_i,k_i\}}(\ell,t)\rangle \;=\; & \frac{1}{\sqrt{N_{tri,\{j_i,k_i\}}(\ell,t)}}\Big(|\Psi_{tri,\{j_i,k_i\}}\rangle - \mathrm{i}t\sum_{\{K_i\}}[Z(tri)_\ell^{\{j_i\}}]^{\{K_i\}}{}_{\{k_i\}}|\Psi_{tri,\{j_i,K_i\}}\rangle\\ & -\frac{1}{2}t^2\sum_{s=0}^{2\ell}\sum_{\{K_i\}}[Z(tri)_s^{\{j_i\}}]^{\{K_i\}}{}_{\{k_i\}}|\Psi_{tri,\{j_i,K_i\}}\rangle\Big)\,,\end{aligned} \tag{7.4.1}$$

where the normalization factor is computed up to fourth order

$$N_{tri,\{j_i,k_i\}}(\ell,t) = 1+\mathcal{O}(t^4)\,. \tag{7.4.2}$$

The transition matrix Z is expressed in terms of $6j$-symbols according to the general formula (7.1.6) for the action of the loop operator $\widehat{\chi}_\ell$,

$$[Z(tri)_\ell^{\{j_i\}}]^{\{K_i\}}{}_{\{k_i\}} \;=\; (-1)^{\sum_{i=1}^3(j_i+k_i+K_i+\ell)}\begin{Bmatrix} j_1 & k_2 & k_3\\ \ell & K_3 & K_2\end{Bmatrix}\begin{Bmatrix} j_2 & k_3 & k_1\\ \ell & K_1 & K_3\end{Bmatrix}\begin{Bmatrix} j_3 & k_1 & k_2\\ \ell & K_2 & K_1\end{Bmatrix}$$

$$\times \prod_{i=1}^{3} \sqrt{(2k_i+1)(2K_i+1)}\,. \tag{7.4.3}$$

The initial spin network state is a basis state, thus is fully separable with vanishing entanglement. Via tracing over $\mathcal{H}_B \otimes \mathcal{H}_C$, the reduced density matrix is read

$$\begin{aligned}
&\rho_{tri_A}(t) = \mathrm{Tr}_{BC}\rho_{tri_{ABC}}(t) \quad \in \mathrm{End}(\mathcal{H}_A)\\
=&\frac{1}{N_{tri,\{j_i,k_i\}}(\ell,t)}\Bigg(\Big(1-t^2\sum_{s=0}^{2\ell}[Z(tri)_s^{\{j_i\}}]^{\{K_i\}}{}_{\{k_i\}}\Big)|j_1,k_2,k_3\rangle\langle j_1,k_2,k_3|_A\\
&+t^2\sum_{K_1,K_2,K_3}\Big([Z(tri)_\ell^{\{j_i\}}]^{K_1K_2K_3}{}_{\{k_i\}}\Big)^2|j_1,K_2,K_3\rangle\langle j_1,K_2,K_3|_A+\mathcal{O}(t^4)\Bigg)\,.
\end{aligned} \tag{7.4.4}$$

This is a diagonal matrix with respect to basis $|j_1,K_2,K_3\rangle \in \mathcal{H}_A$, thus the eigenvalues of $\rho_{tri_A}(t)$ can be directly read off from the expression above:

$$\begin{aligned}
&\lambda_{\rho_{tri_A}}[K_2,K_3] \qquad\qquad (7.4.5)\\
=\;&\Bigg(1-t^2\sum_{s=0}^{2\ell}(-1)^{\sum_{i=1}^3(j_i+2k_i+s)}\begin{Bmatrix}j_1&k_2&k_3\\ s&k_3&k_2\end{Bmatrix}\begin{Bmatrix}j_2&k_3&k_1\\ s&k_1&k_3\end{Bmatrix}\begin{Bmatrix}j_3&k_1&k_2\\ s&k_2&k_1\end{Bmatrix}\\
&\qquad\times\prod_{i=1}^{3}(2k_i+1)\Bigg)\delta_{k_2}^{K_2}\delta_{k_3}^{K_3}\\
&+t^2\sum_{K_1=|k_1-\ell|}^{k_1+\ell}\begin{Bmatrix}j_1&k_2&k_3\\ \ell&K_3&K_2\end{Bmatrix}^2\begin{Bmatrix}j_2&k_3&k_1\\ \ell&K_1&K_3\end{Bmatrix}^2\begin{Bmatrix}j_3&k_1&k_2\\ \ell&K_2&K_1\end{Bmatrix}^2\prod_{i=1}^{3}(2K_i+1)(2k_i+1)\\
&+\mathcal{O}(t^4)\,.
\end{aligned}$$

The eigenvalues are labeled by the two spins K_2 and K_3. This gives us the bipartite entanglement entropy of $\mathcal{H}_A|\mathcal{H}_B\otimes\mathcal{H}_C$ up to second order in t:

$$\begin{aligned}
&\frac{1}{2}S_{lin}(\rho_{tri_A}) = \frac{1}{2}\left(1-\sum_{K_2,K_3}\lambda_{\rho_{tri_A}}[K_2,K_3]^2\right) \qquad (7.4.6)\\
=\;&t^2\Bigg(\sum_{s=0}^{2\ell}(-1)^{j_1+j_2+j_3+2k_1+2k_2+2k_3+3s}\begin{Bmatrix}j_1&k_2&k_3\\ s&k_3&k_2\end{Bmatrix}\begin{Bmatrix}j_2&k_3&k_1\\ s&k_1&k_3\end{Bmatrix}\begin{Bmatrix}j_3&k_1&k_2\\ s&k_2&k_1\end{Bmatrix}\\
&\qquad\times\prod_{i=1}^{3}(2k_i+1)\\
&-\sum_{K_1=|k_1-\ell|}^{k_1+\ell}\begin{Bmatrix}j_1&k_2&k_3\\ \ell&k_3&k_2\end{Bmatrix}^2\begin{Bmatrix}j_2&k_3&k_1\\ \ell&K_1&k_3\end{Bmatrix}^2\begin{Bmatrix}j_3&k_1&k_2\\ \ell&k_2&K_1\end{Bmatrix}^2\\
&\qquad\times(2K_1+1)(2k_1+1)(2k_2+1)^2(2k_3+1)^2\Bigg)+\mathcal{O}(t^4)\,.
\end{aligned}$$

As for the candy graph, no 1st-order of t appears at all and the leading order is directly in t^2.

One gets the linear entropies for the vertices B and C by a straightforward cyclic permutation of the labels. Generally, the three bipartite entanglement entropies have different values due to the a priori different values of the initial spins. Nonetheless, when $\ell \in \mathbb{N} + \frac{1}{2}$, all three bipartite entanglement entropies are equal to each other at the leading order in t^2. We trace this back to the triangle condition on the $\{6j\}$-symbols, which eliminates the second term in the entropy formula above. Hence we conclude

Result 7.10. *For an half-integer holonomy spin $\ell \in N + \frac{1}{2}$, the bipartite entanglement entropies on triangle graph satisfy $S_{lin}(\rho_{tri_A}) = S_{lin}(\rho_{tri_B}) = S_{lin}(\rho_{tri_C})$ at leading order in t^2. This common leading order term is given*

$$\begin{aligned}\frac{1}{2}S_{lin}(\rho_{tri_A}) \;\sim\; t^2\Bigg(\sum_{s=0}^{2\ell}(-1)^{j_1+j_2+j_3+2k_1+2k_2+2k_3+3s}\begin{Bmatrix} j_1 & k_2 & k_3 \\ s & k_3 & k_2\end{Bmatrix}\begin{Bmatrix} j_2 & k_3 & k_1 \\ s & k_1 & k_3\end{Bmatrix} \\ \times\begin{Bmatrix} j_3 & k_1 & k_2 \\ s & k_2 & k_1\end{Bmatrix}\prod_{i=1}^{3}(2k_i+1)\Bigg). \qquad (7.4.7)\end{aligned}$$

Those triangle inequalities further implies that that $S_{lin}(\rho_{tri_A}) = S_{lin}(\rho_{tri_B}) = S_{lin}(\rho_{tri_C})$ reach the same plateau value when the holonomy operator spin is larger than its critical value, $\ell > \min\{2k_1, 2k_2, 2k_3\}$, no matter whenever ℓ is half-integer or integer.

We now compare the bipartite entanglement to the tripartite entanglement, defined as the geometric entanglement.

7.4.1 Tripartite entanglement

In order to quantify the multipartite entanglement on the triangle graph, we use the geometric entanglement. We can compute the geometric measure of entanglement as explained previously: the geometric entanglement is given by the maximal projection of the evolving state onto the spin network basis, which is, at very early times t, its projection onto the initial spin network basis state, that is by the contribution $K_{1,2,3} = k_{1,2,3}$:

$$\begin{aligned}&\lambda_{\max} = \big|\langle\Psi_{tri,\{j_i,k_i\}}(\ell,0)|\Psi_{tri,\{j_i,k_i\}}(\ell,t)\rangle\big|^2 \\ =\;& \frac{1}{N_{tri,\{j_i,k_i\}}(\ell,t)}\Bigg[1 + t^2\Big([Z(tri)_\ell^{\{j_i\}}]^{\{k_i\}}{}_{\{k_i\}}\Big)^2 - t^2\sum_{s=0}^{2\ell}[Z(tri)_s^{\{j_i\}}]^{\{k_i\}}{}_{\{k_i\}} \\ &- \frac{1}{4}t^4\Big(\sum_{s=0}^{2\ell}[Z(tri)_s^{\{j_i\}}]^{\{k_i\}}{}_{\{k_i\}}\Big)^2\Bigg]. \qquad (7.4.8)\end{aligned}$$

Hence it leads to the geometric measure of entanglement on triangle graph:

$$\begin{aligned}&S_g[\Psi_{tri,\{j_i,k_i\}}(\ell,t)] \\ =\;& t^2\prod_{i=1}^{3}(2k_i+1)\sum_{s=0}^{2\ell}(-1)^{\sum_{i=1}^{3}(j_i+2k_i+s)}\begin{Bmatrix} j_1 & k_2 & k_3 \\ s & k_3 & k_2\end{Bmatrix}\begin{Bmatrix} j_2 & k_3 & k_1 \\ s & k_1 & k_3\end{Bmatrix}\begin{Bmatrix} j_3 & k_1 & k_2 \\ s & k_2 & k_1\end{Bmatrix}\end{aligned}$$

$$-t^2\prod_{i=1}^{3}(2k_i+1)^2\begin{Bmatrix} j_1 & k_2 & k_3 \\ \ell & k_3 & k_2\end{Bmatrix}^2\begin{Bmatrix} j_2 & k_3 & k_1 \\ \ell & k_1 & k_3\end{Bmatrix}^2\begin{Bmatrix} j_3 & k_1 & k_2 \\ \ell & k_2 & k_1\end{Bmatrix}^2+\mathcal{O}(t^4)\,. \quad (7.4.9)$$

This is a straightforward extension of the formula (7.3.13) derived for the candy graph, where we've added the relevant $\{6j\}$-symbols. As earlier, the geometric entanglement excitation reaches a plateau, due to the triangle inequalities on the spins, when the holonomy operator spin grows beyond a critical value, $\ell > \min\{2k_1, 2k_2, 2k_3\}$. Moreover, when the spin is half-integer, $\ell \in \mathbb{N}+\frac{1}{2}$, the second term in (7.4.9) vanishes, as for the bipartite entanglement in last subsection.

The plots 7.16 compare the bipartite entanglement entropies and geometric entanglement:

- (i) they are equal when the holonomy spin is half-integer, $\ell \in \mathbb{N}+\frac{1}{2}$;
- (ii) for small spins ℓ, those measures of entanglement are clearly distinct, but they tend to converge as the spin ℓ increases, and they are eventually constant and equal beyond the critical value $\ell > \min\{2k_1, 2k_2, 2k_3\}$.

One could also have computed the geometric entanglement by gauge-fixing and working out the closure defect's probability distribution. Since the bulk graph consists in a single loop made of three edges, there are three ways to gauge-fix: choosing k_1 as the "loopy spin", i.e. the edge which is not gauge-fixed and gauge-fixing the edges associated with k_2 and k_3, plus the two other possibilities of choosing k_2 or k_3 as the "loopy spin".

For instance, contracting the edges carrying k_2 and k_3 and keeping k_1, we obtain the probability distribution of the closure defect as

$$p_{k_1}(J) = (2J+1)(2k_2+1)(2k_3+1)\sum_L (2L+1)\begin{Bmatrix} j_3 & j_2 & L \\ k_1 & k_1 & J \\ k_2 & k_3 & j_1\end{Bmatrix}^2\,, \quad (7.4.10)$$

with the normalization $\sum_J p_{k_1}(J) = 1$. This probability distribution gives the 2nd-order time derivative of geometric entanglement:

$$\begin{aligned}\frac{1}{2}\frac{\mathrm{d}^2 S_g}{\mathrm{d}t^2}\Big|_{t=0} \;=\; & \sum_{J,L}(2J+1)(2L+1)(2k_1+1)(2k_2+1)(2k_3+1)\begin{Bmatrix} j_3 & j_2 & L \\ k_1 & k_1 & J \\ k_2 & k_3 & j_1\end{Bmatrix}^2 \\ & \times\sum_{s=0}^{2\ell}(-1)^{J+s+2k_1}\begin{Bmatrix} J & k_1 & k_1 \\ s & k_1 & k_1\end{Bmatrix} \\ & -\Bigg(\sum_{J,L}(2J+1)(2L+1)(2k_1+1)(2k_2+1)(2k_3+1)\begin{Bmatrix} j_3 & j_2 & L \\ k_1 & k_1 & J \\ k_2 & k_3 & j_1\end{Bmatrix}^2 \\ & \times(-1)^{J+\ell+2k_1}\begin{Bmatrix} J & k_1 & k_1 \\ s & k_1 & k_1\end{Bmatrix}\Bigg)^2\,. \end{aligned} \quad (7.4.11)$$

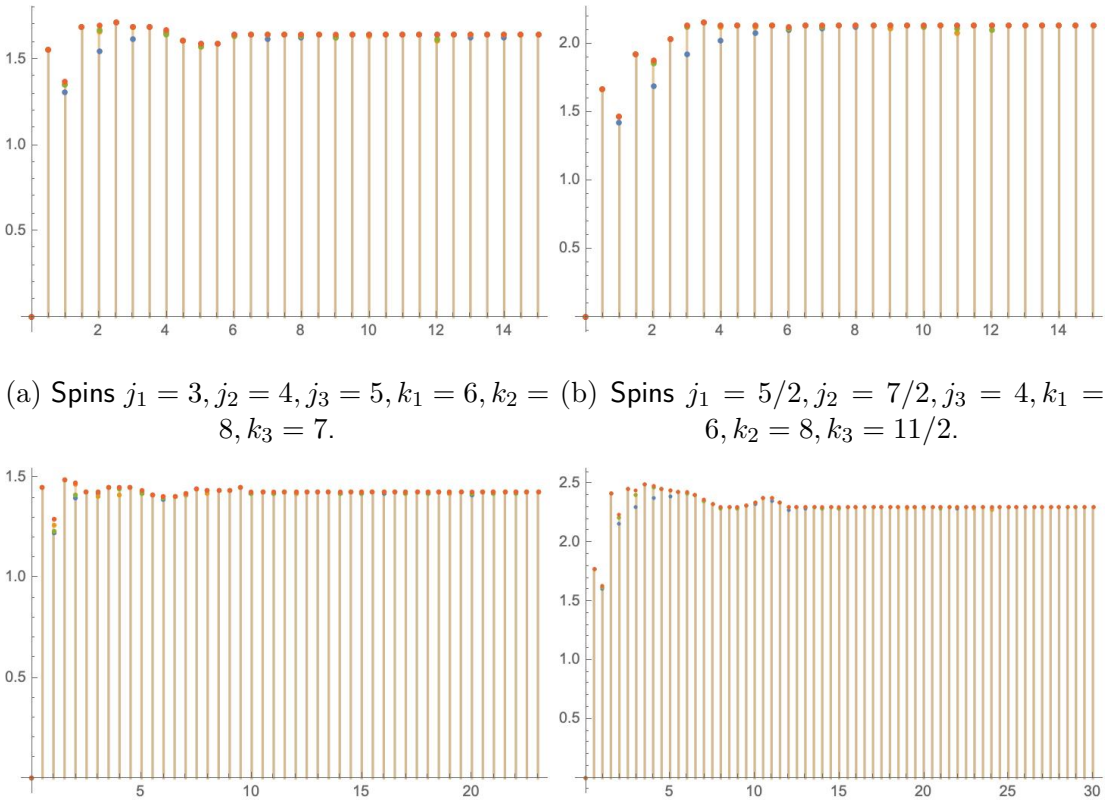

(a) Spins $j_1 = 3, j_2 = 4, j_3 = 5, k_1 = 6, k_2 = 8, k_3 = 7$.

(b) Spins $j_1 = 5/2, j_2 = 7/2, j_3 = 4, k_1 = 6, k_2 = 8, k_3 = 11/2$.

(c) Spins $j_1 = 6, j_2 = 9, j_3 = 7, k_1 = 12, k_2 = 11, k_3 = 10$.

(d) Spins $j_1 = 9/2, j_2 = 11/2, j_3 = 7, k_1 = 12, k_2 = 16, k_3 = 27/2$.

Figure 7.16: The comparison between bipartite entanglement entropies and geometric measure of entanglement, where blue point is for $\frac{1}{2}S(\rho_{tri_A})$, orange point for $\frac{1}{2}S(\rho_{tri_B})$, green point for $\frac{1}{2}S(\rho_{tri_C})$ and red point for S_g.

It is straightforward to check that these results does not actually depend on the choice of gauge-fixing and that it gives the same expression for the leading order entanglement computed above in eqn.(7.4.9). This can be shown by using the Biedenharn-Elliott identity. More precisely, we need to prove the following relation:

$$\begin{Bmatrix} j_1 & k_2 & k_3 \\ \ell & k_3 & k_2 \end{Bmatrix} \begin{Bmatrix} j_2 & k_3 & k_1 \\ \ell & k_1 & k_3 \end{Bmatrix} \begin{Bmatrix} j_3 & k_1 & k_2 \\ \ell & k_2 & k_1 \end{Bmatrix}$$

$$= (-1)^{\sum_{i=1}^{3}(j_i+2k_i+\ell)} \sum_{J,L} (2J+1)(2L+1) \begin{Bmatrix} j_3 & j_2 & L \\ k_1 & k_1 & J \\ k_2 & k_3 & j_1 \end{Bmatrix}^2 (-1)^{J+\ell+2k_1} \begin{Bmatrix} J & k_1 & k_1 \\ \ell & k_1 & k_1 \end{Bmatrix} . \tag{7.4.12}$$

Starting from the left side, we use the Biedenharn-Elliot identity twice: we first recouple the first two $6j$-symbols via the Biedenharn-Elliot identity, which results in three $6j$-symbols, then we take one of them and recouple it to the third $6j$-symbol of the original

prooductone via the Biedenharn-Elliot identity again. This gives:

$$\begin{aligned} & \begin{Bmatrix} \ell & k_3 & k_3 \\ j_1 & k_2 & k_2 \end{Bmatrix} \begin{Bmatrix} \ell & k_1 & k_1 \\ j_2 & k_3 & k_3 \end{Bmatrix} \begin{Bmatrix} \ell & k_2 & k_2 \\ j_3 & k_1 & k_1 \end{Bmatrix} \\ = & \sum_{L',J} (-1)^{j_1+j_2+j_3+2k_1+2k_2+2k_3+\ell} (-1)^{J+\ell+2k_1} \begin{Bmatrix} k_1 & k_1 & J \\ k_1 & k_1 & \ell \end{Bmatrix} (2J+1)(2L'+1) \\ & \times \begin{Bmatrix} j_1 & j_2 & L' \\ k_1 & k_2 & k_3 \end{Bmatrix}^2 \begin{Bmatrix} J & j_3 & L' \\ k_2 & k_1 & k_1 \end{Bmatrix}^2 , \end{aligned} \tag{7.4.13}$$

Finally, we deal with the two squared $6j$-symbols by the contraction formula of Racah coefficients (see [204], page 143)

$$(-1)^{2h+2d} \sum_c (2c+1) \begin{Bmatrix} a & i & k \\ f & b & c \end{Bmatrix} \begin{Bmatrix} a & b & c \\ d & e & f \\ g & h & i \end{Bmatrix} = \begin{Bmatrix} a & i & k \\ h & d & g \end{Bmatrix} \begin{Bmatrix} b & f & k \\ d & h & e \end{Bmatrix} , \tag{7.4.14}$$

which allows to write

$$\begin{aligned} & \sum_{L'} (2L+1) \begin{Bmatrix} j_1 & j_2 & L' \\ k_1 & k_2 & k_3 \end{Bmatrix}^2 \begin{Bmatrix} J & j_3 & L' \\ k_2 & k_1 & k_1 \end{Bmatrix}^2 \\ = & \sum_{L,L''} (2L+1)(2L''+1) \begin{Bmatrix} j_1 & j_2 & L' \\ j_3 & J & L \end{Bmatrix} \begin{Bmatrix} j_1 & j_2 & L' \\ j_3 & J & L'' \end{Bmatrix} \begin{Bmatrix} j_1 & J & L \\ k_2 & k_1 & j_3 \\ k_3 & k_1 & j_2 \end{Bmatrix} \begin{Bmatrix} j_1 & J & L'' \\ k_2 & k_1 & j_3 \\ k_3 & k_1 & j_2 \end{Bmatrix} \\ = & \begin{Bmatrix} j_1 & J & L \\ k_2 & k_1 & j_3 \\ k_3 & k_1 & j_2 \end{Bmatrix}^2 , \end{aligned} \tag{7.4.15}$$

By symmetry of $9j$-symbol, this proves the wanted eqn.(7.4.12).

Finally, we can look at the semi-classical regime at large spins $\{j_i, k_i\}$, in which the spin network has a clear interpretation in terms of dual triangulation: the triangle graph is dual to a open tetrahedron to which one has removed one triangle, as drawn on fig.7.17. This missing triangle corresponds to the the boundary edge of the graph, decorated with the spins (j_1, j_2, j_3). For large spins, assuming that $\ell \ll \{j_i, k_i\}$, one can apply Racah's approximation (7.3.18) for $6j$-symbols to the geometric entanglement formula (7.4.9) and write it in terms of Legendre polynomials in the cosine of the triangle angles, as illustrated on figure 7.17:

$$\begin{aligned} S_g[\Psi_{tri,\{j_i,k_i\}}(\ell,t)] \sim & \; t^2 \sum_{s=0}^{2\ell} P_s(\cos\theta_1) P_s(\cos\theta_2) P_s(\cos\theta_3) \\ & -t^2 [P_s(\cos\theta_1) P_s(\cos\theta_2) P_s(\cos\theta_3)]^2 + \mathcal{O}(t^4) \end{aligned} \tag{7.4.16}$$

with the convention that half-integer Legendre polynomials $P_\ell(x)$ vanish, for $\ell \in \mathbb{N} + \frac{1}{2}$. The angles are given in terms of the spins by

$$\begin{aligned}
\cos\theta_1 &= \frac{k_2(k_2+1)+k_3(k_3+1)-j_1(j_1+1)}{2\sqrt{k_2(k_2+1)k_3(k_3+1)}}\,,\\
\cos\theta_2 &= \frac{k_3(k_3+1)+k_1(k_1+1)-j_2(j_2+1)}{2\sqrt{k_3(k_3+1)k_1(k_1+1)}}\,,\\
\cos\theta_3 &= \frac{k_1(k_1+1)+k_2(k_2+1)-j_3(j_3+1)}{2\sqrt{k_1(k_1+1)k_2(k_2+1)}}\,.
\end{aligned} \tag{7.4.17}$$

This expression allows us to study how the entanglement varies with respect to the spin network initial data.

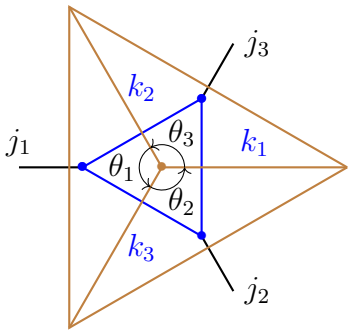

Figure 7.17: The dual triangulation (brown lines) on triangle graph. The angles are given by (7.4.17).

As for the bipartite system defined on the candy graph, the extremal configurations for the entanglement excitation by the holonomy operator are given by extremal geometries: spiky tetrahedral geometries with flatten triangles and maximal curvature. More precisely, to start with, vanishing angles $\theta_1 = \theta_2 = \theta_3 = 0$ maximizes the multipartite entanglement excitation, as for the candy graph geometry. It corresponds to the asymptotic limit of spiky tetrahedron, as drawn on fig.7.18, where the summit is sent to infinity, which is interpreted as an extremal bulk curvature. Similarly, angular configurations $\theta_1 = 0, \theta_2 = \theta_3 = \pi$, and its two other permutations, also produce a maximal entanglement growth. In terms of spins and thus of edge lengths, this corresponds to $j_1 \ll k_2, k_3$, $j_2 \approx k_1 + k_3$, $j_3 \approx k_1 + k_2$, which satisfy the triangular inequalities for (j_1, j_2, j_3).

On the contrary, the angle configurations $\theta_1 = \theta_2 = 0, \theta_3 = \pi$ and its other two permutations, as well as $\theta_1 = \theta_2 = \theta_3 = \pi$, all lead to a minimal entanglement, i.e. vanishing entanglement excitation at leading order in t^2. Translating in terms of spins and edge lengths, the former case corresponds to $j_1, j_2 \ll k_1, k_2, k_3$, $j_3 \approx k_1 + k_2$, which doesn't satisfy the triangular inequalities for (j_1, j_2, j_3), and thus is not an allowed spin network configuration. The latter case, with equal angles $\theta_1 = \theta_2 = \theta_3 = \pi$, corresponds to $j_1 \approx k_2 + k_3$, $j_2 \approx k_3 + k_1$, $j_3 \approx k_1 + k_2$, which is allowed by the triangular inequalities.

To conclude this section, we extended to the triangular graph our analysis of the entanglement excitation by the loop holonomy operator on a spin network basis state. This

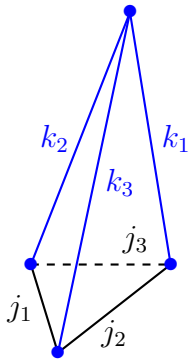

Figure 7.18: A spike triangulation.

has confirmed our general analysis of the geometric entanglement for an arbitrary graph. More precisely, we have computed analytically and numerically both the linear entanglement entropies for bipartitions of the graph and the geometric entanglement and checked that they match at leading order in the time t. Since the initial state is unentangled, the evolution starts with a vanishing entanglement then grows in t^2. Moreover, we have identified the spin network configurations with extremal entanglement excitations, which unsurprisingly correspond to discrete geometries with extremal curvature. This is a positive step towards establishing a more thorough and precise dictionary between quantum entanglement, quantum geometry and its dynamics in the framework of loop quantum gravity.

This chapter is dedicated to the study of entanglement in loop quantum gravity. More precisely, we looked into the evolution of entanglement under the action of the holonomy operator. Intuitively, the holonomy operator acting on a loop of a spin network state will act at once on all the intertwiners living at the nodes on the loop and will entangle them. More precisely, we studied the unitary evolution generated by a holonomy operator on an initial state given by a spin network basis state. Such an initial state has fixed spins and intertwiners. It is thus a separable state carrying absolutely no entanglement. The evolution will naturally create entanglement between the vertices of the spin network and our goal was to compute the excitation of entanglement by the holonomy operator. The holonomy around a loop representing a discretized measure of curvature, this leads to a relation between excitations of the geometry - "quanta of curvature" - and excitations of the information -multipartite entanglement- over spin network basis states. This fits in the larger program of interpreting and reconstructing the quantum geometry of space-time from quantum information concepts.

At the technical level, we introduced geometric entanglement to measure the multipartite entanglement carried by a spin network state, defined as the distance between that state and the set of separable states, identified (up to minor subtleties) to the set of spin network basis states. This is understood as a witness of how much the intertwiners of a spin network are entangled. Starting from an initial spin network basis state, thus with vanishing entanglement, we find that the first order time derivative at the initial time always vanishes, so the leading order behavior is a quadratic growth of the entanglement. We show that the second-order derivative is simply given by the dispersion of the holonomy operator, which can, in turn, be computed from the probability distribution of the "closure defect" around the loop (i.e., the total spin recoupling the spins of all the edges attached to the loop). Considering holonomy operators with arbitrary spin $\ell \in \mathbb{N}/2$, we find that this entanglement excitation grows with the spin ℓ and exhibits a plateau behavior: the entanglement excitation saturates and reaches its maximal value when the spin ℓ becomes larger than all the spins around the loop.

We illustrate this analysis through its application to the simplest spin networks with non-trivial bulk and boundary: the candy graph, consisting of two vertices linked by a single loop, and the triangle graph, consisting of three vertices linked by a single loop, both with arbitrary number of boundary edges poking out of the bulk vertices. These configurations allow studying of explicitly the correlation and entanglement between the intertwiners living at the graph vertices. We compute the geometric entanglement and express it in terms of 6j-symbols from spin recoupling, which allows for studying its low-spin and large-spin regimes. We further compute the bipartite entanglement created by the holonomy operator, defined as the entropy of the reduced density matrix, and show that it fits exactly at leading order with the notion of geometric entanglement we introduced.

Since holonomy operators are the basic building blocks of the Hamiltonian dynamics of loop quantum gravity, this work gives a first hint of the effect of the dynamics on the quantum information carried by spin network states.

Note that in this chapter we only consider the partition with respect to every individual node. The next chapter 8 we will consider a more general partition that admits a subsystem comprising multi-node.

Chapter 8

Spin Network Entanglement: Coarse-graining

The chapter follows the question at the end of the previous chapter, i.e., what about the case that admits a more arbitrary partition on a spin network. Following the question, we explore the entanglement between spin sub-networks, referred to as *spin network entanglement*, which is a direct generalization for intertwiner entanglement. Then we study spin network entanglement in the context of coarse-graining (via gauge-fixing). Indeed, once the relation between sub-networks is involved, it inevitably introduces boundaries that admit coarse-graining procedures.

The key function now played by the holographic principle as a guide for quantum gravity has put a great emphasis on the role of boundaries. It pushes us to include (spatial) boundaries in the description of quantum geometries, not just as mere classical boundary conditions but as legitimate quantum boundary states. This translates a shift of perspective from a global description of space(-time) as a whole to a quasi-local description where any bounded region of space(-time) is considered an open quantum system. Following the idea, the question — where are the quantum gravity degrees of freedom, could be phrased to be a snapshot of the interlaced issues: the coarse-graining of quantum geometry states from the Planck scale to larger scales, the definition of quantum dynamics consistent with the holographic principle, and the implementation of (discretized) diffeomorphism at the quantum level as the fundamental gauge symmetry of the theory (or, in other words, the implementation of a relativity principle for quantum geometry) [44].

This chapter is based on [54], aiming at exploring the relation between coarse-graining and holography, with the notion of spin network entanglement. Partitioning spin network inevitably introduces boundaries (e.g., Fig.8.1a), and every spin sub-network is a spin network with nonempty boundary evolving along time (e.g., Fig.8.1b). On the other hand, we can coarse-grain sub-network into a simpler graph-structure, presenting the sub-network with a single vertex and boundary edges (e.g., Fig.8.1a). The coarse-grained spin network state can be defined based on the coarse-grained graph. We want to answer the questions: (a) Can we study spin network entanglement from the coarse-grained graph? (b) If we can, then will it be effective if we take some evolution into account? The answers are positive for the cases the loop holonomy operator generates evolution.

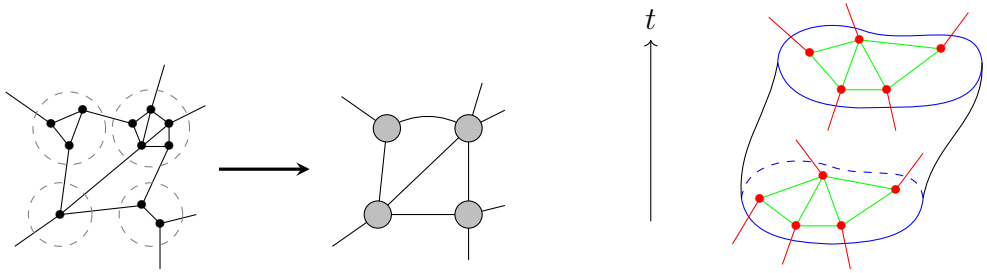

(a) An illustration of the partitioning of the graph in order to coarse-grain the spin network state.

(b) Spin sub-network of right-upper Fig.8.1a evolves along time.

Figure 8.1: Coarse-graining and spin network with non-empty boundary.

Section 8.1 presents the definition of spin network entanglement. The main result of this part is presented in Result 8.2, stating that spin network entanglement can be coarse-grained, and the spin network entanglement exactly gets reflected on the coarse-grained graph. Section 8.2 generalizes the coarse-graining approach for spin network entanglement: we explore the evolution generated by loop holonomy operator, as considered in the previous chapter. The most important results in this part are two-fold: (a) The exact transformation is built between the loop holonomy operators on graph and the corresponding coarse-grained graph, as presented in Result 8.3. (b) The coarse-graining for spin network entanglement still holds under the implementation of the operator, presented in Result 8.4. In a word, not only can one study the spin network entanglement from a simpler graph, but one can also study the evolution of the spin network entanglement from this simpler graph.

Section 8.3 applies these general results of coarse-graining for explicit examples, studying entanglement excitation generated by holonomy operator for the sake of looking evolution of spin entanglement. We present examples with one-loop triangle graph, square graph, and a simple two-loop graph, where the latter exhibits how the path-dependency (the path acted by holonomy operator) can be converted to the dependency of self-loop spin and reveals a deeper relation between entanglement and curvature.

8.1 Entanglement between spin sub-networks

The section aims to define the spin network entanglement and to present how to study the entanglement under coarse-graining. The goal is to show that the coarse-graining via gauge-fixing exactly preserves the spin network entanglement at the kinematical level.

8.1.1 Reduced density matrices on spin network

This subsection is meant to define the spin network entanglement. A graph Γ is partitioned by starting from partitioning the set of vertices. The set of vertices $\mathscr{V} =$

$\{v_1\,, v_2\,, \cdots\}$ is partitioned into subsets

$$\mathscr{V} = \bigsqcup_{i=1}^{n} \mathscr{V}_i \tag{8.1.1}$$

such that the vertices of every subset $\mathscr{V}_i$ can be connected by a path. Then every $\mathscr{V}_i$ defines a subgraph Γ_i by this way: (i) For the bulk of Γ_i, i.e. Γ_i^o, the set of vertices is $\mathscr{V}_i$, and the set of bulk edges consists of the edges in Γ whose two-end vertices are both in $\mathscr{V}_i$. (ii) For those edges whose two-end vertices are in different subsets, they are split into two piecewise. For instance, suppose an edge e whose $s(e) \in \mathscr{V}_i,\ t(e) \in \mathscr{V}_j$ and $i \neq j$, then e is split into two piecewise $e_i,\ e_j$ such that $e = e_i \sqcup e_j$. (iii) All one-end edges whose source vertex or target vertex belongs to $\mathscr{V}_i$, define the boundary of Γ_i, i.e. $\partial\Gamma_i$. Therefore, the graph Γ is partitioned by

$$\Gamma = \bigsqcup_{i=1}^{n} \Gamma_i\,, \qquad \Gamma_i = \Gamma_i^o \sqcup \partial\Gamma_i\,, \qquad \partial\Gamma_i \equiv \mathcal{B}_i\,. \tag{8.1.2}$$

Based on the partition, the spin network Hilbert space satisfies the set-relation

$$\mathcal{H}_\Gamma \subset \bigotimes_{i=1}^{n} \mathcal{H}_{\Gamma_i}\,. \tag{8.1.3}$$

Every $\mathcal{H}_{\Gamma_i}$ is the spin sub-network Hilbert space based on the corresponding Γ_i. Here the $\subset$ sign is due to the spin-matching constraint imposed amongst $\mathcal{H}_{\partial\Gamma_i}$.

Above definition can be viewed as a generalization for the particular situation that vertices are partitioned into sole vertex as Eq.(7.2.1) and Eq.(7.2.2), i.e. every sole vertex and its attached edges make up a sub-graph based on single vertex. Here the $\subset$ sign is due to the spin-matching constraint imposed amongst every bulk edge which would likely introduce entanglement between the vertices or sub-networks to which it connects, as in previous chapter that entanglement is introduced by spin-superposition.

Up to now we generalize the partition from $\bigotimes_{v\in\Gamma} \mathcal{H}_v$ to $\bigotimes_{i=1}^{n} \mathcal{H}_{\Gamma_i}$, i.e. from vertices to sub-networks.

To define the entanglement between sub-networks, we start from entanglement between vertices. A generic spin network state can be decomposed as a superposition over spin network basis states:

$$|\psi_\Gamma\rangle = \sum_{\{I_v\}} C_\Gamma(\{I_v\}) \bigotimes_{v\in\Gamma} |\Psi_{v,I_v}\rangle\,, \qquad \text{where} \quad |\Psi_{\Gamma,\{I_v\}}\rangle = \bigotimes_{v\in\Gamma} |\Psi_{v,I_v}\rangle\,. \tag{8.1.4}$$

Here the intertwiner basis state $|\Psi_{v,I_v}\rangle \in \mathcal{H}_v$ have definite spins and intertwiner, with spins and internal intertwiner indices packaged in the labels I_v. Then the coefficients $C_\Gamma(\{I_v\})$ for a general state admits superpositions of both spins and intertwiners, thus leads to correlation between intertwiner states located at different vertices.

Since spin network basis states can be factorized as the tensor product of intertwiner basis state $|\Psi_{v,I_v}\rangle \in \mathcal{H}_v$, we can group up the intertwiner basis states within every sub-network, which defines a factorization for spin network basis state $|\Psi_{\Gamma,\{I_v\}}\rangle \in \mathcal{H}_\Gamma$ with

respect to spin sub-networks basis states $|\Psi_{\Gamma_i,\{I_v\}_{v\in\Gamma_i}}\rangle \in \mathcal{H}_{\Gamma_i}$,

$$|\Psi_{\Gamma,\{I_v\}}\rangle \;=\; \bigotimes_{i=1}^{n} |\Psi_{\Gamma_i,\{I_v\}_{v\in\Gamma_i}}\rangle\,, \qquad \text{where} \quad |\Psi_{\Gamma_i,\{I_v\}_{v\in\Gamma_i}}\rangle = \bigotimes_{v\in\Gamma_i} |\Psi_{v,I_v}\rangle\,. \tag{8.1.5}$$

It allows to re-group the coefficients $C_\Gamma(\{I_v\}) = C_\Gamma([\{I_v\}_{v\in\Gamma_i}]_i)$ where every square bracket $[,]_i$ is adopted to cluster the vertices belonging to respect Γ_i. In this way, the Eq.(8.1.4) can be also written as

$$|\psi_\Gamma\rangle = \sum_{\{I_v\}_{v\in\Gamma_i}} C_\Gamma([\{I_v\}_{v\in\Gamma_i}]_i) \bigotimes_{i=1}^{n} |\Psi_{\Gamma_i,\{I_v\}_{v\in\Gamma_i}}\rangle\,. \tag{8.1.6}$$

The entanglement of $|\psi_\Gamma\rangle$ between sub-graphs is encoded into the unfactorizability with respect to $\bigotimes_{i=1}^{n} \mathcal{H}_{\Gamma_i}$, which can be studied via the formalism of density matrix.

Given any pure spin network state $|\psi_\Gamma\rangle$, it corresponds to pure density matrix $\rho_\Gamma[\psi] = |\psi_\Gamma\rangle\langle\psi_\Gamma|$. It is straightforward to generalize the following procedure to the cases of mixed density matrix ρ_Γ, since any mixed density matrix admits decomposition $\rho = \sum_k W_k|\psi_k\rangle\langle\psi_k|$. The reduced density matrix for sub-network Γ_i is defined via partial trace over its complementary $\Gamma \setminus \Gamma_i$:

$$\rho_{\Gamma_i}[\psi] = \mathrm{Tr}_{\mathcal{H}_{\Gamma\setminus\Gamma_i}} \rho_\Gamma[\psi] \quad \in \mathrm{End}\Big[\mathcal{H}_{\Gamma_i}\Big]\,, \qquad \Gamma\setminus\Gamma_i = \bigsqcup_{j\neq i}^{n} \Gamma_j\,. \tag{8.1.7}$$

This partial trace is implemented by choosing an orthonormal basis for $\mathcal{H}_{\Gamma\setminus\Gamma_i}$,

$$|\Psi_{\Gamma\setminus\Gamma_i},\{I_v\}_{v\notin\Gamma_i}\rangle = \bigotimes_{j\neq i}^{n} |\Psi_{\Gamma_j,\{I_v\}_{v\in\Gamma_j}}\rangle\,, \qquad \text{where} \quad |\Psi_{\Gamma_j,\{I_v\}_{v\in\Gamma_j}}\rangle = \bigotimes_{v\in\Gamma_j} |\Psi_{v,I_v}\rangle\,, \tag{8.1.8}$$

therefore, Eq.(8.1.7) can be expressed by

$$\rho_{\Gamma_i}[\psi] = \sum_{\{I_v\}_{v\notin\Gamma_i}} \langle\Psi_{\Gamma\setminus\Gamma_i},\{I_v\}_{v\notin\Gamma_i}|\,\rho_\Gamma[\psi]\,|\Psi_{\Gamma\setminus\Gamma_i},\{I_v\}_{v\notin\Gamma_i}\rangle \quad \in \mathrm{End}\Big[\mathcal{H}_{\Gamma_i}\Big]\,. \tag{8.1.9}$$

According to Eq.(8.1.6), the scalar product $\langle\Psi_{\Gamma\setminus\Gamma_i},\{I_v\}_{v\notin\Gamma_i}|\psi_\Gamma\rangle$ is presented by

$$|\psi_\Gamma\rangle = \sum_{\{I_v\}_{v\in\Gamma_i}} \sum_{\{I_{v'}\}_{v'\notin\Gamma_i}} C_\Gamma(\{I_v\}_{v\in\Gamma_i},\{I_{v'}\}_{v'\notin\Gamma_i})|\Psi_{\Gamma_i,\{I_v\}_{v\in\Gamma_i}}\rangle \otimes |\Psi_{\Gamma\setminus\Gamma_i},\{I_{v'}\}_{v'\notin\Gamma_i}\rangle\,, \tag{8.1.10}$$

$$\langle\Psi_{\Gamma\setminus\Gamma_i},\{I_{v'}\}_{v'\notin\Gamma_i}|\psi_\Gamma\rangle = \sum_{\{I_v\}_{v\in\Gamma_i}} C_\Gamma(\{I_v\}_{v\in\Gamma_i},\{I_{v'}\}_{v'\notin\Gamma_i})|\Psi_{\Gamma_i,\{I_v\}_{v\in\Gamma_i}}\rangle\,, \tag{8.1.11}$$

thus the reduced density $\rho_{\Gamma_i}[\psi]$ in Eq.(8.1.9) is expressed as

$$\rho_{\Gamma_i}[\psi] = \sum_{\{I_{v'}\}_{v'\notin\Gamma_i}} \sum_{\{I_v\}_{v\in\Gamma_i}} \sum_{\{\widetilde{I}_v\}_{v\in\Gamma_i}} C_\Gamma(\{I_v\}_{v\in\Gamma_i},\{I_{v'}\}_{v'\notin\Gamma_i})\overline{C_\Gamma(\{\widetilde{I}_v\}_{v\in\Gamma_i},\{I_{v'}\}_{v'\notin\Gamma_i})}$$

$$|\Psi_{\Gamma_i,\{I_v\}_{v\in\Gamma_i}}\rangle\langle\Psi_{\Gamma_i,\{\widetilde{I}_v\}_{v\in\Gamma_i}}|\,. \tag{8.1.12}$$

The reduced density matrix $\rho_{\Gamma_i}[\psi]$ encodes the information about intertwiners located in Γ_i, so the spin network entanglement is the generalization for intertwiner entanglement [190]. We can think that the entirety of the intertwiners located in a subgraph defines a 'cluster-intertwiner'. In other words, the entanglement between these spin sub-networks amounts to being entanglement between the corresponding 'cluster-intertwiner'.

So far we have discussed the entanglement structure of spin networks, and the definition of reduced density matrices for spin sub-networks. The next subsection is to apply coarse-graining via gauge-fixing to the spin network entanglement.

8.1.2 Spin network entanglement and cluster intertwiner entanglement

In this part, we investigate the coarse-graining for spin network entanglement. Suppose that Γ is partitioned into $\Gamma = \bigsqcup_{i=1}^{n}\Gamma_i$. We will show that the entanglement between these sub-graphs $\{\Gamma_i\}_{i=1}^{n}$, can be reflected in coarse-grained graph $\Gamma_{(R)}$ made up by loopy graphs $\{\Upsilon_i\}_{i=1}^{n}$.

Let us apply the viewpoint of dual boundary Hilbert space for this goal. Any partition, needless to say, introduces boundaries. The dual boundary Hilbert spaces inherit the entanglement structure Eq.(8.1.3)

$$(\mathcal{H}_{\partial\Gamma})^* \subset \bigotimes_{i=1}^{n}(\mathcal{H}_{\partial\Gamma_i})^*\,. \tag{8.1.13}$$

Here every $(\mathcal{H}_{\partial\Gamma_i})^*$ is the dual boundary Hilbert space associative with spin sub-network Γ_i. As the correspondence between $|\psi_{\partial\Gamma}\rangle \in (\mathcal{H}_{\partial\Gamma})^*$ and $|\psi_\Gamma\rangle \in \mathcal{H}_\Gamma$, the density matrix $\rho_{\partial\Gamma^*} \in \mathrm{End}\Big[(\mathcal{H}_{\partial\Gamma})^*\Big]$ corresponds to $\rho_\Gamma \in \mathrm{End}\Big[\mathcal{H}_\Gamma\Big]$ in same way (remember the difference between notations $|\psi_{\partial\Gamma}\rangle$ and $|\psi_\Gamma\rangle$ mentioned in subsection 5.4.1). Due to Eq.(5.4.9), the information they contain is identical. The next step is to check that the scalar product for $\mathcal{H}_{\Gamma_i}$ and the scalar product for $(\mathcal{H}_{\partial\Gamma_i})^*$ are equivalent with respect to partial trace. This is again expected due to Eq.(5.4.9), but notice the subtlety

$$\mathcal{H}_{\Gamma_i} \ni \langle\Psi_{\Gamma\setminus\Gamma_i,\{I_v\}_{v\notin\Gamma_i}}|\psi_\Gamma\rangle \overset{!}{=} \mathcal{G}_{\mathcal{B}_i} \triangleright \langle\Psi_{\partial(\Gamma\setminus\Gamma_i),\{I_v\}_{v\notin\Gamma_i}}|\psi_{\partial\Gamma}\rangle \in (\mathcal{H}_{\partial\Gamma_i})^*\,. \tag{8.1.14}$$

The left-hand side is computed from the spin network Hilbert space that all information can be encoded in spins and intertwiners, and holonomies are absent in the formulation. But right-hand side is computed from the dual boundary Hilbert space keeping the $\mathcal{G}_{\mathcal{B}_i}$. Here sign $\overset{!}{=}$ is adopted to indicate the equivalence and notice the slight subtlety.

Of course, the subtlety can also be understood from spin network wave-function: the holonomy is split in terms of group multiplication when the edge is cut. Then partial trace removes one piecewise holonomy without integration. So $\mathcal{H}_\Gamma$ and $(\mathcal{H}_{\partial\Gamma})^*$ perspectives are entirely equivalent.

The boundary holonomies do not affect the scalar product for $(\mathcal{H}_{\partial\Gamma_i})^*$, thus they do not change the Schmidt eigenvalues of the reduced density matrix. Indeed, from the viewpoint of subsection 5.4.2, the $\mathcal{G}_{\mathcal{B}_i}$ should be understood as a unitary transformation for $(\mathcal{H}_{\partial\Gamma_i})^*$ for the whole sub-network Γ_i, i.e. $\mathcal{G}_{\mathcal{B}_i}$ is a local unitary transformation associated to Γ_i. Therefore, $\mathcal{G}_{\mathcal{B}_i}$ can not affect the entanglement between spin sub-networks.

Proposition 8.1. *Let $\rho_\Gamma \in \mathrm{End}\Big[\mathcal{H}_\Gamma\Big]$ be the density matrix for spin network Hilbert space $\mathcal{H}_\Gamma$, which allows decomposition $\rho_\Gamma = \sum_k W_k |\psi^{(k)}_\Gamma\rangle\langle\psi^{(k)}_\Gamma|$. Since every $|\psi^{(k)}_\Gamma\rangle$ offers a bulk-boundary map $|\psi^{(k)}_{\partial\Gamma}\rangle$, then in the dual boundary Hilbert space $(\mathcal{H}_{\partial\Gamma)})^*$, the corresponding density matrix [1] is $\rho_{\partial\Gamma^*} = \sum_k W_k |\psi^{(k)}_{\partial\Gamma}\rangle\langle\psi^{(k)}_{\partial\Gamma}| \in \mathrm{End}\Big[(\mathcal{H}_{\partial\Gamma})^*\Big]$. The density matrices ρ_Γ and $\rho_{\partial\Gamma^*}$ encode identical entanglement between spin sub-networks.*

In fact, any bulk-boundary map for $\partial\Gamma$ can be expressed by 'gluing' $\bigcup\!\!\!\!\times$ bulk-boundary maps associative with Γ_i,

$$|\psi_{\partial\Gamma}(\{g_e\}_{e\in\Gamma^o})\rangle = \sum_{\{I_v\}_{v\in\Gamma_i}} C_\Gamma([\{I_v\}_{v\in\Gamma_i}]_i) \bigcup\!\!\!\!\times_{i=1}^{n} \mathcal{G}_{\partial\Gamma_i} \triangleright |\Psi_{\partial\Gamma_i,\{I_v\}_{v\in\Gamma_i}}(\{g_e\}_{e\in\Gamma^o_i})\rangle\,. \quad (8.1.15)$$

Here notation $\bigcup\!\!\!\!\times$ means gluing the sub-networks with boundary holonomies $\mathcal{G}_{\partial\Gamma_i}$ along the interfacing edges. This is how we acquire a boundary state from a spin network state: every vertex and its edges make up simplest open spin network, then bulk holonomies glue these vertices together, and the rest of the open edges make up the boundary Hilbert space (as illustrated in Fig.2.2). In this sense, bulk holonomies and spin-matching constraint play as 'glue', and spin network wave-function then plays as 'coarse-grainer' that maps these 'glues' to boundary edges. Moreover, this understanding can be applied to time-like boundaries. We recommend that interested readers refer to [188].

The advantage of the viewpoint of dual boundary Hilbert is that we can coarse-grain sub-networks. To see this, let us revisit partial trace Eq.(8.1.9), which requires computing Eq.(8.1.11), but this time we compute it based on Eq.(8.1.15). Now, for any spin sub-network, the scalar product can be computed via Eq.(5.4.15), i.e.,

$$\langle\phi_{\Gamma_i}|\psi_{\Gamma_i}\rangle = \langle\phi_{\partial\Gamma_i}|\psi_{\partial\Gamma_i}\rangle = \langle\phi_{\partial\Upsilon_i}|\psi_{\partial\Upsilon_i}\rangle\,, \quad (8.1.16)$$

where the left side is computed from spin sub-network Hilbert space $\mathcal{H}_{\partial\Gamma_i}$, middle from dual boundary Hilbert space $(\mathcal{H}_{\partial\Gamma_i})^*$, and right side from loopy dual boundary Hilbert space $(\mathcal{H}_{\partial\Upsilon_i})^*$.

Following the analysis, we coarse-grain spin sub-networks into loopy spin networks via gauge-fixing. Given graph Γ and partition $\Gamma = \bigsqcup_{i=1}^n \Gamma_i$, the coarse-grained graph $\Gamma_{(R)}$ is obtained via gauge-fixing every Γ_i to make every Γ_i a loopy spin network Υ_i, then glue Υ_i back and acquire the coarse-grained graph (e.g. Fig.8.2)

$$\Gamma_{(R)} = \bigsqcup_{i=1}^{n} \Upsilon_i\,. \quad (8.1.17)$$

[1] We use a 'star' sign $*$ to emphasize the density matrix associative with dual boundary Hilbert space, also to reminder readers not to confuse it with the induced boundary density matrix $\rho_{\partial\Gamma}$ in Chapter 6.

The coarse-grained graph preserves the entanglement between spin sub-networks. Indeed, one can understand the entanglement preservation from the statement in Proposition 5.4: gauge-fixing Γ_i amounts to implementing a local unitary transformation with respect to $(\mathcal{H}_{\mathcal{B}_i})^*$. In general, in Heisenberg picture,

$$\begin{aligned}|\Psi_{\partial\Gamma,\{I_v\}}(\{g_e\}_{e\in\Gamma^o})\rangle &= \sum_{\{I_{u_i}\}} \bigotimes_{i=1}^{n} \left(\left[\mathcal{U}_{\Upsilon_i}\right]^{I_{u_i}}_{\{I_v\}_{v\in\Gamma_i}} \circ \mathcal{G}_{\mathcal{B}_i} \triangleright |\Psi_{\partial\Upsilon_i,I_{u_i}}(\{G_e\}_{e\in\Upsilon_i^o})\rangle \right) \\ &= \sum_{\{I_{u_i}\}} \left(\prod_{i=1}^{n} \left[\mathcal{U}_{\Upsilon_i}\right]^{I_{u_i}}_{\{I_v\}_{v\in\Gamma_i}} \right) \circ \left(\bigotimes_{i=1}^{n} \mathcal{G}_{\mathcal{B}_i} \triangleright |\Psi_{\partial\Upsilon_i,I_{u_i}}(\{G_e\}_{e\in\Upsilon_i^o})\rangle \right) .\end{aligned} \tag{8.1.18}$$

Here every $\mathcal{U}_{\Upsilon_i}$ represents channel transformation for loopy intertwiner in $\mathcal{H}_\Upsilon$, and every $\mathcal{G}_{\mathcal{B}_i}$ represents boundary holonomies for $\mathcal{H}_{\partial\Gamma_i}$. They do not change the boundary spins, thus all spin-matching constraints hold. Every $\mathcal{U}_{\Upsilon_i}$ and $\mathcal{G}_{\mathcal{B}_i}$ are local unitary transformation for respect $(\mathcal{H}_{\mathcal{B}_i})^*$ so we factorize $\mathcal{U}_{\Upsilon_i}$ and keep $\mathcal{G}_{\mathcal{B}_i}$ in gluing operation. Notably, boundary holonomies on $\mathcal{B}_i$ never change the scalar products for $\mathcal{H}_{\mathcal{B}_i}$ and $(\mathcal{H}_{\mathcal{B}_i})^*$. We then have transformation between density matrices:

$$\rho_{\partial\Gamma^*} = \mathcal{U}^\dagger_{\mathcal{B}_1} \cdots \mathcal{U}^\dagger_{\mathcal{B}_n} \, \rho_{\partial\Gamma^*_{(R)}} \, \mathcal{U}_{\mathcal{B}_1} \cdots \mathcal{U}_{\mathcal{B}_n} . \tag{8.1.19}$$

Again, every $\mathcal{U}_{\mathcal{B}_i}$ is to be interpreted as a local unitary transformations with respect to $(\mathcal{H}_{\mathcal{B}_i})^*$. Therefore, the $\rho_{\partial\Gamma^*}$ and $\rho_{\partial\Gamma^*_{(R)}}$ carry equal spin network entanglement with respect to the partition, since any entanglement measure is required to be invariant under local unitary transformations according to Axioms 3.1 [137, 136, 138, 139, 134].

Result 8.2. *Let $\mathcal{E}$ be any entanglement measure. Given a partition $\Gamma = \bigsqcup_{i=1}^n \Gamma_i$. Let $\Gamma_{(R)} = \bigsqcup_{i=1}^n \Upsilon_i$ be the coarse-grained graph for Γ where Υ_i are loopy graphs for respect Γ_i. For any spin network state based on the Γ, the corresponding coarse-grained state based on the $\Gamma_{(R)}$ is defined via gauge-fixing. Then for density matrix $\rho_{\partial\Gamma^*}$ and the corresponding density matrix $\rho_{\partial\Gamma^*_{(R)}}$ for the coarse-grained state, the reduced density matrices $\rho_{\partial\Gamma_i^*}$ and $\rho_{\partial\Upsilon_i^*}$ are related by*

$$\rho_{\partial\Gamma_i^*} = \mathcal{U}^\dagger_{\mathcal{B}_i} \, \rho_{\partial\Upsilon_i^*} \, \mathcal{U}_{\mathcal{B}_i} . \tag{8.1.20}$$

Here $\mathcal{U}_{\mathcal{B}_i}$ is unitary map for $(\mathcal{H}_{\mathcal{B}_i})^*$. Moreover, $\rho_{\partial\Gamma^*}$ and $\rho_{\partial\Gamma^*_{(R)}}$ carry equal spin network entanglement,

$$\mathcal{E}[\rho_{\partial\Gamma^*}] = \mathcal{E}[\rho_{\partial\Gamma^*_{(R)}}] . \tag{8.1.21}$$

Due to the Proposition 8.1, $\mathcal{E}[\rho_\Gamma] = \mathcal{E}[\rho_{\Gamma_{(R)}}]$.

At the end of the day, we have shown that spin network entanglement admits to be coarse-grained, thus one can study the entanglement by studying (loopy) intertwiner entanglement on coarser graph.

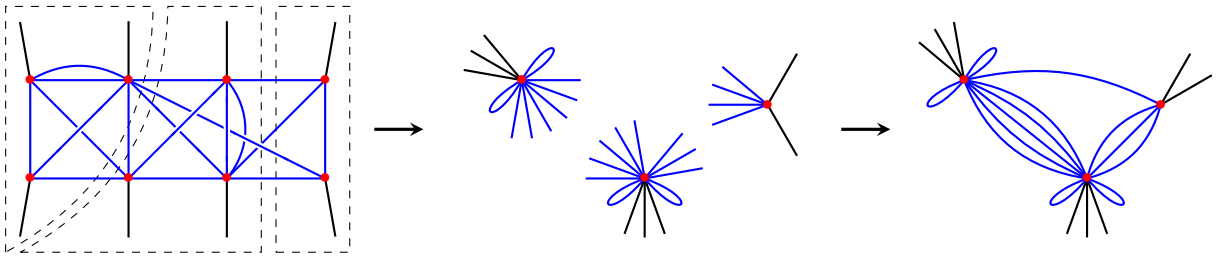

Figure 8.2: Illustrations for coarse-graining: from fine-graph to coarse-grained graph. To consider the entanglement between the three dashed sub-networks (left side), we coarse-grain every sub-networks via gauge-fixing such that they are represented by loop graphs (middle). Then we glue them back (right side). The spin network entanglements on left side and right side are identical, i.e. the coarse-graining preserves the spin network entanglement.

8.2 Coarse-graining: holonomy operators

One of the goals of this part is to show that the action of loop holonomy operator on a graph can be exactly represented by the action on its coarse-grained graph, up to some unitary transformations. We give the transformation rule for the two actions. Based on that, we show that the loop holonomy dynamics of spin network entanglement can be studied exactly from the coarse-grained graph.

8.2.1 The transformation between holonomy operators based on finer and coarser graph

Coarse-graining the loop W is done by keeping the edges that are not coarse-grained, then by gluing them into loop to be referred to $W_{(R)}$, e.g. Fig.8.3.

Two trivial situations are not to be considered: (i) W is completely isolated in certain Γ_i. (ii) Trivial coarse-graining $W_{(R)} = W$.

According to Proposition 7.1, the evolution on these loopy spin sub-networks $\{\Upsilon_i\}$ is determined by the bouquet spins and the spins on the loop edges. So the transition matrix Z (7.1.8) can be obtained by studying the type of particular graphs that the bouquet spins are represented by boundary spins, such as Fig.8.3.

Now consider two evolutions: (a) Evolution $|\psi_\Gamma\rangle \to |\psi_\Gamma(t)\rangle$ generated by loop holonomy operator acting on $W \subset \Gamma$. (b) Evolution $|\psi_{\Gamma_{(R)}}\rangle \to |\psi_{\Gamma_{(R)}}(t)\rangle$ generated by loop holonomy operator action on $W_{(R)} \subset \Gamma_{(R)}$. Then we arrive at the following result:

Result 8.3. *Suppose the oriented loop* $W[v_1 \overset{e_1}{\to} \cdots \overset{e_{p-1}}{\to} v_p \overset{e_p}{\to} v_1]$ *is partitioned by* n *sub-networks* $\{\Gamma_i\}_{i=1}^n$, *i.e.* $W = \bigsqcup_{i=1}^n W_i$ *where* $W_i \subset \Gamma_i$. *For every* Γ_i, *we relabel the bouquet spins* j_α *and bulk spins* k_α *along the* W_i *and denote them by*

$$\{j_\alpha^{(i)}\} \equiv \{j_1^{(i)}, \cdots, j_{p_i}^{(i)}\}, \qquad \{k_\alpha^{(i)}\} \equiv \{k_0^{(i)}, k_1^{(i)}, \cdots, k_{p_i}^{(i)}\} = \{k_\alpha^{o(i)}\} \sqcup \{k_\alpha^{\partial(i)}\}$$

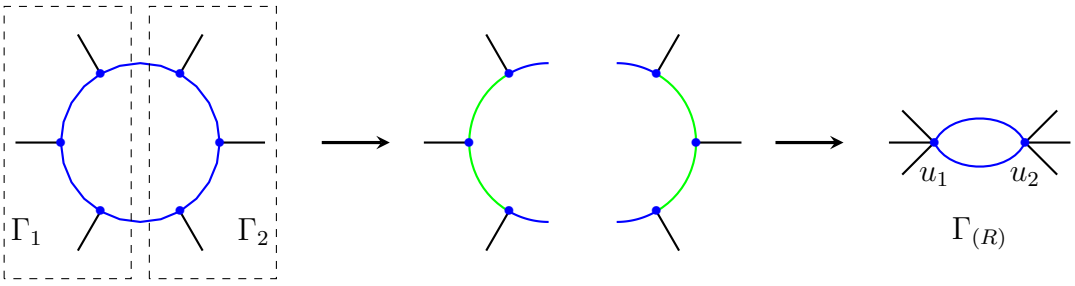

Figure 8.3: The sub-networks Γ_1 and Γ_2 are coarse-grained to Υ_1 and Υ_2 for $\Gamma_{(R)}$ via gauge-fixing along the maximal trees T_1 and T_2 (green). The W and coarse-grained loop $W_{(R)}$ are colored in blue.

with the implicit convention $k_{p_i}^{(i)} = k_0^{(i+1)}$ *due to the spin-matching constraint, where*

$$\{k_\alpha^{o(i)}\} \equiv \{k_1^{(i)}, \cdots, k_{p_i-1}^{(i)}\}, \qquad \{k_\alpha^{\partial(i)}\} \equiv \{k_0^{(i)}, k_{p_i}^{(i)}\},$$

because $\{k_\alpha^{o(i)}\}$ *are bulk spins for* Γ_i*, and* $\{k_\alpha^{\partial(i)}\}$ *are part of boundary spins for* Γ_i*. Spins* $\{j_\alpha^{(i)}, k_\alpha^{\partial(i)}\}$ *define cluster intertwiners*

$$I_{u_i} \in \mathrm{Inv}_{\mathrm{SU}(2)}\Big[\mathcal{V}_{k_0^{(i)}} \otimes \mathcal{V}_{k_{p_i}^{(i)}} \otimes \bigotimes_{\alpha=1}^{p_i} \mathcal{V}_{j_\alpha}\Big]. \tag{8.2.1}$$

Now the cluster intertwiner is labeled by $\{j_\alpha^{(i)}, k_\alpha^{(i)}\}$*, and recoupling spins* $\{j_\alpha^{(i)}, k_\alpha^{\partial(i)}\}$ *leads to the representation* $\mathcal{U}_{\Upsilon_i} : \mathcal{H}_{\Upsilon_i} \longrightarrow \mathcal{H}_{\Upsilon_i}$ *for channel transformation:*

$$\Big[\mathcal{U}_{\Upsilon_i}^{\{j_\alpha^{(i)}, k_\alpha^{\partial(i)}\}}\Big]^{I^o_{u_i}}{}_{\{k_\alpha^{o(i)}\}} = \langle \Psi_{\Upsilon_i, I_{u_i}} | \Psi_{\Upsilon_i, \{j_\alpha^{(i)}, k_\alpha^{(i)}\}} \rangle . \tag{8.2.2}$$

Here $I_{u_i} = \{j_\alpha^{(i)}, k_\alpha^{\partial(i)}\} \cup I^o_{u_i}$ *equivalently labels the cluster intertwiner* $\{j_\alpha^{(i)}, k_\alpha^{(i)}\}$ *(illustrated as Fig.8.4). Tensoring representations leads to*

$$\Big[\mathcal{U}_{\Gamma_{(R)}}\Big]^{\{I_u\}}{}_{\{j_\alpha, k_\alpha\}} = \prod_{i=1}^{n} \Big[\mathcal{U}_{\Upsilon_i}^{\{j_\alpha^{(i)}, k_\alpha^{\partial(i)}\}}\Big]^{I^o_{u_i}}{}_{\{k_\alpha^{o(i)}\}} . \tag{8.2.3}$$

Then the transition matrices based on Γ *and* $\Gamma_{(R)}$ *satisfy*

$$\Big[Z(\Gamma)_{\chi_\ell \triangleright W}\Big]^{\{J_\alpha, K_\alpha\}}{}_{\{j_\alpha, k_\alpha\}} = \sum_{\{I^o_{u_i}\}} \sum_{\{\widetilde{I}^o_{u_i}\}} \overline{\Big[\mathcal{U}_{\Gamma_{(R)}}\Big]^{\{\widetilde{I}_{u_i}\}}{}_{\{J_\alpha, K_\alpha\}}} \Big[Z(\Gamma_{(R)})_{\chi_\ell \triangleright W_{(R)}}\Big]^{\{\widetilde{I}_{u_i}\}}{}_{\{I_{u_i}\}}$$
$$\Big[\mathcal{U}_{\Gamma_{(R)}}\Big]^{\{I_{u_i}\}}{}_{\{j_\alpha, k_\alpha\}} \prod_{\alpha=1}^{p} \delta_{J_\alpha j_\alpha} , \tag{8.2.4}$$

where $I_{u_i} = \{j_\alpha^{(i)}, k_\alpha^{\partial(i)}\} \cup I^o_{u_i}$ *and* $\widetilde{I}_{u_i} = \{J_\alpha^{(i)}, K_\alpha^{\partial(i)}\} \cup \widetilde{I}^o_{u_i}$*, and the transition matrix* $Z(\Gamma_{(R)})$ *is given by*

$$\Big[Z(\Gamma_{(R)})_{\chi_\ell \triangleright W_{(R)}}\Big]^{\{\widetilde{I}_u\}}{}_{\{I_u\}}$$

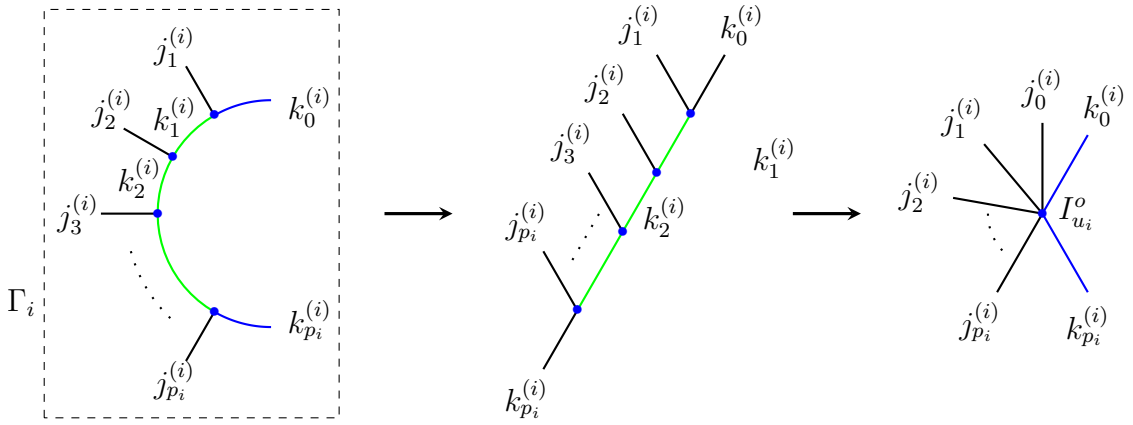

Figure 8.4: The illustration for recoupling spins to acquire cluster intertwiner I_{u_i}.

$$= \int \prod_{e\in W_{(R)}} \mathrm{d}g_e \, {}_\partial\langle \Psi_{\partial\Gamma_{(R)},\{\tilde{I}_u\}}(\{g_e\}_{e\in W_{(R)}}) | \chi_\ell(G_{W_{(R)}}) | \Psi_{\partial\Gamma_{(R)},\{I_u\}}(\{g_e\}_{e\in W_{(R)}}) \rangle_\partial \,. \tag{8.2.5}$$

The proof of the proposition is in Appendix C. One can refer to Fig.8.4 and Fig.8.5 for the outline of the proof. In Fig.8.5, the unitary map $\mathcal{U}_\mathcal{B}$ for dual boundary Hilbert space is implemented by first gauge-fixing the holonomy along $e_{\alpha+1}$ such that the holonomy operator acts trivially on $e_{\alpha+1}$, then gluing two bouquet edges and switching channel. Thus the $e_{\alpha+1}$ is coarse-grained, so it is unseen when the holonomy operator is implemented.

Particularly, a direct corollary of Result 8.3, is that we can compute expectations Eq.(7.2.26) $\langle \widehat{\chi^2_\ell} \triangleright_W \rangle$ and Eq.(7.2.27) $\langle \widehat{\chi_\ell} \triangleright_W \rangle$ from loopy spin network.

Now that we can see, the exponential evolution that is generated by loop holonomy operator $\widehat{\chi_\ell} \triangleright_W$ on Γ, is related to the exponential evolution that is generated by loop holonomy operator $\widehat{\chi_\ell} \triangleright_{W(R)}$ on $\Gamma_{(R)}$ via the following transformation:

$$\exp\left[-\mathrm{i}t\, Z(\Gamma)_{\chi_\ell \triangleright W}\right] = \mathcal{U}^\dagger_{\Upsilon_1} \cdots \mathcal{U}^\dagger_{\Upsilon_n} \exp\left[-\mathrm{i}t\, Z(\Gamma_{(R)})_{\chi_\ell \triangleright_{W_{(R)}}}\right] \mathcal{U}_{\Upsilon_1} \cdots \mathcal{U}_{\Upsilon_n} \,. \tag{8.2.6}$$

Every $\mathcal{U}_{\Upsilon_i}$ is a unitary transformation for internal space of intertwiner at u_i, thus they do not affect the spin-matching constraints between interfacing edges. Instead, they are to be interpreted as local unitary transformations at u_i, i.e., these unitary transformations do not affect spin entanglement. Indeed, following transformation Eq.(8.1.19), the density matrix $\rho_{\partial\Gamma^*}$'s evolution is now given by

$$\rho_{\partial\Gamma^*}(t) = \mathcal{U}^\dagger_{\mathcal{B}_1} \cdots \mathcal{U}^\dagger_{\mathcal{B}_n} \rho_{\partial\Gamma^*_{(R)}}(t) \mathcal{U}_{\mathcal{B}_1} \cdots \mathcal{U}_{\mathcal{B}_n} \,, \tag{8.2.7}$$

$$\rho_{\partial\Gamma^*_{(R)}}(t) = \exp\left[-\mathrm{i}(t-t_0)\, Z(\Gamma)_{\chi_\ell \triangleright_{W_{(R)}}}\right] \rho_{\partial\Gamma^*_{(R)}}(t_0) \exp\left[\mathrm{i}(t-t_0)\, Z(\Gamma)_{\chi_\ell \triangleright_{W_{(R)}}}\right] \,. \tag{8.2.8}$$

Partial tracing ρ_Γ over sub-networks $\Gamma \setminus \Gamma_i$ is equivalent to partial tracing $\rho_{\partial\Gamma^*}$ over $(\mathcal{H}_{\mathcal{B}^c_i})^*$ where $\mathcal{B}^c_i \equiv \partial(\Gamma \setminus \Gamma_i)$. It leads to the reduced density matrix for $(\mathcal{H}_{\mathcal{B}_i})^*$,

$$\rho_{\partial\Gamma^*_i}(t) = \mathrm{Tr}_{(\mathcal{H}_{\mathcal{B}^c_i})^*}\left[\rho_{\partial\Gamma^*}(t)\right] = \mathcal{U}^\dagger_{\mathcal{B}_i} \rho_{\partial\Upsilon^*_i}(t) \mathcal{U}_{\mathcal{B}_i} \,. \tag{8.2.9}$$

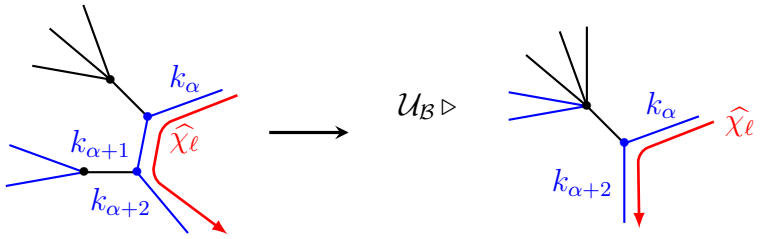

Figure 8.5: The illustration for unitary transformation on loop holonomy operator: on the left-hand side one is able to gauge fix the holonomy associated to spin $k_{\alpha+1}$ into $\mathbb{I}$, then implement channel transformation $\mathcal{U}_\mathcal{B}$ in order to coarse-grain $k_{\alpha+1}$.

Therefore, the reduced density matrices $\rho_{\partial\Gamma_i^*}(t)$ and $\rho_{\partial\Upsilon_i^*}(t)$ are equivalent up to a unitary transformation for dual boundary Hilbert space $(\mathcal{H}_{\mathcal{B}_i})^*$.

Result 8.4. *Given a partition $\Gamma = \bigsqcup_{i=1}^n \Gamma_i$, and an oriented loop W on Γ. Let the coarse-grained graph for Γ be $\Gamma_{(R)} = \bigsqcup_{i=1}^n \Upsilon_i$ where Υ_i are loopy graphs for respect Γ_i, and the coarse-grained loop $W_{(R)}$ for W on $\Gamma_{(R)}$. Let $\mathcal{E}$ be any entanglement measure. Consider evolutions generated by loop holonomy operators $\widehat{\chi}_\ell \triangleright_W$ and the corresponding $\widehat{\chi}_\ell \triangleright_{W_{(R)}}$. Then the evolution of spin network entanglement between Γ_i is identical to the evolution of intertwiner entanglement between Υ_i, i.e.,*

$$\mathcal{E}[\rho_\Gamma(t)] = \mathcal{E}[\rho_{\Gamma_{(R)}}(t)]\,. \tag{8.2.10}$$

At the end of the day, we have shown that the evolution of spin network entanglement admits to be coarse-grained at least for the evolution generated by loop holonomy operator, thus one can study the evolution of entanglement from coarse-grained graph.

8.3 Examples

We would like to conclude this chapter with explicit examples of spin network entanglement coarse-graining.

8.3.1 Triangle graph

We consider the holonomy operator acting on the loop of triangle graph Fig.8.6. We compute explicitly the bipartite entanglement between $\mathcal{H}_A$ and $\mathcal{H}_B \otimes \mathcal{H}_C$. Then we show that the bipartite entanglement can be studied from coarse-grained graph.

Start with an initial spin network basis state $|\Psi_{tri,\{j_i,k_i\}}\rangle = |j_1,k_1,k_3\rangle_A \otimes |j_2,k_2,k_1\rangle_B \otimes |j_3,k_3,k_2\rangle_C$, as the case studied in Chapter 7,

$$\widehat{\chi}_\ell : \bigotimes_{i=1}^3 \mathrm{Inv}_{\mathrm{SU}(2)}\Big(\mathcal{V}_{j_i} \otimes \mathcal{V}_{k_i} \otimes \mathcal{V}_{k_{i-1}}\Big) \to \bigoplus_{\{K_i\}} \bigotimes_{i=1}^3 \mathrm{Inv}_{\mathrm{SU}(2)}\Big(\mathcal{V}_{j_i} \otimes \mathcal{V}_{K_i} \otimes \mathcal{V}_{K_{i-1}}\Big)\,.$$

Now we concern the bipartition $\mathcal{H}_A \otimes \mathcal{H}_B \otimes \mathcal{H}_B$, as what we have done in there, the transition matrix Z, reduced density matrix $\rho_{tri_A}(t)$, and its eigenvalues are given by Eq.(7.4.3), Eq.(7.4.4) and Eq.(7.4.5) respectively.

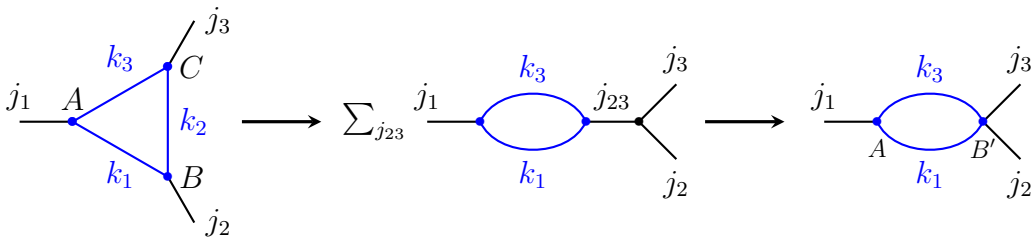

Figure 8.6: Coarse-graining triangle graph to candy graph.

Now we look at the entanglement excitation on the coarse-grained graph. For bipartition $\mathcal{H}_A$ and $\mathcal{H}_B \otimes \mathcal{H}_C$, we gauge fix $g_2 \to \mathbb{I}$, then contract vertices B, C along e_2, acquiring a 4-valent vertex with spins j_2, j_3, k_1, k_3 as Fig.8.6. The spin network coarse-grained state from the triangle graph to the candy graph is given by

$$|\psi_{tc,\{j_i,k_i\}}\rangle = |j_1, k_1, k_3\rangle_A \otimes \sum_{j_{23}} \mathcal{U}^{k_2,j_{23}}_{\{j,k\}_{B'}} |\{j_2, j_3, k_3, k_1\}, j_{23}\rangle_{B'} \,. \tag{8.3.1}$$

As initial spin network state associated to the triangle graph, the initial spin network state $|\psi_{tc,\{j_i,k_i\}}\rangle$ associated to the coarse-grained graph is a product state. But the later is not a spin network basis state. The intertwiner at B' is a superposition of basis states $|\{j_2, j_3, k_3, k_1\}, j_{23}\rangle_{B'}$ with respect to internal spin j_{23}. The unitary matrix

$$\mathcal{U}^{k_2,j_{23}}_{\{j,k\}_{B'}} = (-1)^{2k_2+k_3-k_1+j_2+j_3} \sqrt{(2k_2+1)(2j_{23}+1)} \begin{Bmatrix} j_2 & j_3 & j_{23} \\ k_3 & k_1 & k_2 \end{Bmatrix} \tag{8.3.2}$$

is account for the channel transformation, and the matrix elements are all real numbers, and the unitarity is verified by the orthogonality of $6j$-symbols,

$$\begin{aligned} \sum_{j_{23}} \mathcal{U}^{k_2,j_{23}}_{\{j,k\}_{B'}} \mathcal{U}^{\tilde{k}_2,j_{23}}_{\{j,k\}_{B'}} =& \sum_{j_{23}} \sqrt{(2k_2+1)(2\tilde{k}_2+1)}(2j_{23}+1) \begin{Bmatrix} j_2 & j_3 & j_{23} \\ k_3 & k_1 & k_2 \end{Bmatrix} \begin{Bmatrix} j_2 & j_3 & j_{23} \\ k_3 & k_1 & \tilde{k}_2 \end{Bmatrix} \\ =& \delta_{k_2\tilde{k}_2} \,. \end{aligned} \tag{8.3.3}$$

The unitarity requires the two $\mathcal{U}$ having same $\{j,k\}$ labeling since they are external labels for the intertwiner. On the other hand, the k_2, j_{23} are internal labels for the intertwiner, so we also have

$$\sum_{k_2} \mathcal{U}^{k_2,j_{23}}_{\{j,k\}_{B'}} \mathcal{U}^{k_2,\tilde{j}_{23}}_{\{j,k\}_{B'}} = \delta_{j_{23}\tilde{j}_{23}} \,. \tag{8.3.4}$$

The unitary map $\mathcal{U}_{B'}$ links the transition matrices $Z(tri)$ and $Z(tc)$,

$$[Z(tri)_\ell]^{\{j_i,K_i\}}{}_{\{j_i,k_i\}} = \sum_{j_{23},J_{23}} \mathcal{U}^{K_2,J_{23}}_{\{j,K\}_{B'}} [Z(tc)_\ell]^{j_1,J_{23},K_1,K_3}{}_{j_1,j_{23},k_1,k_3} \mathcal{U}^{k_2,j_{23}}_{\{j,k\}_{B'}} \,, \tag{8.3.5}$$

where the transition matrix for $Z(tc)$ is given by

$$[Z(tc)_\ell]^{J_1,J_{23},K_1,K_3}{}_{j_1,j_{23},k_1,k_3} = (-1)^{j_1+j_{23}+K_1+k_1+K_3+k_3+2\ell} \begin{Bmatrix} j_1 & k_1 & k_3 \\ \ell & K_3 & K_1 \end{Bmatrix} \begin{Bmatrix} j_{23} & k_1 & k_3 \\ \ell & K_3 & K_1 \end{Bmatrix}$$

$$\times \sqrt{(2k_1+1)(2K_1+1)(2k_3+1)(2K_3+1)}\delta_{j_1J_1}\delta_{j_{23}J_{23}}\,. \tag{8.3.6}$$

Explicitly, the transformation is expressed in terms of $6j$-symbols:

$$\begin{aligned}
&(-1)^{\sum_{i=1}^3(j_i+k_i+K_i+\ell)}\begin{Bmatrix} j_1 & k_1 & k_3 \\ \ell & K_3 & K_1\end{Bmatrix}\begin{Bmatrix} j_2 & k_2 & k_1 \\ \ell & K_1 & K_2\end{Bmatrix}\begin{Bmatrix} j_3 & k_3 & k_2 \\ \ell & K_2 & K_3\end{Bmatrix}\\
=&\sum_{j_{23}}(-1)^{2\ell+j_1+j_{23}+2K_1+2k_3+2k_2-2K_2}(2j_{23}+1)\begin{Bmatrix} j_2 & j_3 & j_{23} \\ K_3 & K_1 & K_2\end{Bmatrix}\begin{Bmatrix} j_1 & k_1 & k_3 \\ \ell & K_3 & K_1\end{Bmatrix}\\
&\times\begin{Bmatrix} j_{23} & k_1 & k_3 \\ \ell & K_3 & K_1\end{Bmatrix}\begin{Bmatrix} j_2 & j_3 & j_{23} \\ k_3 & k_1 & k_2\end{Bmatrix}\,.
\end{aligned}\tag{8.3.7}$$

This is a manifestation of Result 8.3, describing the holonomy operator coarse-graining in the triangle graph. Similar to what we have done for Eq.(7.3.17), this identity is related to Biedenharn-Elliot identity.

Let us compute the Schmidt eigenvalues from $|\psi_{tc,\{j_i,k_i\}}\rangle$. Similarly, starting with initial coarse-grained spin network state $|\psi_{tc,\{j_i,k_i\}}\rangle$ as Eq.(8.3.1), we consider the evolution generated by the loop holonomy operator $\widehat{\chi}_\ell$,

$$\begin{aligned}
\widehat{\chi}_\ell:\quad &\mathrm{Inv}_{\mathrm{SU}(2)}\Big(\mathcal{V}_{j_1}\otimes\mathcal{V}_{k_1}\otimes\mathcal{V}_{k_3}\Big)\otimes\mathrm{Inv}_{\mathrm{SU}(2)}\Big(\mathcal{V}_{j_2}\otimes\mathcal{V}_{j_3}\otimes\mathcal{V}_{k_3}\otimes\mathcal{V}_{k_1}\Big)\\
&\to\bigoplus_{K_1,K_3}\mathrm{Inv}_{\mathrm{SU}(2)}\Big(\mathcal{V}_{j_1}\otimes\mathcal{V}_{K_1}\otimes\mathcal{V}_{K_3}\Big)\otimes\mathrm{Inv}_{\mathrm{SU}(2)}\Big(\mathcal{V}_{j_2}\otimes\mathcal{V}_{j_3}\otimes\mathcal{V}_{K_3}\otimes\mathcal{V}_{K_1}\Big)\,.
\end{aligned}$$

Following the same logic in bipartition in the triangle graph. Readers should notice that notation $|\Psi_{tc,\{j_i,K_i\}}\rangle\equiv|\Psi_{sc,\{j_i,K_1,k_2,K_3\}}\rangle$, i.e. the spin k_2 is now fixed under the action of $\widehat{\chi}_\ell$ on the candy graph. The transition matrix is given by Eq.(8.3.6), and the normalization factor $N_{tc,\{j_i,k_i\}}(\ell,t)=N_{tri,\{j_i,k_i\}}(\ell,t)$ due to Eq.(8.3.7).

Repeat the same procedure on spin network state $|\Psi_{tc,\{j_i,k_i\}}\rangle$, as what we have done for Eq.(7.4.5), then we obtain the eigenvalues of $\rho_{tc_A}(t)$ read as

$$\begin{aligned}
&\lambda_{\rho_{tc_A}}[K_1,K_3]\\
=\;&\delta_{k_1}^{K_1}\delta_{k_3}^{K_3}\Bigg(1-t^2\sum_{j_{23}}(-1)^{2\ell+j_1+j_{23}+2k_1+2k_3}(2j_{23}+1)\begin{Bmatrix} j_2 & j_3 & j_{23} \\ K_3 & K_1 & K_2\end{Bmatrix}\begin{Bmatrix} j_1 & k_1 & k_3 \\ \ell & K_3 & K_1\end{Bmatrix}\\
&\times\begin{Bmatrix} j_{23} & k_1 & k_3 \\ \ell & K_3 & K_1\end{Bmatrix}\begin{Bmatrix} j_2 & j_3 & j_{23} \\ k_3 & k_1 & k_2\end{Bmatrix}\Bigg)+t^2\sum_{j_{23}}\begin{Bmatrix} j_{23} & j_2 & j_3 \\ k_2 & k_3 & k_1\end{Bmatrix}^2\begin{Bmatrix} j_1 & k_1 & k_3 \\ \ell & K_3 & K_1\end{Bmatrix}^2\\
&\times\begin{Bmatrix} j_{23} & k_1 & k_3 \\ \ell & K_3 & K_1\end{Bmatrix}^2\prod_{i=1}^3(2k_i+1)(2K_1+1)(2K_3+1)(2j_{23}+1)\Bigg)+O(t^4)\,.
\end{aligned}\tag{8.3.8}$$

One can compare the eigenvalue with Eq.(7.4.5), and verify $\lambda_{\rho_{tri_A}}[K_1,K_3]=\lambda_{\rho_{tc_A}}[K_1,K_3]$ by Eq.(8.3.7). Hence the entanglement excitation is preserved under the coarse-graining.

8.3.2 Square graph

This subsection looks at the holonomy operator acting on the loop of square graph Fig.8.7. We compute explicitly the bipartite entanglement between Γ_1 and Γ_2 where Γ_1 comprises vertices A, D and their adjacent edges, Γ_2 comprises vertices B, C and their adjacent edges. Then we show that the bipartite entanglement can be studied by its coarse-grained graph as Fig.8.7. In fact, similar to the previous case, it is enough to check

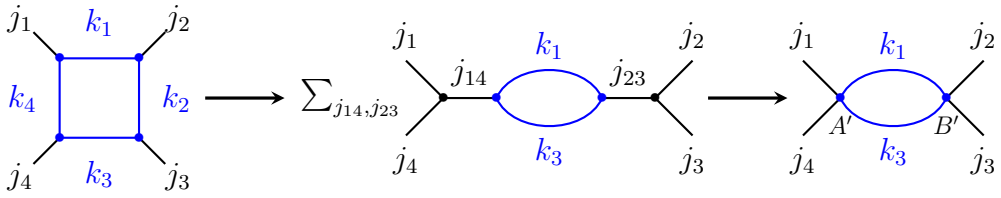

Figure 8.7: Coarse-graining square graph to candy graph.

the transformation between representations of holonomy operator on the square graph and the candy graph (coarse-grained graph of the former).

Considering bipartition $\mathcal{H}_A \otimes \mathcal{H}_D$ and $\mathcal{H}_B \otimes \mathcal{H}_C$, we gauge fix $g_2 \to \mathbb{I}$ and $g_4 \to \mathbb{I}$, then contract vertices A, D along e_4 and vertices B, C along e_2, to acquire two 4-valent vertices with respect spins j_1, j_4, k_1, k_3 and j_2, j_3, k_1, k_3 as Fig.8.7. The coarse-grained spin network state from the square graph is given by

$$|\psi_{sc,\{j_i,k_i\}}\rangle = \sum_{j_{14}} \mathcal{U}^{k_4,j_{14}}_{\{j,k\}_{A'}} |\{j_1, j_4, k_1, k_3\}, j_{14}\rangle_{A'} \otimes \sum_{j_{23}} \mathcal{U}^{k_2,j_{23}}_{\{j,k\}_{B'}} |\{j_2, j_3, k_2, k_3\}, j_{23}\rangle_{B'} \,. \quad (8.3.9)$$

It has intertwiner superposition for $\mathcal{H}_{A'}$ and $\mathcal{H}_{B'}$ with respect to internal spins j_{14} and j_{23}. The $|\{j_1, j_4, k_1, k_3\}, j_{14}\rangle_{A'}$ and $|\{j_2, j_3, k_2, k_3\}, j_{23}\rangle_{B'}$ are intertwiners for the two respect 4-valent vertices A' and B', and $\mathcal{U}^{k_4,j_{14}}_{\{j,k\}_{A'}}$ and $\mathcal{U}^{k_2,j_{23}}_{\{j,k\}_{B'}}$ are unitary transformations for respect $\mathcal{H}_{A'}$ and $\mathcal{H}_{B'}$,

$$\begin{aligned} \mathcal{U}^{k_4,j_{14}}_{\{j,k\}_{A'}} =& (-1)^{2k_4+k_1-k_3+j_1+j_4} \sqrt{(2k_4+1)(2j_{14}+1)} \begin{Bmatrix} j_1 & j_4 & j_{14} \\ k_3 & k_1 & k_4 \end{Bmatrix} , \\ \mathcal{U}^{k_2,j_{23}}_{\{j,k\}_{B'}} =& (-1)^{2k_2+k_3-k_1+j_2+j_3} \sqrt{(2k_2+1)(2j_{23}+1)} \begin{Bmatrix} j_2 & j_3 & j_{23} \\ k_3 & k_1 & k_2 \end{Bmatrix} . \end{aligned} \quad (8.3.10)$$

They are real numbers. The unitarity of $\mathcal{U}^{k_4,j_{14}}_{\{j,k\}_{A'}}$ and $\mathcal{U}^{k_2,j_{23}}_{\{j,k\}_{B'}}$ are verified by the orthogo-

nality of $6j$-symbols,

$$\begin{aligned}\sum_{j_{14}}\mathcal{U}^{k_4,j_{14}}_{\{j,k\}_{A'}}\mathcal{U}^{\tilde{k}_4,j_{14}}_{\{j,k\}_{A'}} =&\sum_{j_{14}}\sqrt{(2k_4+1)(2\tilde{k}_4+1)}(2j_{14}+1)\begin{Bmatrix} j_1 & j_4 & j_{14}\\ k_3 & k_1 & k_4\end{Bmatrix}\begin{Bmatrix} j_1 & j_4 & j_{14}\\ k_3 & k_1 & \tilde{k}_4\end{Bmatrix}\\ =&\delta_{k_4\tilde{k}_4}\,,\\ \sum_{j_{23}}\mathcal{U}^{k_2,j_{23}}_{\{j,k\}_{B'}}\mathcal{U}^{\tilde{k}_2,j_{23}}_{\{j,k\}_{B'}} =&\sum_{j_{23}}\sqrt{(2k_2+1)(2\tilde{k}_2+1)}(2j_{23}+1)\begin{Bmatrix} j_2 & j_3 & j_{23}\\ k_3 & k_1 & k_2\end{Bmatrix}\begin{Bmatrix} j_2 & j_3 & j_{23}\\ k_3 & k_1 & \tilde{k}_2\end{Bmatrix}\\ =&\delta_{k_2\tilde{k}_2}\,.\end{aligned} \tag{8.3.11}$$

As Eq.(8.3.4), the unitarity requires the two $\mathcal{U}$ having same $\{j,k\}$ and for the internal labels,

$$\sum_{k_4}\mathcal{U}^{k_4,j_{14}}_{\{j,k\}_{A'}}\mathcal{U}^{k_4,\widetilde{j}_{14}}_{\{j,k\}_{A'}}=\delta_{j_{14}\widetilde{j}_{14}}\,,\qquad \sum_{k_2}\mathcal{U}^{k_2,j_{23}}_{\{j,k\}_{B'}}\mathcal{U}^{k_2,\widetilde{j}_{23}}_{\{j,k\}_{B'}}=\delta_{j_{23}\widetilde{j}_{23}}\,. \tag{8.3.12}$$

The unitary transformations $\mathcal{U}_{A'}$ and $\mathcal{U}_{B'}$ link the transition matrices $Z(squ)$ and $Z(sc)$,

$$[Z(squ)_\ell]^{\{j_i,K_i\}}{}_{\{j_i,k_i\}}=\sum_{j_{14}}\sum_{j_{23}}\mathcal{U}^{K_4,j_{14}}_{\{j,K\}_{A'}}\mathcal{U}^{K_2,j_{23}}_{\{j,K\}_{B'}}[Z(sc)_\ell]^{j_{14},j_{23},K_1,K_3}{}_{j_{14},j_{23},k_1,k_3}\mathcal{U}^{k_4,j_{14}}_{\{j,k\}_{A'}}\mathcal{U}^{k_2,j_{23}}_{\{j,k\}_{B'}}\,, \tag{8.3.13}$$

where the transition matrix for $Z(sc)$ is given by

$$\begin{aligned}[Z(sc)_\ell]^{J_{14},J_{23},K_1,K_3}{}_{j_{14},j_{23},k_1,k_3} =&(-1)^{j_{14}+j_{23}+K_1+k_1+K_3+k_3+2\ell}\begin{Bmatrix} j_{14} & k_1 & k_3\\ \ell & K_3 & K_1\end{Bmatrix}\begin{Bmatrix} j_{23} & k_1 & k_3\\ \ell & K_3 & K_1\end{Bmatrix}\\ &\times\sqrt{(2k_1+1)(2K_1+1)(2k_3+1)(2K_3+1)}\delta_{J_{14}j_{14}}\delta_{J_{23}j_{23}}\,,\end{aligned} \tag{8.3.14}$$

or explicitly, the transformation is expressed as below identity in terms of $6j$-symbols:

$$\begin{aligned}&(-1)^{\sum_{i=1}^4(j_i+k_i+K_i+\ell)}\begin{Bmatrix} j_1 & k_1 & k_4\\ \ell & K_4 & K_1\end{Bmatrix}\begin{Bmatrix} j_2 & k_2 & k_1\\ \ell & K_1 & K_2\end{Bmatrix}\begin{Bmatrix} j_3 & k_3 & k_2\\ \ell & K_2 & K_3\end{Bmatrix}\begin{Bmatrix} j_4 & k_4 & k_3\\ \ell & K_3 & K_4\end{Bmatrix}\\ =&\sum_{j_{14}}\sum_{j_{23}}(-1)^{j_{14}+j_{23}+k_1+K_1+k_3+K_3+2\ell+2k_2+2k_4-2K_2-2K_4}(2j_{14}+1)(2j_{23}+1)\begin{Bmatrix} j_1 & j_4 & j_{14}\\ K_3 & K_1 & K_4\end{Bmatrix}\\ &\times\begin{Bmatrix} j_2 & j_3 & j_{23}\\ K_3 & K_1 & K_2\end{Bmatrix}\begin{Bmatrix} j_{14} & k_1 & k_3\\ \ell & K_3 & K_1\end{Bmatrix}\begin{Bmatrix} j_{23} & k_1 & k_3\\ \ell & K_3 & K_1\end{Bmatrix}\begin{Bmatrix} j_1 & j_4 & j_{14}\\ k_3 & k_1 & k_4\end{Bmatrix}\begin{Bmatrix} j_2 & j_3 & j_{23}\\ k_3 & k_1 & k_2\end{Bmatrix}\,.\end{aligned} \tag{8.3.15}$$

This is a manifestation of Result 8.3 in the case of square graph. Following the same logic as done in triangle graph, we know that the entanglement is preserved under the coarse-graining.

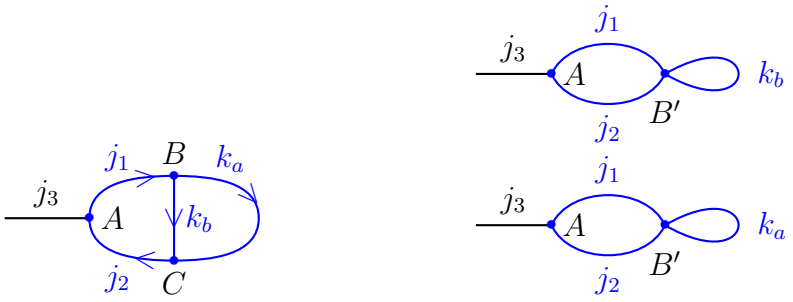

(a) Holonomy operator acts along path $j_1 \to k_a \to j_2$ or path $j_1 \to k_b \to j_2$.

(b) The coarse-grained graphs for path choices. Now the path dependency is reflected on the spin of self-loop.

Figure 8.8: The illustration for holonomy operator's path-dependency. The path-dependency can be converted to spin-dependency via coarse-graining method.

8.3.3 Path-dependency on simplest two-loop graph

This subsection considers an example that appears as a different manner. We act holonomy operator on the graph Fig.8.8a either along path $j_1 \to k_a \to j_2$ or path $j_1 \to k_b \to j_2$. We look at the bipartite entanglement between $\mathcal{H}_A$ and $\mathcal{H}_B \otimes \mathcal{H}_C$. We show the entanglement excitation's dependency on the choices of path along which the holonomy operator acts. We also study the path-dependency from coarse-grained graph, which allows us to convert the path-dependency in the case to the spin-dependency of self-loop.

For the sake of simplicity, we consider a simple spin network with spins $k_a = 1, k_b = \frac{1}{2}$ and $j_1 = j_2 = \frac{1}{2}, j_3 = 1$, and set loop holonomy spin $\ell = \frac{1}{2}$.

Look at the holonomy acting along the path $j_1 \to k_a \to j_2$. The spin network state can be labeled by spin-shifting $|j_1 j_2 K_a k_b\rangle \equiv |j_1 j_2 K_a\rangle_a$, since spin k_b is fixed as holonomy acting along the path. Note that j_1 and j_2 can not be shifted as spin-0 at the same time. The shorthand of the initial state is $|\frac{1}{2}\frac{1}{2}1\rangle_a$. Following the same way presented in Section 7.4, the truncated state of exponential evolution (up to 2nd-order) reads,

$$\begin{aligned}|\psi_a(t)\rangle =&(1-\frac{7}{18}t^2)|\frac{1}{2}\frac{1}{2}1\rangle_a + \frac{it}{2\sqrt{3}}|01\frac{1}{2}\rangle_a + \frac{it}{2\sqrt{3}}|10\frac{1}{2}\rangle_a + \frac{it}{3\sqrt{6}}|11\frac{1}{2}\rangle_a - \frac{4it}{3\sqrt{3}}|11\frac{3}{2}\rangle_a \\ &- \frac{t^2}{6\sqrt{3}}|\frac{1}{2}\frac{1}{2}0\rangle_a + \frac{\sqrt{2}t^2}{9}(|\frac{1}{2}\frac{3}{2}1\rangle_a + |\frac{3}{2}\frac{1}{2}1\rangle_a) + \frac{\sqrt{10}t^2}{36}|\frac{3}{2}\frac{3}{2}1\rangle_a - \frac{5t^2}{6\sqrt{6}}|\frac{3}{2}\frac{3}{2}2\rangle_a + O(t^3)\,.\end{aligned} \tag{8.3.16}$$

Likewise, look at the action acting along the path $j_1 \to k_b \to j_2$. The spin network state can be labeled by spin-shifting $|j_1 j_2 k_a K_b\rangle \equiv |j_1 j_2 K_b\rangle_b$, for the same reason that acting on the path does not change the spin k_a. The shorthand of the initial state is $|\frac{1}{2}\frac{1}{2}\frac{1}{2}\frac{1}{2}\rangle_b$, the truncated state of exponential evolution (up to 2nd-order) reads,

$$|\psi_b(t)\rangle = \frac{1-13t^2}{27}|\frac{1}{2}\frac{1}{2}\frac{1}{2}\frac{1}{2}\rangle_b + \frac{\sqrt{2}it}{3}|011\rangle_b + \frac{\sqrt{2}it}{3}|101\rangle_b + \frac{\sqrt{2}it}{3}|110\rangle_b + \frac{2\sqrt{2}it}{3\sqrt{3}}|111\rangle_b$$

$$-\frac{5\sqrt{5}}{54}|\frac{3}{2}\frac{3}{2}\frac{3}{2}\frac{3}{2}\rangle_b-\frac{2\sqrt{2}t^2}{27}(|\frac{1}{2}\frac{1}{2}\frac{3}{2}\frac{3}{2}\rangle_b+|\frac{1}{2}\frac{3}{2}\frac{1}{2}\frac{3}{2}\rangle_b+|\frac{3}{2}\frac{1}{2}\frac{1}{2}\frac{3}{2}\rangle_b)+\frac{2\sqrt{10}t^2}{27}(|\frac{1}{2}\frac{3}{2}\frac{3}{2}\frac{3}{2}\rangle_b$$
$$+|\frac{3}{2}\frac{1}{2}\frac{3}{2}\frac{3}{2}\rangle_b+|\frac{3}{2}\frac{3}{2}\frac{1}{2}\frac{3}{2}\rangle_b)+O(t^3)\,. \tag{8.3.17}$$

Via partial tracing over $\mathcal{H}_B\otimes\mathcal{H}_C$, it is straightforward to compute the linear entropy up to 2nd-order of t, and it is easy to see the path-dependency,

$$S_{lin}(\rho_{aA})=\frac{7t^2}{9}+O(t^3)\,, \tag{8.3.18}$$

$$S_{lin}(\rho_{bA})=\frac{26t^2}{27}+O(t^3)\,. \tag{8.3.19}$$

The linear entanglement entropy can also be derived from the coarse-grained graph as Fig.8.8b. The coarse-grained graph shows that a loopy vertex affects the transition matrix through bouquet spin recoupling at vertex B'. In this sense, the information regarding the path is coarse-grained into the information of the 4-valent vertex B', reflected on the self-loop spin attached to B'. Hence the path-dependency is translated into the spin-dependency on the self-loop. The different entanglement excitations are interpreted by different local curvature excitations carried by the loop-spin.

This chapter explores the spin entanglement coarse-graining at the kinematical level, and its entanglement evolution under the action of loop holonomy operator. To be more specific, given a graph, we study the entanglement between its subgraphs defined by a partition. Then we show that the entanglement can be exactly reflected upon the coarse-grained graph where each subgraph is represented by a loop spin network (one vertex plus some edges). In this sense, we claim that spin network entanglement is preserved under coarse-graining (via gauge-fixing), as presented in Result 8.2. Furthermore, we show that the spine network preservation holds under the action of loop holonomy operator, namely, the evolution of spin network entanglement associated with the graph can be, again, exactly reflected upon the coarse-grained graph, as presented in Result 8.4. In this sense, spin network entanglement is perfectly preserved under the coarse-graining.

Here the key is the transformation between representations of holonomy operator on the graph and the coarse-grained graph, respectively. We present it in the Result 8.3. At the technical level, we utilize the point of view of bulk-boundary map in Chapter 5, especially the content in Section 5.4.2, i.e. understanding coarse-graining as local unitary transformation for dual boundary Hilbert space. Then the coarse-graining (via gauge-fixing) plays a double-role: (1) to build the relation between the spin network states based on graph and the coarse-grained graph; (2) to build the transformation between the holonomy operators on the graph and on the coarse-grained graph. More important, the coarse-graining is a unitary transformation defined locally with respect to the dual boundary Hilbert space associated with the subgraph. Hence the conclusion is universal for any entanglement measure, according to the requirement that any entanglement measure should be invariant under local unitary transformation.

We wish to shed light on the quantum gravity degrees of freedom. The coarse-graining feature of spin network entanglement implies that the graphical degrees of freedom can be considerably reduced.

On the other hand, the coarse-graining feature emphasizes the degrees of freedom related to interfacing edges and self-loops. More precisely, the entanglement between spin sub-networks is exactly reflected in the entanglement between loopy spin sub-networks to which coarse-graining gives rise. Every loopy sub-network is made up of a single vertex plus boundary edges and self-loops (resulting from gauge-fixing). The bulk topology is reflected in the number of self-loops. Thus for spin network entanglement, the intertwiner at the single vertex encodes all the information about the sub-graph, associated with boundary spins and self-loop spins via recoupling. As already known, the spin along the self-loop reflects the loop curvature at the node. Thus, according to the coarse-graining approach, we can claim that entanglement gets reflected in the averaging curvature with respect to the subregion.

Following the coarse-graining feature of spin network entanglement, we can consider a simple situation: starting with a closed spin network and partitioning it into a bipartite system, we then ask for the maximal entanglement entropy between the subsystems. In line with our result, the entanglement entropy can be studied on the coarse-grained graph with two loopy vertices, say u and v. Then the maximal entanglement entropy has a bound, which is determined by the minor dimension of the two loopy intertwiner spaces. Say N is the number of interfacing edges, and u is the loopy vertex with the number L of

self-loops. Suppose that the intertwiner space associated with u has a minor dimension. Then the maximal entanglement entropy could be converted to a $\mathrm{U}(N + 2L)$ problem about computing dimension [173]. In particular, if one further assumes BF dynamics as considered in [44] such that the self-loops could be removed at all, then it becomes a 2-vertex model with $L = 0$ [203, 211]. In this case, it is likely to see the maximal entanglement entropy in accord with the area-entropy law at a certain limit [173].

Moreover, we extended the result in the previous chapter in some sense. We can reverse the coarse-graining approach: given a spin network where vertices typically have high valency. Then we can refine the graph by unfolding the high-valent vertices (as Fig.2.1b) such that a high-valent vertex is represented by a subgraph where all vertices are trivalent. According to the coarse-graining approach, the entanglement on a coarser spin network (typical high-valency) gets reflected in the entanglement on the finer spin network (trivalency). That is, we reverse the application of the coarse-graining approach such that we can compute the entanglement for a high-valency graph.

Furthermore, we wish this chapter shed light on non-local degrees of freedom in loop quantum gravity. Further works will investigate the various operators in loop quantum gravity, especially taking the full dynamics of loop quantum gravity into account. We want to characterize them in the sense of correlations and entanglement, i.e., whether the evolution generated by an operator is preserved under coarse-graining or not. It could help guide a deeper understanding of dynamics and formulate the precise mathematical framework for holography and renormalization flows in loop quantum gravity.

Conclusion

The studies of bulk-to-boundary relation and entanglement in the context of loop quantum gravity are the two cores of the thesis. The two cores aim at orbiting around the central topics of the field of quantum gravity, the problem of localization, and the implication of boundaries or holography. They are two interlacing issues worth to be understood deeply. The problem of localization requires that the physical operators should be defined relationally, and the implication of boundaries requires that the formulation of theory should be presented quasi-locally.

A number of topics of equal importance are involved more or less to the two: the topic of coarse-graining, which amounts to the transition from microscopic scale to macroscopic scale; the topic of the semi-classical regime, which amounts to recovering the classical continuum general relativity; the topic of emergence, which amounts to defining geometry from entanglement and correlation, or revealing diverse phenomena from complex relations and connectivity.

It is very likely to envision and prospect the exploration of quantum gravity accompanied by the development of quantum information. Indeed, this is not a new story and is still going forwards. Many works and progress have been made in the last decade. Although we are still far from achieving and understanding everything from diversity and connectivity in the sense of developing theoretical science, the endeavors are deserved and worth it. Instead of extracting knowledge from an axiomatic system, we are facing a partial theory of quantum gravity. Our principal motivation is to shed some light on what the full theory of quantum gravity should look like and which ingrained notions should be relaxed. Indeed, we are advocating a coherent approach to these interlacing topics.

The main goal of my work was two-fold: (a) to establish a quasi-local formulation for loop quantum gravity to explore holography and renormalization flows in the future; (b) to reconstruct quantum geometry in the formulation of quantum information theory to explore physical relevant operators in the context of full loop quantum gravity dynamics. We hope the work can provide some hints for further works, and uncover the physical picture of quantum gravity, reveal quantum gravity phenomenology from the point of view of emergence.

The working philosophy in this thesis was to build bulk-to-boundary relation in the formulation of quantum information theory, and vice versa, to exploit quantum information concepts on the bulk-to-boundary relation in the context of loop quantum gravity. As presented in Chapter 5, considering the potential holographic behavior of loop quantum gravity, we introduced explicit 2d boundaries to the 3d space, i.e., spacetime corners. This 2d boundary admits a Hilbert space of boundary states, understood as quantum

boundary conditions.

Then loop quantum gravity's spin network states for the bulk geometry become what we call *bulk-boundary maps*. In this perspective, spin networks are understood as maps sending bulk data to boundary Hilbert space. This resembles the categorical viewpoint: spin networks are promoted to morphisms from objects, and morphisms are promoted in a higher algebraic structure. Bulk wave-functions can be interpreted as quantum circuits acting on the boundary states. Then we define dual boundary Hilbert space by equipping the scalar product of spin network Hilbert space where spin network wave-functions (linear forms) are vectors of the dual space. The idea follows the definition of diffeomorphism invariant Hilbert space.

In some sense, bulk-to-boundary relation is a coarse-graining procedure: it makes bulk information reflected on the boundary, transmitting information but with the possibility of losing some information. Hence our work can be understood as working on coarse-graining procedures. We study two kinds of coarse-graining procedures, and both procedures reflect information in a quasi-local way reducing the graphic information of spin networks.

To be specific, let me sum up the work through the line of coarse-graining procedures.

The first coarse-graining procedure explored in the work is presented in Section 5.2. It defines by gauge-fixing bulk holonomies, reflecting bulk information on self-loops and boundary holonomies. Two remarks are presented. One is stated that: the configuration of flat holonomies is always a stationary point for the bulk probability function (Proposition 5.2). A potential meaning from the remark is that the Ponzano-Regge model could be seen as being a stationary configuration in extended topological quantum field theory. Another is stated that the coarse-graining via gauge-fixing is a unitary map with respect to dual boundary Hilbert space (Proposition 5.4), and we will exploit the remark in later chapters.

The following consequences of the coarse-graining via gauge-fixing are present in Chapter 7 and Chapter 8. In Chapter 7 we studied the unitary evolution generated by holonomy operator on an initial state given by a spin network basis state. Such an initial state has fixed spins and intertwiners, thus it is a separable state carrying no entanglement. The evolution will naturally create entanglement between the vertices of the spin network and our goal was to compute the excitation of entanglement due to the holonomy operator. The holonomy around a loop is a discretized version of gauge curvature, leading to a relation between excitations of the geometry - "quanta of curvature" - and excitations of the information -multipartite entanglement- over spin network basis states. This fits in the larger program of interpreting and reconstructing the quantum geometry of spacetime from quantum information concepts. Our main Result 7.9 was to show that the second order derivative is simply given by the dispersion of the holonomy operator, which can in turn, be computed from the probability distribution of the "closure defect" around the loop (i.e., the total spin recoupling the spins of all the edges attached to the loop).

In Chapter 8, we generalized this approach to the cases in which spin networks are partitioned into subgraphs, each comprising a multiple number of nodes. The partition defines boundaries between these subgraphs. Then we implement the procedure of coarse-graining via gauge-fixing. One main results are Result 8.2 at a purely kinematical level, stating that spin network entanglement on a graph can get reflected on its coarse-grained

graph where a loopy spin network represents each subgraph, and Result 8.4 stating that the coarse-graining approach can be generalized to the situation where the evolution is generated by loop holonomy operator, namely, the evolution of spin network entanglement still gets reflected on the coarse-grained graph. Following the logic, we are able to say that, we extended the result in Chapter 7. We can reverse the coarse-graining approach: given a spin network where vertices typically have high-valency, then we can study the entanglement on finer spin network (lower-valency) which is equivalent to the entanglement on coarser spin network (higher-valency).

Since holonomy operators are the basic building blocks of the Hamiltonian dynamics of loop quantum gravity, the two chapters gave a first hint of the dynamics of the quantum information carried by spin network states. Further exploration would be stepped into the issue of loop quantum gravity's Hamiltonian dynamics. Even though the understanding of the Hamiltonian dynamics still needs to be improved, we hope the works done here to provide an information-theoretic guide toward the complete description of dynamics. Eventually, we wish shed light on the question of the quantum gravity degrees of freedom, and understand loop quantum gravity in a holographic viewpoint, at least in the sense of quantum entanglement and correlations.

The second coarse-graining procedure studied in the thesis is presented in Chapter 6, following the perspective of the previous chapter 5. The coarse-graining procedure is defined via trace over bulk data - bulk holonomies, then obtain a density matrix for the boundary states. This boundary density matrix encodes all that we can know about the quantum state of geometry from probing the boundary if we do not have access to any bulk observable. Our main result, presented in Result 6.2, is proof that any gauge-covariant boundary density matrix can be induced from a pure spin network state whose bulk graph comprises a single vertex and a single loop. In quantum information, this universal reconstruction process purifies arbitrary mixed boundary states into pure bulk states. Since such a boundary density matrix can correspond to various bulk states, a relevant question to the non-uniqueness of purification is whether different bulk states could be seen as physically equivalent under to-be-determined gauge transformations.

From a quantum information-theoretic perspective, this bulk-to-boundary coarse-graining via tracing-bulk defines a quantum reference frame à la SU(2)-twirling operation and obtains a SU(2)-invariant density matrix, which is, typically, a mixed state because of randomization over unitary transformations. We can envisage, similar to what is done in chapter 8, that the spin sub-networks subordinated to a certain entire spin network can be coarse-grained via tracing-bulk, respectively. It defines a coarse-grained graph, and there is no self-loop associated with coarse-grained vertices. In some sense, the coarse-grained graph now presents as a network with respect to quantum reference frames, and we hope this picture can clarify the notion of reference frames from a quantum view.

Furthermore, a more ambitious hope is to tackle the spin network dynamics and reformulate it in light of the bulk-boundary relation. This means projecting the bulk dynamics onto the boundary and expressing evolution in terms of boundary evolution operators. Loop quantum gravity's boundary dynamics would then read in terms of completely positive maps (CP map), admitting an operator-sum representation in terms of Kraus operators $\{E_k,\, k = 1, 2, \cdots\}$, which leave invariant the trace of quantum states. We wish

to describe boundary evolution and measurements in loop quantum gravity in terms of CPTP maps, taking Kraus operators as representations for boundary dynamics.

Through all, the further goal is to investigate in depth the implementation of the holographic principle in loop quantum gravity in the context of full loop quantum gravity dynamics and move forward in the study of the coarse-graining procedures of the theory and its renormalization flows from the Planck scale to the macroscopic scale. Moreover, exploring the complete set of physical operators that can be reconstructed from the boundary is meaningful. Applying quantum information theory will likely be beneficial in developing and establishing the operator-reconstruction program.

Although we have reached the end of my thesis, there are still plenty of work to be done regarding the work I have presented here: the relation between boundary entanglement and bulk entanglement, the consistency between various proposals of Hamiltonian constraint operator, the ability of reconstruction from the boundary, the quantum operational boundary dynamics, the topological entanglement in loop quantum gravity or spin foam, the entanglement in Newtonian gravity and general relativity, etc. It is still a long journey of mathematics, physics, and excitement.

Appendix A

Examples of entanglement evolution

A.1 Time-dependent Bell state

Let $|\Psi(t)\rangle = \cos t|00\rangle + \sin t|11\rangle$. The Hermitian operator in the case has matrix representation $\widehat{H} = \begin{pmatrix} 0 & -\mathrm{i} \\ \mathrm{i} & 0 \end{pmatrix}$ with respect to basis $\{|00\rangle, |11\rangle\}$. This bipartite state initiates with the unentangled state $|00\rangle$. Within $t \in [0, \pi/4)$, the $|\Phi(t)\rangle$ is chosen as $|00\rangle$, while within $t \in (\pi/4, 3\pi/4)$, the $|\Phi(t)\rangle$ is chosen as $|11\rangle$. At the instant $t = \pi/4$, there is ambiguity to define the unique $|\Phi(t)\rangle$. Also, the $|\Phi(t)\rangle$ is discontinuous at $t = \pi/4$. However, the maximal projection $|\langle\Phi(t)|\Psi(t)\rangle|^2$ is still differentiable along $t \to s+$ and $t \to s-$ where $s+$ stands for approaching from $t > s$ and $s-$ for approaching from $t < s$ (the left and right derivative could be different).

A.2 Black hole evaporation toy model

We give another simple example whose maximal projection $|\langle\Phi(t)|\Psi(t)\rangle|^2$ is also differentiable. Consider a two particles system with the Hamiltonian $\widehat{H} = \mathrm{i}(a^\dagger b^\dagger - ab)$. Choosing the initial state to be the unentangled vacuum state $|0\rangle_A \otimes |0\rangle_B$, the evolution produces the entangled quantum state:

$$|\Psi(t)\rangle = \frac{1}{\cosh t} \sum_{n=0}^{\infty} \tanh^n t |n\rangle_A \otimes |n\rangle_B \,. \tag{A.1}$$

The Schmidt eigenvalues are labelled by an interger n and read $\lambda_n = \tanh^{2n} t / \cosh^2 t$. The bipartite entanglement entropy as a function of the time t is given by:

$$S(t) = \ln \cosh^2 t - \sinh^2 t \ln \tanh^2 t \,, \qquad \text{with} \quad \lim_{t\to 0} \frac{\mathrm{d}S(t)}{\mathrm{d}t} = 0 \,, \quad \lim_{t\to 0} \frac{\mathrm{d}^2 S(t)}{\mathrm{d}t^2} \to \infty \,. \tag{A.2}$$

This entropy evolution function grows asymptotically linearly as $2t$. However, the maximal Schmidt eigenvalue is always given by the 0-mode, for the number of quanta $n = 0$, since $|\tanh^2 t| < 1$, so that the separable projection is constant, $|\Phi(t)\rangle = |0\rangle_A \otimes |0\rangle_B$ for

all times t. Then the maximal Schmidt eigenvalue $\lambda_{\max}(t) = \lambda_0 = 1/\cosh^2 t$ is smooth and gives the geometric measure of entanglement.

Appendix B

Proof of Proposition 5.2

The proof of Proposition 5.2 is outlined as follows.

Proof. To show $\mathcal{P}_{GF}(G_1,..,G_L)$ stationary at flat SU(2) connection amounts to

$$\begin{aligned}&\forall\, i=1,\cdots,L\ :\\ &\mathcal{P}_{GF}(G_1,\cdots,\vec{J}G_i,\cdots,G_L)|_{G_1=\cdots=G_L=\mathbb{I}}=\mathcal{P}_{GF}(G_1,\cdots,G_i\vec{J},\cdots,G_L)|_{G_1=\cdots=G_L=\mathbb{I}}=0\,,\end{aligned} \tag{B.1}$$

where $\vec{J}$ are arbitrary left/right (depending on position relative to G_i) invariant vector with form $\vec{J}=J_a\cdot v_a$ with some basis $J_a\in\mathfrak{su}(2)$ and 3d-vector $v_a\in\mathbb{R}^3$, which is an analogy to directional derivative in calculus. Let us look at G_i separately now, for the first order derivative on G_i, we consider function

$$\mathcal{P}_{G_iF}(G_i)\equiv\mathcal{P}_{GF}(\mathbb{I},\cdots,G_i,\cdots,\mathbb{I})\,. \tag{B.2}$$

As (5.2.12), it inherits $\mathcal{P}_{G_iF}(G_i)=\mathcal{P}_{G_iF}(h\,G_i\,h^{-1})\,,\ \forall\, h\in\mathrm{SU}(2)$, implying that $\mathcal{P}_{G_iF}(G_i)$ can be written as a Fourier series of SU(2) class functions $\chi_j(G)$:

$$\mathcal{P}_{G_iF}(G_i)=\sum_{j\in\frac{\mathbb{N}}{2}}F_j\,\chi_j(G_i)\,. \tag{B.3}$$

This can be shown more explicitly: consider kernel $\delta(g)$ acting on $\mathcal{P}_{G_iF}(G_i)$ and insert $\delta(g)=\sum_j(2j+1)\chi_j(g)$ into it, thus we have

$$\begin{aligned}\mathcal{P}_{G_iF}(G_i)&=\int_{\mathrm{SU}(2)}\sum_{j\in\frac{\mathbb{N}}{2}}(2j+1)\,\chi_j(g)\,\mathcal{P}_{G_iF}(G_i\,g)\,\mathrm{d}g &\text{(B.4)}\\ &=\sum_{j\in\frac{\mathbb{N}}{2}}(2j+1)\int_{\mathrm{SU}(2)}\chi_j(G_i^{-1}\,g)\,\mathcal{P}_{G_iF}(g)\,\mathrm{d}g &\text{(B.5)}\\ &=\sum_{j\in\frac{\mathbb{N}}{2}}(2j+1)\,D^j_{mn}(G_i^{-1})\underbrace{\int_{\mathrm{SU}(2)}D^j_{nm}(g)\,\mathcal{P}_{G_iF}(g)\,\mathrm{d}g}_{\equiv F_{jnm}} &\text{(B.6)}\end{aligned}$$

$$= \sum_{j\in\frac{\mathbb{N}}{2}} (2j+1)\, D^j_{mn}(G_i^{-1})\, F_{jnm}\,, \tag{B.7}$$

where the second equal sign uses invariant property of Haar measure, and the third breaks down the trace of $G_i^{-1}\, g$ into matrices multiplication. Since $\mathcal{P}_{G_iF}(G_i) = \mathcal{P}_{G_iF}(h\, G_i\, h^{-1})$ for every $h \in \mathrm{SU}(2)$, consider

$$\mathcal{P}_{G_iF}(G_i) = \int_{\mathrm{SU}(2)} \mathcal{P}_{G_iF}(h\, G_i\, h^{-1})\, \mathrm{d}h \tag{B.8}$$

$$= \sum_{j\in\frac{\mathbb{N}}{2}} (2j+1)\, F_{jnm} \int_{\mathrm{SU}(2)} D^j_{mm'}(h)\, D^j_{m'n'}(G_i^{-1})\, D^j_{n'n}(h^{-1})\, \mathrm{d}h \tag{B.9}$$

$$= \sum_{j\in\frac{\mathbb{N}}{2}} \underbrace{\left(\sum_{m=-j}^{j} F_{jmm}\right)}_{\equiv F_j} \chi_j(G_i^{-1}) = \sum_{j\in\frac{\mathbb{N}}{2}} F_j\, \chi_j(G_i)\,, \tag{B.10}$$

where the first equal sign uses the property of normalized Haar measure, and from second to third equal sign we employ Peter-Weyl theorem for Wigner D-matrices. Finally, since $\mathcal{P}_{G_iF}(G_i)$ has been decomposed in terms of $\chi_j(G_i)$, it is straightforwards to check below derivatives to complete the proof:

$$\chi_j(\vec{J}\, G_i)|_{G_i=\mathbb{I}} = \chi_j(G_i \vec{J})|_{G_i=\mathbb{I}} = 0\,. \tag{B.11}$$

□

Appendix C

Proof of Result 8.3

The proof is outlined by Fig.8.4 and Fig.8.5.

Proof. The transition matrix Z Eq.(7.1.8) can be computed from the type of graph $\Gamma = W \sqcup \mathcal{E}^\partial$ where $\mathcal{E}^\partial = \partial\Gamma$ is the set of p boundary edges $\{e_1^\partial, \cdots, e_p^\partial\}$, and $\Gamma^o = W$. Let us consider the simplest case $n = 2$. The proof is straightforward to generalize to arbitrary n. Suppose bipartition $\Gamma = \Gamma_1 \sqcup \Gamma_2$,

$$\Gamma_1 = T_1 \sqcup \{e_1^\partial, \cdots, e_q^\partial, e_p^{(1)}, e_q^{(1)}\}\,, \qquad \Gamma_2 = T_2 \sqcup \{e_{q+1}^\partial, \cdots, e_p^\partial, e_p^{(2)}, e_q^{(2)}\}\,. \tag{C.1}$$

where $e_p^{(1)}$, $e_q^{(1)}$, $e_p^{(2)}$, $e_q^{(2)}$ are due to the partition that splits edges e_p and e_q with $e_p = e_p^{(1)} \sqcup e_p^{(2)}$ and $e_q = e_q^{(1)} \sqcup e_q^{(2)}$. The bulks of Γ_1 and Γ_2 are $\Gamma_1^o = T_1[v_1 \overset{e_1}{\to} \cdots \overset{e_{q-2}}{\to} v_{q-1} \overset{e_{q-1}}{\to} v_q]$ and $\Gamma_2^o = T_2[v_{q+1} \overset{e_{q+1}}{\to} \cdots \overset{e_{p-2}}{\to} v_{p-1} \overset{e_{p-1}}{\to} v_p]$, respectively. In particular, $W_1 = T_1 \sqcup \{e_p^{(1)}, e_q^{(1)}\}$ and $W_2 = T_2 \sqcup \{e_p^{(2)}, e_q^{(2)}\}$ so $W = W_1 \sqcup W_2$. An example is illustrated by Fig.8.3. We start by noticing

$$\begin{aligned}
&\Big[Z(\Gamma)_{\chi_\ell \triangleright W}\Big]^{\{J_\alpha, K_\alpha\}}_{\{j_\alpha, k_\alpha\}} \\
&= \int \prod_{e\in W} \mathrm{d}g_e \, {}_\partial\langle \Psi_{\partial\Gamma,\{J_\alpha,K_\alpha\}}(\{g_e\}_{e\in W}) | \chi_\ell(G_W) | \Psi_{\partial\Gamma,\{j_\alpha,k_\alpha\}}(\{g_e\}_{e\in W})\rangle_\partial \qquad \text{(C.2)} \\
&= \int \prod_{e\in W\setminus(T_1\sqcup T_2)} \mathrm{d}h_e \, {}_\partial\langle \Psi_{\partial\Gamma,\{J_\alpha,K_\alpha\}}(\{h_e\}_{e\in W\setminus(T_1\sqcup T_2)}, \{\mathbb{I}\}_{e\in T_1\sqcup T_2}) | \chi_\ell(G_W) \\
&\qquad\qquad |\Psi_{\partial\Gamma,\{j_\alpha,k_\alpha\}}(\{h_e\}_{e\in W\setminus(T_1\sqcup T_2)}, \{\mathbb{I}\}_{e\in T_1\sqcup T_2})\rangle_\partial\,. \qquad \text{(C.3)}
\end{aligned}$$

Let us break down this step: we start from Eq.(7.1.5). Recall Eq.(8.1.15), we can express the bulk-boundary map $|\Psi_{\partial\Gamma,\{j_\alpha,k_\alpha\}}(\{g_e\}_{e\in W})\rangle$ in terms of 'gluing operation' $\bowtie$ for bulk-boundary maps $|\Psi_{\partial\Gamma_1,\{j_\alpha^{(1)},k_\alpha^{(1)}\}}(\{g_{e'}\}_{e'\in T_1})\rangle$ and $|\Psi_{\partial\Gamma_2,\{j_\alpha^{(2)},k_\alpha^{(2)}\}}(\{g_{e''}\}_{e''\in T_2})\rangle$. We then gauge-fix the two bulk-boundary maps such that the holonomies along T_1 and T_2 are gauge-fixed to $\mathbb{I}$ in line with Eq.(5.2.3), i.e.,

$$|\Psi_{\partial\Gamma,\{j_\alpha,k_\alpha\}}(\{g_e\}_{e\in W})\rangle$$

$$
\begin{aligned}
&= \left[h_{e_p^{(1)}} \otimes h_{e_q^{(1)}} \otimes \left(\bigotimes_{e' \in \partial\Gamma_1 \setminus (e_p^{(1)} \sqcup e_q^{(1)})} h_{v(e')}^{\epsilon_{e'}^{v}} \right) |\Psi_{\partial\Gamma_1, \{j_\alpha^{(1)}, k_\alpha^{(1)}\}}(\{\mathbb{I}\}_{e' \in T_1})\rangle \right] \\
&\quad \curlyvee \left[h_{e_p^{(2)}} \otimes h_{e_q^{(2)}} \otimes \left(\bigotimes_{e'' \in \partial\Gamma_2 \setminus (e_p^{(2)} \sqcup e_q^{(2)})} h_{v(e'')}^{\epsilon_{e''}^{v}} \right) |\Psi_{\partial\Gamma_2, \{j_\alpha^{(2)}, k_\alpha^{(2)}\}}(\{\mathbb{I}\}_{e'' \in T_2})\rangle \right] \qquad \text{(C.4)} \\
&= \left(\bigotimes_{e \in \partial\Gamma} h_{v(e)}^{\epsilon_e^{v}} \right) |\Psi_{\partial\Gamma, \{j_\alpha, k_\alpha\}}(\{h_e\}_{e \in W \setminus (T_1 \sqcup T_2)}, \{\mathbb{I}\}_{e \in T_1 \sqcup T_2})\rangle \,. \qquad \text{(C.5)}
\end{aligned}
$$

The advantage with the gauge-fixing is that the action of loop holonomy operator is only nontrivial along piecewise edges $e_p^{(1)}$, $e_q^{(1)}$, $e_q^{(2)}$, $e_p^{(2)}$ (interfacing edges between Γ_1 and Γ_2), and is trivial along other piecewise edges. Notably, gauge-fixing does not change the loop holonomy, i.e.,

$$
G_W = h_{e_p^{(2)}} \cdot h_{e_q^{(2)}} \cdot h_{e_q^{(1)}} \cdot h_{e_p^{(1)}} = G_{W_{(R)}} \,. \qquad \text{(C.6)}
$$

We put Eq.(C.5) back to the Eq.(C.2), and note that the boundary holonomies are erased by the scalar product '$_\partial\langle \ | \ \rangle_\partial$' for $\mathcal{H}_{\partial\Gamma}$ due to $h^\dagger h = \mathbb{I}$, while the holonomies $h_{e_p^{(1)}}$, $h_{e_p^{(2)}}$, $h_{e_q^{(1)}}$, $h_{e_q^{(2)}}$ are not erased by the '$_\partial\langle \ | \ \rangle_\partial$'.

To handle Eq.(C.4), we follow the spirit of Eq.(5.4.10). We glue boundary edges along the T_1 and T_2. The resulting intertwiners allow for decomposition:

$$
\begin{aligned}
|\Psi_{\partial\Gamma_1, \{j_\alpha^{(1)}, k_\alpha^{(1)}\}}(\{\mathbb{I}\}_{e' \in T_1})\rangle &= \sum_{I_{u_1}^o} \left[\mathcal{U}_{\Upsilon_1}^{\{j_\alpha^{(1)}, k_\alpha^{\partial(1)}\}} \right]^{I_{u_1}^o}{}_{\{k_\alpha^{o(1)}\}} |\Psi_{\partial\Upsilon_1, I_{u_1}}\rangle \,, \\
|\Psi_{\partial\Gamma_2, \{j_\alpha^{(2)}, k_\alpha^{(2)}\}}(\{\mathbb{I}\}_{e'' \in T_2})\rangle &= \sum_{I_{u_2}^o} \left[\mathcal{U}_{\Upsilon_2}^{\{j_\alpha^{(2)}, k_\alpha^{\partial(2)}\}} \right]^{I_{u_2}^o}{}_{\{k_\alpha^{o(2)}\}} |\Psi_{\partial\Upsilon_2, I_{u_2}}\rangle \,.
\end{aligned} \qquad \text{(C.7)}
$$

Here the Υ_1 and Υ_2 are coarse-grained graphs of respect Γ_1 and Γ_2. With Eq.(C.7), the boundary state in Eq.(C.5) is rewritten as:

$$
\begin{aligned}
&|\Psi_{\partial\Gamma, \{j_\alpha, k_\alpha\}}(\{h_e\}_{e \in W \setminus (T_1 \sqcup T_2)}, \{\mathbb{I}\}_{e \in T_1 \sqcup T_2})\rangle \\
&= \left[h_{e_p^{(1)}} \otimes h_{e_q^{(1)}} \otimes \sum_{I_{u_1}^o} \left[\mathcal{U}_{\Upsilon_1}^{\{j_\alpha^{(1)}, k_\alpha^{\partial(1)}\}} \right]^{I_{u_1}^o}{}_{\{k_\alpha^{o(1)}\}} |\Psi_{\partial\Upsilon_1, I_{u_1}}\rangle \right] \\
&\quad \curlyvee \left[h_{e_p^{(2)}} \otimes h_{e_q^{(2)}} \otimes \sum_{I_{u_2}^o} \left[\mathcal{U}_{\Upsilon_2}^{\{j_\alpha^{(2)}, k_\alpha^{\partial(2)}\}} \right]^{I_{u_2}^o}{}_{\{k_\alpha^{o(2)}\}} |\Psi_{\partial\Upsilon_2, I_{u_2}}\rangle \right] .
\end{aligned} \qquad \text{(C.8)}
$$

We put Eq.(C.8) back to Eq.(C.3), obtaining the transition matrix along $W_{(R)}$,

$$
\int \left[(h_{e_p^{(1)}} \otimes h_{e_q^{(1)}}) \triangleright |\Psi_{\partial\Upsilon_1, \widetilde{I}_{u_1}}\rangle \curlyvee (h_{e_p^{(2)}} \otimes h_{e_q^{(2)}}) \triangleright |\Psi_{\partial\Upsilon_2, \widetilde{I}_{u_2}}\rangle \right]^\dagger \chi_\ell(h_{e_p^{(2)}} \cdot h_{e_q^{(2)}} \cdot h_{e_q^{(1)}} \cdot h_{e_p^{(1)}})
$$

$$\left[(h_{e_p^{(1)}}\otimes h_{e_q^{(1)}})\triangleright|\Psi_{\partial\Upsilon_1,I_{u_1}}\rangle\bigcirc\!\!\!\!\!\!\backslash\,(h_{e_p^{(2)}}\otimes h_{e_q^{(2)}})\triangleright|\Psi_{\partial\Upsilon_2,I_{u_2}}\rangle\right]\mathrm{d}h_{e_p^{(1)}}\mathrm{d}h_{e_q^{(1)}}\mathrm{d}h_{e_p^{(2)}}\mathrm{d}h_{e_q^{(2)}}$$

$$= \int\prod_{e\in W_{(R)}}\mathrm{d}g_e\,{}_\partial\langle\Psi_{\partial\Gamma_{(R)},\{\widetilde{I}_u\}}(\{g_e\}_{e\in W_{(R)}})|\chi_\ell(G_{W_{(R)}})|\Psi_{\partial\Gamma_{(R)},\{I_u\}}(\{g_e\}_{e\in W_{(R)}})\rangle_\partial$$

$$= \Big[Z(\Gamma_{(R)})_{\chi_\ell\triangleright W_{(R)}}\Big]^{\{\widetilde{I}_u\}}_{\{I_u\}}\prod_{\alpha=1}^{p}\delta_{J_\alpha j_\alpha}\,. \tag{C.9}$$

Here $I_{u_i}=\{j_\alpha^{(i)},k_\alpha^{\partial(i)}\}\cup I^o_{u_i}$ and $\widetilde{I}_{u_i}=\{J_\alpha^{(i)},K_\alpha^{\partial(i)}\}\cup\widetilde{I}^o_{u_i}$. The $\delta_{J_\alpha j_\alpha}$ is imposed by scalar product '${}_\partial\langle\ |\ \rangle_\partial$'. So Eq.(C.9) actually represents the transition matrix on the coarse-grained graph $\Gamma_{(R)}$. Therefore, Eq.(C.3) leads to the transformation for particular case $n=2$,

$$\Big[Z(\Gamma)_{\chi_\ell\triangleright W}\Big]^{\{J_\alpha,K_\alpha\}}_{\{j_\alpha,k_\alpha\}}$$

$$= \sum_{\{I^{(o)}_{u_i}\}}\sum_{\{\widetilde{I}^{(o)}_{u_i}\}}\overline{\Big[\mathcal{U}_{\Upsilon_1}^{\{J_\alpha^{(1)},K_\alpha^{\partial(1)}\}}\Big]^{\widetilde{I}^o_{u_1}}_{\{K_\alpha^{o(1)}\}}\Big[\mathcal{U}_{\Upsilon_2}^{\{J_\alpha^{(2)},K_\alpha^{\partial(2)}\}}\Big]^{\widetilde{I}^o_{u_2}}_{\{K_\alpha^{o(2)}\}}}\Big[Z(\Gamma_{(R)})_{\chi_\ell\triangleright W_{(R)}}\Big]^{\{\widetilde{I}_{u_i}\}}_{\{I_{u_i}\}}$$

$$\Big[\mathcal{U}_{\Upsilon_1}^{\{j_\alpha^{(1)},k_\alpha^{\partial(1)}\}}\Big]^{I^o_{u_1}}_{\{k_\alpha^{o(1)}\}}\Big[\mathcal{U}_{\Upsilon_2}^{\{j_\alpha^{(2)},k_\alpha^{\partial(2)}\}}\Big]^{I^o_{u_2}}_{\{k_\alpha^{o(2)}\}}\prod_{\alpha=1}^{p}\delta_{J_\alpha j_\alpha}\,. \tag{C.10}$$

□

Bibliography

[1] S. Weinberg, *The Quantum theory of fields. Vol. 1: Foundations*. Cambridge University Press, 2005.

[2] L. Diósi, "Gravitation and quantummechanical localization of macroobjects," Phys. Lett. A **105** (1984) 199–202, arXiv:1412.0201.

[3] R. Penrose, "On gravity's role in quantum state reduction," Gen. Rel. Grav. **28** (1996) 581–600.

[4] L. Diósi, "Nonlinear Schrödinger equation in foundations: summary of 4 catches," J. Phys. Conf. Ser. **701** (2016), no. 1, 012019, arXiv:1602.03772.

[5] R. Ligez, R. B. MacKenzie, V. Massart, M. B. Paranjape, and U. A. Yajnik, "What is the Gravitational Field of a Mass in a Spatially Nonlocal Quantum Superposition?," arXiv:2110.13866.

[6] C. Rovelli and F. Vidotto, *Covariant Loop Quantum Gravity: An Elementary Introduction to Quantum Gravity and Spinfoam Theory*. Cambridge Monographs on Mathematical Physics. Cambridge University Press, 11, 2014.

[7] S. Carlip, "Quantum gravity: A Progress report," Rept. Prog. Phys. **64** (2001) 885, arXiv:gr-qc/0108040.

[8] G. Esposito, "An Introduction to quantum gravity," in *Section 6.7.17 of the EOLSS Encyclopedia by UNESCO*. 2011. arXiv:1108.3269.

[9] J. Polchinski, *String theory. Vol. 1: An introduction to the bosonic string*. Cambridge Monographs on Mathematical Physics. Cambridge University Press, 2007.

[10] J. Polchinski, *String theory. Vol. 2: Superstring theory and beyond*. Cambridge Monographs on Mathematical Physics. Cambridge University Press, 2007.

[11] D. Tong, "String Theory," arXiv:0908.0333.

[12] A. Ashtekar and J. Lewandowski, "Background independent quantum gravity: A Status report," Class. Quant. Grav. **21** (2004) R53, arXiv:gr-qc/0404018.

[13] M. Han, W. Huang, and Y. Ma, "Fundamental structure of loop quantum gravity," Int. J. Mod. Phys. D **16** (2007) 1397–1474, arXiv:gr-qc/0509064.

[14] T. Thiemann, *Modern canonical quantum general relativity.* Cambridge University Press, 2008.

[15] P. Dona and S. Speziale, "Introductory lectures to loop quantum gravity," in *Gravitation Théorie et Expérience.Proceedings, Troisième école de physique théorique de Jijel: Jijel, Algeria, September 26–October 03, 2009*, pp. 89–140. 2013. arXiv:1007.0402.

[16] C. Rovelli, "Zakopane lectures on loop gravity," PoS **QGQGS2011** (2011) 003, arXiv:1102.3660.

[17] A. Ashtekar and E. Bianchi, "A short review of loop quantum gravity," Rept. Prog. Phys. **84** (2021), no. 4, 042001, arXiv:2104.04394.

[18] M. P. Reisenberger and C. Rovelli, "'Sum over surfaces' form of loop quantum gravity," Phys. Rev. D **56** (1997) 3490–3508, arXiv:gr-qc/9612035.

[19] J. C. Baez, "Spin foam models," Class. Quant. Grav. **15** (1998) 1827–1858, arXiv:gr-qc/9709052.

[20] L. Freidel and K. Krasnov, "Spin foam models and the classical action principle," Adv. Theor. Math. Phys. **2** (1999) 1183–1247, arXiv:hep-th/9807092.

[21] D. Oriti, "Spin foam models of quantum space-time," other thesis, 11, 2003.

[22] A. Perez, "Spin foam models for quantum gravity," Class. Quant. Grav. **20** (2003) R43, arXiv:gr-qc/0301113.

[23] E. R. Livine, *The Spinfoam Framework for Quantum Gravity.* PhD thesis, Lyon, IPN, 2010. arXiv:1101.5061.

[24] M. Dupuis, *Spin Foam Models for Quantum Gravity and semi-classical limit.* PhD thesis, Lyon, Ecole Normale Superieure, 2010. arXiv:1104.2765.

[25] A. Perez, "The Spin Foam Approach to Quantum Gravity," Living Rev. Rel. **16** (2013) 3, arXiv:1205.2019.

[26] M. Assanioussi, *New dynamics for canonical loop quantum gravity.* PhD thesis, Warsaw U., 2017.

[27] I. Mäkinen, *Dynamics in canonical models of loop quantum gravity.* PhD thesis, Warsaw U., 2019. arXiv:1910.00469.

[28] R. De Pietri, L. Freidel, K. Krasnov, and C. Rovelli, "Barrett-Crane model from a Boulatov-Ooguri field theory over a homogeneous space," Nucl. Phys. B **574** (2000) 785–806, arXiv:hep-th/9907154.

[29] L. Freidel, "Group field theory: An Overview," Int. J. Theor. Phys. **44** (2005) 1769–1783, arXiv:hep-th/0505016.

[30] D. Oriti, "The Group field theory approach to quantum gravity," arXiv:gr-qc/0607032.

[31] S. Carrozza, *Tensorial methods and renormalization in Group Field Theories*. PhD thesis, Orsay, LPT, 2013. arXiv:1310.3736.

[32] D. Oriti, "Group Field Theory and Loop Quantum Gravity," 8, 2014. arXiv:1408.7112.

[33] D. Oriti, J. P. Ryan, and J. Thürigen, "Group field theories for all loop quantum gravity," New J. Phys. **17** (2015), no. 2, 023042, arXiv:1409.3150.

[34] D. Oriti, "The microscopic dynamics of quantum space as a group field theory," in *Foundations of Space and Time: Reflections on Quantum Gravity*, pp. 257–320. 10, 2011. arXiv:1110.5606.

[35] C. Rovelli, "Relational quantum mechanics," Int. J. Theor. Phys. **35** (1996) 1637–1678, arXiv:quant-ph/9609002.

[36] C. Rovelli, "The Relational Interpretation of Quantum Physics," arXiv:2109.09170.

[37] J. Eisert, M. Cramer, and M. B. Plenio, "Area laws for the entanglement entropy - a review," Rev. Mod. Phys. **82** (2010) 277–306, arXiv:0808.3773.

[38] E. R. Livine and D. R. Terno, "Reconstructing quantum geometry from quantum information: Area renormalisation, coarse-graining and entanglement on spin networks," arXiv:gr-qc/0603008.

[39] B. Dittrich, F. Hellmann, and W. Kaminski, "Holonomy Spin Foam Models: Boundary Hilbert spaces and Time Evolution Operators," Class. Quant. Grav. **30** (2013) 085005, arXiv:1209.4539.

[40] E. R. Livine, "Deformation Operators of Spin Networks and Coarse-Graining," Class. Quant. Grav. **31** (2014) 075004, arXiv:1310.3362.

[41] B. Dittrich, M. Martín-Benito, and E. Schnetter, "Coarse graining of spin net models: dynamics of intertwiners," New J. Phys. **15** (2013) 103004, arXiv:1306.2987.

[42] B. Dittrich and S. Steinhaus, "Time evolution as refining, coarse graining and entangling," New J. Phys. **16** (2014) 123041, arXiv:1311.7565.

[43] C. Charles and E. R. Livine, "The Fock Space of Loopy Spin Networks for Quantum Gravity," Gen. Rel. Grav. **48** (2016), no. 8, 113, arXiv:1603.01117.

[44] E. R. Livine, "From Coarse-Graining to Holography in Loop Quantum Gravity," EPL **123** (2018), no. 1, 10001, arXiv:1704.04067.

[45] W. Donnelly and L. Freidel, "Local subsystems in gauge theory and gravity," JHEP **09** (2016) 102, arXiv:1601.04744.

[46] L. Freidel, E. R. Livine, and D. Pranzetti, "Gravitational edge modes: from Kac-Moody charges to Poincaré networks," Class. Quant. Grav. **36** (2019), no. 19, 195014, arXiv:1906.07876.

[47] L. Freidel, M. Geiller, and D. Pranzetti, "Edge modes of gravity. Part I. Corner potentials and charges," JHEP **11** (2020) 026, arXiv:2006.12527.

[48] L. Freidel, M. Geiller, and D. Pranzetti, "Edge modes of gravity. Part II. Corner metric and Lorentz charges," JHEP **11** (2020) 027, arXiv:2007.03563.

[49] L. Freidel, M. Geiller, and D. Pranzetti, "Edge modes of gravity. Part III. Corner simplicity constraints," JHEP **01** (2021) 100, arXiv:2007.12635.

[50] D. Oriti, "Disappearance and emergence of space and time in quantum gravity," Stud. Hist. Phil. Sci. B **46** (2014) 186–199, arXiv:1302.2849.

[51] P. W. Anderson, "More Is Different," Science **177** (1972), no. 4047, 393–396.

[52] Q. Chen and E. R. Livine, "Loop quantum gravity's boundary maps," Class. Quant. Grav. **38** (2021), no. 15, 155019, arXiv:2103.08409.

[53] Q. Chen and E. R. Livine, "Intertwiner Entanglement Excitation and Holonomy Operator," arXiv:2204.03093.

[54] Q. Chen, "Spin network entanglement: coarse-graining," arXiv:2205.11205.

[55] R. M. Wald, *General Relativity*. Chicago Univ. Pr., Chicago, USA, 1984.

[56] G. W. Gibbons and S. W. Hawking, "Action Integrals and Partition Functions in Quantum Gravity," Phys. Rev. **D15** (1977) 2752–2756.

[57] J. York, "Boundary terms in the action principles of general relativity," Found. Phys. **16** (1986) 249–257.

[58] A. Perez and C. Rovelli, "Physical effects of the Immirzi parameter," Phys. Rev. D **73** (2006) 044013, arXiv:gr-qc/0505081.

[59] L. Freidel and A. Starodubtsev, "Quantum gravity in terms of topological observables," arXiv:hep-th/0501191.

[60] L. Freidel, D. Minic, and T. Takeuchi, "Quantum gravity, torsion, parity violation and all that," Phys. Rev. D **72** (2005) 104002, arXiv:hep-th/0507253.

[61] S. Mercuri, "Fermions in Ashtekar-Barbero connections formalism for arbitrary values of the Immirzi parameter," Phys. Rev. D **73** (2006) 084016, arXiv:gr-qc/0601013.

[62] G. Hayward, "Gravitational action for space-times with nonsmooth boundaries," Phys. Rev. D **47** (1993) 3275–3280.

[63] D. Brill and G. Hayward, "Is the gravitational action additive?," Phys. Rev. D **50** (1994) 4914–4919, arXiv:gr-qc/9403018.

[64] L. Lehner, R. C. Myers, E. Poisson, and R. D. Sorkin, "Gravitational action with null boundaries," Phys. Rev. D **94** (2016), no. 8, 084046, arXiv:1609.00207.

[65] L. B. Szabados, "Quasi-Local Energy-Momentum and Angular Momentum in General Relativity," Living Rev. Rel. **12** (2009) 4.

[66] J. D. Brown and J. W. York, Jr., "Quasilocal energy and conserved charges derived from the gravitational action," Phys. Rev. **D47** (1993) 1407–1419, arXiv:gr-qc/9209012.

[67] I. S. Booth and R. B. Mann, "Moving observers, nonorthogonal boundaries, and quasilocal energy," Phys. Rev. D **59** (1999) 064021, arXiv:gr-qc/9810009.

[68] G. Odak and S. Speziale, "Brown-York charges with mixed boundary conditions," JHEP **11** (2021) 224, arXiv:2109.02883.

[69] J. Baez and J. P. Muniain, *Gauge fields, knots and gravity*. 1995.

[70] S. Holst, "Barbero's Hamiltonian derived from a generalized Hilbert-Palatini action," Phys. Rev. D **53** (1996) 5966–5969, arXiv:gr-qc/9511026.

[71] S. W. Hawking and G. T. Horowitz, "The Gravitational Hamiltonian, action, entropy and surface terms," Class. Quant. Grav. **13** (1996) 1487–1498, arXiv:gr-qc/9501014.

[72] E. Poisson, *A Relativist's Toolkit: The Mathematics of Black-Hole Mechanics*. Cambridge University Press, 12, 2009.

[73] P. Dirac, *Lectures on Quantum Mechanics*. Belfer Graduate School of Science. Monographs series.

[74] M. Henneaux and C. Teitelboim, *Quantization of gauge systems*. 1992.

[75] A. Ashtekar, "New Variables for Classical and Quantum Gravity," Phys. Rev. Lett. **57** (1986) 2244–2247.

[76] D. Lovelock, "The Einstein tensor and its generalizations," J. Math. Phys. **12** (1971) 498–501.

[77] M. Crisostomi, K. Noui, C. Charmousis, and D. Langlois, "Beyond Lovelock gravity: Higher derivative metric theories," Phys. Rev. **D97** (2018), no. 4, 044034, arXiv:1710.04531.

[78] D. Langlois, "Dark energy and modified gravity in degenerate higher-order scalar–tensor (DHOST) theories: A review," Int. J. Mod. Phys. **D28** (2019), no. 05, 1942006, arXiv:1811.06271.

[79] L. Heisenberg, "A systematic approach to generalisations of General Relativity and their cosmological implications," Phys. Rept. **796** (2019) 1–113, arXiv:1807.01725.

[80] C. Rovelli, *Quantum gravity*. Cambridge Monographs on Mathematical Physics. Univ. Pr., Cambridge, UK, 2004.

[81] B. Dittrich, "Partial and complete observables for Hamiltonian constrained systems," Gen. Rel. Grav. **39** (2007) 1891–1927, arXiv:gr-qc/0411013.

[82] B. Dittrich, "Partial and complete observables for canonical general relativity," Class. Quant. Grav. **23** (2006) 6155–6184, arXiv:gr-qc/0507106.

[83] A. Ashtekar, "New Hamiltonian Formulation of General Relativity," Phys. Rev. D **36** (1987) 1587–1602.

[84] J. F. Barbero G., "Real Ashtekar variables for Lorentzian signature space times," Phys. Rev. D **51** (1995) 5507–5510, arXiv:gr-qc/9410014.

[85] G. Immirzi, "Real and complex connections for canonical gravity," Class. Quant. Grav. **14** (1997) L177–L181, arXiv:gr-qc/9612030.

[86] G. Immirzi, "Quantum gravity and Regge calculus," Nucl. Phys. B Proc. Suppl. **57** (1997) 65–72, arXiv:gr-qc/9701052.

[87] C. Charles and E. R. Livine, "Ashtekar-Barbero holonomy on the hyperboloid: Immirzi parameter as a cutoff for quantum gravity," Phys. Rev. D **92** (2015), no. 12, 124031, arXiv:1507.00851.

[88] A. Ashtekar and C. J. Isham, "Representations of the holonomy algebras of gravity and nonAbelian gauge theories," Class. Quant. Grav. **9** (1992) 1433–1468, arXiv:hep-th/9202053.

[89] A. Ashtekar and J. Lewandowski, "Representation theory of analytic holonomy C* algebras," arXiv:gr-qc/9311010.

[90] A. Ashtekar, A. Corichi, and J. A. Zapata, "Quantum theory of geometry III: Noncommutativity of Riemannian structures," Class. Quant. Grav. **15** (1998) 2955–2972, arXiv:gr-qc/9806041.

[91] R. Gambini and J. Pullin, *Loops, knots, gauge theories and quantum gravity*. Cambridge University Press, 2000.

[92] A. Ashtekar and J. Lewandowski, "Projective techniques and functional integration for gauge theories," J. Math. Phys. **36** (1995) 2170–2191, arXiv:gr-qc/9411046.

[93] A. S. Cattaneo and A. Perez, "A note on the Poisson bracket of 2d smeared fluxes in loop quantum gravity," Class. Quant. Grav. **34** (2017), no. 10, 107001, arXiv:1611.08394.

[94] K. Giesel and T. Thiemann, "Algebraic Quantum Gravity (AQG). I. Conceptual Setup," Class. Quant. Grav. **24** (2007) 2465–2498, arXiv:gr-qc/0607099.

[95] K. Giesel and T. Thiemann, "Algebraic Quantum Gravity (AQG). II. Semiclassical Analysis," Class. Quant. Grav. **24** (2007) 2499–2564, arXiv:gr-qc/0607100.

[96] K. Giesel and T. Thiemann, "Algebraic quantum gravity (AQG). III. Semiclassical perturbation theory," Class. Quant. Grav. **24** (2007) 2565–2588, arXiv:gr-qc/0607101.

[97] K. Giesel and T. Thiemann, "Algebraic quantum gravity (AQG). IV. Reduced phase space quantisation of loop quantum gravity," Class. Quant. Grav. **27** (2010) 175009, arXiv:0711.0119.

[98] N. Biggs, N. L. Biggs, and B. Norman, *Algebraic graph theory*. No. 67. Cambridge university press, 1993.

[99] T. Thiemann, "Quantum spin dynamics (QSD)," Class. Quant. Grav. **15** (1998) 839–873, arXiv:gr-qc/9606089.

[100] T. Thiemann, "Quantum spin dynamics (qsd). 2.," Class. Quant. Grav. **15** (1998) 875–905, arXiv:gr-qc/9606090.

[101] T. Thiemann, "Anomaly - free formulation of nonperturbative, four-dimensional Lorentzian quantum gravity," Phys. Lett. B **380** (1996) 257–264, arXiv:gr-qc/9606088.

[102] E. Alesci, M. Assanioussi, J. Lewandowski, and I. Mäkinen, "Hamiltonian operator for loop quantum gravity coupled to a scalar field," Phys. Rev. D **91** (2015), no. 12, 124067, arXiv:1504.02068.

[103] M. Assanioussi, J. Lewandowski, and I. Mäkinen, "New scalar constraint operator for loop quantum gravity," Phys. Rev. D **92** (2015), no. 4, 044042, arXiv:1506.00299.

[104] M. Assanioussi, J. Lewandowski, and I. Mäkinen, "Time evolution in deparametrized models of loop quantum gravity," Phys. Rev. D **96** (2017), no. 2, 024043, arXiv:1702.01688.

[105] E. Alesci, M. Assanioussi, and J. Lewandowski, "Curvature operator for loop quantum gravity," Phys. Rev. D **89** (2014), no. 12, 124017, arXiv:1403.3190.

[106] T. Thiemann, "The Phoenix project: Master constraint program for loop quantum gravity," Class. Quant. Grav. **23** (2006) 2211–2248, arXiv:gr-qc/0305080.

[107] T. Thiemann, "Gauge field theory coherent states (GCS): 1. General properties," Class. Quant. Grav. **18** (2001) 2025–2064, arXiv:hep-th/0005233.

[108] T. Thiemann and O. Winkler, "Gauge field theory coherent states (GCS). 2. Peakedness properties," Class. Quant. Grav. **18** (2001) 2561–2636, arXiv:hep-th/0005237.

[109] T. Thiemann and O. Winkler, "Gauge field theory coherent states (GCS): 3. Ehrenfest theorems," Class. Quant. Grav. **18** (2001) 4629–4682, arXiv:hep-th/0005234.

[110] B. Dittrich and T. Thiemann, "Testing the master constraint programme for loop quantum gravity. I. General framework," Class. Quant. Grav. **23** (2006) 1025–1066, arXiv:gr-qc/0411138.

[111] B. Dittrich and T. Thiemann, "Testing the master constraint programme for loop quantum gravity. II. Finite dimensional systems," Class. Quant. Grav. **23** (2006) 1067–1088, arXiv:gr-qc/0411139.

[112] B. Dittrich and T. Thiemann, "Testing the master constraint programme for loop quantum gravity. III. SL(2,R) models," Class. Quant. Grav. **23** (2006) 1089–1120, arXiv:gr-qc/0411140.

[113] B. Dittrich and T. Thiemann, "Testing the master constraint programme for loop quantum gravity. IV. Free field theories," Class. Quant. Grav. **23** (2006) 1121–1142, arXiv:gr-qc/0411141.

[114] B. Dittrich and T. Thiemann, "Testing the master constraint programme for loop quantum gravity. V. Interacting field theories," Class. Quant. Grav. **23** (2006) 1143–1162, arXiv:gr-qc/0411142.

[115] J. W. Barrett and L. Crane, "Relativistic spin networks and quantum gravity," J. Math. Phys. **39** (1998) 3296–3302, arXiv:gr-qc/9709028.

[116] M. P. Reisenberger and C. Rovelli, "Space-time as a Feynman diagram: The Connection formulation," Class. Quant. Grav. **18** (2001) 121–140, arXiv:gr-qc/0002095.

[117] J. D. Bekenstein, "Black holes and the second law," Lett. Nuovo Cim. **4** (1972) 737–740.

[118] J. D. Bekenstein, "Black holes and entropy," Phys. Rev. D **7** (1973) 2333–2346.

[119] W. G. Unruh, "Notes on black hole evaporation," Phys. Rev. D **14** (1976) 870.

[120] S. W. Hawking, "Particle Creation by Black Holes," Commun. Math. Phys. **43** (1975) 199–220. [Erratum: Commun.Math.Phys. 46, 206 (1976)].

[121] A. Almheiri, D. Marolf, J. Polchinski, and J. Sully, "Black Holes: Complementarity or Firewalls?," JHEP **02** (2013) 062, arXiv:1207.3123.

[122] M. Van Raamsdonk, "Building up spacetime with quantum entanglement," Gen. Rel. Grav. **42** (2010) 2323–2329, arXiv:1005.3035.

[123] M. Van Raamsdonk, "Building up spacetime with quantum entanglement II: It from BC-bit," arXiv:1809.01197.

[124] S. Ryu and T. Takayanagi, "Holographic derivation of entanglement entropy from AdS/CFT," Phys. Rev. Lett. **96** (2006) 181602, arXiv:hep-th/0603001.

[125] J. Maldacena and L. Susskind, "Cool horizons for entangled black holes," Fortsch. Phys. **61** (2013) 781–811, arXiv:1306.0533.

[126] A. Einstein, B. Podolsky, and N. Rosen, "Can Quantum-Mechanical Description of Physical Reality Be Considered Complete?," Phys. Rev. **47** (May, 1935) 777–780.

[127] J. S. Bell, "On the Einstein Podolsky Rosen paradox," Physics Physique Fizika **1** (Nov, 1964) 195–200.

[128] D. Bohm and Y. Aharonov, "Discussion of Experimental Proof for the Paradox of Einstein, Rosen, and Podolsky," Phys. Rev. **108** (Nov, 1957) 1070–1076.

[129] A. Peres and D. R. Terno, "Quantum information and relativity theory," Rev. Mod. Phys. **76** (2004) 93–123, arXiv:quant-ph/0212023.

[130] M. Nielsen and I. Chuang, *Quantum Computation and Quantum Information: 10th Anniversary Edition*. Cambridge University Press, 2010.

[131] E. Witten, "A Mini-Introduction To Information Theory," Riv. Nuovo Cim. **43** (2020), no. 4, 187–227, arXiv:1805.11965.

[132] W. Dur, J. I. Cirac, and R. Tarrach, "Separability and distillability of multiparticle quantum systems," Phys. Rev. Lett. **83** (1999) 3562–3565, arXiv:quant-ph/9903018.

[133] A. Acín, D. Bruß, M. Lewenstein, and A. Sanpera, "Classification of Mixed Three-Qubit States," Phys. Rev. Lett. **87** (Jul, 2001) 040401.

[134] O. Gühne and G. Tóth, "Entanglement detection," Physics Reports **474** (2009), no. 1, 1–75.

[135] E. Chitambar and G. Gour, "Quantum resource theories," Reviews of modern physics **91** (2019), no. 2, 025001.

[136] G. Vidal, "On the characterization of entanglement," J. Mod. Opt. **47** (2000) 355, arXiv:quant-ph/9807077.

[137] V. Vedral and M. B. Plenio, "Entanglement measures and purification procedures," Phys. Rev. A **57** (1998) 1619–1633, arXiv:quant-ph/9707035.

[138] M. Horodecki, P. Horodecki, and R. Horodecki, "Limits for Entanglement Measures," Phys. Rev. Lett. **84** (Feb, 2000) 2014–2017.

[139] T.-C. Wei and P. M. Goldbart, "Geometric measure of entanglement and applications to bipartite and multipartite quantum states," Phys. Rev. A **68** (Oct, 2003) 042307.

[140] D. Manzano, "A short introduction to the Lindblad master equation," Aip Advances **10** (2020), no. 2, 025106.

[141] S. D. Bartlett, T. Rudolph, and R. W. Spekkens, "Reference frames, superselection rules, and quantum information," Rev. Mod. Phys. **79** (2007) 555–609, arXiv:quant-ph/0610030.

[142] G. Gour and R. W. Spekkens, "The resource theory of quantum reference frames: manipulations and monotones," New Journal of Physics **10** (2008), no. 3, 033023.

[143] M. M. Wilde, "From Classical to Quantum Shannon Theory," arXiv:1106.1445.

[144] M.-D. Choi, "Completely positive linear maps on complex matrices," Linear Algebra and its Applications **10** (1975), no. 3, 285–290.

[145] L. D. Landau and L. M. Lifshitz, *Quantum Mechanics Non-Relativistic Theory, Third Edition: Volume 3*. Butterworth-Heinemann, 3 ed., Jan., 1981.

[146] P. Tommasini, E. Timmermans, and A. F. R. de Toledo Piza, "The Hydrogen atom as an entangled electron proton system," Am. J. Phys. **66** (1998) 881, arXiv:quant-ph/9709052.

[147] S. M. Chandran and S. Shankaranarayanan, "Divergence of entanglement entropy in quantum systems: Zero-modes," Phys. Rev. D **99** (2019), no. 4, 045010, arXiv:1810.03888.

[148] S. Qvarfort, S. Bose, and A. Serafini, "Hydrogenic entanglement," New J. Phys. **22** (2020), no. 9, 093062, arXiv:2002.10383.

[149] K. Huang, "Statistical Mechanics," Statistical Mechanics (1987) 512.

[150] J. D. Hey, "On the momentum representation of hydrogenic wave functions: Some properties and an application," American Journal of Physics **61** (1993), no. 1, 28–35.

[151] V. S. Buyarov, P. López-Artés, A. Martínez-Finkelshtein, and W. V. Assche, "Information entropy of Gegenbauer polynomials,".

[152] M. Bander and C. Itzykson, "Group Theory and the Hydrogen Atom (I)," Rev. Mod. Phys. **38** (Apr, 1966) 330–345.

[153] M. Bander and C. Itzykson, "Group Theory and the Hydrogen Atom (II)," Rev. Mod. Phys. **38** (Apr, 1966) 346–358.

[154] J. Avery and J. Avery, *Hyperspherical Harmonics and Their Physical Applications*. World Scientific, 2017.

[155] W. Van Assche, R. J. Yáñez, R. González-Férez, and J. S. Dehesa, "Functionals of Gegenbauer polynomials and D-dimensional hydrogenic momentum expectation values," Journal of Mathematical Physics **41** (2000), no. 9, 6600–6613.

[156] J. S. Dehesa and D. Puertas-Centeno, "Multidimensional hydrogenic states: position and momentum expectation values," Journal of Physics B: Atomic, Molecular and Optical Physics **54** (mar, 2021) 065006.

[157] T. Szymanski and J. Freericks, "Algebraic derivation of Kramers–Pasternack relations based on the Schrödinger factorization method," European Journal of Physics **42** (2021), no. 2, 025409.

[158] R. J. Yáñez, W. Van Assche, and J. S. Dehesa, "Position and momentum information entropies of the D-dimensional harmonic oscillator and hydrogen atom," Phys. Rev. A **50** (Oct, 1994) 3065–3079.

[159] F. Pinheiro and A. T. Piza, "Quantum entanglement of bound particles under free center of mass dispersion," Physica Scripta **85** (2012) 065002, `arXiv:1106.4812`.

[160] V. Buyarov, J. S. Dehesa, A. Martinez-Finkelshtein, and J. Sanchez-Lara, "Computation of the entropy of polynomials orthogonal on an interval," 2004.

[161] J. F. Sánchez Lara, "On the asymptotic expansion of the entropy of Gegenbauer polynomials," Journal of Computational and Applied Mathematics **142** (2002), no. 2, 401–409.

[162] J. Sánchez-Ruiz, "Information entropy of Gegenbauer polynomials and Gaussian quadrature," Journal of Physics A: Mathematical and General **36** (apr, 2003) 4857–4865.

[163] J. I. de Vicente, S. Gandy, and J. Sánchez-Ruiz, "Information entropy of Gegenbauer polynomials of integer parameter," Journal of Physics A: Mathematical and Theoretical **40** (jul, 2007) 8345–8361.

[164] I. V. Toranzo, D. Puertas-Centeno, N. Sobrino, and J. S. Dehesa, "Analytical Shannon information entropies for all discrete multidimensional hydrogenic states," International Journal of Quantum Chemistry **120** (Nov, 2019).

[165] J. S. Dehesa, "High Dimensional Atomic States of Hydrogenic Type: Heisenberg-like and Entropic Uncertainty Measures," Entropy **23** (2021), no. 10,.

[166] J. S. Dehesa and N. Sobrino, "Complexity-like properties and parameter asymptotics of Lq-norms of Laguerre and Gegenbauer polynomials," Journal of Physics A: Mathematical and Theoretical **54** (nov, 2021) 495001.

[167] A. Feller and E. R. Livine, "Ising Spin Network States for Loop Quantum Gravity: a Toy Model for Phase Transitions," Class. Quant. Grav. **33** (2016), no. 6, 065005, `arXiv:1509.05297`.

[168] S. K. Asante, B. Dittrich, and J. Padua-Arguelles, "Effective spin foam models for Lorentzian quantum gravity," Class. Quant. Grav. **38** (2021), no. 19, 195002, `arXiv:2104.00485`.

[169] E. R. Livine and D. R. Terno, "The Entropic boundary law in BF theory," Nucl. Phys. B **806** (2009) 715–734, arXiv:0805.2536.

[170] L. Freidel, A. Perez, and D. Pranzetti, "Loop gravity string," Phys. Rev. **D95** (2017), no. 10, 106002, arXiv:1611.03668.

[171] L. Freidel and E. R. Livine, "Bubble networks: framed discrete geometry for quantum gravity," Gen. Rel. Grav. **51** (2019), no. 1, 9, arXiv:1810.09364.

[172] A. Feller and E. R. Livine, "Quantum Surface and Intertwiner Dynamics in Loop Quantum Gravity," Phys. Rev. **D95** (2017), no. 12, 124038, arXiv:1703.01156.

[173] L. Freidel and E. R. Livine, "The Fine Structure of SU(2) Intertwiners from U(N) Representations," J. Math. Phys. **51** (2010) 082502, arXiv:0911.3553.

[174] E. F. Borja, L. Freidel, I. Garay, and E. R. Livine, "U(N) tools for Loop Quantum Gravity: The Return of the Spinor," Class. Quant. Grav. **28** (2011) 055005, arXiv:1010.5451.

[175] E. R. Livine and J. Tambornino, "Spinor Representation for Loop Quantum Gravity," J. Math. Phys. **53** (2012) 012503, arXiv:1105.3385.

[176] M. Dupuis, S. Speziale, and J. Tambornino, "Spinors and Twistors in Loop Gravity and Spin Foams," PoS **QGQGS2011** (2011) 021, arXiv:1201.2120.

[177] E. R. Livine and J. Tambornino, "Holonomy Operator and Quantization Ambiguities on Spinor Space," Phys. Rev. D **87** (2013), no. 10, 104014, arXiv:1302.7142.

[178] E. Alesci, A. Dapor, J. Lewandowski, I. Mäkinen, and J. Sikorski, "Coherent State Operators in Loop Quantum Gravity," Phys. Rev. **D92** (2015), no. 10, 104023, arXiv:1507.01153.

[179] E. Bianchi, L. Hackl, and N. Yokomizo, "Entanglement entropy of squeezed vacua on a lattice," Phys. Rev. **D92** (2015), no. 8, 085045, arXiv:1507.01567.

[180] E. Bianchi, J. Guglielmon, L. Hackl, and N. Yokomizo, "Squeezed vacua in loop quantum gravity," arXiv:1605.05356.

[181] F. Markopoulou, "Quantum causal histories," Class. Quant. Grav. **17** (2000) 2059–2072, arXiv:hep-th/9904009.

[182] E. Hawkins, F. Markopoulou, and H. Sahlmann, "Evolution in quantum causal histories," Class. Quant. Grav. **20** (2003) 3839, arXiv:hep-th/0302111.

[183] L. Freidel and E. R. Livine, "Spin networks for noncompact groups," J. Math. Phys. **44** (2003) 1322–1356, arXiv:hep-th/0205268.

[184] E. R. Livine and D. R. Terno, "Bulk Entropy in Loop Quantum Gravity," Nucl. Phys. **B794** (2008) 138–153, arXiv:0706.0985.

[185] F. Anzà and G. Chirco, "Typicality in spin-network states of quantum geometry," Phys. Rev. **D94** (2016), no. 8, 084047, arXiv:1605.04946.

[186] J. W. Barrett and I. Naish-Guzman, "The Ponzano-Regge model," Class. Quant. Grav. **26** (2009) 155014, arXiv:0803.3319.

[187] E. R. Livine, "Area Propagator and Boosted Spin Networks in Loop Quantum Gravity," Class. Quant. Grav. **36** (2019), no. 18, 185009, arXiv:1902.02722.

[188] E. R. Livine, "The Ponzano–Regge cylinder and propagator for 3d quantum gravity," Class. Quant. Grav. **38** (2021), no. 21, 215009, arXiv:2107.03264.

[189] E. Bianchi, H. M. Haggard, and C. Rovelli, "The boundary is mixed," Gen. Rel. Grav. **49** (2017), no. 8, 100, arXiv:1306.5206.

[190] E. R. Livine, "Intertwiner Entanglement on Spin Networks," Phys. Rev. **D97** (2018), no. 2, 026009, arXiv:1709.08511.

[191] A. Feller and E. R. Livine, "Surface state decoherence in loop quantum gravity, a first toy model," Class. Quant. Grav. **34** (2017), no. 4, 045004, arXiv:1607.00182.

[192] W. Donnelly, "Entanglement entropy in loop quantum gravity," Phys. Rev. **D77** (2008) 104006, arXiv:0802.0880.

[193] W. Donnelly, "Decomposition of entanglement entropy in lattice gauge theory," Phys. Rev. **D85** (2012) 085004, arXiv:1109.0036.

[194] W. Donnelly, "Entanglement entropy and nonabelian gauge symmetry," Class. Quant. Grav. **31** (2014), no. 21, 214003, arXiv:1406.7304.

[195] A. Ashtekar, J. Baez, A. Corichi, and K. Krasnov, "Quantum geometry and black hole entropy," Phys. Rev. Lett. **80** (1998) 904–907, arXiv:gr-qc/9710007.

[196] M. Domagala and J. Lewandowski, "Black hole entropy from quantum geometry," Class. Quant. Grav. **21** (2004) 5233–5244, arXiv:gr-qc/0407051.

[197] E. R. Livine and D. R. Terno, "Quantum black holes: Entropy and entanglement on the horizon," Nucl. Phys. **B741** (2006) 131–161, arXiv:gr-qc/0508085.

[198] I. Agullo, G. J. Fernando Barbero, E. F. Borja, J. Diaz-Polo, and E. J. S. Villasenor, "The Combinatorics of the SU(2) black hole entropy in loop quantum gravity," Phys. Rev. D **80** (2009) 084006, arXiv:0906.4529.

[199] E. R. Livine and D. R. Terno, "Entropy in the Classical and Quantum Polymer Black Hole Models," Class. Quant. Grav. **29** (2012) 224012, arXiv:1205.5733.

[200] O. Asin, J. Ben Achour, M. Geiller, K. Noui, and A. Perez, "Black holes as gases of punctures with a chemical potential: Bose-Einstein condensation and logarithmic corrections to the entropy," Phys. Rev. **D91** (2015) 084005, arXiv:1412.5851.

[201] L. Amico, R. Fazio, A. Osterloh, and V. Vedral, "Entanglement in many-body systems," Rev. Mod. Phys. **80** (2008) 517–576, arXiv:quant-ph/0703044.

[202] V. Bonzom, E. R. Livine, and S. Speziale, "Recurrence relations for spin foam vertices," Class. Quant. Grav. **27** (2010) 125002, arXiv:0911.2204.

[203] E. F. Borja, J. Diaz-Polo, I. Garay, and E. R. Livine, "Dynamics for a 2-vertex Quantum Gravity Model," Class. Quant. Grav. **27** (2010) 235010, arXiv:1006.2451.

[204] D. Brink and G. Satchler, *Angular Momentum*. Oxford library of the physical sciences. Clarendon P., 1968.

[205] J. Yang and Y. Ma, "Graphical calculus of volume, inverse volume and Hamiltonian operators in loop quantum gravity," Eur. Phys. J. C **77** (2017), no. 4, 235, arXiv:1505.00223.

[206] I. Mäkinen, "Introduction to SU(2) Recoupling Theory and Graphical Methods for Loop Quantum Gravity," arXiv:1910.06821.

[207] J. Yang, C. Zhang, and Y. Ma, "Relating spin-foam to canonical loop quantum gravity by graphical calculus," Phys. Rev. D **104** (2021), no. 4, 044025, arXiv:2102.05881.

[208] G. Ponzano and T. Regge, "Semiclassical limits of Racah coefficients," pp 1-58 of Spectroscopic and Group Theoretical Methods in Physics. Block, F. (ed.). New York, John Wiley and Sons, Inc., 1968.

[209] J. Roberts, "Classical 6j-symbols and the tetrahedron," Geom. Topol. **3** (1999), no. 1, 21–66, arXiv:math-ph/9812013.

[210] E. R. Livine and M. Martin-Benito, "Classical Setting and Effective Dynamics for Spinfoam Cosmology," Class. Quant. Grav. **30** (2013) 035006, arXiv:1111.2867.

[211] E. Aranguren, I. n. Garay, and E. R. Livine, "Classical dynamics for Loop Gravity: The 2-vertex model," arXiv:2204.00307.